REPUBLIC OF TÜRKİYE

YILDIZ TECHNICAL UNIVERSITY

GRADUATE SCHOOL OF SCIENCE AND ENGINEERING

WATER BUDGET CALCULATION USING REMOTE SENSING IN DATA-SCARCE CATCHMENTS: KUNDUZ CATCHMENT, AFGHANISTAN

Ahmad Shah FRAHMAND

DOCTOR OF PHILOSOPHY THESIS

Department of Geomatic Engineering

GIS and Remote Sensing Program

Prof. Dr. Fusun BALIK ŞANLI

Co-Supervisor

Assoc. Prof. Dr. Dilek Eren AKYÜZ

September 2023

REPUBLIC OF TÜRKİYE

YILDIZ TECHNICAL UNIVERSITY

GRADUATE SCHOOL OF SCIENCE AND ENGINEERING

WATER BUDGET CALCULATION USING REMOTE SENSING IN DATA-SCARCE CATCHMENTS: KUNDUZ CATCHMENT, AFGHANISTAN

A thesis submitted by Ahmad Shah FRAHMAND in partial fulfillment of the requirements for the degree of DOCTOR OF PHILOSOPHY is approved by the committee on 01-09-2023 in the Department of Geomatic Engineering Program.

Prof. Dr. Fusun BALIK ŞANLI Yıldız Technical University Supervisor	Assoc. Prof. Dr. Dilek Eren AKYÜZ İstanbul University - Cerrahpasa Co- supervisor

Approved By the Examining Committee

Prof. Dr. Fusun BALIK ŞANLI, Supervisor
Yıldız Technical University _____

Prof. Dr. Fatmagül KILIÇ GÜL, Member
Yıldız Technical University _____

Prof. Dr. Ali Melih BAŞARANER, Member
Yıldız Technical University _____

Assoc. Dr. Filiz BEKTAŞ BALÇIK, Member
İstanbul Technical University _____

Assoc. Dr. Saygin ABDİKAN, Member
Hacettepe University _____

I hereby declare that this thesis is my original work and has not been submitted for any other degree or award at any other university or institution. All sources used in the preparation of this thesis have been properly acknowledged and cited in accordance.

I take full responsibility for the design, implementation, and interpretation of the research results presented in this thesis. I affirm that any ethical issues related to this research have been addressed and all necessary approvals have been obtained.

I have considered the principles of scientific research and ethics during my Thesis Study under the title of Estimation of Water Budget using Remote Sensing Observation and GLDAS-2.1 supervised by my supervisor, Prof. Dr. Fusun BALIK ŞANLI. In the case of the discovery of a false statement, I am to acknowledge any legal consequence.

Ahmad Shah FRAHMAND

Signature

Dedicated to my mother and father.

ACKNOWLEDGEMENTS

I extend my heartfelt gratitude to all those who have made significant contributions to the completion of my PhD thesis. Foremost, I am deeply thankful to my esteemed supervisors, Prof. Dr. Fusun BALIK ŞANLI and Prof. Dr. Dilek Eren AKYÜZ, for their invaluable guidance, unwavering encouragement, and steadfast support throughout my research journey. Their wealth of expertise, constructive feedback, and remarkable patience have been pivotal in shaping my research concepts and ensuring the overall quality of my work. I also wish to express my appreciation to the esteemed members of my thesis committee: Prof. Dr. Fatmagül KILIÇ GÜL, Prof. Ali Melih BAŞARANER, Assoc. Dr. Filiz BEKTAŞ BALÇIK, and Assoc. Dr. Saygin ABDİKAN. Their thoughtful insights and suggestions have significantly enriched the quality of my thesis. My sincere thanks are also extended to the Department of Geomatic Engineering at Yildiz Technical University for providing the essential resources and facilities that facilitated my research. I would like to extend special thanks to Mr. Fayez Azizi and Azim Zahed for their vital support, providing the observed data that made this study possible. I would also like to acknowledge and express my gratitude to the four professors who have significantly influenced my academic journey: Dr. Akhter Ali, who has supported me since my master's studies in India; Prof. Naim Eqrar, whose guidance in water studies has been invaluable; the highly respected Prof. Sayed Massod; and Prof. Dr. Fazlul Hadi Wazeen, whose spiritual support has been a source of strength. I extend my warm regards and thanks to a very important friend, Assoc. Prof. Murat Hudaverdi from Yildiz Technical University, whose support was instrumental in the final stages of my thesis. His selflessness even extended to providing me with his personal computer to write my thesis. Simultaneously, I wish to express my gratitude to Mr. Ramzi for his generous provision of numerous resources during the initial stages of my study and for introducing me to the concept of Linux in geospatial data analysis.

I would like to express my heartfelt gratitude and remember my mother, who recently passed, and my father, who continues to stand by my side, for their

unwavering support and invaluable guidance throughout my academic pursuits. Their influence has been immeasurable, shaping the person I am today. To my beloved wife, your unwavering love and support across every facet of this journey have been my rock. Your sacrifices and encouragement have carried me through the most challenging times, and I'm profoundly thankful for having you by my side. I'm equally appreciative of the steadfast support from my family members, including my sister and brother, Ahmad Zaki Frahmand, who have been unwavering sources of inspiration and motivation throughout my studies.

I would like to convey my warm regards and thanks to my family members, Mohamad Sami Amiri and Muhibullah Fruten, for their financial support during my most challenging times. Once again, I am truly grateful to everyone who has contributed to this work, and I hope that my thesis will contribute to the advancement of knowledge in my field.

Ahmad Shah Frahmand

TABLE OF CONTENTS

LIST OF ABBREVIATIONS **vii**

LIST OF FIGURES **ix**

LIST OF TABLES **xiv**

ABSTRACT **xvi**

ÖZET **xviii**

1 INTRODUCTION **1**

1.1 Introduction....1

1.2 Literature Review....4

1.2.1 Precipitation (P)....4

1.2.2 Evapotranspiration (ET)....6

1.2.3 Runoff (Q)....8

1.2.4 Terrestrial Water Storage (TWS)....9

1.2.5 Water Budget (WB)....10

1.2.6 Downscaling Water Budget Components....12

1.2.7 A Literature Rivew on the Study Area....14

1.3 Objective and Gap Filling of the Thesis....16

1.4 Hypothesis....18

2 STUDY AREA **20**

2.1 Study Area....20

2.2 Databases....23

2.2.1 Precipitation, Air Temperature, Runoff and Evapotranspiration at Gage Stations....23

2.2.2 Remote Sensing and GLDAS based Precipitation....25

2.2.3 Remote Sensing and GLDAS based Evapotranspiration....26

2.2.4 Runoff from Rs-Based and GLDAS CLSM Datasets....27

2.2.5 Rs-Based and GLDAS CLSM Terrestrial Water Storage (TWS)....30

2.2.6 RS, land surface model (LSM) products....32

3 METHODOLOGY **35**

3.1 A Holistic Methodology for Water Budget Analysis....35

3.2 Estimation of Precipitation....38

3.3 Estimation of Evapotranspiration using Various Approaches....38

3.3.1 Estimation of ET Rates using Local Meteorological Station Data...38
3.3.2 SEBAL ET Calculation Method...40
3.3.3 Estimation of Evapotranspiration (ET) from MODIS SSEBop and GLDAS-CLSM...44
3.4 Estimation of Runoff using Various Approaches...45
3.5 Terrestrial Water Storage (TWS)...45
3.6 Terrestrial Water Storage Change (TWSC)...46
3.7 Downscaling with Geographically Weighted Regression (GWR)...47
3.8 Statistical Analysis...52
4 RESULT **55**
4.1 Precipitation...55
4.1.1 CHIRPS precipitation...55
4.1.2 PERSIANN Precipitation...69
4.1.3 GLDA CLSM Precipitation...84
4.2 Evapotranspiration (ET)...100
4.2.1 ET Rates Using Local Meteorological Station Data...101
4.2.2 SEBAL ET Result...102
4.2.3 MODIS SSEBop Evapotranspiration...103
4.2.4 GLDAS CLSM Evapotranspiration...106
4.3 GRACE and GLDAS CLSM Terrestrial Water Storage (TWS)...117
4.4 Temporal Variations in Terrestrial Water Storage Change (TWSC)...119
4.5 Runoff...128
4.6 Assessment of Water Budget Estimation Using Remote Sensing-Based and GLDAS CLSM Data...134
4.7 Uncertainty Analysis...146
4.8 Statistical Tests and Findings...150
4.9 Discussion of Statistical Result...159
5 CONCLUSION **162**
5.1 General Conclusion...162
5.2 Precipitation...163
5.3 Evapotranspiration (ET)...164
5.4 Runoff...165
5.5 Terrestrial Water Storage (TWS)...166
5.6 Water Budget (WB)...166

5.7 Reducing Water Budget Uncertainty through Downscaling in Kunduz Catchment.....167
5.8 Recommendations for the Study Area.....170
5.9 Future Works 171
REFERENCES **172**
PUBLICATIONS FROM THE THESIS **188**

LIST OF SYMBOLS

dT	Temperature Differential for each pixel
EF	Reference Evapotranspiration Fraction
ET24	Daily Values of Evapotranspiration
G	Gravitational Constant (9.81 m/s^2)
G	Soil Heat Flux
H	Sensible Heat Flux (W/m^2)
LAI	Leaf Area Index
L	Monin-Obukhov Length
cp	Air Specific Heat (1004 J/kg/K)
P	Density of Air (kg/m^2)
Rah	Aerodynamic Resistance to Heat Transport
Rn	Net Radiation
S-Albedo	Surface Albedo
LSE	Land Surface Emissivity
Ta	Air Temperature
TOA	Top of the Atmosphere Albedo and Radiance
Ts	Surface Temperature (K)
u*	Friction Velocity
u200	Wind Speed at 200 m
Z_om	Momentum Roughness Length (m)
z1, z2	Height above the Zero Plane Displacement
Ψh	Stability Correction Factor for Sensible Heat Flux
Ψm	Stability Correction Factor for Momentum
εa	Atmospheric Emissivity

LIST OF ABBREVIATIONS

Abt	Abtew
CH	CHIRPS
CPC	Climate Prediction Center
CMORPH	Climate Prediction Center Morphing Technique
CHIRPS	Climate Hazards group InfraRed Precipitation with Station
D	Downscaled
DD	Downscaled Data
DEM	Digital Elevation Model
ET	Evapotranspiration
Elev	Elevation
GL	GLDAS
GLDAS	Global Land Data Assimilation System
GRACE	Gravity Recovery and Climate Experiment
H	Sensible Heat Flux
HS	Hargreaves-Samani
JPL	Jet Propulsion Laboratory
LST	Land Surface Temperature
LSM	Land Surface Model
M a.s.l	Meters Above Sea Level
MAK	Makkink
MODIS	Moderate Resolution Imaging Spectroradiometer
MSWEP	Multi-Source Weighted-Ensemble Precipitation
NASA	National Aeronautics and Space Administration
NDVI	Normalized Difference Vegetation Index
O	Original
Obs	Observed
OD	Original Data
PERSIANN	Precipitation Estimation from Remotely Sensed Information using Artificial Neural Networks

PERS	PERSIANN
PM	Penman-Monteith
PT	Priesley-Taylor
RH	Relative Humidity
RHmax	Maximum RH
RHmin	Minimum RH
RS	Remote Sensing
Rn	Net Radiation
SEBAL	Surface Energy Balance Algorithm for Land
SSEBop	Simplified Surface Energy Balance for Evapotranspiration
T	Air Temperature
Tavg	Average of T
Tmax	Maximum of T
Tmin	Minimum of T
TRMM	Tropical Rainfall Measuring Mission
TWSC	Terrestrial Water Storage Change
WB	Water Budget
mm/Year	Millimeter per year
ΔS	Water Storage

LIST OF FIGURES

Figure 2.1 a) World map, b) Afghanistan, c) Amu River Basin, d) Kunduz Catchment with elevation and hydro-meteorological stations **.....21**

Figure 2.2 Kunduz Catchment Land Cover Classes**.....22**

Figure 2.3 Kunduz Catchment Gauge Stations Location **.....22**

Figure 2.4 Temporal Variations of Observed Precipitation in the Kunduz Catchment from 2009 to 2019 **.....24**

Figure 2.5 Temporal Variations of Observed Temperature in the Kunduz Catchment from 2009 to 2019 **.....24**

Figure 2.6 Temporal Variations of Observed Kunduz catchment Runoff from 2009 to 2019**.....25**

Figure 2.7 Remote Sensing (RS), Temporal Variations of PERSIANN, CHIRPS, GLDAS Precipitation in the Kunduz Catchment from 2009 to 2019 **.26**

Figure 2.8 Temporal Variations of MODIS SSEBop ET, in the Kunduz Catchment from 2009 to 2019**.....28**

Figure 2.9 Temporal Variations of GLDAS ET, in the Kunduz Catchment from 2009 to 2019 **.....28**

Figure 210 Temporal Variations of surface runoff from GLDAS CLSM (mm/year) in Kunduz Catchment from 2009 to 2019 **.....29**

Figure 2.11 Temporal Variations of surface runoff from GLDAS-CLSM (mm/year) in Kunduz Catchment from 2009 to 2019**.....29**

Figure 2.12 Temporal Variations of GRACE JPL Terrestrial Water Storage in the Kunduz Catchment from 2009 to 2017 (mm/year)**.....31**

Figure 2.13 GLDAS-CLSM Terrestrial Water Storage in the Kunduz Catchment from 2009 to 2019 (mm/year)**.....31**

Figure 2.14 Temporal Variations of Normalized Difference Vegetation Index (NDVI) in the Kunduz Catchment from 2008 to 2019 **.....32**

Figure 2.15 Temporal Variations of Land Surface Temperature in the Kunduz Catchment from 2008 to 2019 **.....33**

Figure 3.1 Flowchart, explaining the sequential steps in the calculation of the Water Budget for the Kunduz Catchment **.....37**

Figure 3.2 Flowchart of the SEBAL Model Calculating ET Using Landsat 8 Data with Six Standard ET Calculation Methods **.....43**

Figure 3.3 GWR model graphical user interface, reading the dependent and independent variables**.....48**

Figure 3.4 Model properties, variable locations, kernel type, and geographical variability test are represented in red, while the dependent and independent variables are shown in green.....**48**

Figure 3.5 Kernel properties, Search type, and goodness of fit for GWR represented in red.....**50**

Figure 4.1 Comparison of Downscaled (D), Original (O), and Observed (0bs) Data CHIRPS Precipitation data.....**58**

Figure 4.2 Comparison of Downscaled (D), Original (O), and Observed (0bs) Data CHIRPS Precipitation data.....**59**

Figure 4.3 Comparison of Downscaled (D), Original (O), and Observed (0bs) Data CHIRPS Precipitation data.....**60**

Figure 4.4 Original (O), Downscaled (D) CHIRPS Precipitation data from 2009 to 2019.....**61**

Figure 4.5 Monthly Variation of Downscaled (D) CHIRPS Precipitation at Chahar Dara, Gerdab, Baghlan and Balay-i-Kelagai Stations in the Kunduz Catchment from 2009 to 2019.....**64**

Figure 4.6 Monthly Variation of CHIRPS Precipitation (Downscaled) at Doshi, Pul-i-Kundasang, Tang-i-Nahrin and Doab Stations in the Kunduz Catchment from 2009 to 2019.....**65**

Figure 4.7 Monthly Variation of CHIRPS Precipitation (Downscaled) at Dasht-i-Safid, Ahangran and Bamyan Stations in the Kunduz Catchment from 2009 to 2019.....**66**

Figure 4.8 Seasonal (DJF, MAM, JJA, SON) Mean of Downscaled RS-Based CHIRPS (CH) Precipitation in Kunduz Catchment (2009-2019) by Station (mm/season).....**68**

Figure 4.9 Comparison of Downscaled (D), Original (O), and Observed (Obs) Data PERSIANN (PER) Precipitation data.....**73**

Figure 4.10 Comparison of Downscaled (D), Original (O), and Observed (Obs) Data PERSIANN (PER) Precipitation data.....**74**

Figure 4.11 Comparison of Downscaled (D), Original (O), and Observed (Obs) Data PERSIANN (PER) Precipitation data.....**75**

Figure 4.12 Original (O), Downscaled (D) PERSIANN Precipitation (PCP) data (mm/year).....**77**

Figure 4.13 Monthly Variation of PERSIANN Precipitation (Downscaled) at Chahar Dara, Gerdab, Baghlan and Balay-i-Kelagai in the Kunduz Catchment from 2009 to 2019.....**80**

Figure 4.14 Monthly Variation of PERSIANN Precipitation (Downscaled) at Doshi, Pul-i-Kundasang, Tang-i-Nahrin and Doab Stations in the Kunduz Catchment from 2009 to 2019.....**81**

Figure 4.15 Monthly Variation of PERSIANN Precipitation (Downscaled) at Dasht-i-Safid, Ahangaran and Bamyan Stations in the Kunduz Catchment from 2009 to 2019.....**82**

Figure 4.16 Seasonal (DJF, MAM, JJA, SON) Mean of Downscaled RS-Based PERSIANN (PER) Precipitation in Kunduz Catchment (2009-2019) by Station (mm/season) **83**

Figure 4.17 Comparison of Downscaled (D), Original (O), and Observed (Obs) Data GLDAS Precipitation data **87**

Figure 4.18 Comparison of Downscaled (D), Original (O), and Observed (Obs) Data GLDAS Precipitation data **88**

Figure 4.19 Comparison of Downscaled (D), Original (O), and Observed (Obs) Data GLDAS Precipitation data **89**

Figure 4.20 Original (O), Downscaled (D) GLDAS CLSM Precipitation data (mm/year) **90**

Figure 4.21 Monthly Variation of GLDAS CLSM Precipitation (Downscaled) at Chahar Dara, Gerdab, Baghlan and Balay-i-Kelagai Stations in the Kunduz Catchment from 2009 to 2019 ..... **93**

Figure 4.22 Monthly Variation of GLDAS CLSM Precipitation (Downscaled) at Doshi, Pul-i-Kundasang, Tang-i-Nahrin and Dasht-i-Safid Stations in the Kunduz Catchment from 2009 to 2019 ..... **94**

Figure 4.23 Monthly Variation of GLDAS CLSM Precipitation (Downscaled) at Doshi, Pul-i-Kundasang, Tang-i-Nahrin and Dasht-i-Safid Stations in the Kunduz Catchment from 2009 to 2019 ..... **95**

Figure 4.24 Seasonal (DJF, MAM, JJA, SON) Mean of Downscaled GLDAS CLSM Precipitation in Kunduz Catchment (2009-2019) by Station (mm/season) **98**

Figure 4.25 Normalized Difference Vegetation Index (NDVI) – (*a)*; Leaf Area Index (LAI) – (*b)*; Surface Temperature – (c), and Surface Albedo values – (*d*)in Kunduz Catchment, North of Afghanistan **103**

Figure 4.26 Instantaneous hourly ET – (*a*) and ET daily – (*b)* for 18th and 27th September 2016 ..... **103**

Figure 4.27 ET values derived from MODIS SSEBop model for the period spanning from 2009 to 2019 in Kunduz Catchment **109**

Figure 4.28 ET values derived from GLDAS CLSM Original (O), Downscaled DD model for the period spanning from 2009 to 2019 in Kunduz Catchment **112**

Figure 4.29 ET values vs precipitation from downscaled RS-Base precipitation in Chahar Dara, Gerdab and Baghlan stations for the period spanning from 2009 to 2019 in Kunduz Catchment **113**

Figure 4.30 ET values vs precipitation from downscaled Rs-base precipitation in Balay-i-Kelagai. Doshi and Pul-i-Kundasang for the period spanning from 2009 to 2019 in Kunduz Catchment **114**

Figure 4.31 ET values vs precipitation from downscaled Rs-base precipitation in Tang-i-Nahrin, Doab and Dasht-i-Safid for the period spanning from 2009 to 2019 in Kunduz Catchment **115**

Figure 4.32 ET values vs precipitation from downscaled RS-base precipitation Ahangran and Bamyan stations for the period spanning from 2009 to 2019 in Kunduz Catchment **116**

Figure 4.33 Original GRACE JPL Data (O) for Total Water Storage Availability in the Kunduz Catchment **118**

Figure 4.34 Original GLDAS Data (O) for Total Water Storage (TWS) Availability in the Kunduz Catchment **119**

Figure 4.35 Original (O) Total Water Storage Change (TWSC) in the Kunduz Catchment from 2009 to 2017 ..... **122**

Figure 4.36 Downscaled (D) Total Water Storage Change (TWSC) in the Kunduz Catchment from 2009 to 2017 ..... **122**

Figure 4.37 illustrates the Mean Monthly Basin-wise Downscaled (D) Total Water Storage Change (TWSC) in the Kunduz Catchment from 2009 to 2019 ..... **123**

Figure 4.38 Presents a scatter plot comparing the Mean Monthly (D) and (O) datasets of GRACE from 2009 to 2019 ..... **123**

Figure 4.39 Original (O) Total Water Storage Change (TWSC) in the Kunduz Catchment from 2009 to 2019 ..... **124**

Figure 4.40 Downscaled (D) Total Water Storage Change (TWSC) in the Kunduz Catchment from 2009 to 2019 ..... **125**

Figure 4.41 illustrates the Mean Monthly Basin-wise GLDAS CLSM (P-ET-SR) vs GLDAS CLSM in the Kunduz Catchment from 2009 to 2019 ..... **125**

Figure 4.42 Scatter plot of P-ET-R from GLDAS CLSM with GLDAS CLSM TWSC **127**

Figure 4.43 illustrates the residual from CHIRPS, a RS-based dataset, from 2009 to 2017 ..... **129**

Figure 4.44 illustrates the residual from PERSIANN, a RS-based dataset, from 2009 to 2017 ..... **129**

Figure 4.45 Present the residual from GLDAS CLSM (O) dataset, from 2009 to 2019 ..... **131**

Figure 4.46 Present the residual from GLDAS CLSM (D) dataset, from 2009 to 2019 ..... **131**

Figure 4.47 GLDAS CLSM Surface Runoff - Original (O) and Downscaled (D) in Kunduz Catchment (2009-2019) (mm/year) **133**

Figure 4.48 illustrates the monthly comparison between GLDAS CLSM surface runoff and observed runoff within the Kunduz Catchment for the period spanning from 2009 to 2019 ..... **134**

Figure 4.49 Original (O) Total Amount of RS-Based (CHIRPS) Water Budget Components in Kunduz Catchment (2009-2017) **142**

Figure 4.50 Original (O) Total Amount of RS-Based (PERSIANN Data) Water Budget Components in Kunduz Catchment (2009-2017) **142**

Figure 4.51 Original (O) Total Amount of GLDAS CLSM Data Water Budget Components in Kunduz Catchment (2009-2019) **143**

Figure 4.52 Downscaled (D) Total Amount of RS-Based (CHIRPS Data) Water Budget Components in Kunduz Catchment (2009-2017) **143**

Figure 4.53 Downscaled (D) Total Amount of RS-Based (PERSIANN Data) Water Budget Components in Kunduz Catchment (2009-2017) **144**

Figure 4.54 Downscaled (D) Total Amount of GLDAS CLSM Data Water Budget Components in Kunduz Catchment (2009-2019) **144**

Figure 4 55 GLDAS CLSM Downscaled and Original Surface Runoff vs CHIRPS Downscaled and Original Residual **156**

Figure 4 56 GLDAS CLSM Downscaled and Original Surface Runoff vs Observed Runoff **157**

LIST OF TABLES

Table 1.1 A summary of studies that have utilized remote sensing (RS) to estimate and test the efficiency of (WBC) closure measures. **15**

Table 2.1 Location of Gauge Stations in Kunduz Catchment. **23**

Table 2.2 Main Datasets Analyzed for Hydrological Variables in Kunduz Catchment. **33**

Table 2.3 GRACE JPL Data Availability and Missing Months for Kunduz Catchment. **34**

Table 4.1 Correlation Assessment of CHIRPS (CH) RS Downscaled (D), Original (O) Precipitation data vs. Observed (Obs) Precipitation data. **62**

Table 4.2 CHIRPS Monthly Median Values Over Gauge Stations in Kunduz Catchment During 2009 to 2019 (mm/month). **67**

Table 4.3 Seasonal Mean of Downscaled RS-Based CHIRPS (CH) Precipitation in Kunduz Catchment (2009-2019) by Station (mm/season). **68**

Table 4.4 Correlation assessment of PERSIANN (PER) RS based Downscaled (D), Original (O) vs Observed (Obs) precipitation. **76**

Table 4.5 PERSIANN Monthly Median Values Over Gauge Stations in Kunduz Catchment During 2009 to 2019. **83**

Table 4.6 Seasonal Mean of Downscaled RS-Based PERSIANN (PER) Precipitation in Kunduz Catchment (2009-2019) by Station (mm/season). **84**

Table 4.7 Correlation assessment of GLDAS Downscaled (D), Original (O) vs Observed (Obs) precipitation. **91**

Table 4.8 GLDAS CLSM Monthly Median Values Over Gauge Stations in Kunduz Catchment During 2009 to 2019. **96**

Table 4.9 Seasonal Mean of Downscaled RS-Based GLDAS CLSM Precipitation in Kunduz Catchment (2009-2019) by Station (mm/season). **98**

Table 4.10 ET Values (mm/day) on September 18th and September 27th, 2016: SEBAL and Widely Used Conventional Methods. **101**

Table 4.11 Presents the Monthly Mean MODIS SSEBop ET data for gauge stations within the Kunduz Catchment from 2009 to 2019 (mm/month). **109**

Table 4.12 Seasonal Mean of RS-Based MODIS SSEBop ET in Kunduz Catchment (2009-2019) by Station (mm/season). **110**

Table 4.13 Presents the Monthly Mean GLDAS CLSM ET data for gauge stations within the Kunduz Catchment from 2009 to 2019 (mm/month). **110**

Table 4.14 Seasonal Mean of GLDAS CLSM ET in Kunduz Catchment (2009-2019) by Station (mm/season). **111**

Table 4.15 Comparison of RS-Based and GLDAS CLSM Total Water Budget Components - Original (O) and Downscaled (D). **145**

Table 4.16 Uncertainty Analysis of the Precipitation (P) Water Budget Component from RS-Based and GLDAS CLSM Sources in Both (O) and (D) Datasets, Including Minimum (Min), Maximum (Max), Standard Deviation (Std Dev), and Uncertainty (U). **148**

Table 4.17 Uncertainty Analysis of Evapotranspiration (ET) Component from RS-Based and GLDAS CLSM Sources in Both (O) and (D) Datasets. ..**149**

Table 4.18 Uncertainty Analysis of TWSC Component from RS- Based (GRACE) and GLDAS CLSM Sources in Both (O) and (D) Datasets. **150**

Table 4.19 Statistical Analysis of Rs-Based CHIRPS Downscaled (CH (D)) and Original (CH (O)), PERSIANN Downscaled (PERS (D)) and Original (PERS (O)), and GLDAS CLSM Downscaled (GL (D)) and Original (GL (O)) Residuals (Inferred Runoff) Compared to Observed Runoff from Kunduz Catchment Gauge Stations. **154**

Table 4.20 Statistical Analysis of Rs-Based CHIRPS Downscaled (CH (D)) and Original (CH (O)), PERSIANN Downscaled (PERS (D)) and Original (PERS (O)), and GLDAS CLSM Surface Runoff Downscaled (GLSR (D)) and Original Surface Runoff (GLSR (O)) Residuals (Inferred Runoff) Compared to Observed Runoff from Kunduz Catchment Gauge Stations. **156**

Table 4.21 Monthly statistical analysis result for Rs based and GLDAS CLSM residual (P-ET-TWSC) vs observed runoff. **157**

Table 4.22 Accuracy assessment of SEBAL result using two meteorological station data. **158**

Table 4.23 Statistics of albedo, Nb-Emissivity, NDVI, LAI, and LST in Kunduz Catchment. **158**

Table 4.24 Statistical properties of energy balance parameters, in Kunduz Catchment. **158**

Table 4.25 MODIS SSEBop and GLDAS CLSM ET Percentages (CHIRPS (CH), PERSIANN (PERS) and GLDAS (GL) %). **160**

ABSTRACT

Water Budget Calculation Using Remote Sensing in Data-Scarce Catchments: Kunduz Catchment, Afghanistan

Ahmad Shah FRAHMAND

Department of Geomatic Engineering

Doctor of Philosophy Thesis

Supervisor: Prof. Dr. Fusun BALIK ŞANLI

Co- supervisor: Assoc. Prof. Dr. Dilek Eren AKYÜZ

This study focuses on estimating monthly and annual water budget components within the Kunduz catchment from 2009 to 2019. It utilizes satellite observations and the GLDAS-2.1 CLSM model. Datasets, including Precipitation (P), Evapotranspiration (ET), and Terrestrial Water Storage (TWS), were obtained from diverse sources, such as PERSIANN, CHIRPS, MODIS SSEBop, GRACE, and GLDAS CLSM. Inferred runoff data were derived by calculating residual values within the water balance equation and showed differences from the observed runoff. Furthermore, acknowledging that numerous studies have highlighted the difficulty posed by the coarse resolution in remote sensing and GLDAS, which can impact the accuracy of water budget estimations, this study endeavors to improve and enhance water budget inputs. Thus, in this study, downscaling techniques such as Geographical Weighted Regression (GWR) are employed on both the remote sensing data and the GLDAS datasets. Both remote sensing and GLDAS CLSM Original and Downscaled data results compared with observed data and showed some level of consistency between remotely sensed and GLDAS P data, vs

observed data. As known, in this catchment, ET exhibited a direct relationship with precipitation. TWS showed significant uncertainties, warranting further investigation in future research. The assessment of downscaled water budget components, including P, unveiled moderate to strong correlations between remote sensing data and actual rainfall measurements, quantified by the Pearson correlation coefficient ranging from 0.2 to 0.88. Also, a strong negative correlation was observed between downscaled precipitation layers as -0.66. However, caution should be exercised when using monthly downscaled data obtained from remote sensing (RS) and GLDAS sources for accurately predicting water budget components and discharge values. Conversely, annual downscaled datasets from both GLDAS and RS showed a broader performance spectrum, with coefficient determination (R^2) values ranging from 0.04 to 0.55. Notably, Downscaled NSE -0.44 to the Original lowest -12.2, the CHIRPS Downscaled dataset indicated a -12% Percent Bias (PBIAS), indicating underestimation of discharge values for the entire catchment, while PERSIANN, demonstrated an overestimation of 102.3%. On the other hand, volumetric efficiency of downscaled data shows that 0.54 to 0.64 water delivered at proper time in the catchment. This study highlighted the strengths and weaknesses of remote sensing-based and GLDAS-2.1 CLSM in water budget analyses and estimation, particularly within the Afghanistan Kunduz catchment having scarcity in terms of observed data. As a result of this study, it has been observed that these methods are particularly successful in sub-basins, especially in areas where data is limited, for conducting water budget studies. Considering this information, it will enhance the successes of the studies involving a water budget aspect, such as sustainable basin management, predicting anthropogenic impacts, reservoir operation, and more. Furthermore, within the scope of the thesis, downscaling the spatial resolution of water budget parameters (precipitation, evaporation, runoff, TWS) to 1 km makes it possible to approach sustainability goals in micro-scale planning.

Keywords: ET, GLDAS-2.1 CLSM, Water budget estimation, Remote Sensing, Residue, Inferred runoff.

ÖZET

Az Ölçüm Verisi Olan Havzalarda Uzaktan Algılama Kullanarak Su Bütçesi Hesaplama: Kunduz Havzası, Afganistan

Ahmad Shah FRAHMAND

Department of Geomatic Engineering

Doctor of Philosophy Thesis

Supervisor: Prof. Dr. Fusun BALIK ŞANLI

Co- supervisor: Assoc. Prof. Dr. Dilek Eren AKYÜZ

Bu çalışma, 2009 ile 2019 yılları arasında Kunduz Nehri Havzası içinde aylık ve yıllık su bütçesi bileşenlerini tahmin etmeyi amaçlamıştır. Bu amaçla uydu gözlemleri ve GLDAS-2.1 CLSM modeli kullanılmıştır. Veri setleri, PERSIANN, CHIRPS, MODIS SSEBop, GRACE ve GLDAS CLSM gibi farklı kaynaklardan temin edilen Yağış (P), Evapotranspirasyon (ET) ve Karasal Toplam Su Depolama (TWS) içermektedir. Çıkarılan akış verileri, su bütçesi denklemi içindeki artık değerleri hesaplayarak elde edilmiş ve gözlemlenen akıştan farklılıklar göstermiştir. Ayrıca, birçok çalışma, uzaktan algılama ve GLDAS'ın düşük çözünürlüğünün, su bütçesi tahminlerinin doğruluğunu etkileyebileceğini vurgulamış olup, bu çalışma su bütçesi girdilerini geliştirmeyi ve artırmayı amaçlamaktadır. Bu nedenle, bu çalışma, hem uzaktan algılama verileri hem de GLDAS verileri üzerinde ölçek iyileştirme (downscaling) teknikleri özellikle Coğrafi Ağırlıklı Regresyon (Geographical Weighted Regression: GWR) kullanılmıştır. Orijinal ve ölçeklenmiş sonuçlar gözlemlenen verilerlele

karşılaştırılmış ve uzaktan algılanan P, GLDAS verileri ile gözlemlenen veriler arasında bir dereceye kadar tutarlılık göstermiştir. Bilindiği üzere, bu havzada da ET ile yağış doğrudan bir ilişki göstermiştir. TWS'de belirgin şekilde belirsizlikler mevcut olup, gelecekteki araştırmalarda incelenmesi gerekmektedir. Ölçeklenmiş yağış verilerini içeren su bütçesi bileşenlerinin değerlendirilmesi, uzaktan algılanan verilerle gerçek yağış ölçümleri arasında Pearson korelasyon katsayısı 0,2 ile 0,88 arasında değişken bir korelasyon göstermiştir. Ayrıca, ölçeklenmiş yağış katmanla rı arasında güçlü bir negatif korelasyon gözlenmiştir (-0,66). Bununla birlikte, uzaktan algılamadan (RS) ve GLDAS kaynaklarından elde edilen aylık ölçeklenmiş veriler, su bütçesi bileşenlerini ve deşarj değerlerini doğru bir şekilde tahmin edebilmesi için dikkatli kullanılması gerekir. Aynı zamanda, hem GLDAS hem de RS'den yıllık ölçeklenmiş veriler, determinasyon katsayısı (R^2) değerlerinin 0,04 ile 0,55 arasında değiştiği daha geniş bir performans yelpazesi sergilemiştir. Özellikle, CHIRPS ölçeklenmiş veri seti, havzanın tamamı için deşarj değerlerini Yüzde Hata Göstergesi (PBIAS) %-12 hesaplanmıştır. RS veri seti ise özellikle PERSIANN deşarj değerlerini %102,3 oranında daha yüksek bulunmuştur. Öte yandan ölçekle nmiş verilerin hacimsel verimliliği kriter değeri 0,54 ile 0,64 arasında hesaplanmıştır. Bu çalışma, uzaktan algılama temelli su bütçesi analizleri ve GLDAS-2.1 CLSM modelinin su bütçesi tahminindeki güçlü ve zayıf yönlerine dikkat çekerek Afganistan Kunduz havzası özelinde de hesaplanmıştır. Çalışma sonucunda bu yöntemler sisteminin veri eksikliği olan havzalarda su bütçesi çalışmaları için özellikle alt havzalarda başarlı sonuç verdiği gözlemlenmiştir. Bu bilgiler ışığında, sürdürülebilir havza yönetimi, antropojenik etkilerin tahmini, reservuar işletmesi gibi su bütçesini içeren veya ihtiyaç duyan tüm çalışmaların başarısını arttıracağı için önem taşımaktadır. Ayrıca tez kapsamında ölçek iyileştirme ile su bütçesi (yağış, buharlaşma, debi, TWS) değerlerinin mekansal çözünürlüğü 1km'ye kadar düşürülmüş olması mikro ölçekli planlamada sürdürülebilirlik hedefine daha yaklaşmasını mümkün kılmaktadır.

Anahtar Kelimeler: GLDAS-2.1 CLSM, Su Bütçesi Tahmini, Uzaktan Algılama, Artık hata, Dolaysız Akış.

1
INTRODUCTION

1.1 Introduction

Water stands as a critical resource for sustaining life on Earth. However, its availability faces threats due to climate change, pollution, and unsustainable practices, and the scarcity of freshwater, which constitutes only 2.5% of Earth's water, further underscores its limited abundance. The urgency to address these challenges necessitates effective water resource management.

According to the World Health Organization [1], safe drinking water remains inaccessible for 2.2 billion people, and proper sanitation services are lacking for 4.2 billion people. Notably, agriculture consumes around 70% of global freshwater withdrawals [2]. Water scarcity is particularly pronounced in regions like the Middle East and North Africa, characterized by chronic shortages [3]. Climate change is expected to exacerbate this issue, especially in water-stressed areas [4]. In addition to scarcity, water quality concerns arise from pollution and inadequate sanitation infrastructure, leading to environmental degradation and health issues [3]. Alarmingly, the Global Water Institute forecasts that severe water scarcity could displace around 700 million people by 2030 [5].

Given these challenges, understanding terrestrial water budget (WB) components gains significance for various applications, including water resource management, flood and drought prediction, wastewater treatment, and energy provision [6, 7]. The WB principle, capturing changes in water storage by measuring inflows and outflows over time, is expressed as Equation (1.1).

$$\Delta S = P - ET - Q - Baseflow \pm \Delta TWS - other\ components = 0 \qquad (1.1)$$

This formula signifies the difference between precipitation (P), evapotranspiration (ET), ΔTWS represents the change in Terrestrial Water Storage, while the remaining components encompass factors such as interception, soil moisture, storage of shallow and deep groundwater, as well as snow and glaciers, among others. While gauge stations ensure accurate WB estimates, their limited coverage

in some regions, especially developing areas, poses challenges. Gauge measurements have conventionally been regarded as the most precise approach for monitoring WB components. Nevertheless, in many areas around the world, particularly in developing regions, there is a notable scarcity or even a complete absence of gauge stations. This scarcity is primarily attributed to the substantial expenses associated with establishing and maintaining such stations. On the contrary, some components of the water budget, such as ET, necessitate dense gauge networks to accurately predict the climatic conditions in the region [8, 9]. In recent times, WB studies have entered a new phase owing to advanced satellite remote sensing (RS) techniques. These techniques enable us to regularly monitor remote or even hard-to-reach areas on Earth and areas with scarce hydrometeorological observed data. While satellite RS observations may not match the precision of gauge measurements, they provide substantial cost advantages and the capability to collect data globally, irrespective of political situations. RS products offer unparalleled temporal resolution, at times capturing data down to sub-hourly intervals, and deliver impressive spatial detail, achieving resolutions typically ranging from 500 m to 300-400 kilometers. This extensive coverage is available worldwide [10]. Most satellite products used in water budget studies have historically possessed coarse resolutions, raising concerns about the accuracy of their results. However, with the launch of the GRACE satellite in April 2002, there has been a significant increase in research focused on water budgets. Scientists have not only leveraged GRACE's high-precision monthly solutions for changes in terrestrial water storage (TWS) but have also begun to explore rescaling and downscaling techniques [11]. These techniques aim to refine the coarse resolution data, thereby improving accuracy in numerous regions across the globe. This enhanced data availability, coupled with innovative downscaling approaches, has propelled researchers to investigate water budgets with greater precision and has broadened the understanding of water resource dynamics, particularly in developing regions with scarce data. Before the GRACE mission, remote sensing products like PERSIANN and CHIRPS for P and MODIS for ET were available. However, GRACE data availability has greatly facilitated global water budget studies. Although satellite remote sensing cannot directly measure discharge (Q), this limitation is expected to be addressed by the Surface Water and Ocean

Topography (SWOT) mission, commencing in November 2022 [12]. Runoff, while not directly provided by satellite data, can be inferred as a residual component within the water budget [13-15]. On the other hand, The Global Land Data Assimilation System (GLDAS), provided by the National Aeronautics and Space Administration (NASA), is responsible for the provision of consistent and frequent data concerning water and energy components [16]. This system combines remote sensing and ground-based observations, delivering quantities (such as evapotranspiration, runoff, and snow water equivalence) that cannot be directly observed by satellites [16] or provided by simplistic models. Despite the presence of advanced Land Surface Models (LSMs) such as GLDAS, the simulation of human-induced modifications within extensive basins remains a formidable challenge [14, 15, 17-19]. Nevertheless, owing to their heightened spatial resolution, hydrological models at smaller scales (microscale models) may be deemed appropriate for reconciling the water budget.

Satellite remote sensing plays a vital role in water resources management, offering global coverage and consistent data compared to ground-based measurements. It provides reliable, fine-grained precipitation estimates globally, particularly in data-sparse regions, a key advantage of Earth-observing satellites [20]. Recent studies [21-26] support the use of satellite-based rainfall estimates, emphasizing their promise in data-scarce areas. However, it's worth noting that regions with elevation variations can exhibit significant spatial variability in satellite-based precipitation estimates [27]. Remotely estimated evapotranspiration relies on geophysical parameters observed through satellite sensors. Researchers have assessed the effectiveness of evapotranspiration products derived from spaceborne remote sensing data [28-33]. Despite uncertainties, these studies have demonstrated the advantages of satellite-based evapotranspiration products over costly conventional methods. While acknowledging certain limitations, satellite remote sensing holds substantial promise for estimating the water budget, with uncertainties exhibiting variability across different basins [30, 34]. Thus, more studies over different basins can better reveal the potential of satellite-based water budget estimation.

1.2 Literature Review

While researchers acknowledge the valuable role of satellite remote sensing in basin hydrology, it's important to note that remote sensing products encounter significant uncertainties. These uncertainties arise from factors such as changes in satellite orbits, infrequent data sampling, imperfections in retrieval algorithms, intricate topographical features, and variations in cloud reflectance [9, 14, 35].

In order to estimate the water budget of a basin accurately, it is necessary to have data about the various water-related factors, including precipitation, evapotranspiration, runoff, as well as surface and groundwater storage and its changes.

1.2.1 Precipitation (P)

Precipitation serves as the primary input to the water budget, encompassing various forms of water, including rainfall, snowfall, and other types. Precipitation is quantified using various techniques, such as rain gauges, snow gauges, weather radar, and satellite data. Precipitation is measured directly through in situ methods using rain gauges and remote sensing techniques employing satellite sensors and weather radars [21, 36]. In gauge-based observations, spatial variations become resolvable when gauge density is sufficient [15]. However, in point-based observations like these, the uncertainty in precipitation values tends to increase with greater distance from the measuring station [20, 21]. Moreover, in regions with limited gauge stations, particularly in mountainous areas, point-based rainfall observations result in an uneven distribution of data. Collecting rainfall data on the ground is typically challenging due to its high cost and limited availability in remote areas [15]. Various remote sensing-based precipitation data sources are available for water budget assessments. Notable among these sources are Precipitation Estimation from Remotely Sensed Information using Artificial Neural Networks (PERSIANN), Climate Hazards Group InfraRed Precipitation with Station (CHIRPS), among many others. These datasets effectively serve as the primary parameter for global-scale water budget analysis. For instance, in a study by [37], four distinct precipitation (P) datasets were employed in combination with all four precipitation layers to reduce hydrological imbalances. The researchers found that

the best results were obtained when they combined a precipitation product called the Global Precipitation Climatology Project (GPCP). Furthermore, a study conducted by [15] emphasized that remote sensing-based precipitation played a significant role in generating hydrological imbalances across thirteen major river basins in the United States. The study authors conducted a comparison between remotely sensed P and gauge observations. They utilized the Variable Infiltration Capacity (VIC) model to assess uncertainties related to precipitation parameters and other components of the water budget, using data derived from remote sensing. The analysis results indicated that the estimated runoff (Q) exceeded the gauge measurements. This was attributed to the overestimation of P and the underestimation of ET and TWS. In a study analyzing rainfall climatic patterns in Bangladesh, researchers employed data from the Tropical Rainfall Measuring Mission (TRMM) which a remote sensing base precipitation layer. The investigation focused on distinct seasons—pre-monsoon, monsoon, and post-monsoon—utilizing ground-based rainfall data as a reference. Both TRMM versions 4 and 5 3B42 were utilized. Findings from this analysis indicated that while TRMM holds promise for long-term water resource management analysis, its applicability for short-term events, such as flood forecasting, appears limited [38]. Similarly, in another study, TRMM precipitation data were used to estimate runoff within the Xinjiang catchment of the Poyang Lake basin [39]. This estimation involved the use of a distributed hydrological model. Studies [13, 15], and [40] revealed that the primary source of errors in water budget estimation is remote sensing-based precipitation data. The authors attempted to combine the precipitation data using the Multi-Source Weighted Ensemble Precipitation (MSWEP) to reduce the imbalance in the first parameter of the water budget, which is precipitation. In regions with sparse gauge stations, particularly in mountainous areas like the Kunduz watershed, the uneven spatial distribution of gauge data remains a significant challenge for estimating precipitation. This is due to the reliance on point-based rainfall observation. Ground-based rainfall observation further adds to this challenge, primarily due to high costs and limited availability in remote areas, as noted in prior research [15].

[41] suggests that satellite remote sensing has the potential to facilitate real-time global monitoring of the Earth's surface, particularly in sparsely populated or economically disadvantaged regions where in situ observations of precipitation are often lacking. Consequently, space-borne remote sensing of hydrological variables is gaining prominence as a viable approach for monitoring the water cycle and its associated components. This shift in focus is particularly valuable for regions facing data scarcity or limitations in traditional ground-based monitoring methods.

1.2.2 Evapotranspiration (ET)

Evapotranspiration, the second crucial parameter in the water budget, encompasses the combined loss of water from the land surface through evaporation and from plants through transpiration. ET is influenced by multiple factors, including solar radiation, air and land temperature, surface winds, humidity, soil properties, and vegetation characteristics such as type and coverage. Precise estimation of soil water content and actual ET within a catchment relies on accurate input data. While ground-based observations provide localized insights, remotely sensed data are essential for capturing broader spatial patterns. However, measuring ET and terrestrial water storage changes at larger scales through in situ methods poses challenges, introducing uncertainties into ET and terrestrial water storage assessments [14, 15, 34, 42, 43]. Since 1988, various algorithms, including the Surface Energy Balance Algorithm for Land (SEBAL), have been developed to estimate ET, utilizing satellite imagery and computational models to assess land surface energy balance. SEBAL, for instance, has undergone verification across 30 countries, consistently achieving impressive accuracy levels of 85 percent on a daily scale and 95 percent on an annual basis [44]. This progress highlights the significance of satellite-based approaches for assessing water budget components and enhancing our understanding of hydrological processes. Researchers in Brazilian tropical savannas applied a MODIS-based energy balance model to calculate ET on clear-sky days, using the results for water resource management [45]. The MODIS satellite mission employs the Temperature-Vegetation Index (Ts-VI) method to provide ET data, relying on remotely sensed vegetation indices and surface temperature [46]. Notably, MODIS ET exhibits a strong correlation with measurements from flux towers in the United States, especially when hourly surface

radiation data from Geostationary Operational Environmental Satellites (GOES) are integrated. However, it's essential to acknowledge that the utility of MODIS ET is limited to North America due to constraints in GOES data coverage.

In contrast, researchers in China's Yellow River basin adopted an alternative approach to estimate ET, utilizing a water balance equation incorporating various inputs, including precipitation, runoff, and ΔTWS data from GRACE. Findings unveiled consistent bias patterns in monthly mean ET values, with MODIS ET surpassing water balance ET from May to August but falling short during September-October and January-February [47]. In research [37] endeavors were made to optimize combinations of P and ET datasets to minimize imbalances within the water budget component. The study identified that the most favorable agreement between estimated values and gauge measurements of discharge (Q) occurred when employing the Global Precipitation Climatology Project (GPCP) product for P alongside the University of Montana (MON) product for ET. This combination yielded Q estimations closely aligning with gauge measurements, with deviations within 1 mm/day. This finding underscores the importance of selecting appropriate datasets for precipitation and evapotranspiration to enhance the accuracy and reliability of water budget assessments.

Furthermore, studies [13, 15], and [40], emphasized that remote sensing-based P primarily contributes to water budget errors in South America. To enhance the precision of water budget parameter estimations, especially for Q, these investigations recommended using a multi-source evapotranspiration dataset, such as the Global Land Evaporation Amsterdam Model (GLEAM), to significantly reduce errors in runoff estimation. Additionally, researchers employed the Priestley-Taylor equation in conjunction with the Ts/NDVI space, utilizing MODIS NDVI data and Global Land Data Assimilation System (GLDAS) meteorological data to compute ET in ungauged basins, without relying on field data. However, an important limitation of the Ts/NDVI method for ET estimation is related to the range of NDVI values. Consequently, this approach is applicable only when a substantial range of NDVI values is present to generate an expected trapezoidal shape in the Ts/NDVI space. It's crucial to note that this method does not account for nighttime and cloudy daytime ET estimation [32].

1.2.3 Runoff (Q)

Runoff, an integral component of the water budget, encompasses precipitation that does not infiltrate the soil or become absorbed by vegetation. Instead, it flows over the land surface, eventually reaching rivers and streams. Accurately estimating runoff is crucial for effective water resource management, flood control, and ecological sustainability. However, this task is intricate and depends on various factors such as precipitation, evapotranspiration, land use, soil characteristics, terrain, and climate conditions.

Multiple methods have been developed to estimate runoff, including empirical, physical, and numerical models, each with its own set of advantages and limitations. Monitoring runoff variability is traditionally reliant on hydrological stations. Still, the insufficient availability or sparse distribution of these stations in many basins worldwide poses significant challenges [15, 34]. Multiple studies have assessed the degree of water budget closure by examining the deviation of calculated runoff (represented in Equation 1.1) from gauge-measured runoff data [13, 15, 37, 40, 48, 49]. A higher degree of closure indicates a closer alignment between calculated and gauge-measured runoff, signifying greater accuracy in water budget estimations.

In a comprehensive study of the Mississippi River basin [13], researchers conducted extensive validations of remote sensing (RS) products against various reference datasets, including in-situ measurements, land surface models, and reanalysis data. Their findings revealed a tendency for calculated runoff to overestimate gauge-measured runoff. This overestimation was primarily attributed to a noticeable positive bias in RS-based precipitation estimates, particularly during the summer season. A separate study encompassing 13 major river basins in the United States utilized a Variable Infiltration Capacity model platform to compare RS-based precipitation data with gauge observations. The aim was to assess uncertainties in RS-based evapotranspiration and water storage estimates, considering the limited availability of in-situ measurements for ET and surface storage. The results indicated an overestimation of calculated runoff compared to gauge-measured runoff, attributed to the overestimation of P and the underestimation of ET and surface storage [15]. The significant runoff and soil erosion observed in the Mandri river watershed underscores the importance of

accurately assessing these factors within the water budget. These phenomena directly impact key components of the budget, such as runoff and surface water storage, emphasizing the need for comprehensive management strategies to maintain a sustainable and balanced water budget in the region [22]. Additionally, the integration of remote sensing data with GLDAS data layers provides a means to indirectly estimate runoff, as demonstrated in prior studies [13-15, 50]. This approach opens new avenues for enhancing the accuracy of runoff estimation by incorporating diverse data sources and models, thereby improving our understanding of the complex spatial and temporal variations in hydrological processes.

1.2.4 Terrestrial Water Storage (TWS)

Estimating water storage using conventional methods can be intricate and prone to errors, especially when considering factors like changes in total terrestrial water storage (ΔTWS), snowmelt, and soil moisture. These factors become crucial when estimating various components of the water budget, such as precipitation, evapotranspiration (ET), and runoff. While certain aspects of terrestrial water storage (TWS), including surface water and soil moisture, can be monitored using various satellite data sources, a comprehensive assessment of TWS through remote sensing is uniquely achievable with data from the Gravity Recovery and Climate Experiment (GRACE) satellite mission [27, 51]. GRACE satellite data has revolutionized our ability to study changes in global water mass by observing shifts in gravity, a capability previously unattainable within the scientific community [27, 43, 52]. In a Canadian case study, GRACE-derived water storage anomalies significantly improved water budget estimates. These GRACE values were cross validated with precipitation, ET, and streamflow records, demonstrating a robust correlation. However, minor discrepancies may still exist due to inherent uncertainties in terrestrial water storage data [53].

In regions lacking sufficient or accurate water level measurements, satellite altimetry plays a crucial role in tracking changes in surface water levels. In such cases, GRACE satellite gravimetry aligns well with the geometric changes observed through altimetry measurements [54]. Additionally, [55] employed three distinct approaches to estimate groundwater storage using satellite data. The first

method involved scrutinizing water budgets to validate GRACE-derived TWS values. The second approach entailed determining trends in groundwater anomalies using both GRACE TWS data and satellite-derived variables, followed by comparing these trends with hydrological models. The third method directly contrasted GRACE-derived groundwater estimations with in-situ groundwater levels.

Within the context of the GLDAS CLSM (Global Land Data Assimilation System - Catchment Land Surface Model), Total Water Storage Anomaly (TWSA) represents the difference between the current total water storage and the historical average total water storage, typically over a specific period [56]. The GLDAS-CLSM is a hydrological model that assimilates various observational data sources to simulate land surface processes and estimate hydrological variables. This comprehensive exploration of terrestrial water storage enhances our understanding of the water budget, shedding light on its intricate components and their interactions.

1.2.5 Water Budget (WB)

In the preceding sections, individual water budget components received separate consideration. This section offers a consolidated view of these fundamental components.

Water budgets play a pivotal role for water agencies, aiding in long-term planning, resource assessment, data gap identification, and the formulation of effective management strategies [57]. The implementation of a water budget framework facilitates the empowerment of water managers to make informed decisions, ensuring the sustainable and efficient utilization of water resources. In today's world, the management and allocation of water within basins and across borders have assumed a significant role [15, 19]. Climate change adds complexity to the availability of water, impacting both ecosystems and societies [19, 58, 59]. A comprehensive assessment of a basin's water budget necessitates data encompassing soil, vegetation, and various components such as precipitation, evapotranspiration (ET), runoff, and surface and groundwater storage [21, 36]. It is essential to note that gauge-based observations are beset by limitations in spatial

resolution and an increase in precipitation uncertainties with distance from measuring stations [15, 20]. The quantification of water fluxes, including precipitation, ET, and runoff, is of utmost importance for maintaining a watershed's hydrological balance. Notably, precipitation can detect large-scale variations if gauge density is sufficient [14, 15, 34].

The estimation of ET and changes in terrestrial water storage (TWSC) poses challenges, mainly due to gauge distribution, especially in remote regions. Consequently, observations of ET and TWS remain relatively deficient when compared to precipitation at continental scales [43, 60]. To address these challenges, some authors have turned to remote sensing data to finalize water budget assessments in the regions of their study. In an initial study conducted by [13], an attempt was made to balance the water budget equation using remote sensing (RS) data for the Mississippi River basin. Thorough validation against reference data sources, including in-situ measurements, land surface models (LSMs), and reanalysis data, revealed a consistent pattern where estimated runoff (Q) exceeded gauge-measured runoff. This overestimation was primarily attributed to a notable positive bias in RS-derived precipitation (P), especially during the summer months. Notably, significant progress was made in reducing the water budget closure gap after correcting this bias in the RS precipitation data. In the [15] study identified RS-based P as the primary contributor to non-closure issues across thirteen major US river basins. The research involved comparing RS-derived P data with gauge observations and utilized the Variable Infiltration Capacity (VIC) model to assess uncertainties in RS-based ET and terrestrial water storage change (ΔS) data due to limited in-situ measurements for ET and ΔS. The results consistently indicated that estimated Q exceeded gauge-measured runoff due to overestimation of P and underestimation of ET and TWS. The increasing availability of RS data has allowed researchers to select more suitable data combinations for each WB component. In their study [37], researchers explored various combinations of four different P datasets and two different ET datasets to identify the most effective combinations that reduced water budget non-closure. Their analysis revealed that the highest level of agreement between estimated and gauge-measured Q occurred when they utilized the Global Precipitation Climatology Project (GPCP) P product

in conjunction with the University of Montana (MON) ET product, resulting in differences of less than 1 mm/day. In a study conducted by [49], an investigation was carried out to determine the feasibility of achieving WB closure in the data-scarce Rufiji basin, located in Tanzania, using solely RS products. The findings pointed to a limited correlation between estimated and observed Q, with estimated Q typically falling short of observed Q. Additionally, the analysis led to the conclusion that long-term assessments of water resources yield more consistent results compared to short-term assessments. In their study, [48] observed a significant overestimation of estimated Q compared to observed Q, primarily attributable to the underestimation of remote sensing-based ET. Building on the findings from [13] and [15], [40] also highlighted the dominant role of remote sensing-based P in WB errors, particularly in South America. They found that WB closure errors were minimized when employing the Multi-Source Weighted-Ensemble Precipitation (MSWEP) dataset for P and the Global Land Evaporation Amsterdam Model (GLEAM) for ET. Worldwide studies have employed various methodologies, providing valuable insights into the utility of remote sensing data, as well as data assimilated from GLDAS. Researchers have also made efforts to enhance the spatial resolutions of satellite data using downscaling techniques, all with the goal of improving the accuracy of water budget assessments. The upcoming literature review section will explore these research efforts in greater detail.

1.2.6 Downscaling Water Budget Components

Numerous studies have explored methods and techniques to enhance the precision and reliability of estimating water budget components, aligning with the central theme of water budget analysis. Downscaling, which has been extensively researched, serves as a key method to improve the accuracy of water budget assessments. For instance, in a study conducted by [61]**,** spatial downscaling techniques were applied to daily precipitation data, significantly enhancing the accuracy of discharge estimates related to water budget calculations. This improvement extends beyond reducing model bias; it also enables a better representation of overall flow variability, especially during extreme events. Additionally, it enhances the accuracy of capturing the timing and shape of

hydrographs. Another approach to enhance spatial resolution involves utilizing coarse-scale datasets that integrate data from diverse remote sensors. Downscaling is a method employed to increase spatial resolution by disaggregating the original dataset (OD) through the application of statistical relationships [62], However, it's essential to note that downscaling typically requires high-resolution information [63-65]. To illustrate, Liu and Wu employed the spatial and temporal adaptive reflectance fusion model (STARFM) to downscale 1-km ETa data, a significant aspect of water budget analysis [66]. Similarly, Yasir H. Kaheil developed an algorithm combining the discrete wavelet transform (DWT) and support vector machines (SVMs) to downscale and forecast ET values, providing valuable input for water budget calculations, at a spatial resolution of 15 m [67] This resolution is comparable to that of [68, 69]. Additionally, the U.S. Geological Survey explored the potential of downscaling simplified surface energy balance (SSEBop ET)-derived ETa data from 1 km to 250 m. This process involved establishing correlations between the ET data and NDVI values from MODIS, contributing to more precise water budget assessments [70]. Moreover, researchers have consistently validated NASA's GRACE for accurately monitoring monthly variations in groundwater storage, a critical aspect of water budget analysis, in major global aquifer systems [71-73]. Notable examples include the Ogallala aquifer, Northwestern India, California's Central Valley, South America's Guarani aquifer, the Middle East, the North China Plain, and other locations [55, 74, 75], These studies employed three distinct techniques to derive estimates of groundwater storage via satellite data, enhancing the groundwater component of water budget analysis. The first technique involved assessing the water budget to verify the TWS value obtained from GRACE, an essential element of water budget calculations. The second technique entailed determining the trend in groundwater anomaly using both GRACE TWS values and satellite-derived variables, followed by a comparison with a hydrological model. The third technique involved a direct comparison of the groundwater estimates derived from GRACE with in-situ groundwater levels, contributing valuable data to refine water budget assessments. Indeed, a literature review with a focus on the Kunduz catchment area can yield valuable insights into the specific water budget components of this region. Such a review will provide a comprehensive understanding of the status of the water

budget, including the use of satellite or GLDAS data in their original or downscaled forms. It will serve as a crucial resource for uncovering essential information about the area's water resources, as well as the diverse data sources and methodologies utilized in prior research efforts.

1.2.7 A Literature Rivew on the Study Area

The Kunduz River, located in Northern Afghanistan, is a significant tributary of the Amu Darya Basin. The basin is home to numerous communities that have relied on the water resources of the Kunduz River for their livelihoods for many generations.

The Kunduz River, which derives from the northern slope of the Hindukush Mountain, traverses the expansive lowlands of Baghlan before ultimately confluence with the primary Amu Darya stream at Qala-i-Zal area. Encompassing an area of 28,024 km^2, the Kunduz watershed accounts for 4.5% of the nation's territory [76]. The study cited as [77], focusing on the Kunduz River Basin in Afghanistan, reveals a shift towards drier conditions in the region. This change is driven by a significant warming trend, with temperatures exceeding 2 °C since the 1960s, combined with a substantial precipitation decrease of over -30%. Consequently, river discharge has notably decreased. However, increased glacier melting has compensated for this reduction, primarily in the upper catchment's highland areas. In a recent study [78] conducted in 2023, titled "Water Balance Assessment in Three Northern Provinces of Afghanistan (Kunduz, Balkh & Jawzjan)," researchers focused on a specific sub-region within the Kunduz and its neighboring provinces, which constitutes approximately 3% of the total catchment area. Through an examination of observed data sourced from the Ministry of Energy and Water of Afghanistan, the study unveiled a yearly runoff of approximately 2.9 billion cubic meters (BCM) in this area. This finding provides valuable insights into the water balance dynamics of the Kunduz catchment. Table 1.1 provides a compact overview and extensive citations of critical discoveries from various global water budget investigations that harnessed remote sensing data to attain water budget closure.

Table 1.1 A summary of studies that have utilized remote sensing (RS) to estimate and test the efficiency of (WBC) closure measures.

Ref	P	ET	Q	ΔS	Region	Conclusions
[13]	TRMM CMORPH	PM	Gauge	GRACE	Mississippi river basin	The main source of persistence errors arose from the significant positive bias leading to a pronounced overestimation of remote sensing precipitation (RS P), especially during the summer season.
[15]	TRMM CMORPH PERSIANN	MODIS	Gauge	GRACE-VIC	9 major US river basins	The water budget's lack of closure was mainly due to overestimated precipitation P and underestimated evapotranspiration (ET) and changes in terrestrial water storage (ΔS).
[37]	GPCP-TRMM CMORPH PERSIANN	MON-PRI	Gauge	GRACE	Amazon basin	Using the GPCP precipitation product MON evapotranspiration (ET) yielded a highly accurate agreement between observed and estimated streamflow Q of 1 m/day
[60]	CPC-CRU-WM GPCC	SEBS-ERA-MPI-VIC	Gauge	GRACE-LSM	32 global rivers basins	Merging weights for RS products were determined from reference data error variances. These errors were then reintroduced into the wideband WB components using CKF.
[18]	TRMM	MODIS	Gauge	GRACE	3 largest Brazilian river basins	The primary reason for overestimating the Estimated Q was the overestimation of TRMM P.
[9]	TRMM	MODIS	Gauge	GRACE	Australia	Annual mean Q was below 10 mm/year, the GRACE TWSC exhibited a statistically significant decrease in comparison to the P-ET.
[48]	TRMM	MODIS	Gauge	GRACE	Upper Paraguay river basin	Negative bias in RS ET was the main source. Of non-closure errors.

1.3 Objective and Gap Filling of the Thesis

Previous research in the field of water budget assessment primarily focused on larger global basins, a preference largely driven by the limitations associated with the GRACE satellite mission. While GRACE provided precise data for these larger basins [74, 75, 79-84], its precision waned as basin size decreased, a consistent observation across various studies [18, 40, 85-115]. Concerns emerged about the applicability of GRACE data to smaller basins, particularly those below 100,000 km², where disparities of up to 130% were observed [40]. Furthermore, uncertainties lingered regarding the accuracy of GRACE's TWS estimates in basins with areas below 150,000 km² [116]. The estimation of evapotranspiration (ET) posed another challenge in water budget assessments due to its inherent lower accuracy compared to measurements of precipitation (P) and runoff (Q). Previous attempts to estimate ET using remote sensing (RS) data often relied on land surface models (LSMs) or empirical formulas, both of which introduced uncertainties. To comprehensively address these challenges, this study emphasizes the pivotal role of downscaling techniques. These techniques are considered indispensable for overcoming spatial resolution limitations in water resource management. In this research, the complexities of water budget assessment, particularly in smaller basins like the Kunduz catchment, have been thoroughly examined. The approach employed utilized Precipitation, Evapotranspiration, and Total Water Storage data from the GRACE mission as remote sensing inputs, in conjunction with GLDAS CLSM components for Precipitation, ET, and TWS. These components have been utilized, and the approach has been complemented with advanced downscaling techniques. This integration is augmented with advanced downscaling techniques. Downscaling, a pivotal process in climate research, involves the transformation of coarse-scale data into high-resolution spatial and temporal data [117]. Two primary downscaling methods exist: creating relationships between coarse-scale inputs and fine-resolution outputs using techniques like classification, regression, Markov chains, and statistical inversion [118, 119]. While these methods offer flexibility, they rely on comprehensive input and target data. Dynamical models, on the other hand, use numerical simulations to replicate the physical processes driving climate variability, demanding detailed information on relevant processes and boundary

conditions. Although computationally intensive, dynamical models provide high-resolution and accurate data [120]. The downscaling process is crucial in climate research and hydrological data [121-123].

This study deviates from prior research, which selectively applied downscaling methods to one or two components of the WB. Instead, it employs statistical approaches with spatial data inputs for all WB components, including precipitation, evapotranspiration, and total water storage layers from both remote sensing data and GLDAS layers. This comprehensive approach enables an integrated analysis of all water balance components, yielding a more holistic understanding of the water cycle's dynamics. By applying downscaling methods to all WB components, a more accurate and complete representation of the water balance is achieved, a crucial aspect for informed decision-making in water resource management. It will mark a significant advancement in the application of downscaling techniques to WB analysis within the academic context. Its uniqueness is further accentuated when considering the geographical boundaries of the Kunduz catchment, located in the northern region of Afghanistan. It distinguishes itself as the first-ever investigation employing remote sensing and GLDAS layers to study water budget components, utilizing various techniques to enhance data quality and accuracy. Indeed, this study addresses a critical gap in the existing literature and paves the way for future research in the Kunduz Catchment area. The use of remote sensing data holds promise in providing more accurate and comprehensive information on the water balance components in the Kunduz River Basin, making a significant contribution to the fields of hydrology and remote sensing research. This investigation will now proceed to address the following research questions:

1) How can various components of water budgets, including evapotranspiration, precipitation, and terrestrial water storage, be accurately estimated within the context of a river basin using remote sensing data and GLDAS CLSM data for effective water resource management and planning?
2) What methodologies can be explored to investigate and improve the accuracy of water budget estimation in a river basin, utilizing remote sensing and Earth system model data (GLDAS)?

3) How can the distribution of evapotranspiration across the entire catchment be analyzed and compared with other ET models, such as PM, HS, and others, to enhance understanding of this crucial water cycle component?
4) How effective are different remote sensing products, including CHIRPS, PERSIANN, MODIS-SSEBop ET, and GLDAS, in accurately estimating precipitation within the river basin?

This research aims to investigate methodologies for accurately estimating various components of water budgets in a river basin, utilizing remote sensing and Earth system model data. It seeks to provide valuable insights into the accuracy and reliability of remote sensing data for estimating water budgets and their components, which hold critical significance for water resource management and planning. The findings of this study will contribute to the understanding of hydrological processes and water management in the river basin, providing valuable information for policymakers to make informed decisions regarding water allocation and management.

1.4 Hypothesis

The integration of remote sensing data and downscaling techniques is expected to enhance the precision and resolution of water balance component estimations in the Kunduz catchment, which covers a smaller scale of approximately 28,024 km2, in comparison to relying solely on traditional data sources. The underlying hypothesis posits that the combined utilization of remote sensing data and GLDAS CLSM, along with downscaling methodologies, will result in improved accuracy and resolution of water balance component estimations within the river basin, surpassing what can be achieved using original data (OD) without downscaling. This hypothesis suggests that integrating remote sensing, GLDAS, and spatial downscaling procedures will offer a more comprehensive and detailed insight into the water balance components, a crucial aspect for efficient water resource management.

To evaluate this hypothesis, water balance components derived from remote sensing and the GLDAS CLSM model, with downscaling techniques, will be

compared to the original remote sensing and original GLDAS CLSM data, which lack spatial downscaling. Additionally, a comparison will be made with observed data, both downscaled and original, to thoroughly assess the effectiveness of the downscaling approach. Through statistical analyses, it will be ascertained whether the downscaled approach provides a more precise and detailed depiction of the water budget components within the river basin.

2
STUDY AREA

2.1 Study Area

The Kunduz Catchment, situated in the northern region of the Hindukush Mountain and stretching through the broad lowlands of Baghlan, eventually merges with the main Amu Darya River. This catchment holds significant importance within the Amu River Basin, as illustrated in Figure 2.1 (d) and (c). Covering an area of 28,024 km², which accounts for approximately 4.5% of the nation's total landmass, the Kunduz Catchment concentrates around 1.9% of the country's population. Its topography varies, with elevations reaching up to 4000 meters above sea level in the upper southern areas, gradually decreasing to 300-400 meters above sea level in the lowlands of Baghlan [77]. The geological composition of the Kunduz catchment mainly comprises Paleogene and Neogene sediments, overlaid by a substantial layer of Loess deposits, ranging from 30 meters to over 100 meters in thickness at its central region. Within the basin's floodplain, alluvial deposits, including gravel, sands, and silt, are prevalent. Closer to the mountainous regions, coarser deposits like gravel, pebbles, cobbles, and various detritus materials are common [124]. The higher altitude regions of the basin are predominantly employed for rain-fed agriculture, though deforestation is a recurring issue in these areas [77]. The fertile medium-drained soils in the flood plains offer excellent agricultural land, serving as the primary economic hub of the basin The Kunduz Catchment, which encompasses 27% of the entire basin [125], is supplied by multiple rivers, including the central Hindu Kush, Khanjan, Andarab, Bamyan, and Payandeh rivers, as depicted in Figure 2.1 (d), Figure 2.3, and Table 2.1, which provide information on the locations of gauge stations within the Kunduz catchment. These rivers converge to form the Kunduz River, ultimately flowing into the Aral Sea through the Amu River (Figure 2.1.(c)). This catchment plays a pivotal role in the national economy due to its significant potential for agriculture and energy production. Additionally, it supports the biodiversity of a national park situated in the Saighan and Kuhmard area. However, due to limited hydro-

meteorological data and the absence of lysimeters for comprehensive measurement of water balance components throughout the river basin, further research is essential to enhance the understanding of the hydrological processes in the region.

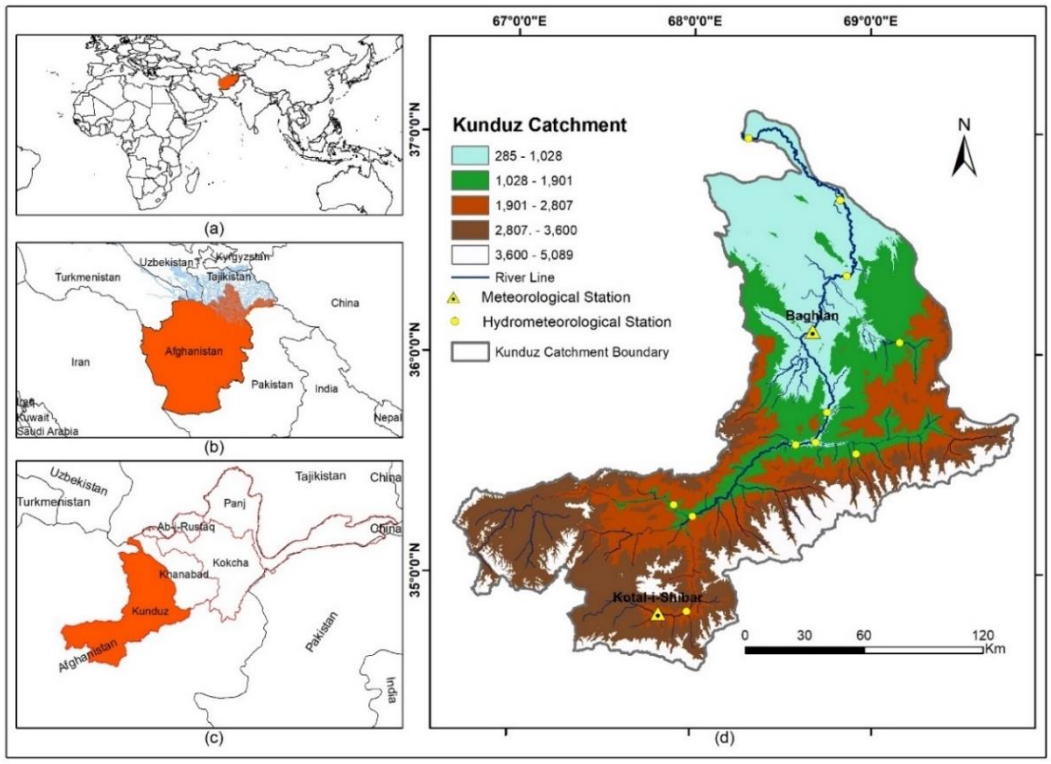

Figure 2.1 a) World map, b) Afghanistan, c) Amu River Basin, d) Kunduz Catchment with elevation and hydro-meteorological stations

The Kunduz Catchment encompasses seven distinct land cover classes, as depicted in Figure 2.2. These classes are categorized based on their coverage area, with rangeland being the most extensive, covering 57.9% of the region. It is followed by bare soil at 21.5%, agricultural areas at 14.3%, forest at 2.2%, water bodies at 1.1%, snow cover at 2.3%, and urban areas at 0.7%. The predominant land cover classes in the Kunduz Catchment hold significant implications for agriculture and livestock. This region is known for cultivating valuable crops such as wheat, rice, melons, and vineyards [126, 127]. Given the catchment's reliance on agricultural activities, the conservation and management of water resources within the catchment are of utmost importance for sustained economic development and the livelihoods of local communities. The hydrological characteristics of the Kunduz Catchment are primarily shaped by the towering peaks of the Hindukush Mountains. Upstream areas feature narrow and deep-water channels with year-

round flow. Runoff patterns are dominated by snowmelt, resulting in peak discharges typically occurring between April and June [77].

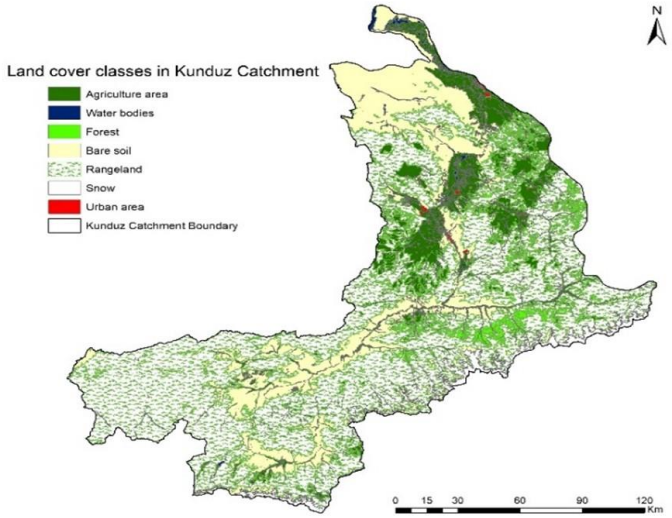

Figure 2.2 Kunduz Catchment Land Cover Classes

Notably, the small glaciered area in the upstream catchment, particularly at the Doab station Table 2.1, significantly impacts the flow regime. The region experiences precipitation in the form of rain, drizzle, snowfall, and hail, with higher intensity during winter months [128]. The water originating from the river plays a crucial role in supporting the intensive irrigated agriculture that serves as the cornerstone of the region's economy. Multiple river gauging stations are strategically positioned within the Catchment, as depicted in Figure 2.1 (d) and Figure 2.2.

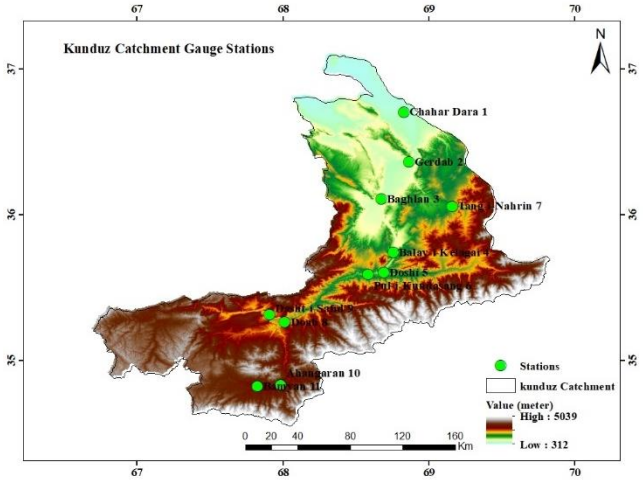

Figure 2.3 Kunduz Catchment Gauge Stations Location

Table 2.1 Location of Gauge Stations in Kunduz Catchment.

ST#	Station	Lat	Lon	Elev (meter)
1	Chahar Dara	36.70	68.83	376
2	Gerdab	36.36	68.86	474
3	Baghlan	36.11	68.67	538
4	Balay-i-Kelagai	35.74	68.76	746
5	Doshi	35.60	68.69	841
6	Pul-i-Kundasang	35.59	68.58	887
7	Tang-i-Nahrin	36.06	69.16	1177
8	Doab	35.26	68.01	1448
9	Dasht-i-Safid	35.32	67.91	1601
10	Ahangaran	34.83	67.98	2368
11	Bamyan	34.82	67.83	2501

2.2 Databases

2.2.1 Precipitation, Air Temperature, Runoff and Evapotranspiration at Gage Stations

The data used in this study was collected from gauge stations operated by the Afghanistan Ministry of Energy and Water, as detailed in Table 2.1 and Figures 2.3. It comprises mean monthly measurements of precipitation and maximum temperature, as well as annual runoff in million cubic meters for Figures 2.4, 2.5, and 2.6. These observations were used as a basis for comparing remote sensing-derived water balance component estimations. The data primarily covers the period from 2009 to 2019, and any missing values were filled using a simple averaging technique, mainly for air temperature values. However, it's important to note that the Kunduz Catchment in Afghanistan lacks sufficient observed data on evapotranspiration. None of the stations listed in Table 2.1 collect ET values, which are crucial for understanding water dynamics in the region. To address this data gap, remote sensing and GLDAS datasets are employed to estimate evapotranspiration and enhance water budget study.

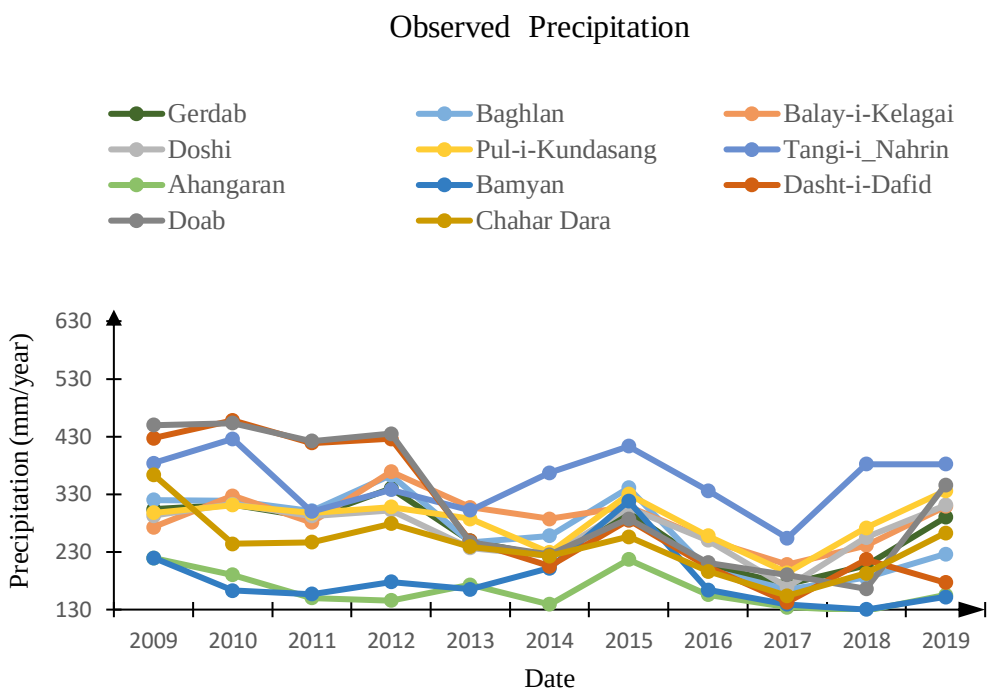

Figure 2.4 Temporal Variations of Observed Precipitation in the Kunduz Catchment from 2009 to 2019

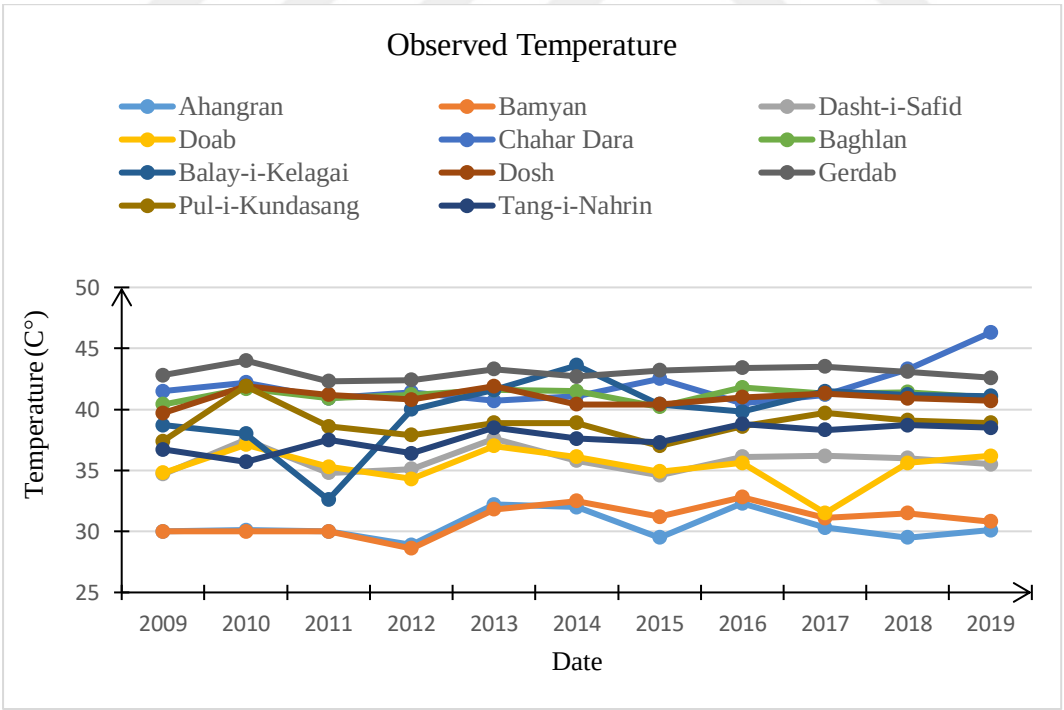

Figure 2.5 Temporal Variations of Observed Temperature in the Kunduz Catchment from 2009 to 2019

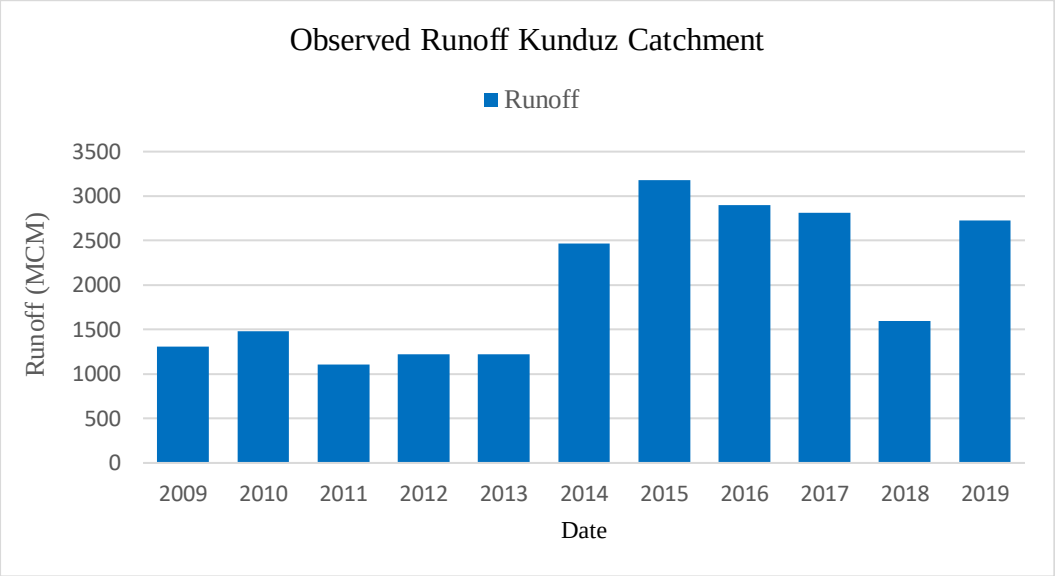

Figure 2.6 Temporal Variations of Observed Kunduz catchment Runoff from 2009 to 2019

2.2.2 Remote Sensing and GLDAS based Precipitation

Two Remote Sensing (RS)-based precipitation products, namely Precipitation Estimation from Remotely Sensed Information using Artificial Neural Networks (PERSIANN) [129] and Climate Hazards group InfraRed Precipitation with Station data (CHIRPS) [26], were employed in the study. Data from various sources are illustrated in Figure 2.7, while comprehensive descriptions of the dataset properties, along with download links, are provided in Table 2.2. Alongside satellite-based precipitation data, the GLDAS 2.1 CLSM model's [130], precipitation layer was incorporated to calculate a component of the water budget. This calculation was performed using monthly time scale data and averaged accumulated yearly precipitation values. GLDAS-2.1 CLSM model incorporates observational and model data from NOAA/GDAS, GPCP, and AGRMET [131, 132]. GLDAS-2.1 CLSM generates monthly outputs in three categories: water balance (subsurface runoff, evapotranspiration, soil moisture), energy balance (latent and sensible heat flux, ground heat flux), and forcing parameters temperature, wind speed, short- and longwave radiation [16]. The CLSM model incorporates groundwater by relating the distribution of water table depth to catchment topography statistics [133]. It utilizes three non-traditional bulk moisture variables: catchment deficit, surface layer excess, and root zone excess, to represent the catchment's moisture conditions,

encompassing both equilibrium conditions associated with water table distribution and non-equilibrium conditions near the surface [133], Outputs of the GLDAS-2.1 CLSM model are available at spatial resolutions of 0.25° and 1°, respectively (Table 2.2). For evaluation of water budget estimation, satellite-based and GLDAS Figure 2.7 hydrological datasets were acquired from various sources and compared with the model outputs and in-situ observations.

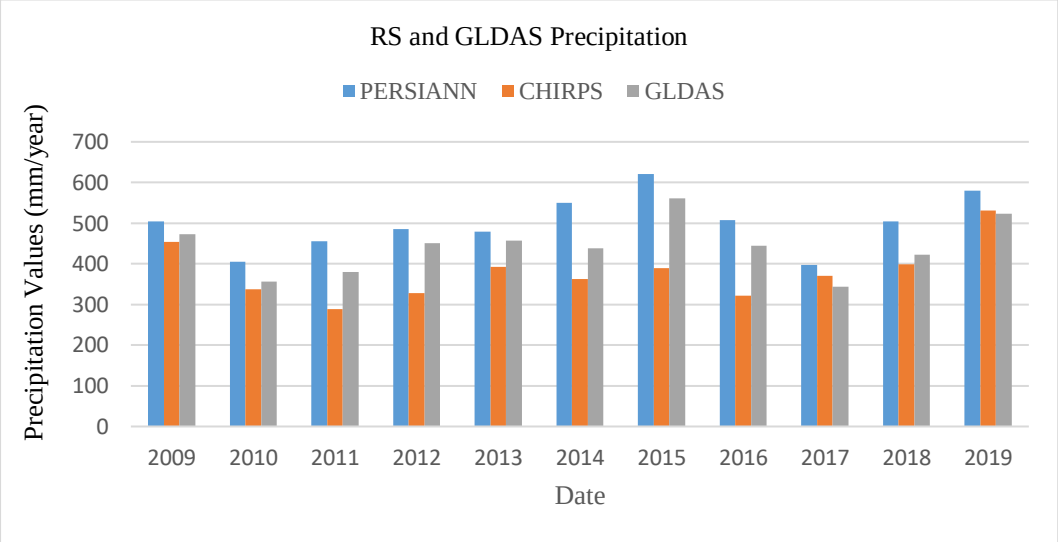

Figure 2.7 RS-based and GLDAS Precipitation, PERSIANN, CHIRPS, GLDAS in Kunduz Catchment from 2009 to 2019

2.2.3 Remote Sensing and GLDAS based Evapotranspiration

Evapotranspiration (ET) was assessed using two remote sensing-based products: Landsat ET-based and annual MODIS SSEBop ET values (Figure 2.8). SSEBop ET, a remote sensing-based method for operational ET estimation, effectively utilizes satellite thermal infrared data from sensors such as MODIS to calculate ET through an energy balance approach. It finds extensive application in agriculture, where it is employed for monitoring crop water use, optimizing irrigation, and assessing drought conditions. Its operational simplicity, including simplifications and assumptions, facilitates practical large-scale applications while providing fine spatial and temporal resolution data. SSEBop ET plays a pivotal role in water resource management, particularly in data-scarce regions, contributing to an enhanced understanding of water balance dynamics. Ground-based measurements are often used to validate the results for specific applications [134], a critical aspect

that is lacking in the Kunduz basin [134]. In addition, the GLDAS CLSM ET dataset (Figure 2.9), along with remote sensing data, were employed to estimate the water budget of the Kunduz Catchment for the water years 2009 and 2019. ET patterns are estimated by GLDAS CLSM, which simulates evaporation from soil and water surfaces and transpiration from vegetation on a global scale. This information is crucial for various applications, including water resource management, water budget studies, agriculture, and climate research. ET estimates from GLDAS CLSM contribute to a comprehensive understanding of Earth's terrestrial water balance and its implications for environmental and societal processes.

2.2.4 Runoff from Rs-Based and GLDAS CLSM Datasets

In accordance with prior sections, it should be noted that remote sensing, while valuable for various hydrological parameters, is unable to directly estimate runoff. Instead, the derivation of runoff involves inferring it as a residual component within the broader water budget framework, as detailed in references [13-15]. Simultaneously, the GLDAS CLSM emerges as an essential resource in this context, notably for surface runoff analysis. As demonstrated in Figure 2.10, GLDAS furnishes yearly mean surface runoff data, and Figure 2.11 presents the mean surface runoff data for the entire study period within the Kunduz catchment. Indeed, the availability of GLDAS-derived surface runoff data is particularly invaluable in regions where runoff data is scarce, facilitating a comprehensive examination of water budget components.

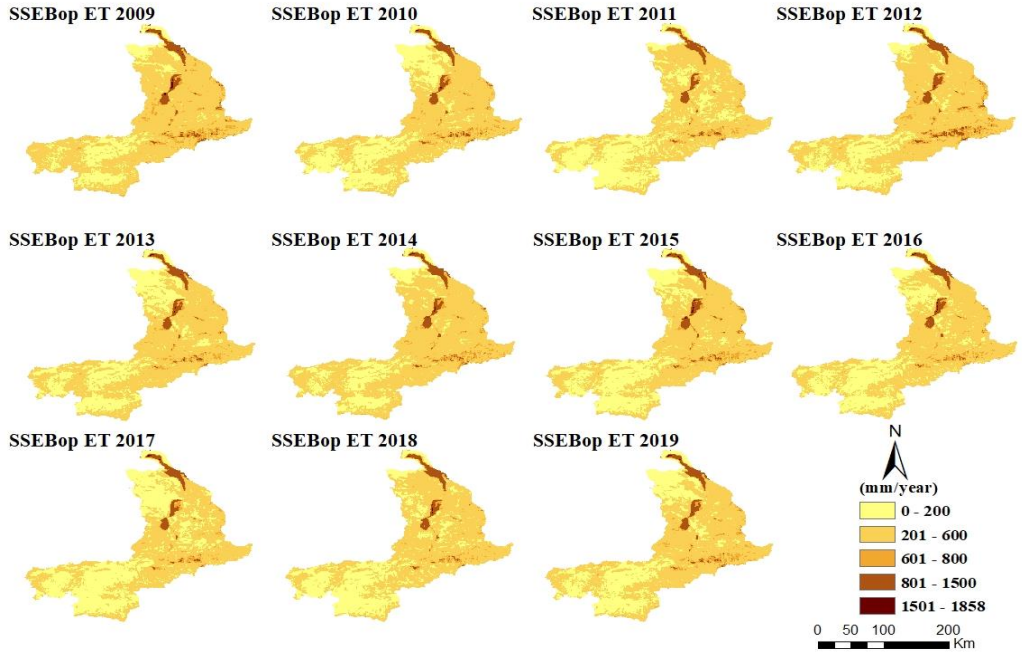

Figure 2.8 Temporal Variations of MODIS SSEBop ET, in the Kunduz Catchment from 2009 to 2019

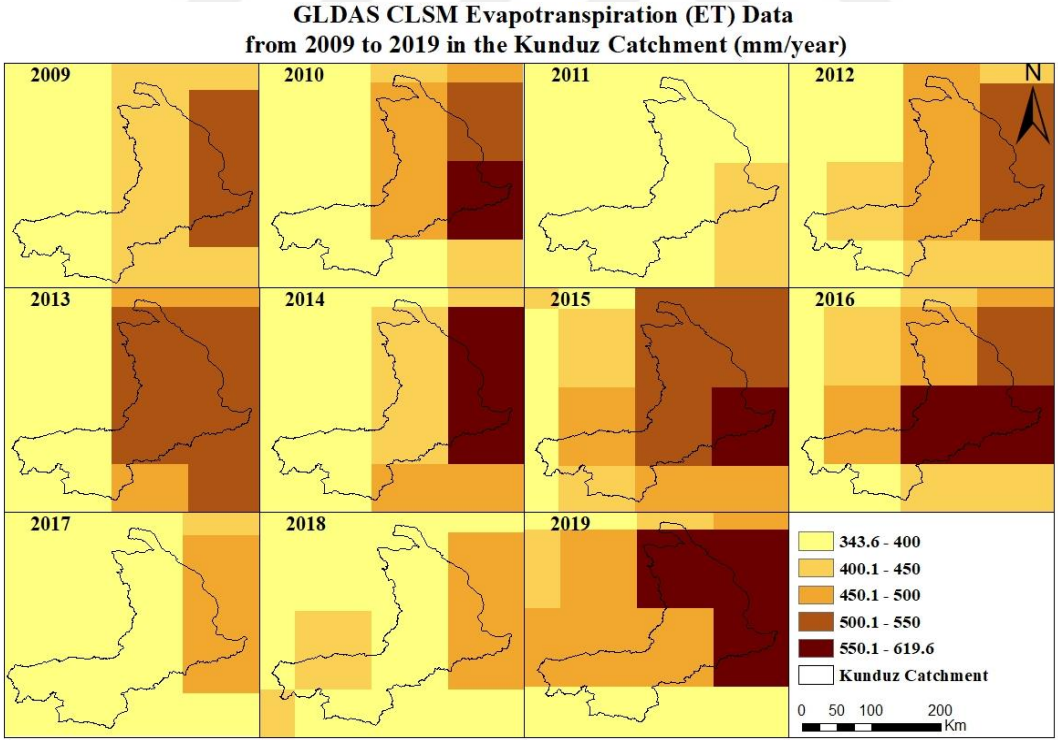

Figure 2.9 Temporal Variations of GLDAS ET, in the Kunduz Catchment from 2009 to 2019

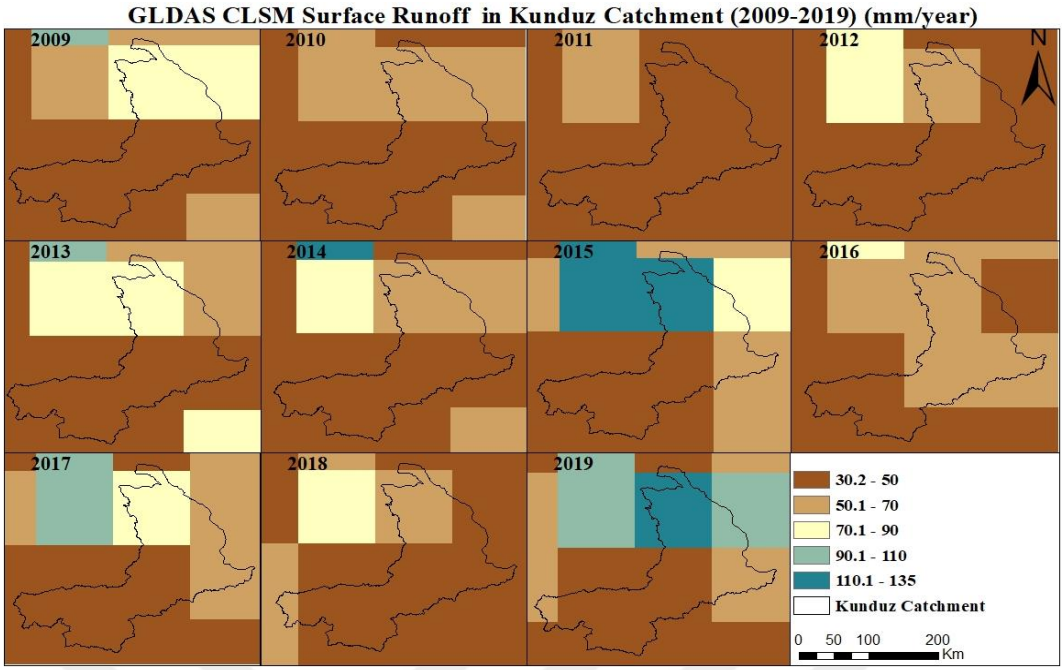

Figure 210 Temporal Variations of surface runoff from GLDAS CLSM (mm/year) in Kunduz Catchment from 2009 to 2019

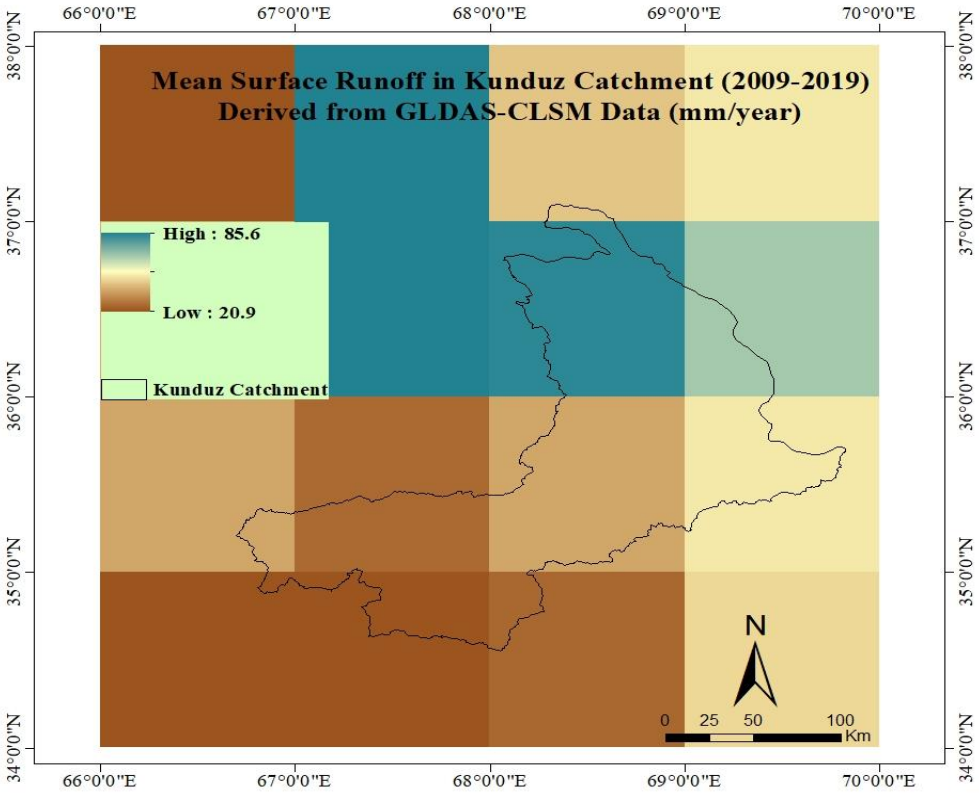

Figure 2.11 Temporal Variations of surface runoff from GLDAS-CLSM (mm/year) in Kunduz Catchment from 2009 to 2019

2.2.5 Rs-Based and GLDAS CLSM Terrestrial Water Storage (TWS)

The mean annual values from the Gravity Recovery and Climate Experiment (GRACE) dataset, as depicted in Figure 2.12 and obtained from the Jet Propulsion Laboratory (JPL), have been employed to derive estimations of changes in terrestrial water storage (TWSC). The GRACE mission deploys two satellites to measure fluctuations in the Earth's gravitational field, enabling the inference of alterations in the planet's water resources. The GRACE dataset falls under the category of assimilation data, amalgamating various data sources, including remote sensing data, ground-based measurements, and modeling outcomes. This amalgamation offers a comprehensive insight into the transformations occurring in terrestrial water storage. Consequently, the utilization of GRACE data is pivotal in the calculation of TWSC solutions and serves as a valuable instrument for monitoring shifts in the Earth's water resources. Simultaneously, this study also incorporated the GLDAS CLSM TWS layer, as illustrated in Figure 2.13 with an annual mean for study period. In the context of hydrology and Earth science, the TWS layer represents the sum of all water stored within a specific area or catchment, including groundwater, soil moisture, snow, and surface water bodies. The GLDAS CLSM Figure 2.13, TWS layer is a product generated by the GLDAS using the Catchment Land Surface Model, which assimilates various sources of data like satellite observations and ground measurements to estimate the water storage dynamics of a specific region over time. This TWS layer provides valuable insights into water availability and distribution, aiding in water resource management, hydrological modeling, and understanding environmental changes. In this study, the utilization of GRACE TWS data extended from 2009 to 2017. Table 2.3 presents a comprehensive overview of data availability, specifically highlighting the months with missing data, which are indicated in red. The decision to discontinue the analysis beyond 2017 was prompted by a substantial data gap observed between 2017 and 2019. This discontinuation was determined based on the recognition of inadequate data quality during that period, rendering meaningful analysis unfeasible. It is noteworthy that GRACE data became accessible with the introduction of GRACE FO data starting from June 2018, as highlighted in green within Table 2.3.

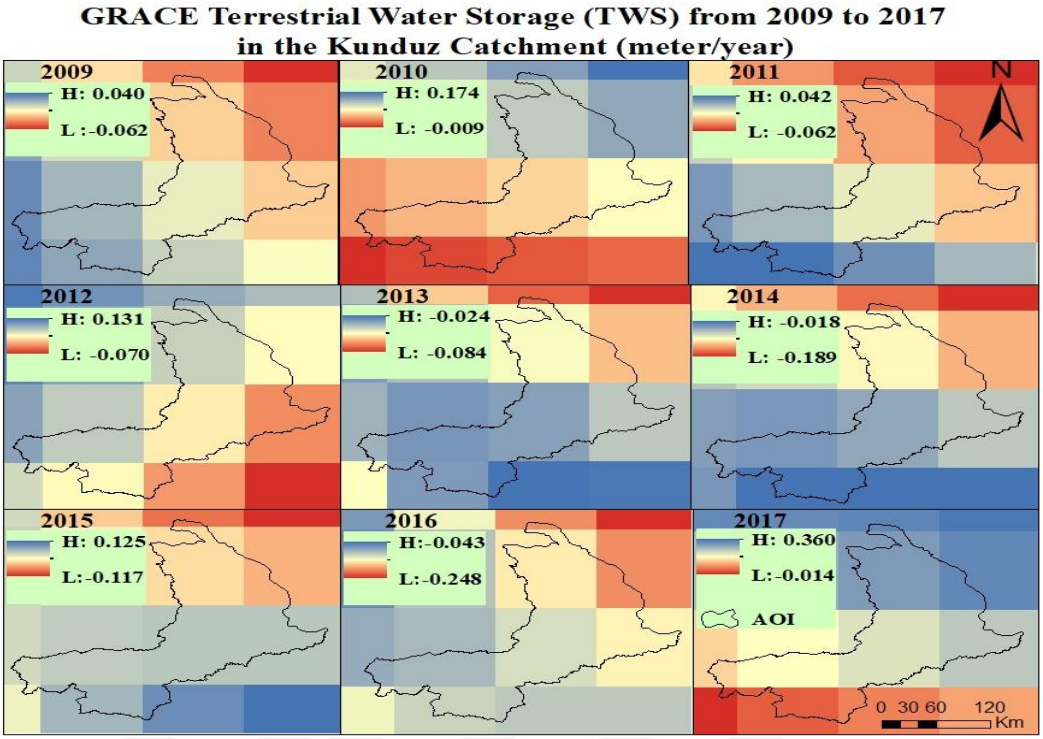

Figure 2.12 Temporal Variations of GRACE JPL Terrestrial Water Storage in the Kunduz Catchment from 2009 to 2017 (mm/year)

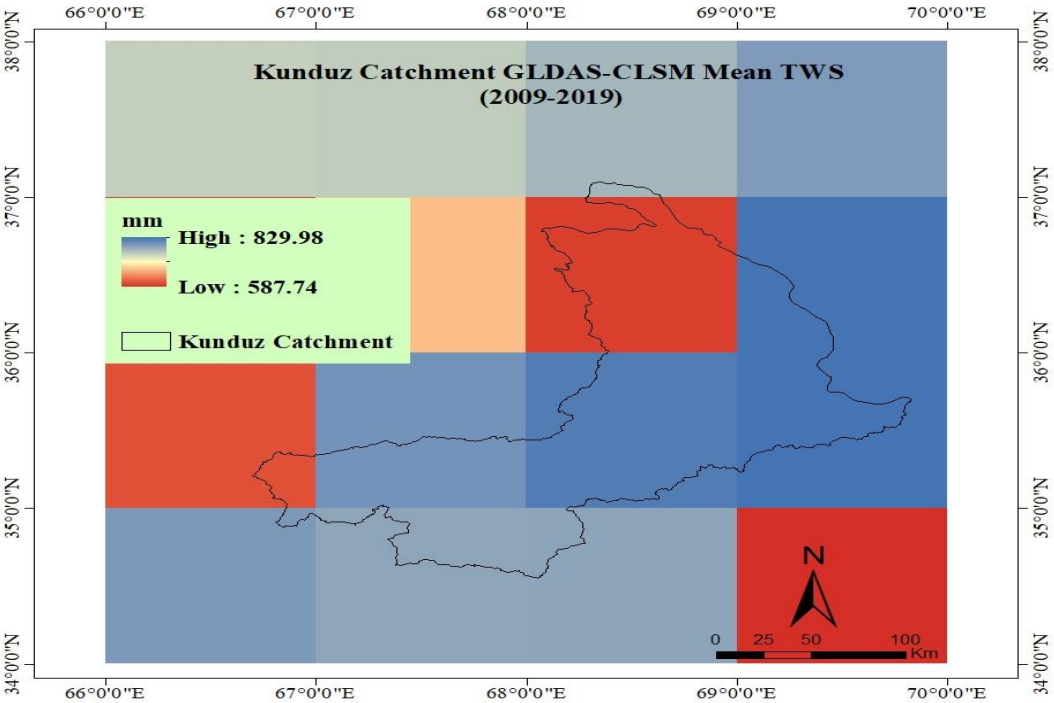

Figure 2.13 GLDAS-CLSM Terrestrial Water Storage in the Kunduz Catchment from 2009 to 2019 (mm/year)

To fill the months with no data, the meaning of the adjacent months and year was utilized. This data gap-filling approach is commonly employed in hydrological and remote sensing studies to maintain dataset continuity and reduce the impact of missing values on analysis outcomes.

2.2.6 RS, land surface model (LSM) products

Along with landcover Figure 2.2, in this study, remote sensing layers played a crucial role, including the utilization of Normalized Difference Vegetation Index (NDVI) values (Figure 2.14) and Land Surface Temperature (LST) data (Figure 2.15). Furthermore, for the delineation of the basin and the mapping of its stream network, a Digital Elevation Model (DEM) with a grid resolution of 1 arc-second (approximately 30 meters), sourced from the Shuttle Radar Topography Mission (SRTM) as depicted in Figure 2.3, was employed.

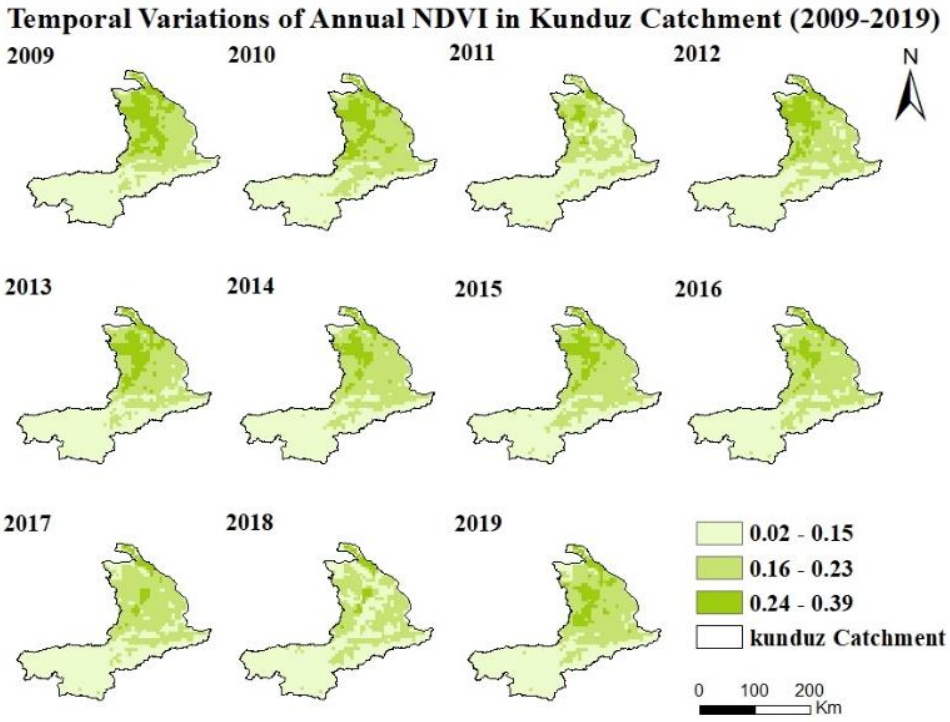

Figure 2.14 Temporal Variations of Normalized Difference Vegetation Index (NDVI) in the Kunduz Catchment from 2008 to 2019

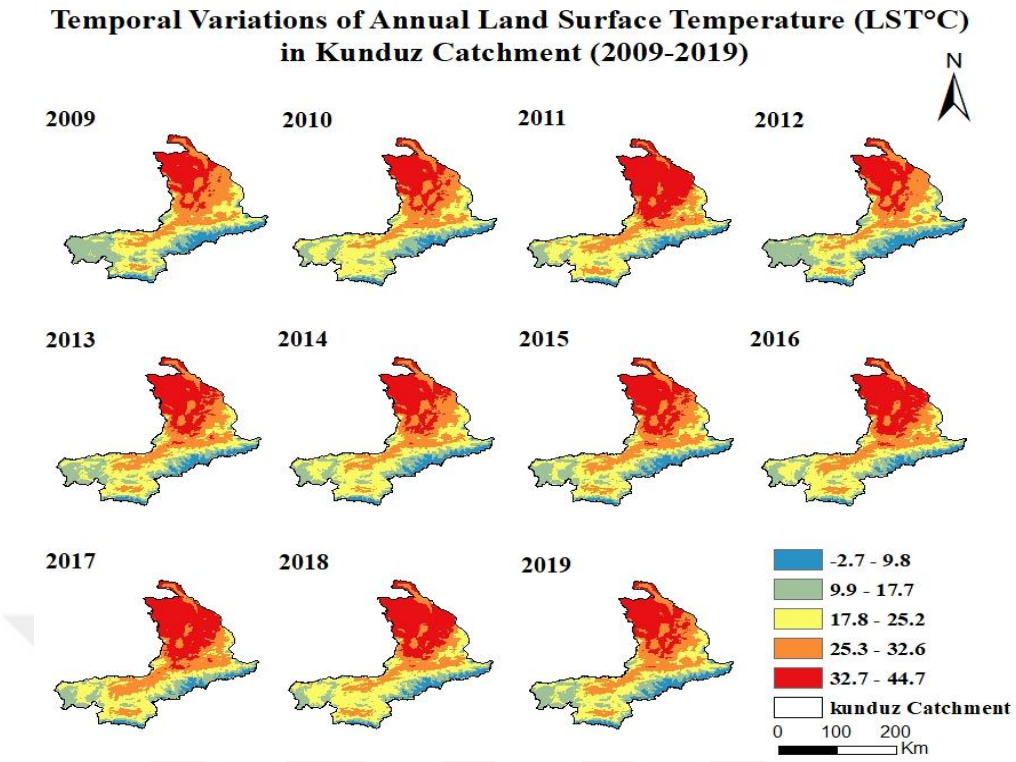

Figure 2.15 Temporal Variations of Land Surface Temperature in the Kunduz Catchment from 2008 to 2019

Table 2.2 Main Datasets Analyzed for Hydrological Variables in Kunduz Catchment.

Variable	Products	Spatial Res	Temporal Res	Source/Website	Time
PR	PERSIANN	0.25°	Monthly	chrsdata.eng.uci.edu/	2009-2019
	CHIRPS V2.0	0.05°	Monthly	chc.ucsb.edu/data/chirps	
	GLDAS	0.1°	Monthly	daac.gsfc.nasa.gov	
ET	GLDAS	1°	Monthly	daac.gsfc.nasa.gov	2009-2019
	SSEBop	1Km	Monthly	climateengine.org	
TWS	GRACE	1°	Monthly	grace.jpl.nasa.gov	2009-2019
	GLDAS	0.1°	Monthly	daac.gsfc.nasa.gov	

Table 2.3 GRACE JPL Data Availability and Missing Months for Kunduz Catchment 2009 to 2019.

Level-3 (JPL)	09	010	011	012	013	014	015	016	017	018	019
Jan	1	1	0	1	1	1	1	1	1	0	1
Feb	1	1	1	1	1	0	1	1	NAN	0	1
Mar	1	1	1	1	0	1	1	1	1	0	1
Apr	1	1	1	1	1	1	1	0	1	0	1
May	1	1	1	0	1	1	1	1	1	0	1
Jun	1	1	0	1	1	1	0	1	1	1	1
Jul	1	1	1	1	1	0	1	1	0	1	1
Aug	1	1	1	1	0	1	1	1	0	0	1
Sep	1	1	1	1	0	1	1	0	0	0	1
Oct	1	1	1	0	1	1	0	0	0	1	1
Nov	1	1	1	1	1	1	0	1	0	1	1
Dec	1	1	1	1	1	0	1	1	0	1	1

Note: A value of 0 (illustrated in red) indicates the absence of data. A value of 1 (illustrated in white) indicates the presence of data. Green represents the GRACE-FO data.

3
METHODOLOGY

3.1 A Holistic Methodology for Water Budget Analysis

To achieve the study's objective, a series of sequential steps were undertaken. Initially, the basin and its stream network were delineated using DEM data (Figure 2.3). This process was executed within the ArcGIS software environment and other spatial software tools. Subsequently, the hydrological raster data, including Precipitation, Evapotranspiration, TWS, and Runoff, underwent image pre-processing to prepare them for analysis. These preparatory steps involved applying scale factors to specific layers, with a particular focus on the GLDAS layers, such as Precipitation, Evapotranspiration, and Surface Runoff.

Following the scaling adjustments, the units of various variables were converted to mm/month. Monthly data were then aggregated to create yearly datasets. Changes in TWS were calculated for GRACE and GLDAS TWS layers by subtracting the TWS values of adjacent months (e.g., subtracting the TWS value of February from that of December to produce the changes for January). This method [135], was employed to determine the changes in TWS for the month of January. To ensure uniformity across all layers and achieve a consistent spatial scale of 1 km, a complex process involving downscaling methods, specifically Geographically Weighted Regression (GWR), was employed. Residuals were obtained from corresponding layers, including P-ET-TWSC, sourced from remote sensing and GLDAS datasets, to estimate residual as inferred runoff, as detailed in previous studies [13, 15]. This estimation was conducted for both the original hydrological layers and the downscaled layers on an annual basis. Subsequently, the ratio between the original annual data and the monthly original data was calculated. Kriging interpolation was then applied to resample this ratio data to a 1km resolution, followed by multiplication with the downscaled layer to derive monthly downscaled data. After the pre-processing stage, basin-averaged values for each variable were extracted on an annual and a monthly basis using Zonal Statistics in GIS platform and converted it to volumetric hydrological units. To calculate the

basin's water budget, monthly data were cumulatively aggregated using cell statistics as mean values, and calculations were performed based on the general water balance equation, as cited in previous studies [15, 34, 43]. The results of the zonal statistical analysis underwent a final step, where the yearly accumulated components were multiplied by the basin's area to derive total annual quantities, after statistical operations applied to find out the uncertainty level for both downscaled and original layers and the final product representing the water budget for the Kunduz catchment, as illustrated in Figure 3.1.

Regarding validation, the studies can be validated through a comparison of the results within situ measurements, remotely sensed data, and model outputs. All the data employed in this study have undergone comprehensive validation, encompassing in situ studies and various other methods.

Independent evaluations have been conducted by numerous researchers on remotely sensed precipitation datasets, such as PERSIANN and CHIRPS [15, 105, 136]. Similarly, assessments have been performed on remotely sensed ET datasets like MODIS SSEBop ET [9, 15, 18], and global evaluations of TWS analysis using GRACE have been reported by [9, 13, 15, 105], . Additionally, GLDAS outputs and the forcing data have been validated in various studies[19, 137, 138].

The remote sensing precipitation datasets, PERSIANN and CHIRPS, along with the GLDAS precipitation layer, were compared to observed precipitation data from gauge stations. Correlation analysis was conducted between these datasets and the observed precipitation data, based on the pixel locations of gauge stations. Meanwhile, both ET layers MODIS SSEBop and GLDAS ET data were plotted against the downscaled CHIRPS precipitation layer to see the ET variations over the months, given the lack of ET values for the Kunduz catchment. To enhance comprehension, an analysis of the precipitation layer was performed to examine rainfall dynamics across different months and seasons. Additionally, thus providing insights into the basin's flow patterns, TWS layer used to generate TWSC, and residual were used to compare observed runoff with remote sensing and GLDAS outcome. For a better explanation of the methods involved each of water budget component are individually explained to provide more detailed information.

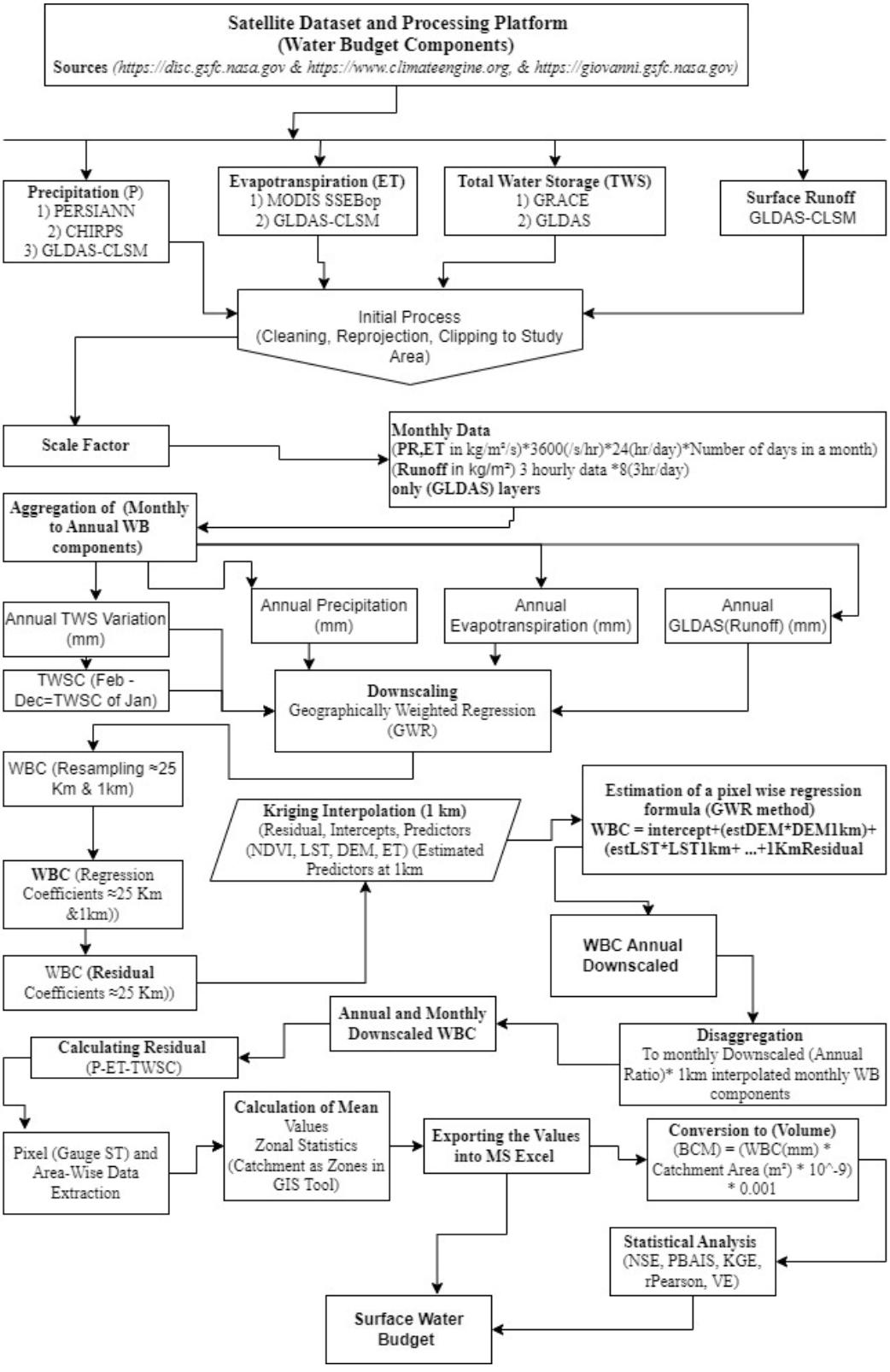

Figure 3.1 Flowchart, explaining the sequential steps in the calculation of the Water Budget for the Kunduz Catchment

3.2 Estimation of Precipitation

In this study, the potential of two remote sensing-derived precipitation datasets, namely PERSIANN-CDR and CHIRPS data, along with GLDAS precipitation data as detailed in Table 2.2, was utilized. These datasets were made use of due to their distinct spatial resolutions and coverage extents, which provide a comprehensive view of precipitation patterns. The PERSIANN data can be accessed from the following link: https://climatedataguide.ucar.edu/climate-data/persiann-cdr-precipitation-estimation-. Similarly, the CHIRPS data is available for download at https://www.chc.ucsb.edu/data/chirps. The data processing approach encompassed the downloading of these datasets and subsequent clipping to match the study area. These curated datasets were then subjected to further processing, ultimately enhancing the understanding of precipitation dynamics. The diverse spatial resolutions and coverage areas inherent in these datasets significantly contribute to the advancement of insights into precipitation patterns.

3.3 Estimation of Evapotranspiration (ET) using Various Approaches

3.3.1 Estimation of ET Rates using Local Meteorological Station Data

ET values calculated using local meteorological data and the SEBAL algorithm, combined with Landsat 8 data (refer to Figure 3.2 for a detailed depiction of the process). The intention was to demonstrate the capability of satellite and remote sensing technologies in supplying higher spatial resolution data for a crucial water budget component, applicable not only at specific points but also across entire catchment areas. In this regard the study focused on the calculation of daily ET rates using data gathered from local meteorological stations. Six widely recognized methods, including Penman-Monteith (PM), Hargreaves-Samani (HS), Priestley-Taylor (PT), Lin, Makkink (Mak), and Abtew (Abt), were applied, utilizing input parameters measured at local meteorological stations. These parameters encompassed air temperature (T), maximum temperature (Tmax), minimum temperature (Tmin), average temperature (Tavg), relative humidity (RH), maximum relative humidity (RHmax), minimum relative humidity (RHmin), and

wind speed. The Penman-Monteith (PM) equation, known for its standardized usage in estimating reference and daily evapotranspiration rates, was employed. This equation utilized local meteorological data collected from meteorological stations. (Figure 2.3 and Table 2.1), including temperature, wind speed, relative humidity, and solar radiation, to estimate the total evaporation and transpiration rates [139]. The PM equation for calculating reference ET is given Equation (3.1).

$$ET_{PM} = 0.408(R_n - G) + \frac{\gamma \frac{900}{T+273} u2(e_s - e_a)}{\Delta + \gamma(1 + 0.34u2)} \quad (3.1)$$

where; ET_{PM} is ET values calculated using PM method (*mm/day*), *Rn* is the net radiation (*MJ/m²/day*), G is the soil heat flux density (*MJ/m²/day*), this parameter for the daily calculation was considered as null (zero), γ is the psychometric constant (*kPa/°C*), T is the mean of the temperature (°*C*), *u2* is wind speed at local station which considered as 2m height (*m/s*), e_s is the vapor pressure of the air saturation (*kPa*), e_a is the actual vapor pressure (*kPa*) and Δ is the slope of the saturation vapor pressure (*kPa/ °C*).

Another method proposed by Hargreaves-Saman [140] is given in Equation (3.2).

$$ET_{HS} = 0.0023 * R_a * (T_{max} - T_{min})^{0.5} * (T + 17.8) \quad (3.2)$$

where R_a is the extraterrestrial solar radiation (*MJ/m²/day*), T_{max} and T_{min} are the maximum and minimum temperature (°C), and *T* is the average air temperature (°C).

The third ET calculation method is given by Priestley-Taylor (PT), [141] is given in Equation (3.3).

$$ET_{PT} = \alpha * \frac{\Delta}{\Delta + \gamma} * \frac{Rn - G}{\lambda} \quad (3.3)$$

where, α is the constant for calibration and it is equal to α=1.26. λ is the latent heat of vaporization (MJ/kg) and in this study it's value used as 2.45 [141].

Another method developed by Lin [142], with considering the air and dew point temperature is given in Equation (3.4).

$$ET_{Lin} = 500 * \frac{\frac{T + 0.006 * A}{100 - \varphi} + 15 * (T - Td)}{80 - T} \quad (3.4)$$

where, A is the local station elevation (m), φ is the latitude of the local station, and Td is dew point temperature (°C).

Makkink developed many equations and in this study Equation (2.5) is used to estimate daily ET [143] is given in Equation (3.5).

$$ET_{Mak} = 0.61 * \frac{\Delta}{\Delta + \gamma} * R_s - 0.12 \quad (3.5)$$

where, R_s is solar radiation (MJ/m^2/day), which relates the shortwave radiation to both extraterrestrial radiation and daily sunshine duration.

The last method developed by Abtew [144], uses the solar radiation to calculate ET as Equation (3.6).

$$ET_{ABT} = K * \frac{Rs}{\lambda} \quad (3.6)$$

where, K is dimensionless coefficient with a value of 0.53.

The ET calculation method remains valuable, even in cases where satellite data or analysis platforms may not be applicable, as it allows for point-wise ET calculation. The flowchart as Figure 3.2 presented here offers a comprehensive visualization of the sequential steps employed in estimating evapotranspiration through the utilization of Landsat data and meteorological station information.

3.3.2 SEBAL ET Calculation Method

The six standard ET calculation methods discussed above can provide point-based evapotranspiration values, which are valuable for water budget estimation for comparing remote sensing result. However, they do not suffice when it comes to understanding the spatial variation of evapotranspiration across an entire basin. In this study, the SEBAL method was employed to showcase the potential of higher-resolution remote sensing satellite data and the feasibility of calculating ET. This was undertaken to demonstrate the capacity of remote sensing in data-scarce regions.

SEBAL, which stands for Surface Energy Balance Algorithm for Land, uses remote sensing data and is based on an energy balance model with a concept of two mutual anchor pixels, one cold and one hot, in an iterative semi-empirical procedure. It is one of the most promising approaches currently available to estimate evapotranspiration. SEBAL, which is explained in Figure 3.2, is designed to calculate most of the energy balance components at both local and regional scales with minimal ground data as shown in Table 4.23. Further information about SEBAL can be found in the work of [145]. SEBAL computes net radiation (Rn), soil heat flux (G), and sensible heat flux (H) for every pixel as a residual (r) of the energy balance equation for the entire catchment, as given in Equation (3.7).

$$\lambda ET = Rn - G - H \tag{3.7}$$

Where, λET is the latent heat flux in W/m^2; Rn – the net radiation in W/m^2; G – the soil heat flux in W/m^2, and H – the sensible heat flux to the air in W/m^2.

Net Radiation (Rn) is the actual radiant energy available and is computed from the balance of short and longwave radiation. It can be achieved by subtracting all outgoing radiant from all incoming radiant [145].

$$Rn = (1 - aS)\, Rs\downarrow - RL\uparrow - (1 - \varepsilon 0)\, RL\downarrow \tag{3.8}$$

Where, aS is the surface albedo; $Rs\downarrow$ – the shortwave energy coming downward.

$RL\downarrow$ – the energy which is coming downward; $RL\uparrow$ – the energy, which is going upward, and $\varepsilon 0$ – the surface thermal emissivity in the broad thermal spectrum.

Soil heat flux (G) is the amount of heat storage into the soil and vegetation, which can be determined by the thermal conductivity of the soil and temperature gradient of topsoil. Two studies explained the derivation of soil heat using multiple functions such as surface albedo, surface temperature, and normalized difference vegetation index (NDVI) [145, 146]. In this study daily evapotranspiration is adopted G as an empirical fraction of the net radiation using NDVI to compute G given in Equation (3.9).

$$G/Rn = Ts/(aS)\,(0.0038\, aS + 0.0047\, aS2)\,(1 - 0.98\, NDVI4) \tag{3.9}$$

where *Ts* is the surface temperature[145] in °C, the values of 0.5 for snow and water, 0.1 for agriculture area and 0.32 for bare land was employed.

NDVI is a ration of the differences in the reflectivity of near infrared and red bands7 to their sum and expressed as Equation (3.10).

$$NDVI = (NIR - RED)\ (NIR + RED) \tag{3.10}$$

where, NIR and RED correspond to Band 5 (near infrared) and Band 4 in Landsat-8 OLI/TIRS, respectively. The sensible heat flux (H) is the rate of heat loss, due to the differences in temperature of two heights.

$$H = \rho air\ Cp\ dT/rah \tag{3.11}$$

Where, *H* is Sensible Heat Flux; ρair – the air density in kg/m3; *Cp* – the air specific heat in 1004 J/kg/K; *dT* is the difference between the air temperature and the aerodynamic temperature near the surface in Kelvin and *rah* is aerodynamic resistance to heat transport in m/s. Due to the existence of two unknown variables (a and b coefficients) calculating *dT* is complicated. So, two anchor pixels must be determined to solve this problem with an iterative trial and error method. Therefore, the *dT* can be calculated using Equation (3.12).

$$dT = aTs + b \tag{3.12}$$

Where; (*a*) and (*b)* are the linear relationship constants. To resolve these constants, SEBAL uses the 'anchor' pixels for which a value for sensible heat flux *(H)* can be reliably estimated, *Ts* is estimated from the thermal bands of Landsat-8 OLI/ TIRS for each pixel, while *dT*, for either the hot or cold pixel, calculated using the relationship [147]. To find constant (*a)* the total difference between the cold and hot pixels must be divided on the total difference temperature between the cold and hot pixels. In case of ($b = (-a)\ T_{sh} + dT_h$) *a* is the correlation coefficient, T_{sh} – the hot pixel temperature, dT_h – the selected hot pixel net radiation and soil heat flux radiation[147].The instantaneous evapotranspiration ET_{inst} for the satellite at the crossing time above the study area is written as in Equation (3.13). [101]

$$ETinst = 3600 \times \lambda ET/\lambda \quad (3.13)$$

Where, ET_{inst} in mm/h is the instantaneous evapotranspiration; 3600 – the time conversion from second to hour; λET – the evaporation latent heat flux, and λ – heat absorbed when a kilogram of water evaporates (J/kg).

The Reference *ET* fraction *ETrF* is a ratio between instantaneous ET_{inst} for each pixel to the reference ET_r calculated from weather data:

A final step in SEBAL calculation is to compute the ET values for 24 h, which is more useful than ET_{inst}. The ET_{24} (mm/day) can be computed as in Equation (3.14).

$$ET_{24} = ETrF \times ETr_{-24} \quad (3.14)$$

where ETr_{-24} is the cumulative 24 h ETr for the day of the image. This is calculated by adding the hourly *ETr* values over the day of the image.

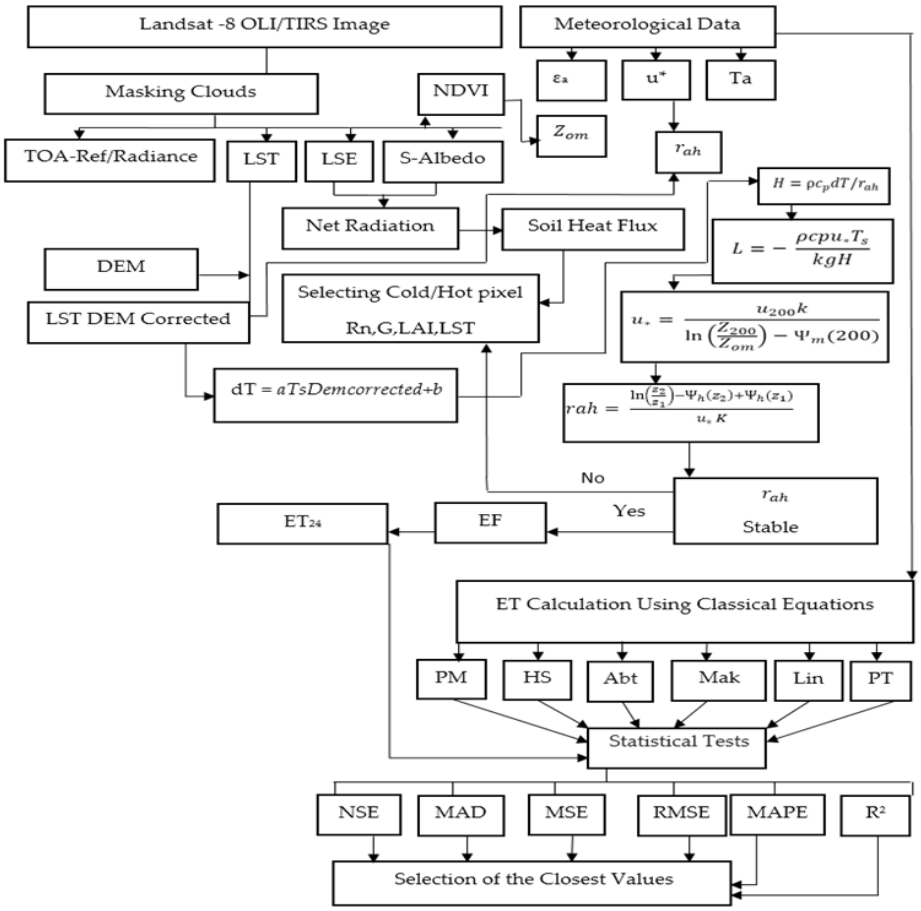

Figure 3.2 Flowchart of the SEBAL Model Calculating ET Using Landsat 8 Data with Six Standard ET Calculation Methods

Note: Here is a brief explanation of the symbols and observations in the flowchart: NDVI is Normalized Difference Vegetation Index, ε_a is the atmospheric emissivity, u* is the friction velocity, Ta is the air temperature, TOA-Ref-Ref/Radiance is Top of the Atmosphere Albedo and Radiance, LST is the Land Surface Temperature, LSE is the Land Surface Emissivity, S-Albedo is the Surface Albedo, Z_om is the Momentum Roughness Length (m), r_{ah} is Aerodynamic Resistance to Heat Transport, DEM is the Digital Elevation Model, Rn is Net Radiation, G is Soil Heat Flux, LAI is Leaf Area Index, H is Sensible Heat Flux (W/m^2), ρ is the density of air (kg/m^2), c_p is the Air Specific Heat (1004 J/kg/K), dT is the Temperature Differential for each pixel, u_* is the Friction Velocity for each pixel, T_s is the Surface Temperature (K), g is the Gravitational Constant (9.81 m/s^2), L is the Monin-Obukhov length, u_{200} is the Wind Speed at 200 m, a+b are the Correlation Coefficients, z_1, z_2 is the Height above the Zero plane Displacement and z_2 is some Distance above the Zero plane Displacement, Ψ_m and Ψ_h are the Stability Correction factors for momentum and Sensible Heat Flux, EF is Reference Evapotranspiration Fraction, ET_{24} is Daily Values of ET. PM: Penman-Monteith, HS: Hargreaves-Samani, Abt: Abtew methods, Mak: Makkink, Lin: Lin, PT: Priestley-Taylor methods ET calculation methods. MAD: Median absolute deviation, MSE: Mean Square Error, RMSE: Root-Mean-Square Error, MAPE: Mean absolute percentage error, NSE: Nash Sutcliffe Error, R^2: coefficient of determination.

3.3.3 Estimation of Evapotranspiration (ET) from MODIS SSEBop and GLDAS CLSM

Following the SEBAL calculation, a demonstration of the capacity of remote sensing for calculating ET was carried out. Another remote sensing ET dataset with a 1km resolution, estimated using MODIS SSEBop ET, was acquired. Additionally, GLDAS CLSM ET data were retrieved from the NASA data archive, the links of downloads are demonstrated in Figure 3.1. These datasets were obtained to address the second parameter in the water budget equation, specifically ET. Various GIS platforms were utilized to geospatially align the data with the study area, establish its spatial boundaries, and apply relevant scaling factors, as specified in reference [148]. ET values were extracted within the designated timeframe to ensure data quality and were subsequently compared with accompanying metadata. The use of

this dependable dataset facilitated the identification of temporal and spatial patterns consistent with the study's objectives. The findings were comprehensively summarized and analyzed in conjunction with other components of the water budget (refer to Figure 3.1).

3.4 Estimation of Runoff using Various Approaches

In this study, the estimation of runoff was approached through two distinct methods. The first method involved the utilization of a satellite image processing technique, incorporating data from sources such as PERSIANN, CHIRPS, and TWSC explained in (Figure 3.1) obtained from GRACE data. This method encompassed a process where precipitation was subtracted from evapotranspiration and Terrestrial Water Storage Change (TWSC) values. The resulting residual, referred to as "residual runoff or inferred runoff," was conceptualized as an indirect indicator of runoff, given the challenges associated with directly deriving runoff from remote sensing data [13-15]. Concurrently, the second method involved the use of an existing GLDAS CLSM layer, readily accessible via download. This approach facilitated the computation of water budget components by integrating precipitation, evapotranspiration, and surface runoff. The GLDAS CLSM data layer served as the foundational framework for the direct quantification of surface runoff, providing an alternative avenue for runoff estimation. The combination of these two methods allowed for a comprehensive exploration of runoff dynamics, incorporating both indirect inference through residual analysis and direct quantification through established hydrological modeling. This methodological duality was chosen to ensure the robustness of runoff estimation [135].

3.5 Terrestrial Water Storage (TWS)

Terrestrial Water Storage is a measure of the total amount of water stored within the Earth's landmass, including groundwater, soil moisture, surface water, snow, and ice. In the context of the study, the method for estimating TWS involves using data from the GRACE satellite mission and the GLDAS model. A similar method applied to extract information from GRACE and GLDAS TWS layer for understanding the changes in total water storage of Kunduz layer Figure 3.1.

3.6 Terrestrial Water Storage Change (TWSC)

To ascertain alterations in water storage, the quantification of Temporal Variations in TWS within the Kunduz basin was undertaken through the computation of Terrestrial Water Storage Changes (TWSCs). This was accomplished by analyzing data pertaining to TWS Anomalies (TWSAs), which were derived from observations conducted by the GRACE satellite, in conjunction with TWS data obtained from the GLDAS. In this study, the traditional water balance method (referred to as Equation 1.1), grounded in the principle of mass conservation [135].

The TWSCs calculation was performed according to the established equation given in Equation (3.15).

$$\frac{ds}{dt} = \frac{TWS(t+1) - TWS(t-1)}{2\Delta t} \tag{3.15}$$

The quantification of temporal variations in e TWS for each month within the study basin was executed using the derivative, ds/dt, which represents the Terrestrial Water Storage Change. This estimation was conducted by averaging two distinct GRACE TWS Anomaly. To ensure consistency with the GRACE terrestrial water storage estimates, a time (Δt) of 1 month was employed in Equation (3.15) for this study. The calculation involved utilizing the TWS values for month t + 1 and t - 1, denoted as TWS (t + 1) and TWS (t - 1), respectively. Through the utilization of this methodology, the study aimed to capture and quantify changes in Terrestrial Water Storage over time within the study catchment, incorporating information derived from the GRACE and GLDAS CLSM terrestrial water storage estimates. As elaborated in Table 2.3, a decision was made in this study to utilize the data available up to 2017 for GRACE data, primarily because of the substantial data gap that was encountered from 2017 onwards but for GLDAS layer the study continue from 2009 to 2019. Due to the very course resolution of both GRACE and GLDAS TWS layers a methodology for enhancing of the spatial resolution applied that will be discussed in the section below, utilizing the GWR method, as depicted in Figure 3.1.

3.7 Downscaling with Geographically Weighted Regression (GWR)

In this study, GWR served as the chosen methodology for downscaling datasets, including PERSIANN, CHIRPS [129], GRACE, and GLDAS [149-151], datasets. The primary objective of this downscaling was to enhance the spatial resolution of the WB components. Specifically, the aim was to improve the quality of these components by transforming them from their original varying spatial resolutions to a uniform 1 km spatial resolution. GWR is a widely utilized spatial regression technique across multiple disciplines, including geography, hydrology, and city planning, to comprehend and forecast variables or processes [152]. It serves as an exploratory tool for detecting non-stationarity within spatial phenomena signifying a significant recent advancement in modeling, particularly regarding spatial heterogeneity [153-155]. In the design of GWR, parameters are estimated across the study area using a dependent variable and known spatial coordinates of one or more independent variables. Observations are weighted based on Tobler's principle of closeness and similarity, where closeness has a stronger influence on parameter estimation compared to distant observations [156]. GWR is an open-source tool. The accompanying figures provide valuable support by visually depicting both the formula and the weighting scheme of the model Figure 3.3.

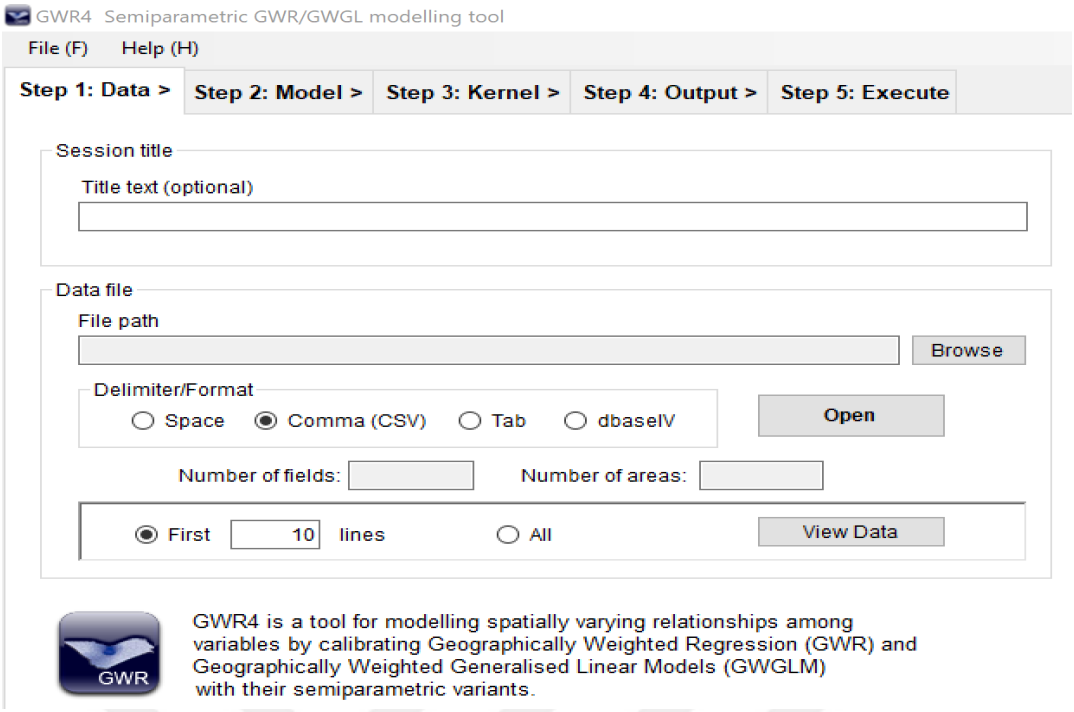

Figure 3.3 GWR model graphical user interface, reading the dependent and independent variables

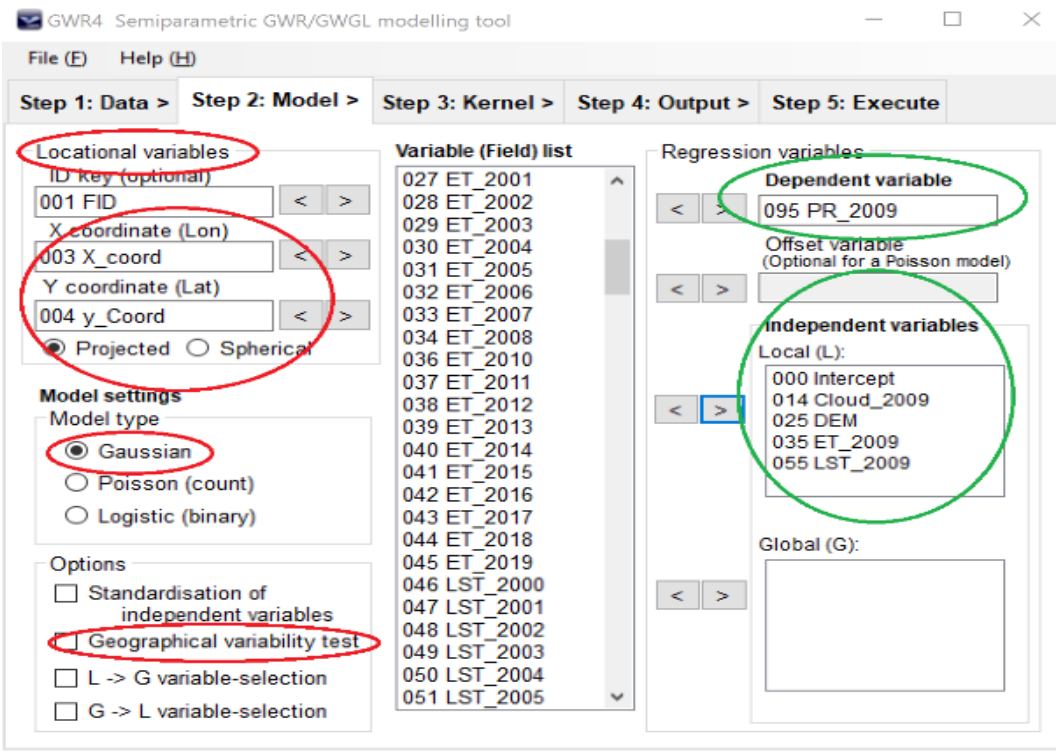

Figure 3.4 Model properties, variable locations, kernel type, and geographical variability test are represented in red, while the dependent and independent variables are shown in green

The initial step in this methodology involves providing a point dataset containing the locations of the dependent and independent variables. This dataset can be extracted from water budget components within a GIS environment. In a dataset containing a dependent variable (y), a set of m independent variables (Xk, k=1…m), and positional information for each of the n observations, GWR implementations typically employ a regression model known as Ordinary Least Squares (OLS), as expressed by Equation (3.16).

$$y_i(p) = B\beta_{0i}(p) + \beta_{1i}(p)xi1 + \beta_{2i}(p)x2i + \cdots + \beta_{ni}(p)xni \qquad (3.16)$$

Where; $B\beta_{0i}(p)$ This formula represents the relationship between the dependent variable (y) and the independent variables (xi1, x2i, ..., xni) at a specific location (p). The parameters in the formula, $B\beta_{0i}(p) + \beta_{1i}(p)$, ..., $\beta_{ni}(p)$, capture the spatially varying effects of these independent variables on the dependent variable.

$B\beta_{0i}(p)$ represents a location-specific parameter describing the baseline or intercept of the relationship. $B\beta_{0i}(p) + \beta_{1i}(p)$, ..., $\beta_{ni}(p)$ represent location-specific coefficients associated with each independent variable, reflecting how their values influence the dependent variable at that specific location.

As illustrated in Figures 3.3 and 3.4, when measurements of independent variables are available at location (p), the prediction of the dependent variable becomes feasible. This approach may initially appear unconventional but gains clarity when considering the influence of geographical weighting. In the second step, the process of geographical weighting was applied to spatial pixels using the Gaussian kernel, as indicated by Equation 3.17.

$$w_i(p) = \left(-0.5\left(\frac{d_i(p)}{h}\right)^2\right) \qquad (3.17)$$

in this formula the $w_i(p)$ represents the weight assigned to the ith data point based on its distance from the location (p), $d_i(p)$ is the distance between the ith data point and the location (p), h is the bandwidth or spatial scale parameter that controls the extent of the kernel. It follows a Gaussian or normal distribution. Gaussian kernel is a weighting function that assigns weights to data points based on their spatial proximity to a specific location. It's a key component of GWR and helps ensure that

the analysis considers the spatial context and captures local variations in relationships between variables. in this study despite the data's initial uniformity, the adaptive approach, combining the bi-square kernel with nearest neighbor (NN) weighting and a golden section search, proved valuable. It allowed the model to tailor the bandwidth to each location, emphasizing nearby data points in dense regions and extending its reach to encompass more distant data points in sparser areas. The use of the corrected Akaike Information Criterion (AICc) for goodness of fit assessment underscored the study's commitment to robust model performance evaluation. This comprehensive approach was applied to enhance the model's capacity to capture intricate spatial relationships, providing deeper insights into spatially varying phenomena even when the initial dataset was uniformly extracted from a water budget component layer including precipitation and evapotranspiration and TWS raster Figure 3.5.

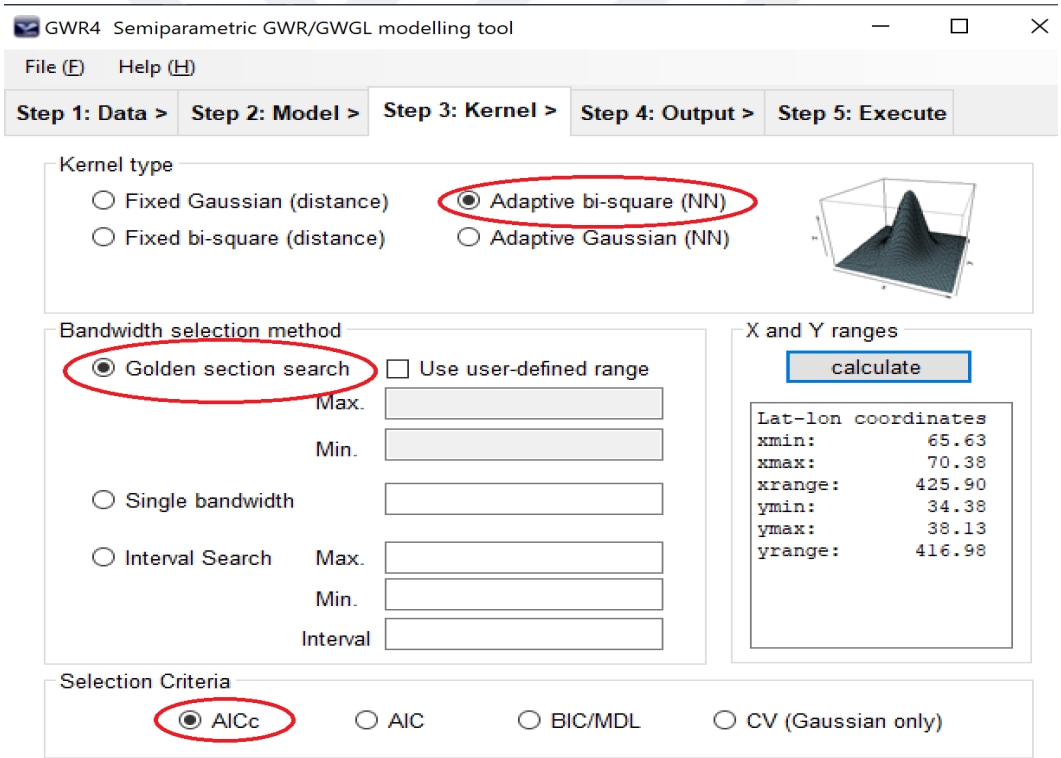

Figure 3.5 Kernel properties, Search type, and goodness of fit for GWR represented in red

In the realm of GWR, the primary measure of goodness of fit that is commonly employed is the corrected Akaike Information Criterion [157]. This criterion is expressed as Equation (3.18).

$$AIC_c\ 2nln_e\ (\widehat{\sigma}\ ) + nln_e\ (2\pi) + n\left(\frac{n + tr(S)}{n - 2 - tr(S)}\right) \quad (3.18)$$

The corrected Akaike Information Criterion (AICc) is a useful tool for comparing models that involve different explanatory variables while considering the complexity of the model. In short, it incorporates the sample size (n), the estimated model variance (σ^), and the trace of the model matrix S. The goal is to find a model with the lowest AICc value, indicating a better trade-off between model fit and complexity Equation 3.18 [158].

In the third step, global regression coefficients (β) corresponding to the independent variables were estimated using Ordinary Least Squares (OLS) models. "Downscaling formula"

$$yi\ =\ \beta 0\ +\ \beta 1x1i\ +\ \beta 2x2i\ +\cdots+\ \beta nxni\ +\ \varepsilon i \quad (3.19)$$

The downscaling formula aimed to utilize Ordinary Least Squares (OLS) to derive the global regression coefficients (β) associated with the independent variables. (3.19):

- Y_i represents the dependent variable value at location i.
- β_0 *intercept,* represents the spatially varying intercept term.
- β_1 *(dem estimated coefficient1km),* β_2 *(ndvi estimated coefficient1km), ...,* β *(raster layer estimated coefficients)* represent the spatially varying coefficients associated with the independent variables X_1i, X_2i, ..., X_ki, respectively.
- $X_1i, X_2i, ..., X_ki$ represent the values of independent variables (DEM, NDVI, LST,
- $\mathcal{E}i$ represents the error term or residual at location i.

The model estimates parameters, including intercept and coefficients at 1km resolution, for each location. This enables the capture of spatial heterogeneity in

variable relationships. The spatially varying coefficients (β intercept) represent local effects of independent variables on the dependent variable, reflecting area-specific relationships. The GWR model is estimated through an iterative process, typically employing weighted least squares or maximum likelihood estimation [152]. The intercept in GWR [159], captures the spatially varying baseline value across the study area. Rather than assuming a single intercept for the entire dataset, GWR estimates a unique intercept for each location or observation. This approach accommodates spatial heterogeneity in the relationship between the dependent and independent variables, recognizing that the intercept may vary across space. In essence, the GWR intercept represents the starting point or baseline value of the dependent variable at each location, considering spatial variations in its relationship with the independent variables. After generating the estimated layer with 1km coefficients from the model, the subsequent step entails crafting the regression equation within the GIS environment. This comes after performing kriging interpolation on the model output, facilitating the conversion of GWR coefficients into a 1km raster format. Additionally, this process involves the correction of the coefficients using the GWR residual layer. The simplified downscaling approach with GWR can be expressed as follows:

"Dependent Variable (PERSIANN (P)) = Intercept + Estimated Coefficient * Original 1km Independent Layer (e.g., DEM, ...) + Residual."

In the study, several environmental variables were employed as independent factors for downscaling precipitation in the Kunduz catchment. These variables were selected based on the hydro-meteorological characteristics of the study area and the primary factors influencing precipitation in the region. The chosen variables comprised the NDVI, Digital Elevation Model (DEM), cloud cover, land surface temperature, and evapotranspiration. The GWR model was utilized to perform spatial downscaling, as explained in previous sections.

3.8 Statistical Analysis

To comprehensively evaluate the performance of the current study, an assessment is conducted through the analysis of three key statistical metrics: Normalized Nash-

Sutcliffe Efficiency (NSE), Percentage Bias (PBAIS), and the coefficient of determination (R^2). These metrics are calculated using Equations (3.20 to 3.25).

$$NSE = 1 - \left[\frac{\sum(sim - obs)^2}{\sum\left(sim - \overline{obs}\right)^2}\right] \tag{3.20}$$

In this study, the existence of a lower limit of negative infinity for the Nash-Sutcliffe Efficiency (NSE) poses challenges. To mitigate this issue and confine the NSE within a normalized range of (0-1) [160].

PBAIS indicator were utilized to quantify the systematic deviation or bias between the simulated and observed annual hydrological data values, expressed as percentages, offering insights into the average overestimation or underestimation of simulated hydrological data relative to observed values. [162, 163].

$$PBIAS = 100\,\frac{\sum_{i=1}^{N}(S_i - O_i)}{\sum_{i=1}^{N} O_i} \tag{3.21}$$

R-squared (R^2) is a statistical measure representing the proportion of explained variance in the dependent variable by the independent variables in a regression model, commonly used for assessing model goodness-of-fit. It is expressed by the following equation: [164].

$$R^2 = \frac{\sum_{i=1}^{T}(y_t - \overline{y})(f_t - \overline{f})}{[\sum_{t=1}^{T}(y_t - \overline{y})^2]\text{^}0.5\ [\sum_{t=1}^{T}(f_t - \overline{f})\text{^}2\ ]\text{^}0.5} \tag{3.22}$$

$$MAD = \frac{\sum(ET_{SEB} - ET_{XY})}{n} \tag{3.23}$$

$$RMSE = \sqrt{\frac{\sum_{i=1}^{N}(ET_{SEB} - ET_{XY})\text{^}2}{N}} \tag{3.24}$$

ET_{SEB} is SEBAL ET value compared with ET from the location of gauge stations.

$$KGE = 1 - \sqrt{[(\mathrm{r} - 1)\hat{}2 + (\alpha - 1)\hat{}2 + (\beta - 1))\hat{}2]} \quad (3.25)$$

Where, r is the Pearson correlation coefficient between observed and simulated values. α is the ratio of the standard deviation of the simulated values to that of the observed values. β is the ratio of the mean of the simulated values to that of the observed values

$$r = \frac{\Sigma\,[(\mathrm{X} - \bar{\mathrm{X}}) * (\mathrm{Y} - \bar{\mathrm{Y}})]}{\sqrt{[\Sigma(\mathrm{X} - \bar{\mathrm{X}})^2 * \Sigma(\mathrm{Y} - \bar{\mathrm{Y}})^2]}} \quad (3.26)$$

r is Pearson correlation coefficient, where X and Y are data points from the two datasets being compared. $\bar{\mathrm{X}}$ and $\bar{\mathrm{Y}}$ are the means (average values) of the X and Y datasets, respectively.

$$VE = 1 - \frac{\sum_{i=1}^{N}[\mathrm{Si} - \mathrm{Oi}\,]}{\sum_{i=1}^{N}(O_i)} \quad (3.27)$$

Volumetric efficiency was introduced as a solution to mitigate certain challenges linked to Nash-Sutcliffe efficiency. This metric is confined within the range of (0 to 1), signifying the proportion of water distributed at the correct timing. Its complementary aspect reflects the fractional volumetric discrepancy.

4
RESULT

4.1 Precipitation

This study employed three distinct precipitation datasets, namely CHIRPS, PERSIANN, and GLDAS CLSM, and the results will be separately presented for each of these datasets, including an annual mean comparison of RS-based and GLDAS CLSM data with observed precipitation. Additionally, catchment-wise results, as well as monthly median and seasonal analysis findings, will be presented. It is worth noting that these datasets have been widely employed in various global water budget studies, as evidenced by prior research [15, 105, 129, 136]. Throughout the result presentation, the names of the gauge stations and their respective station numbers will be used interchangeably to ensure clarity. Additionally, correlation results between remote sensing and GLDAS with observed layers will be presented separately.

4.1.1 CHIRPS precipitation

In Figures 4.1 to 4.3, an analysis of precipitation data from all Kunduz catchment stations was conducted. A comparison was made between the original data (OD) and downscaled data (DD) values, with reference to the observed (Obs) data, aiming to identify any overestimations or underestimations in different years across the datasets.

Figure 4.1 illustrates data from Chahar Dara, Gerdab, Baghlan, and Balay-i-Kelagai stations. In the Chahar Dara station, an overestimation was observed in the year 2010, where DD data exceeded the observed precipitation by 5.01 mm/year, with a more significant margin compared to OD data. In this context, 2010 emerges as the top year for overestimation with 5.01 mm/year. Similarly, the Gerdab station exhibited overestimations, particularly in 2019, with the downscaled data surpassing the observed precipitation by 21.83 mm/year. This overestimation was more pronounced when compared to the original data, making 2019 the year with the highest overestimation of 21.83 mm/year. Overestimations were noticeable in the Baghlan station in 2015, where the downscaled data exceeded the observed

precipitation by 24.70 mm/year, with the downscaled data demonstrating a more substantial overestimation. At the Balay-i-Kelagai station, overestimations occurred in multiple years. In 2010 and 2019, the downscaled data exhibited overestimations of 29.04 mm/year and 26.91 mm/year, respectively, significantly surpassing the observed values.

Figure 4.2 presents the results for the Doshi Station, which also displayed overestimations in several years. In 2014, 2016, and 2017, the DD consistently overestimated the observed precipitation by 34.57 mm/year, 33.28 mm/year, and 38.97 mm/year, respectively. In the case of the Pul-i-Kundasang station, overestimations were observed in 2019, where both the downscaled and original data exceeded the observed values. In 2019, the DD exhibited an overestimation of 10.06 mm/year, with the original data also overestimating the precipitation. The Tang-i-Nahrin station revealed overestimations in multiple years, with the DD showing more substantial overestimations in 2011, 2015, and 2019, with values of 7.99 mm/year, 25.278 mm/year, and 3.435 mm/year, respectively.

Figure 4.3 presents data for the Ahangaran Station, which displayed overestimations in the years 2011, 2014, and 2018. In these years, the DD overestimated the observed precipitation by 0.72 mm/year, 6.54 mm/year, and 8.17 mm/year, respectively. Lastly, the Bamyan station indicated overestimations in multiple years. In 2010 and 2018, the DD consistently exceeded the observed precipitation by 86.22 mm/year and 16.62 mm/year, respectively, with 2010 standing out as the top year for overestimation.

Figure 4.4 presents a comprehensive analysis of the CHIRPS rainfall satellite data for the entire Kunduz catchment, covering the period from 2009 to 2019. This dataset reveals significant variations in precipitation levels within both the DD and OD layers. According to the DD, 2019 was the year that received the highest amount of precipitation in the catchment, with an annual precipitation value of 1141.3 mm/year. This finding is supported by the OD, which also identifies 2019 as the year with highest amount of precipitation, recording a high precipitation value of 1201.6 mm/year. In contrast, the year receiving the least amount of rain in the catchment, based on the DD, was 2016, with a low annual precipitation value of 173.0 mm/year. The OD indicates that the driest year was 2011, with a low

precipitation value of 122.9 mm/year. These observations underscore the substantial annual variations in precipitation levels within the Kunduz catchment, with 2019 identified as the wettest year and 2016 as the driest year in both the DD and OD.

The values presented here are based on the highest and lowest amount of rain over the Kunduz catchment. In the DD CHIRPS Rainfall satellite layer for the entire Kunduz catchment between 2009 and 2018, fluctuations in precipitation levels were observed. In 2009, annual precipitation varied from 967.5 mm/year to 233.5 mm/year. These fluctuations continued in subsequent years, with 2010 ranging from 781.3 mm/year to 152.8 mm/year. Similarly, in 2011, precipitation spanned from 642.2 mm/year to 126.6 mm/year. The trend persisted into 2012, with a range from 674.4 mm/year to 140.0 mm/year, and in 2013, precipitation ranged from 1118.6 mm/year to 167.9 mm/year. In 2014, the range was 957.5 mm/year to 180.1 mm/year, and in 2015, it spanned from 1058.6 mm/year to 167.6 mm/year. The year 2016 varied from 903.8 mm/year to 173.0 mm/year, while 2017 ranged from 974.9 mm/year to 207.0 mm/year. In 2018, the range extended from 1121.9 mm/year to 213.1 mm/year. In the CHIRPS OD layer, data similarly revealed annual fluctuations. In 2009, precipitation ranged from 999.9 mm/year to 225.6 mm/year. In 2010, the range extended from 764.4 mm/year to 144.7 mm/year. The year 2011 varied from 671.6 mm/year to 122.9 mm/year, and in 2012, it ranged from 689.1 mm/year to 133.8 mm/year. In 2013, precipitation spanned from 1199.2 mm/year to 158.3 mm/year, and in 2015, it extended from 1131.9 mm/year to 154.5 mm/year. The year 2016 varied from 936.3 mm/year to 164.8 mm/year, while 2017 ranged from 1086.28 mm/year to 196.6 mm/year. In 2018, the range extended from 1112.71 mm/year to 195.7 mm/year.

Throughout the years from 2010 to 2018, consistent fluctuations in precipitation levels were observed, emphasizing the dynamic nature of precipitation patterns within the Kunduz catchment. The remaining years from 2009 to 2018 similarly exhibited varying degrees of fluctuation in precipitation levels, underlining the dynamic nature of precipitation patterns in this region, where annual precipitation significantly varies from one year to the next.

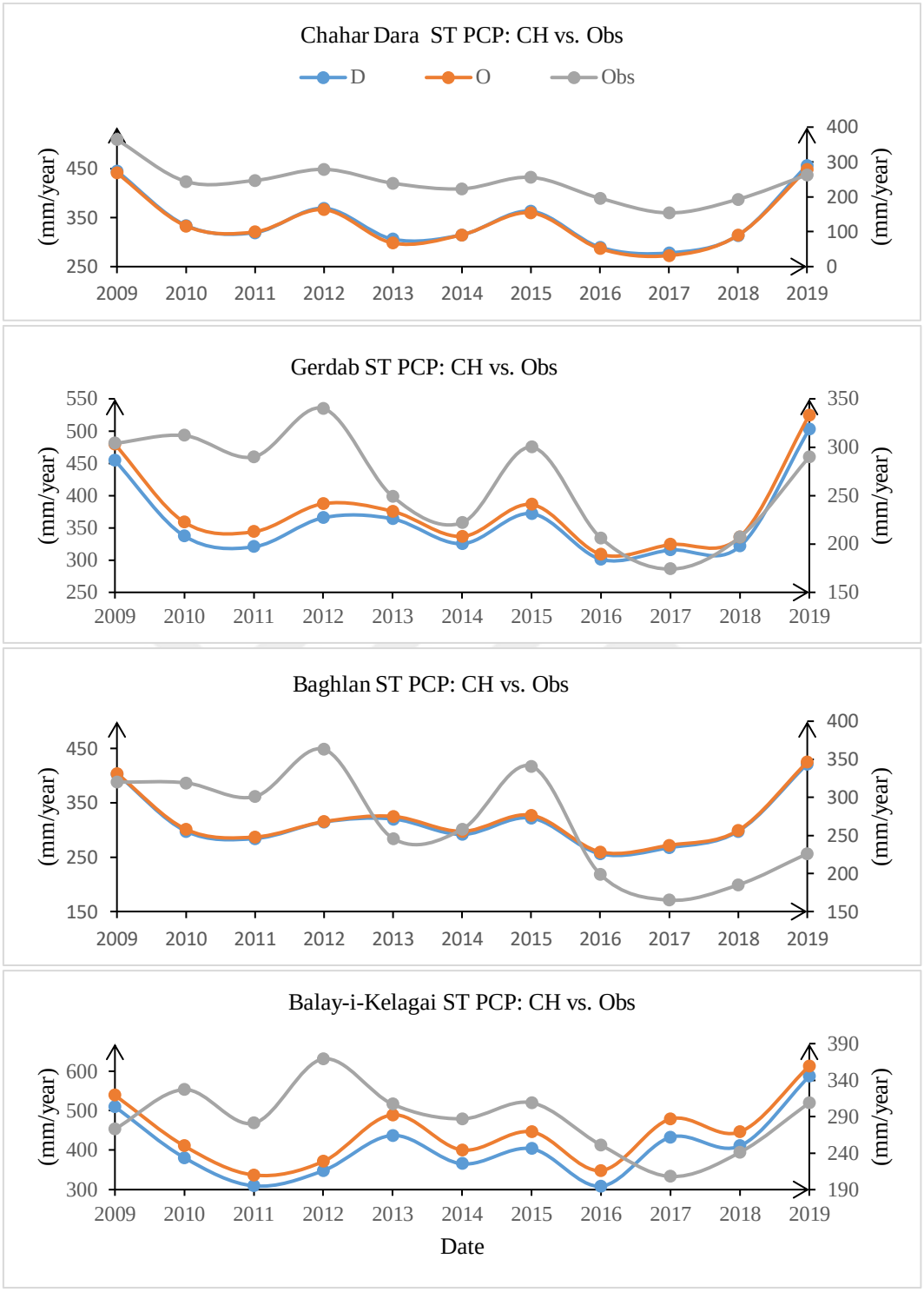

Figure 4.1 Comparison of Downscaled (DD), Original (OD), and Observed (0bs) Data CHIRPS Precipitation data

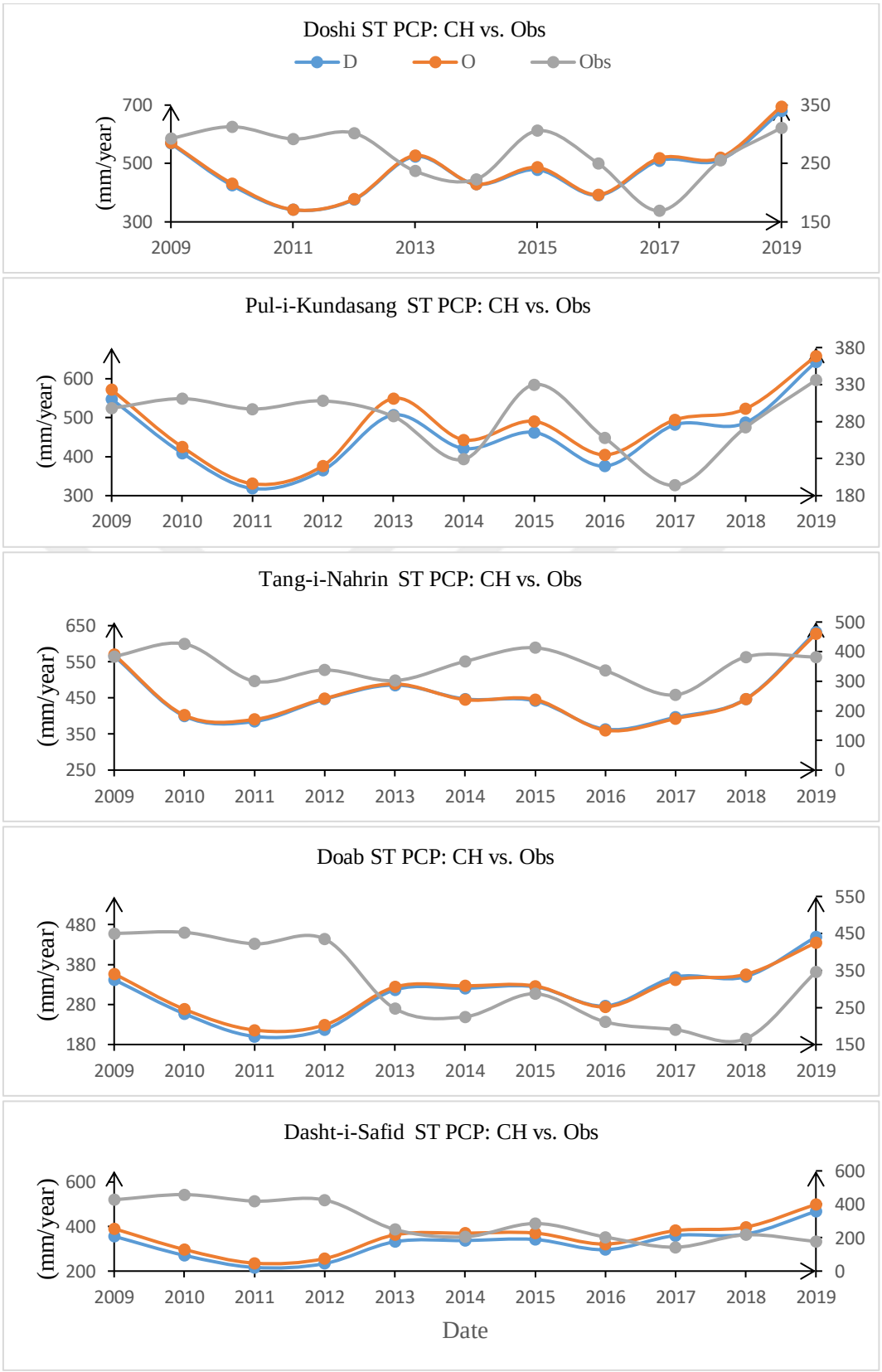

Figure 4.2 Comparison of Downscaled (DD), Original (OD), and Observed (0bs) Data CHIRPS Precipitation data

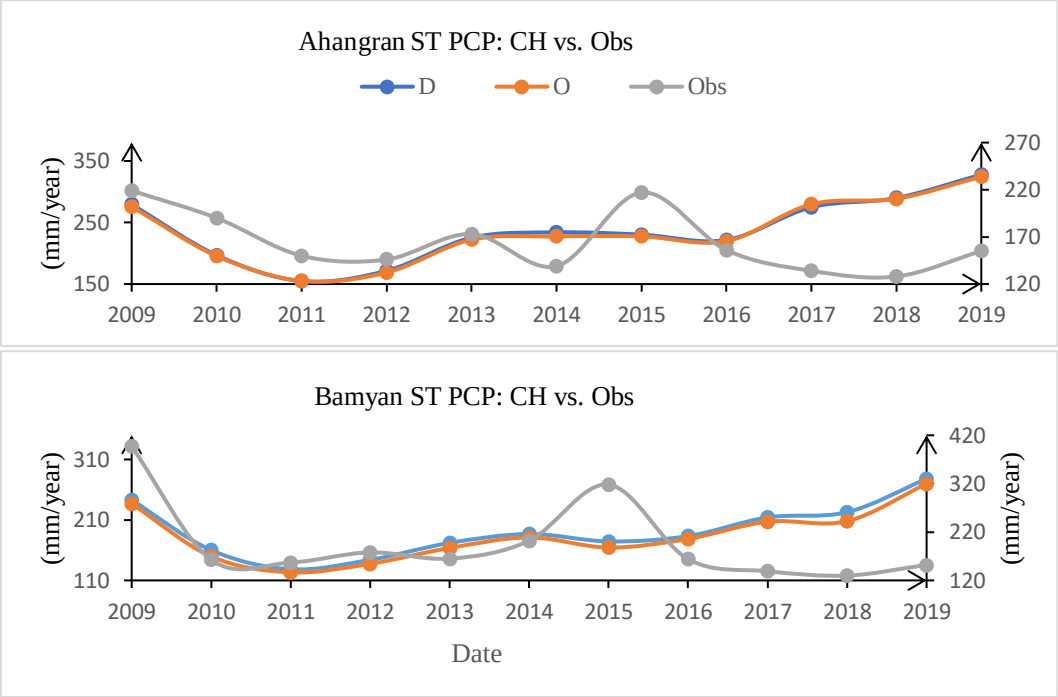

Figure 4.3 Comparison of Downscaled (DD), Original (OD), and Observed (0bs) Data CHIRPS Precipitation data

Simultaneously, a correlation assessment analysis was conducted to examine the correlation between RS-based CHIRPS and observed precipitation. Table 4.1 provides a comprehensive correlation assessment encompassing all study stations throughout the entire study period. The results disclose a spectrum of correlations, both positive and negative in nature. Positive correlations were evident in Station #1 (Chahar Dara), with coefficients of 0.82 for DD vs. observed (Obs) and 0.8 for OD vs. Obs. Similarly, Station #2 (Gerdab) displayed positive correlations, registering 0.56 for DD vs. Obs and 0.51 for OD vs. Obs. These stations emerged as the ones with the most substantial positive correlations between observed precipitation and CHIRPS data. Conversely, Station #9 (Dasht-i-Safid) was notable for its strong negative correlations, measuring -0.66 for DD vs. Obs and -0.65 for OD vs. Obs. The weakest negative correlations were observed in Station #10 (Ahangaran), featuring -0.04 for DD vs. Obs and -0.03 for OD vs. Obs.

These findings illuminate the presence of diverse positive and negative correlations within the dataset, reflecting the intricate dynamics of precipitation patterns and their associations with CHIRPS data across all study stations, as presented in Table 4.1.

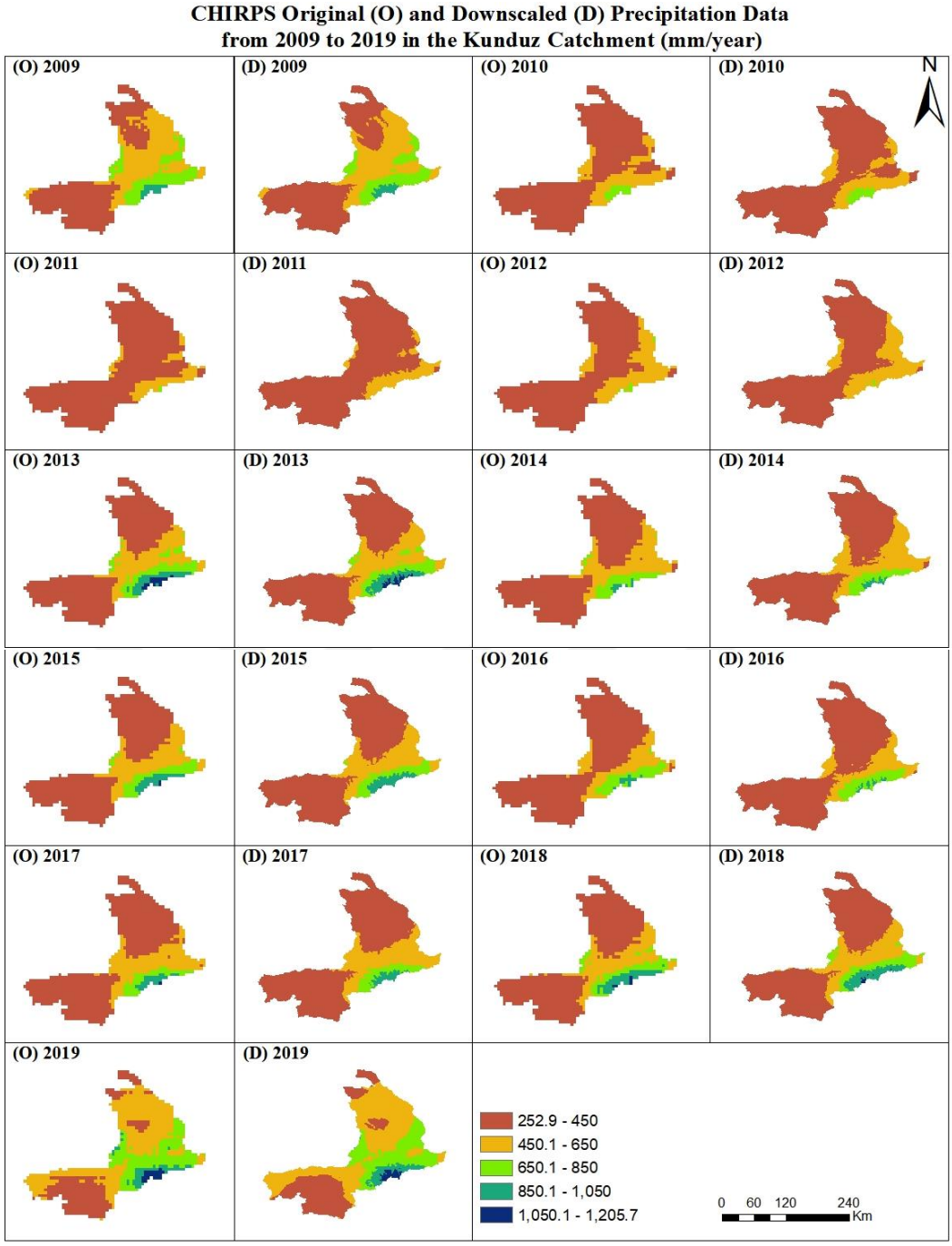

Figure 4.4 Original (O), Downscaled (D) CHIRPS Precipitation data from 2009 to 2019

Table 4.1 Correlation Assessment of CHIRPS (CH) RS Downscaled (D), Original (O) Precipitation data vs. Observed (Obs) Precipitation data.

Station#	CH D&O vs. Obs PCP		
	Data	D	O
1	D	1	
	O	1	1
	Obs	0.82	0.8
2	D	1	
	O	1	1
	Obs	0.56	0.51
3	D	1	
	O	1	1
	Obs	0.26	0.26
4	D	1	
	O	0.99	1
	Obs	-0.07	-0.03
5	D	1	
	O	0.93	1
	Obs	0.3	0.05
6	D	1	
	O	0.99	1
	Obs	0.19	0.18
7	D	1	
	O	1	1
	Obs	0.32	0.31
8	D	1	
	O	0.99	1
	Obs	-0.39	-0.35
9	D	1	
	O	1	1
	Obs	-0.66	-0.65
10	D	1	
	O	1	1
	Obs	-0.04	-0.03
11	D	1	
	O	0.83	1
	Obs	-0.22	0.18

The monthly median analysis, focusing on downscaled data due to its strong positive and negative correlation, was conducted as a key component of this study. As previously emphasized in the earlier sections, the analyses were primarily carried out on an annual, monthly, and seasonal basis. Within the context of

assessing the first parameter of the water budget within the Kunduz catchment, the analysis of monthly median precipitation data, as presented in Figures 4.5 to 4.7 and Table 4.2, reveals noteworthy variations in precipitation levels across the different stations. Specifically, it is consistently observed that February emerges as the month with the highest median precipitation levels, with values ranging from approximately 68 mm/month to 150.48 mm/month. This consistency in the high precipitation levels of February is a notable finding and aligns with data from various stations, confirming its status as the wettest month in the region.

Conversely, the months of June, July, August, and September consistently exhibit a distinct pattern of zero median precipitation across all stations. These months collectively signify a dry spell, characterized by the absence of median precipitation, as indicated by the uniform reporting of 0 mm/month at all stations during this period. For the remaining months, including January, March, April, May, October, November, and December, the data reflects moderate median precipitation levels. These levels vary within the range of approximately 26.72 mm/month to 93 mm/month. It's important to note that while some variability exists among stations, these months collectively display a pattern of moderate median precipitation in the Kunduz catchment. Stations such as Chahar Dara, Baghlan, Balay-i-Kelagai, Doshi, Pul-i-Kundasang, Dasht-i-Safid, Doab, and Ahangaran collectively contribute to this observation, emphasizing the consistent pattern of moderate median precipitation levels throughout these months. The matrix plots provide a valuable visual interpretation of the precipitation datasets, including CHIRPS, PERSIANN, and GLDAS CLSM. These plots effectively illustrate the intensity of precipitation data within the Kunduz catchment area. The color representation within the plots is a key aspect for understanding the variations in precipitation levels. Dark red hues within the plots signify minimal or zero precipitation, while a gradual transition to dark blue indicates higher amounts of precipitation within the Kunduz catchment. These visual representations facilitate a clear comprehension of the spatial distribution of precipitation across the datasets.

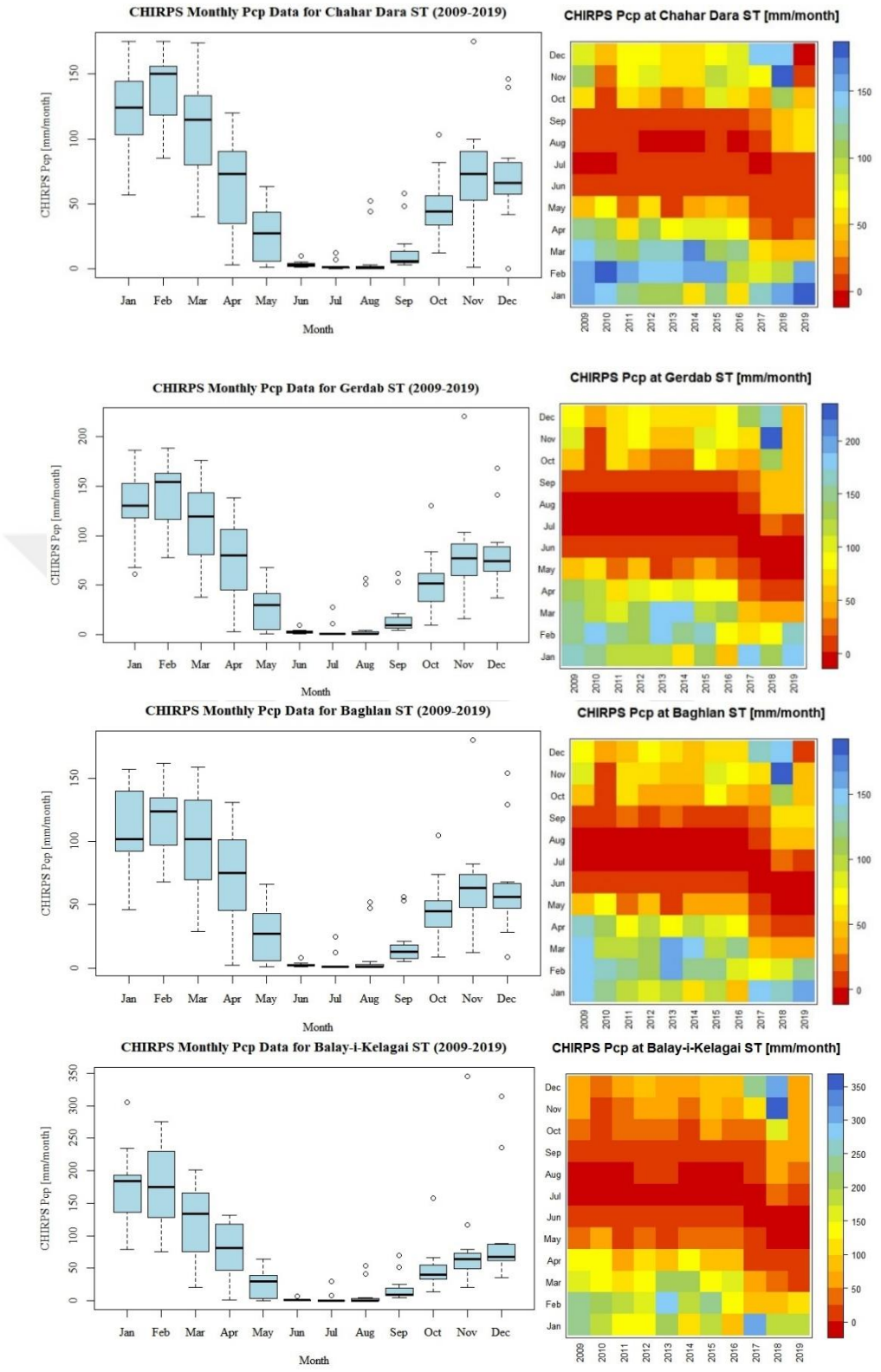

Figure 4.5 Monthly Variation of Downscaled (D) CHIRPS Precipitation at Chahar Dara, Gerdab, Baghlan and Balay-i-Kelagai Stations in the Kunduz Catchment from 2009 to 2019

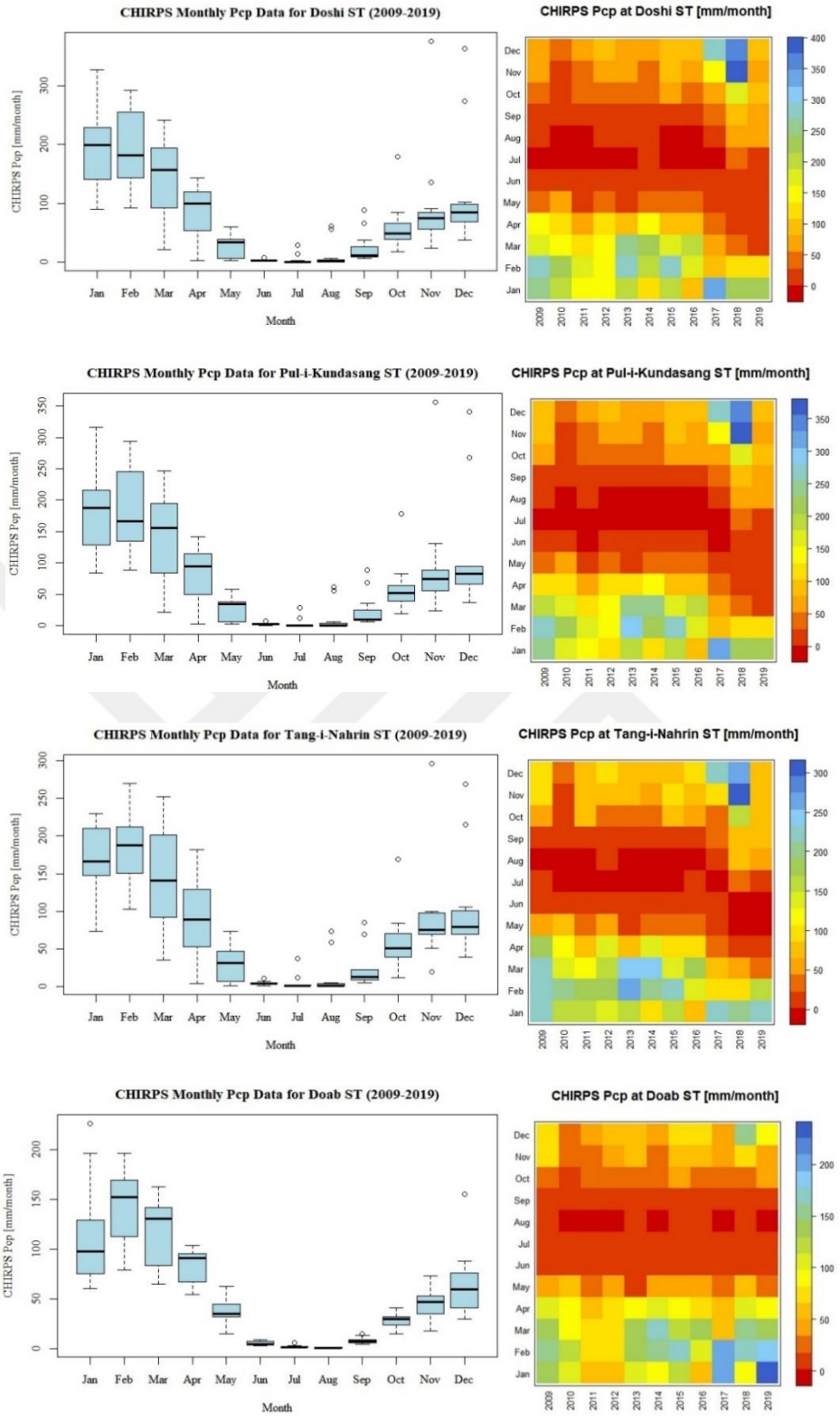

Figure 4.6 Monthly Variation of CHIRPS Precipitation (Downscaled) at Doshi, Pul-i-Kundasang, Tang-i-Nahrin and Doab Stations in the Kunduz Catchment from 2009 to 2019

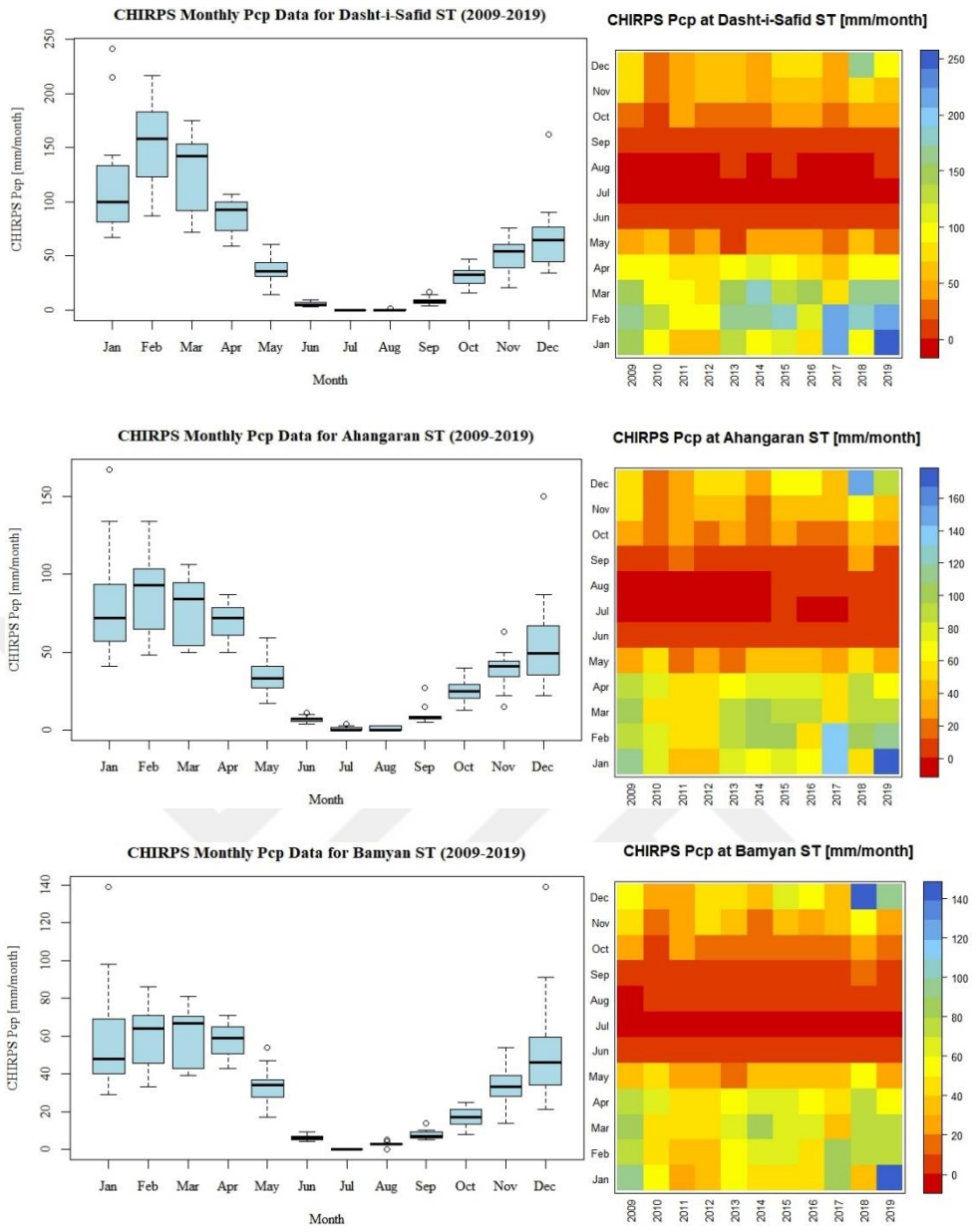

Figure 4.7 Monthly Variation of CHIRPS Precipitation (Downscaled) at Dasht-i-Safid, Ahangran and Bamyan Stations in the Kunduz Catchment from 2009 to 2019

Table 4.2 is employed for the presentation of the actual median values encompassing all the months within the confines of the Kunduz catchment, thus providing a comprehensive depiction of the hydroclimatic conditions observed throughout the extensive study period spanning from 2009 to 2019. Station name and numbers are illustrated in Table 2.1 and Figure 2.3.

Table 4.2 CHIRPS Monthly Median Values Over Gauge Stations in Kunduz Catchment During 2009 to 2019 (mm/month).

ST#	Jan	Feb	Mar	Apr	May	Jun	Jul	Aug	Sep	Oct	Nov	Dec
1	124.1	150.5	115.0	72.7	26.7	3.1	1.2	0.6	6.3	44.3	73.1	65.7
2	130.0	154.0	119.0	80.0	30.0	3.0	1.0	1.0	10.0	52.0	77.0	74.0
3	102.0	124.0	102.0	75.0	27.0	2.0	1.0	1.0	13.0	45.0	63.0	56.0
4	184.0	175.0	134.0	81.0	30.0	1.0	0.0	0.0	9.0	40.0	64.0	67.0
5	199.0	181.0	157.0	99.0	34.0	3.0	0.0	1.0	11.0	49.0	74.0	85.0
6	187.0	166.0	156.0	94.0	34.0	2.0	0.0	0.0	10.0	52.0	74.0	83.0
7	166.0	188.0	141.0	89.0	31.0	4.0	1.0	1.0	13.0	51.0	75.0	79.0
8	100.0	158.0	142.0	93.0	36.0	5.0	0.0	0.0	8.0	33.0	54.0	65.0
9	98.0	152.0	131.0	91.0	35.0	5.0	2.0	1.0	8.0	30.0	47.0	60.0
10	72.0	93.0	84.0	72.0	33.0	7.0	0.0	0.0	8.0	25.0	41.0	49.0
11	48.0	64.0	67.0	59.0	34.0	6.0	0.0	3.0	7.0	17.0	33.0	46.0

As previously stated, the analysis results are presented on a temporal basis, including monthly, yearly, and seasonal data. Figure 4.8 and Table 4.3 illustrate the seasonal analysis, focusing on the DJF (December, January, February) season. During DJF, the highest precipitation of 506.73 mm/season was recorded, with Doshi ST leading the observations. Pul-i-Kundasang closely followed, recording 486.27 mm/season. Balay-i-Kelagai ST and Tang-i-Nahrin ST reported the same value of 455.18 mm/season. Meanwhile, Chahar Dara received 330.13 mm, Gerdab received 354.82 mm, and Dasht-i-Safid received 345.82 mm. A similar value of 345.82 mm was also recorded by Ahangaran. Notably, Bamyan station reported the lowest precipitation for this season, at 174.82 mm.

Transitioning to the MAM (March, April, and May) season, the highest recorded precipitation was 263.27 mm/season, establishing a new benchmark. Doshi ST closely followed, with 254.82 mm/season. Other stations reported 252.18 mm/season, while Dasht-i-Safid ST had the lowest at 152.27 mm/season. In the driest season, JJA (June, July, and August), Tang-i-Nahrin ST received the highest precipitation at 22.82 mm/season, while the lowest was recorded by Ahangaran ST at 6.18 mm. It is important to note the seasonal shift, with precipitation increasing after JJA as the SON (September, October, and December) season commences. During SON, Tang-i-Nahrin ST leads with 179.00 mm/season, while the lowest was reported by Bamyan ST at 58.27 mm/season.

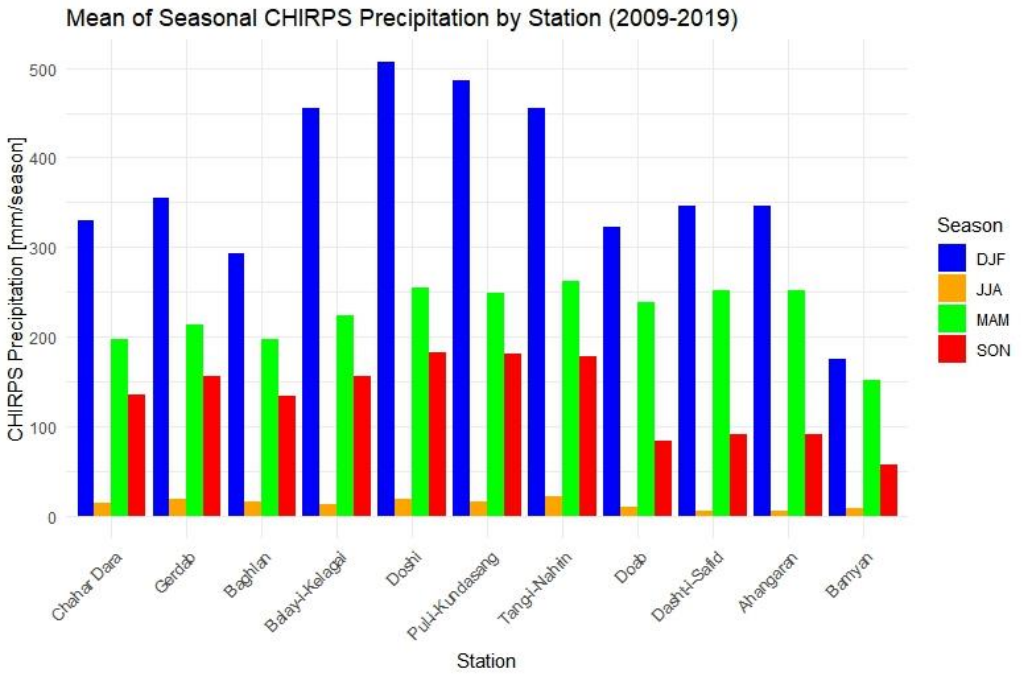

Figure 4.8 Seasonal (DJF, MAM, JJA, SON) Mean of Downscaled RS-Based CHIRPS (CH) Precipitation in Kunduz Catchment (2009-2019) by Station (mm/season)

Table 4.3 Seasonal Mean of Downscaled RS-Based CHIRPS (CH) Precipitation in Kunduz Catchment (2009-2019) by Station (mm/season).

Station	DJF	MAM	JJA	SON
Chahar Dara	330.1	198.2	15	135.9
Gerdab	354.8	214.4	18.7	155.6
Baghlan	292.8	197.3	17	133.5
Balay-i-Kelagai	455.2	223.6	14.2	157.2
Doshi	506.7	254.8	18.5	183.4
Pul-i-Kundasang	486.3	249	17.3	181.8
Tang-i-Nahrin	455.2	263.3	22.8	179
Doab	322.8	238.6	9.7	83.6
Dasht-i-Safid	345.8	252.2	6.2	91.5
Ahangaran	345.8	252.2	6.2	91.5
Bamyan	174.8	152.3	9.3	58.3

4.1.2 PERSIANN Precipitation

Similar to the CHIRPS data analysis, this study explores PERSIANN precipitation data, with a specific emphasis on comparing the original data (OD) and Downscaled data (DD) PERSIANN dataset. These datasets were then compared to the observed (Obs) data obtained from the relevant stations. The results of this annual and pixel-wise (Gauge Stations) analysis within the Kunduz Catchment have revealed valuable insights, as shown in Figures 4.9 to 4.11.

Figure 4.9 displays the consistent overestimation of Obs precipitation by PERSIANN both DD and OD at Chahar Dara station across most of the study years. In 2009, Obs recorded 510 mm/year, while DD and OD reported 506 mm/year, indicating a slight overestimation. In 2015, Obs registered 573.8 mm/year, whereas DD reported 609 mm/year and OD reported 566 mm/year, signifying overestimation. The most substantial disparity occurred in 2019, with Obs at 551.3 mm/year and DD and OD at 584.3 mm/year, raising concerns about dataset accuracy. At Gerdab station, a parallel pattern was observed, with consistent overestimation of Obs precipitation by PERSIANN DD and OD throughout the study years. In 2009, Obs data measured 510 mm/year, while DD and OD reported 506 mm/year, indicating slight overestimation. Similarly, in 2015, Obs recorded 609 mm/year, while DD and OD reported 566 mm/year and 573.8 mm/year, signifying overestimation. The most pronounced overestimation was in 2019, with Obs at 551.3 mm/year, while DD and OD were at 584.3 mm/year, reflecting substantial overestimation. Analyzing the data from Baghlan station revealed a similar trend, with consistent overestimation of Obs precipitation by both DD and OD across the study years. In 2009, Obs recorded 531 mm/year, while DD and OD reported 512 mm/year, indicating overestimation. Similarly, in 2015, Obs measured 605 mm/year, while DD and OD reported 609 mm/year and 605 mm/year, respectively. In 2019, a significant discrepancy was evident, with Obs at 606.2 mm/year and DD and OD at 584.4 mm/year, suggesting substantial overestimation. Balay-i-Kelagai station displayed a comparable pattern, with consistent overestimation of Obs precipitation by both DD and OD of PERSIANN datasets across the study years. In 2009, Obs recorded 545 mm/year, while DD and OD reported 531 mm/year, indicating overestimation. This pattern continued in 2015,

with Obs at 712 mm/year, while DD and OD reported 671 mm/year and 712 mm/year, respectively. The most substantial disparity was in 2019, with Obs at 606.2 mm/year and DD and OD at 597 mm/year, signifying notable overestimation. This consistent overestimation across the stations raises questions about dataset accuracy.

Figure 4.10 reveals a consistent overestimation of Obs precipitation by both the DD and OD of PERSIANN datasets across multiple study years at Doshi Station. In 2009, Obs precipitation measured 293 mm/year, while both DD and OD datasets reported 521 mm/year, indicating significant overestimation. A similar trend continued in 2015, with Obs precipitation at 306 mm/year, while DD and OD datasets indicated 656 mm/year and 680 mm/year, respectively, reflecting substantial overestimation. The most notable overestimation was observed in 2019, with Obs precipitation at 311 mm/year and DD and OD datasets showing values of 619 mm/year and 602 mm/year, signifying substantial overestimation. Pul-i-Kundasang station displayed a parallel trend, with consistent overestimation of Obs precipitation by both the DD and OD of PERSIANN datasets across the study years. In 2009, Obs data recorded 298 mm/year of precipitation, while both DD and OD datasets reported 521 mm/year, indicating notable overestimation. This pattern persisted in 2015, with Obs data at 330 mm/year, while DD and OD reported 656 mm/year and 655 mm/year, respectively, representing substantial overestimation. The most significant overestimation occurred in 2019, with Obs data at 336 mm/year and DD and OD datasets showing values of 619 mm/year and 597 mm/year, signifying substantial overestimation. Tang-i-Nahrin station also demonstrated a similar pattern, with consistent overestimation of Obs precipitation by both the DD and OD of PERSIANN datasets across the study years. In 2009, Obs data recorded 384 mm/year of precipitation, while both DD and OD indicated values of 554 mm/year, signifying substantial overestimation. A parallel pattern continued in 2015, with Obs data at 413 mm/year, while DD and OD datasets reported 660 mm/year and 645 mm/year, respectively, reflecting substantial overestimation. The most significant overestimation was observed in 2019, with Obs data at 382 mm/year and DD and OD datasets showing values of 605 mm/year and 592 mm/year, signifying substantial overestimation. Doab station also

displayed a parallel trend, with consistent overestimation of Obs precipitation by both the DD and OD of PERSIANN datasets across the study years. In 2009, Obs data recorded 450 mm/year of precipitation, while both DD and OD indicated values of 494 mm/year, indicating notable overestimation. This pattern persisted in 2015, with Obs data at 287 mm/year, while DD and OD datasets reported 609 mm/year and 591 mm/year, respectively, representing substantial overestimation. The most substantial overestimation was in 2019, with Obs data at 346 mm/year and DD and OD showing values of 570 mm/year and 536 mm/year, signifying substantial overestimation.

Figure 4.11 presents the analysis of Dasht-i-Safid Station's data for the years 2009 to 2019, indicating that both the DD and OD of PERSIANN datasets consistently overestimated the Obs precipitation data. In 2009, Obs precipitation was recorded at 427 mm/year, while DD and OD reported values of 465 mm/year, indicating significant overestimation. A similar pattern continued in 2015, with Obs precipitation at 285 mm/year, while DD and OD reported 576 mm/year and 577 mm/year, respectively, signifying substantial overestimation. For Ahangaran Station, the analysis across the years 2009 to 2019 demonstrates a consistent overestimation of Obs precipitation by both the DD and OD of PERSIANN datasets. In 2009, observed data recorded 451 mm/year of precipitation, while DD and OD datasets indicated values of 450 mm/year, indicating a slight overestimation. This pattern continued in 2015, with observed data at 592 mm/year, while DD and OD datasets reported 592 mm/year and 598 mm/year, respectively, signifying substantial overestimation. The most significant overestimation was observed in 2019, with observed data at 514 mm/year, while DD and OD datasets showed values of 514 mm/year and 535 mm/year, reflecting substantial overestimation. The analysis of Bamyan Station's data for the years 2009 to 2019 reveals a consistent overestimation of Obs precipitation by both the DD and OD. In 2009, observed precipitation was recorded at 397 mm/year, while DD and OD reported values of 465 mm/year and 450 mm/year, indicating significant overestimation. A parallel pattern persisted in 2015, with observed precipitation at 318 mm/year, while DD and OD reported 591.6 mm/year and 569.9 mm/year, respectively, signifying substantial overestimation. The most substantial

overestimation was in 2019, with observed precipitation at 152 mm/year, while DD and OD datasets showed values of 513.8 mm/year and 520.6 mm/year, signifying notable overestimation.

Figures 4.9 to 4.11 consistently revealed a significant overestimation of observed precipitation by both the DD and OD of PERSIANN datasets across multiple years. This overestimation was evident at various stations throughout the entire study period, with the DD and OD PERSIANN datasets consistently overestimating the Obs precipitation data in the years 2015 and 2019.

A correlation analysis was concurrently conducted to examine the relationship between RS-based (PERSIANN) and observed precipitation. Table 4.4 presents a comprehensive correlation assessment across all study stations and the entire study period, revealing a range of both positive and negative correlations. Notably, Station #7 (Tang-i-Nahrin) exhibited positive correlations, with coefficients of 0.56 for DD vs. Obs and 0.5 for OD vs. Obs. Conversely, Station #8 (Doab) was characterized by strong negative correlations, measuring -0.46 for DD vs. Obs. These findings highlight the presence of various positive and negative correlations in the dataset, shedding light on the complex dynamics of precipitation patterns and their relationships with PERSIANN data across all study stations, as presented in Table 4.4

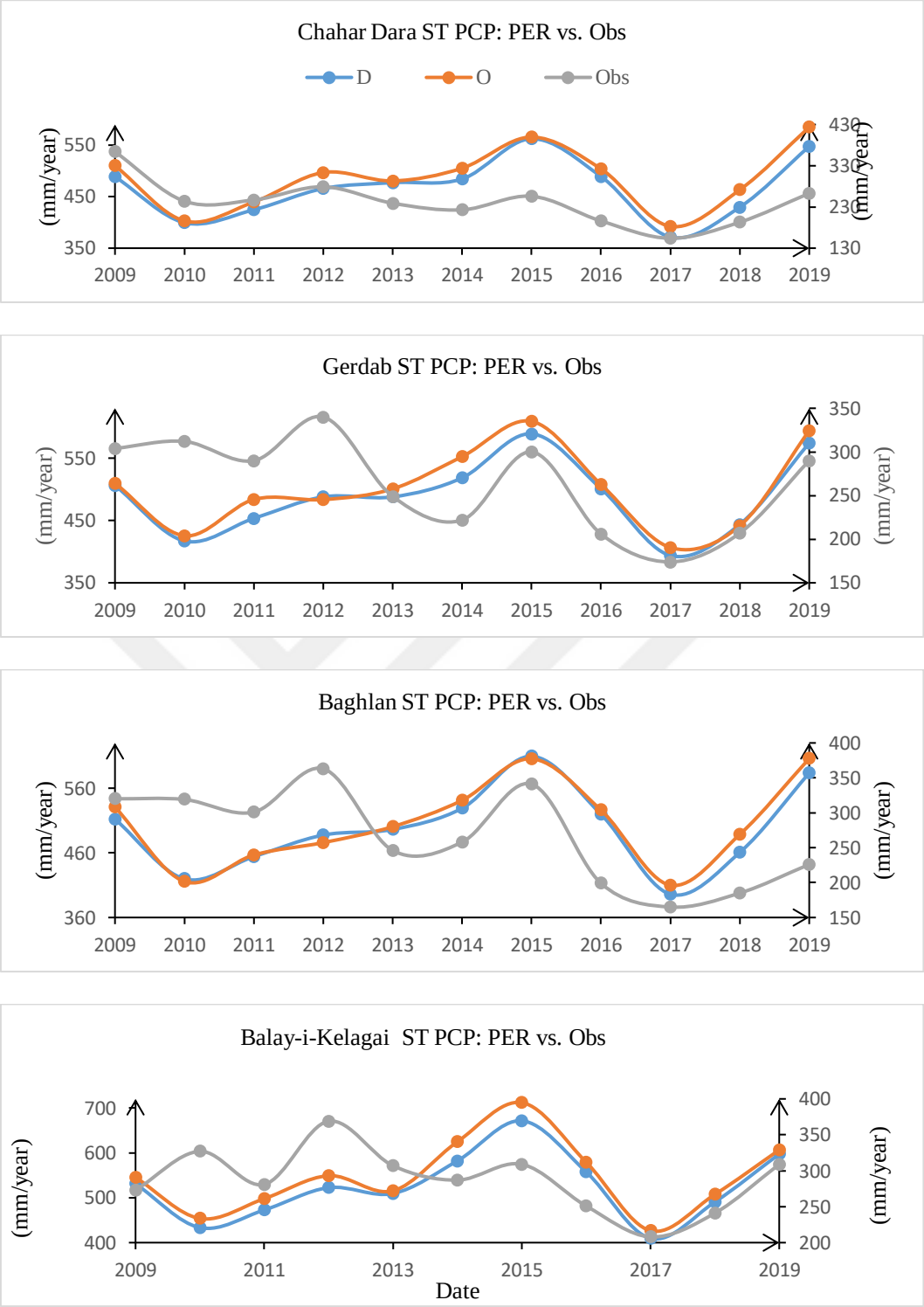

Figure 4.9 Comparison of Downscaled (D), Original (O), and Observed (Obs) Data PERSIANN (PER) Precipitation data



Figure 4.10 Comparison of Downscaled (D), Original (O), and Observed (Obs) Data PERSIANN (PER) Precipitation data

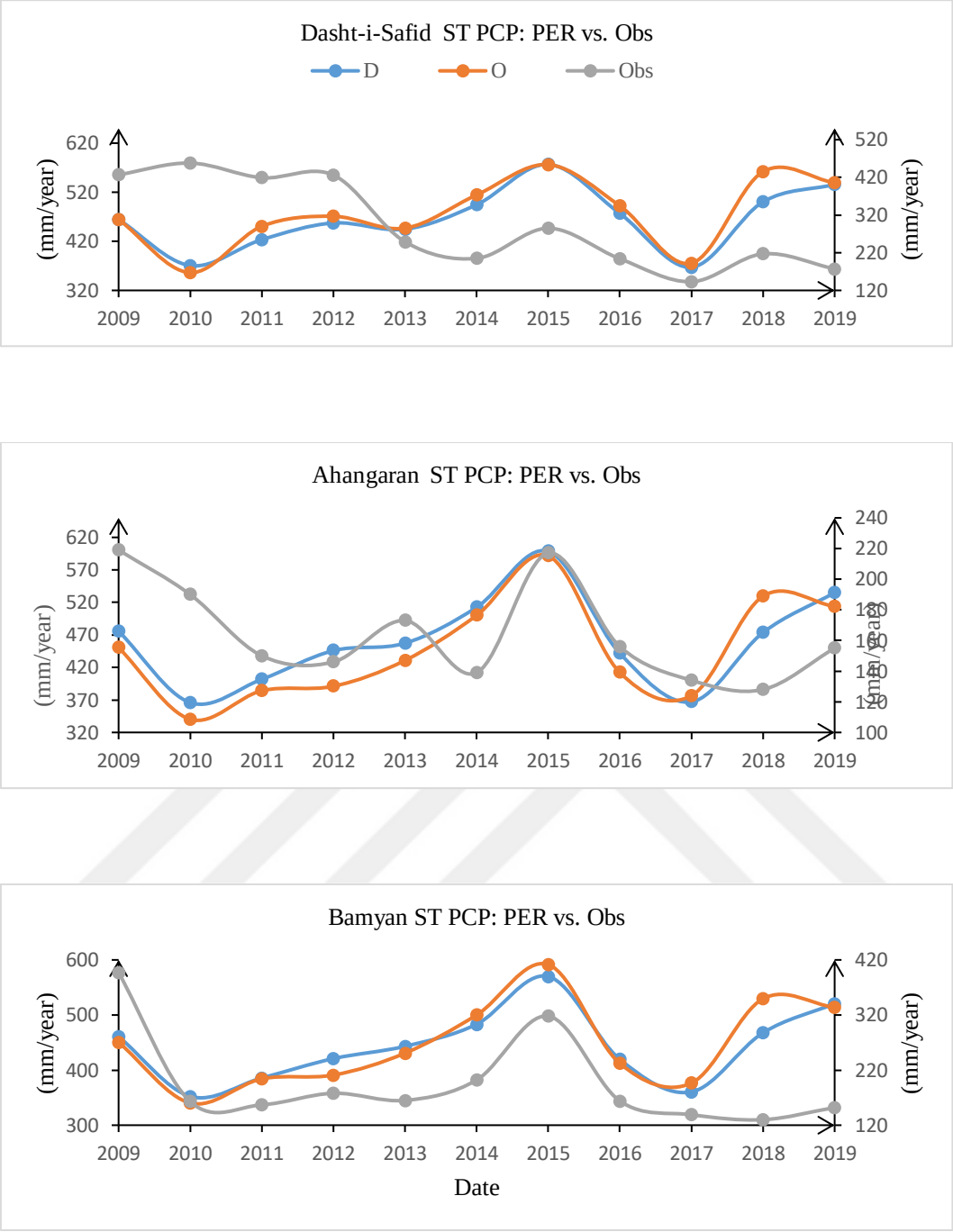

Figure 4.11 Comparison of Downscaled (D), Original (O), and Observed (Obs) Data PERSIANN (PER) Precipitation data

Table 4.4 Correlation assessment of PERSIANN (PER) RS based Downscaled (D), Original (O) vs Observed (Obs) precipitation.

Station#	PER D&O vs. Obs PCP		
	Data	D	O
1	D	1.00	
	O	0.98	1.00
	Obs	0.45	0.40
2	D	1.00	
	O	0.98	1.00
	Obs	0.35	0.30
3	D	1.00	
	O	0.98	1.00
	Obs	0.25	0.11
4	D	1.00	
	O	0.99	1.00
	Obs	0.31	0.30
5	D	1.00	
	O	0.99	1.00
	Obs	0.39	0.36
6	D	1.00	
	O	0.99	1.00
	Obs	0.44	0.38
7	D	1.00	
	O	1.00	1.00
	Obs	0.56	0.50
8	D	1	
	O	0.88	1
	Obs	-0.46	-0.13
9	D	1.00	
	O	0.96	1.00
	Obs	-0.34	-0.29
10	D	1.00	
	O	0.93	1.00
	Obs	0.33	0.18
11	D	1.00	
	O	0.95	1.00
	Obs	0.46	0.35

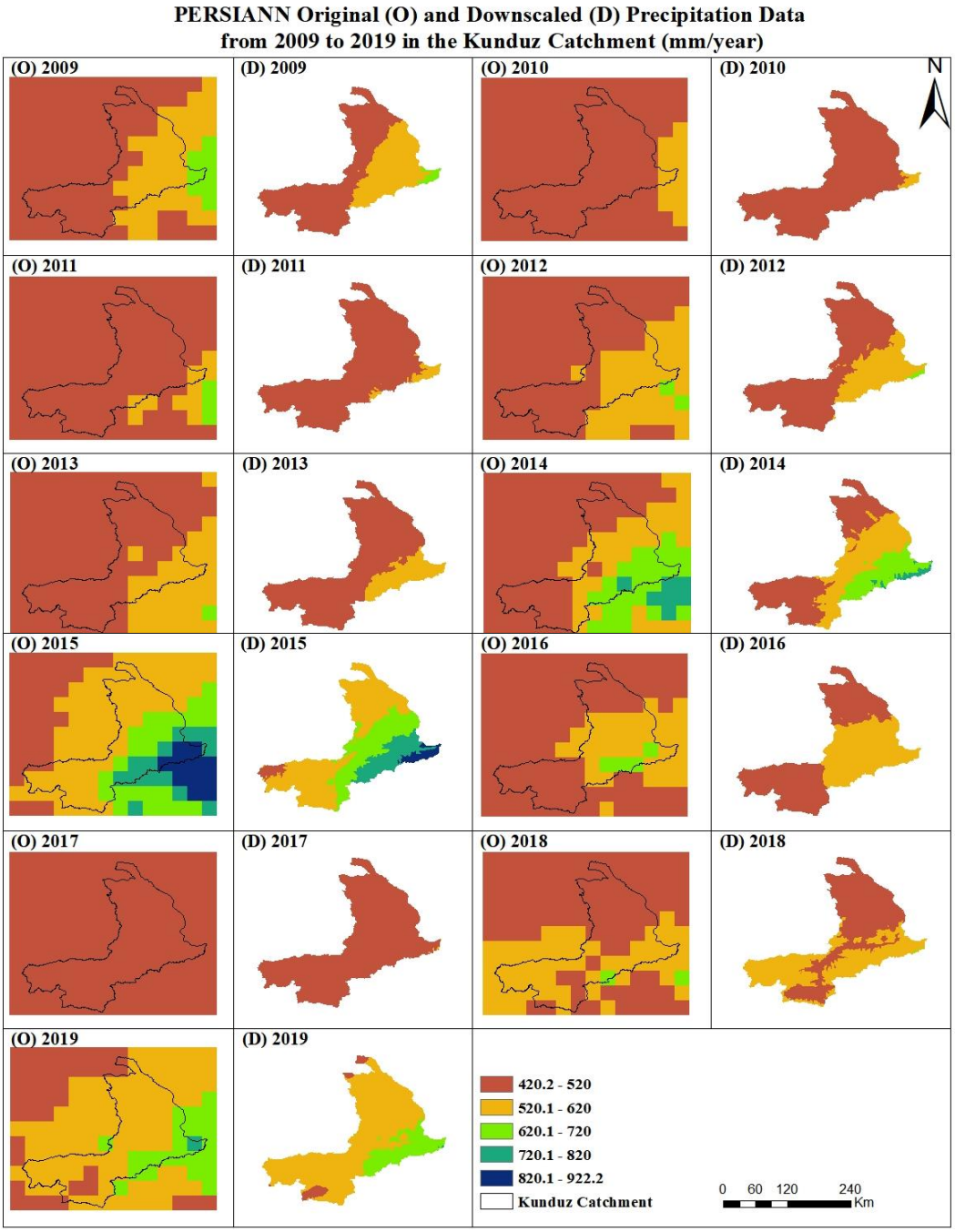

Figure 4.12 Original (O), Downscaled (D) PERSIANN Precipitation (PCP) data (mm/year)

Figure 4.12 presents a comprehensive analysis of PERSIANN precipitation data for the entire Kunduz catchment spanning from 2009 to 2019. Significant variations in precipitation levels are observed within both the DD and OD. The wettest year in the catchment, identified by the DD, was 2015, with annual precipitation values of 913.2 mm/year (high estimate) and 504.9 mm/year (low estimate. This designation

is supported by the OD, which also designates 2015 as the wettest year, recording high precipitation values of 922.2 mm/year (high estimate) and 420.2 mm/year (low estimate). In contrast, the analysis indicates that 2016 witnessed relatively lower precipitation levels, with annual precipitation values of 621.6 mm/year (high estimate) and 380.1 mm/year (low estimate) in the DD. Based on the DD, the driest year was 2011, with an annual precipitation value of 569.5 mm/year (high estimate) and 297.4 mm/year (low estimate). The OD designates 2011 as the driest year, with low precipitation values of 297.4 mm/year (low estimate). This analysis underscores the significance of precise data analysis in hydrological research within the Kunduz catchment.

The analysis of PERSIANN monthly median precipitation data, as presented in Figures 4.13 to 4.15 and Table 4.5, provides a comprehensive overview of precipitation levels across various stations within the Kunduz catchment during the study period from 2009 to 2019. Consistently across all stations which was explained in (Table 2.1), February stands out as the month with the highest median precipitation levels, ranging from approximately 68 mm/month to 123 mm/month. These observations underline February's status as the wettest month in the region and are consistent with patterns observed in the CHIRPS data. On the other hand, the months of June, July, August, and September consistently display a recurring pattern of zero median precipitation across all stations. This pattern is indicative of a dry spell characterized by an absence of median precipitation, as uniformly reported at all stations, including Chahar Dara, Gerdab, Baghlan, Balay-i-Kelagai, Doshi, Pul-i-Kundasang, Tang-i-Nahrin, Dasht-i-Safid, Doab, Ahangaran, and Bamyan, during these months. The remaining months, which include January, March, April, May, October, November, and December, consistently exhibit moderate median precipitation levels. These levels vary within the range of approximately 25 mm/month to 98 mm/month across the mentioned stations. This pattern of moderate median precipitation is observed at Chahar Dara, Gerdab, Baghlan, Balay-i-Kelagai, Doshi, Pul-i-Kundasang, Tang-i-Nahrin, Dasht-i-Safid, Doab, Ahangaran, and Bamyan, providing a comprehensive understanding of the hydroclimatic conditions in the Kunduz catchment over the specified study period.

Following this detailed exploration of monthly patterns, the analysis extends to encompass the seasonal variations in PERSIANN data across the entire catchment.

In this seasonal analysis, noteworthy disparities emerge among the various stations in the Kunduz catchment utilizing PERSIANN dataset. During the DJF season, Tang-i-Nahrin Station stands out as the top performer, recording the highest precipitation levels at 207.9 mm/season, surpassing all other stations. Conversely, Ahangaran station receives the least amount of precipitation during this season, with a total of only 129.3 mm/season, establishing its status as the most modest contributor among the stations. Intriguingly, the MAM season reveals a different scenario, with all stations in the Kunduz catchment experiencing a convergence in precipitation levels, ranging from 200 to 232.5 mm/season. Notably, Ahangaran and Bamyan stations deviate from this general trend, exhibiting distinct patterns in their precipitation levels.

Moving into JJA, a distinct reduction in precipitation levels becomes evident, with values ranging from 26.9 to 16.3 mm/season. This significant seasonal shift is particularly pronounced in Baghlan and Balay-i-Kelagai stations, signifying a substantial decrease in precipitation during this period.

Remarkably, as the SON season unfolds, the catchment witnesses an increase in precipitation levels. Doshi Station takes the lead, registering the highest level of precipitation at 73.6 mm/season, surpassing all other stations within the catchment. These findings furnish valuable insights into the dynamic patterns of precipitation across the Kunduz catchment. For a deeper understanding of the seasonal variations in PERSIANN data, Figure 4.16 and Table 4.6 comprehensively present the data categorized by station and season.

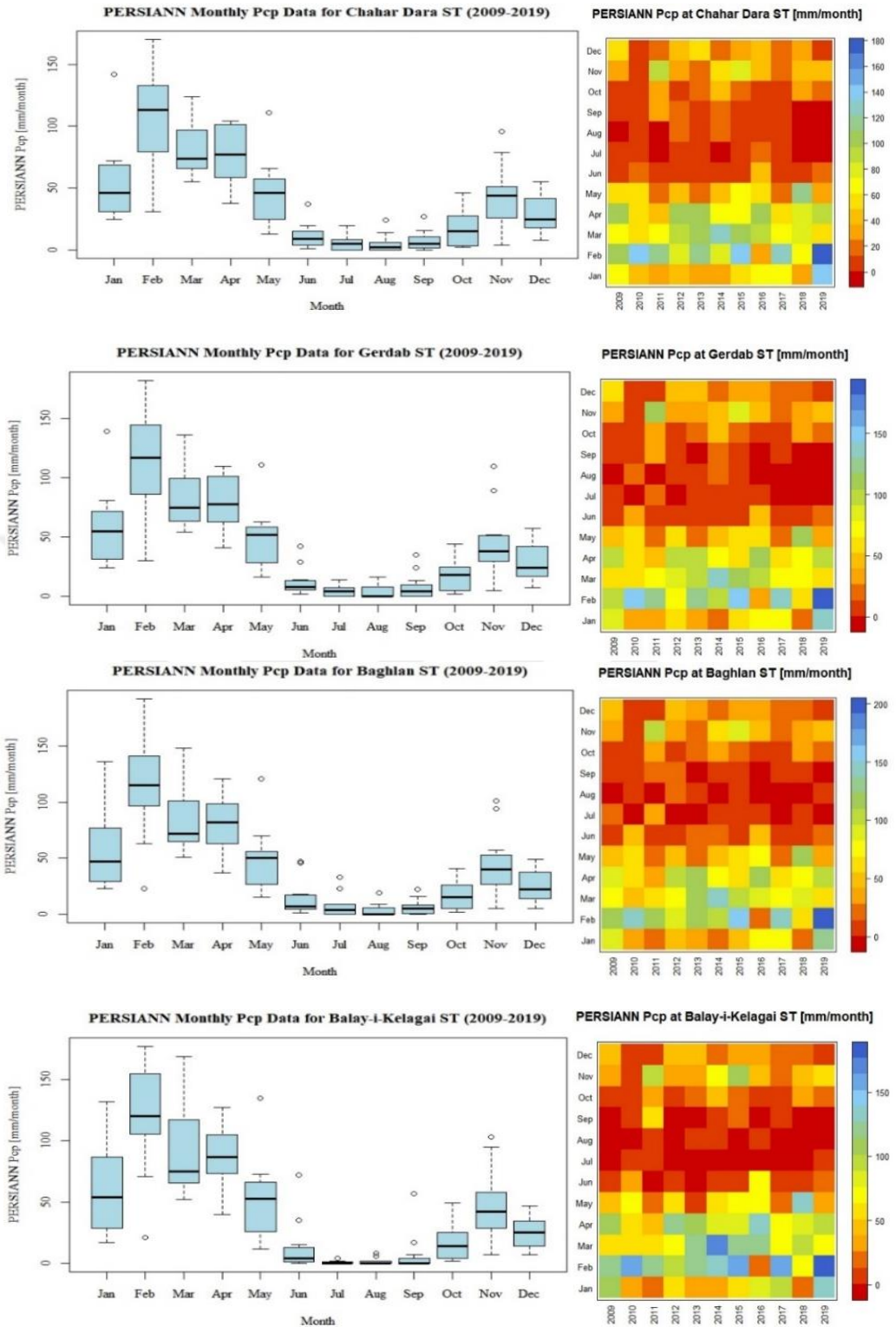

Figure 4.13 Monthly Variation of PERSIANN Precipitation (Downscaled) at Chahar Dara, Gerdab, Baghlan and Balay-i-Kelagai in the Kunduz Catchment from 2009 to 2019

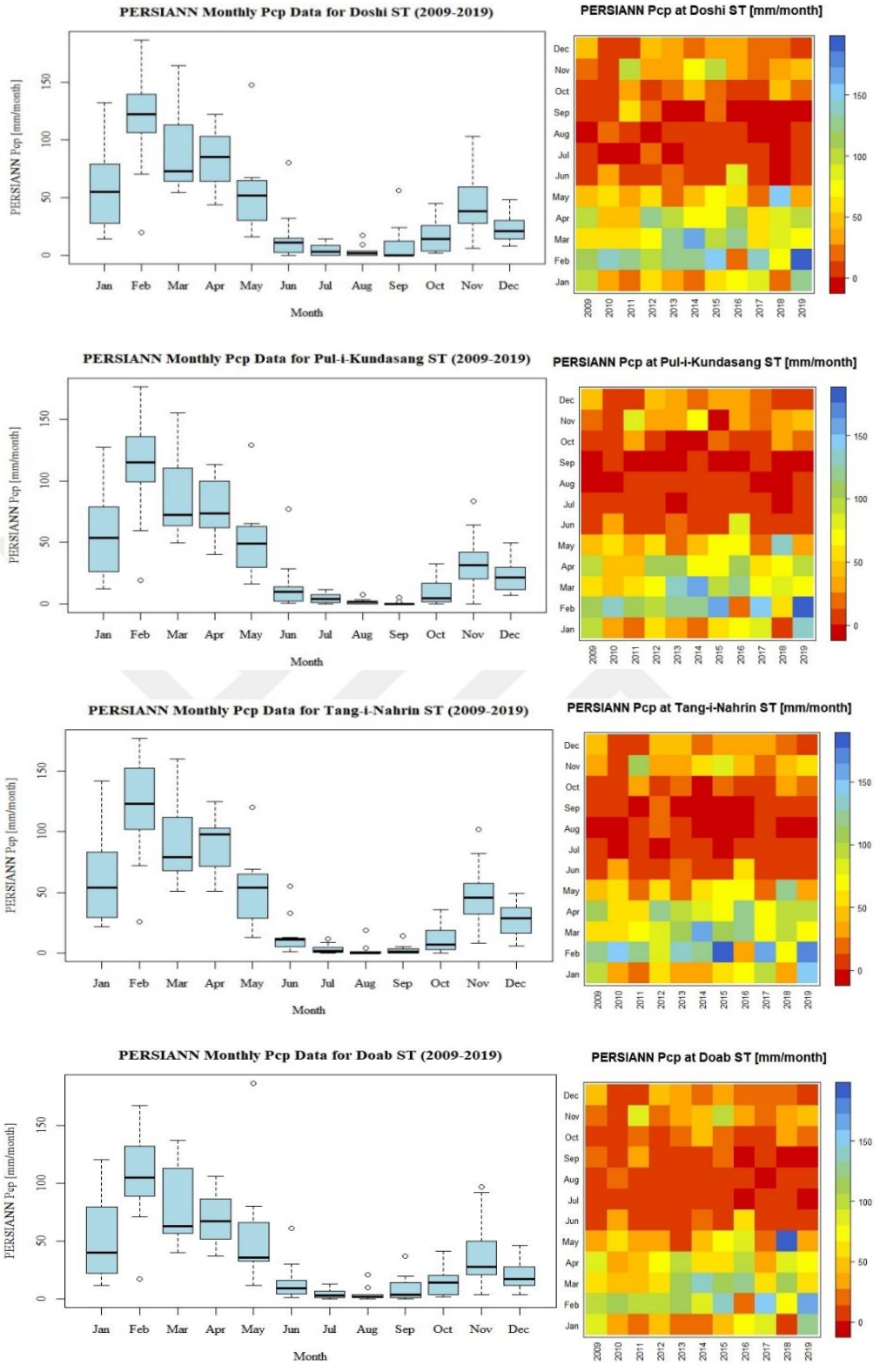

Figure 4.14 Monthly Variation of PERSIANN Precipitation (Downscaled) at Doshi, Pul-i-Kundasang, Tang-i-Nahrin and Doab Stations in the Kunduz Catchment from 2009 to 2019

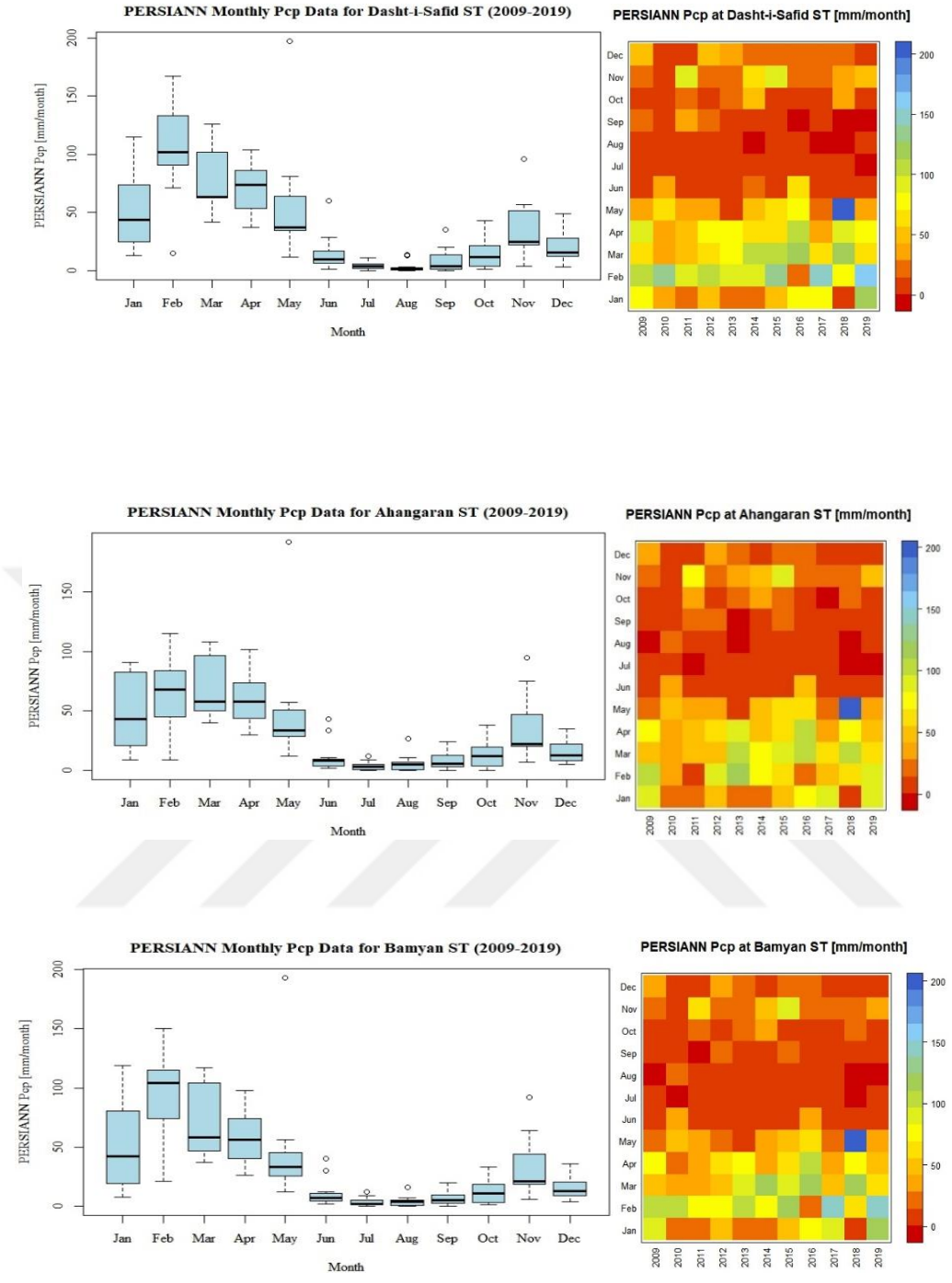

Figure 4.15 Monthly Variation of PERSIANN Precipitation (Downscaled) at Dasht-i-Safid, Ahangaran and Bamyan Stations in the Kunduz Catchment from 2009 to 2019

Table 4.5 PERSIANN Monthly Median Values Over Gauge Stations in Kunduz Catchment During 2009 to 2019.

ST#	Jan	Feb	Mar	Apr	May	Jun	Jul	Aug	Sep	Oct	Nov	Dec
1	46.0	113.0	74.0	77.0	46.0	9.0	5.0	2.0	5.0	15.0	44.0	25.0
2	55.0	117.0	75.0	78.0	52.0	8.0	4.0	0.0	4.0	18.0	38.0	24.0
3	47.0	115.0	72.0	82.0	50.0	7.0	4.0	0.0	5.0	15.0	40.0	22.0
4	54.0	120.0	75.0	87.0	53.0	4.0	0.0	0.0	0.0	14.0	42.0	25.0
5	55.0	122.0	73.0	85.0	52.0	11.0	3.0	2.0	0.0	14.0	38.0	21.0
6	53.7	114.0	93.3	73.8	49.1	10.2	3.9	1.6	0.0	4.4	31.7	21.8
7	54.0	123.0	79.0	98.0	54.0	11.0	2.0	0.0	1.0	7.0	46.0	29.0
8	44.0	102.0	63.0	74.0	37.0	10.0	4.0	1.0	4.0	12.0	25.0	16.0
9	40.0	105.0	63.0	67.0	36.0	9.0	3.0	2.0	4.0	14.0	28.0	17.0
10	43.0	68.0	58.0	58.0	34.0	8.0	3.0	5.0	6.0	12.0	22.0	13.0
11	42.0	104.0	58.0	56.0	33.0	7.0	2.0	4.0	5.0	11.0	21.0	13.0

Note: Table name and numbers explained in Table 2.1.

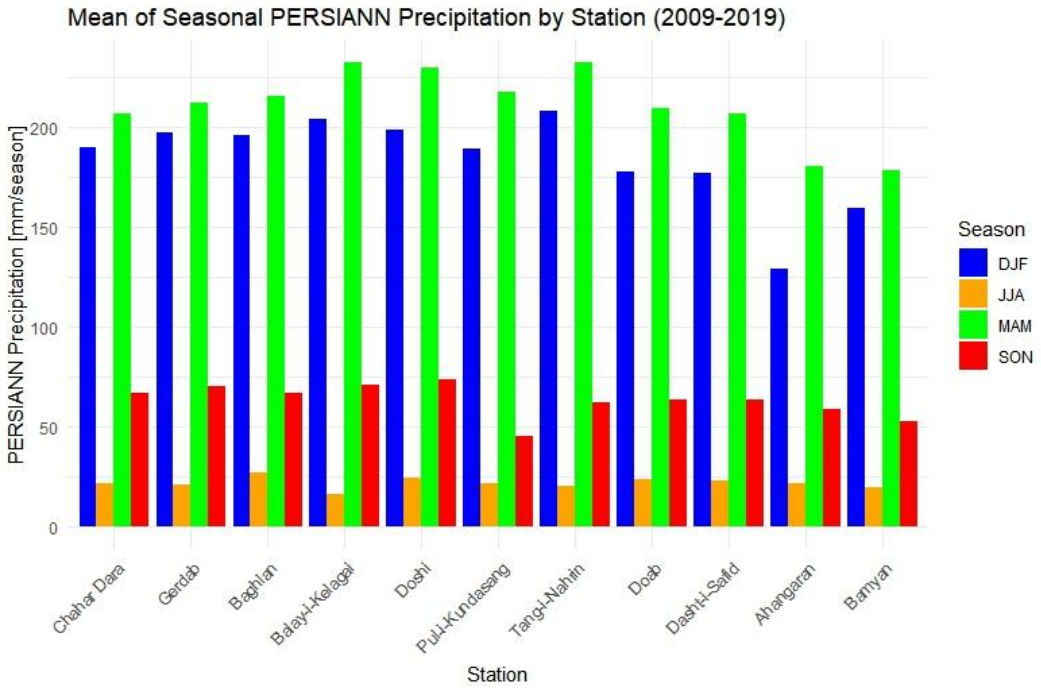

Figure 4.16 Seasonal (DJF, MAM, JJA, SON) Mean of Downscaled RS-Based PERSIANN (PER) Precipitation in Kunduz Catchment (2009-2019) by Station (mm/season)

Table 4.6 Seasonal Mean of Downscaled RS-Based PERSIANN (PER) Precipitation in Kunduz Catchment (2009-2019) by Station (mm/season).

Station	DJF	MAM	JJA	SON
Chahar Dara	189.6	206.7	22.0	67.3
Gerdab	197.5	212.4	21.4	70.6
Baghlan	195.6	215.6	26.9	67.2
Balay-i-Kelagai	204.3	232.5	16.3	71.3
Doshi	198.6	229.6	24.6	73.6
Pul-i-Kundasang	189.4	217.7	21.8	45.0
Tang-i-Nahrin	207.9	232.2	20.3	62.2
Doab	177.6	209.6	23.6	63.3
Dasht-i-Safid	177.1	206.9	23.2	63.6
Ahangaran	129.3	180.6	21.7	59.1
Bamyan	159.6	178.4	19.4	52.6

4.1.3 GLDA CLSM Precipitation

The study utilized CHIRPS and PERSIANN rainfall data and incorporated GLDAS CLSM precipitation to examine precipitation variations within the Kunduz catchment. Figures 4.17 to 4.19 provide a comparative analysis of annual mean precipitation values (mm/year) across various meteorological stations, comparing observed data Obs with the original dataset OD and the downscaled dataset DD. At Chahar Dara Station, the highest overestimation occurred in 2015, with observed data (256 mm/year), surpassing the OD (702 mm/year) and DD (642 mm/year). The lowest overestimation was observed in 2011, with observed data (247 mm/year), compared to the OD dataset (466 mm/year) and the DD (421 mm/year). Similarly, at Gerdab Station, the most substantial overestimation happened in 2015, with observed data (300 mm/year), while the OD (702 mm/year) and DD (654 mm/year) exhibited concurrent data. In 2014, the lowest overestimation was recorded, with observed data (222 mm/year), OD (496 mm/year), and DD (526 mm/year). At Baghlan station, the highest overestimation was in 2015, with observed data (341 mm/year), while the OD (702 mm/year) and DD (650 mm/year) registered higher values. The lowest overestimation occurred in 2018, with observed data (185 mm/year), original dataset (482 mm/year), and DD (443 mm/year). Furthermore, Balay-i-Kelagai Station experienced the highest overestimation in 2015, with

observed data (309 mm/year), exceeding the OD (630 mm/year) and DD (641 mm/year). In 2018, the lowest overestimation was observed, with observed data (241 mm/year), compared to the OD (427 mm/year) and DD (420 mm/year). In Figure 4.18, data from four GLDAS CLSM precipitation stations in the Kunduz catchment was analyzed. At the Doshi station, the data for 2019 was overestimated, with observed data (336 mm/year), surpassing the original dataset (553 mm/year) and DD (565 mm/year). In contrast, the data for 2017 was underestimated, with observed data (194 mm/year), while the OD (345 mm/year) and DD (384 mm/year) indicated lower values. At the Pul-i-Kundasang station, the data for 2019 was overestimated, with observed data (336 mm/year), exceeding the values in the original dataset (553 mm/year) and downscaled dataset (565 mm/year). Additionally, the data for 2017 was found to be underestimated, with observed data (194 mm/year), while the OD (345 mm/year) and DD (384 mm/year) indicated lower values. Moving to the Tang-i-Nahrin station, the data for 2015 was overestimated, with observed data (413 mm/year), surpassing the OD (640 mm/year) and DD (666 mm/year). In contrast, the data for 2010 was underestimated, with observed data (426 mm/year), while the OD (528 mm/year) and DD (496 mm/year) registered lower values. At Doab Station, the data for 2010 was overestimated, with observed data (453 mm/year), exceeding the values found in the OD (413 mm/year) and DD (350 mm/year). In contrast, the data for 2018 was underestimated, with observed data (166 mm/year), while the OD (427 mm/year) and downscaled dataset (430 mm/year) reported lower values. In Figure 4.19, Dasht-i-Safid Station showed overestimated data for 2019, with observed data (177 mm/year), surpassing the OD (513 mm/year) and DD (508 mm/year). The data for 2017 was underestimated, with observed data (143 mm/year), while the OD (357 mm/year) and DD (334 mm/year) recorded lower values. Ahangaran Station in 2015 experienced overestimation, with observed data (592 mm/year), exceeding the OD (468 mm/year) and DD (525 mm/year). In 2010, there was underestimation, with observed data (340 mm/year), while the OD (248 mm/year) and DD (331 mm/year) indicated lower values. Bamyan Station in 2019 encountered overestimation, with observed data (152 mm/year), surpassing the OD (423 mm/year) and DD (460 mm/year). In 2018, there was underestimation, with

observed data (130 mm/year), while the OD (439 mm/year) and DD (417 mm/year) reported lower values.

In Figure 4.20, an examination of the GLDAS precipitation data reveals the years with the highest and lowest precipitation estimates for the entire Kunduz catchment over the study period. Within the OD, the year with the most substantial precipitation estimate was 2015, characterized by a high estimate of 729.608 mm/year. In contrast, the DD pointed to 2019 as the wettest year, recording a high estimate of 680.185 mm/year. Conversely, when considering the years with the lowest precipitation estimates, both datasets concurred. In the OD, 2010 emerged as the driest year, depicting a low estimate of 240.895 mm/year. Similarly, within the DD, 2010 also marked the driest year, registering a low estimate of 264.987 mm/year. It is noteworthy that the determination of the wettest and driest years within the Kunduz catchment, based on the highest and lowest precipitation estimates, was subject to variation between the OD and DD. The OD identified 2015 as the wettest year, whereas the DD pointed to 2019. However, a consensus was reached for the driest year, as both datasets underscored 2010 as the year with the lowest precipitation estimates.

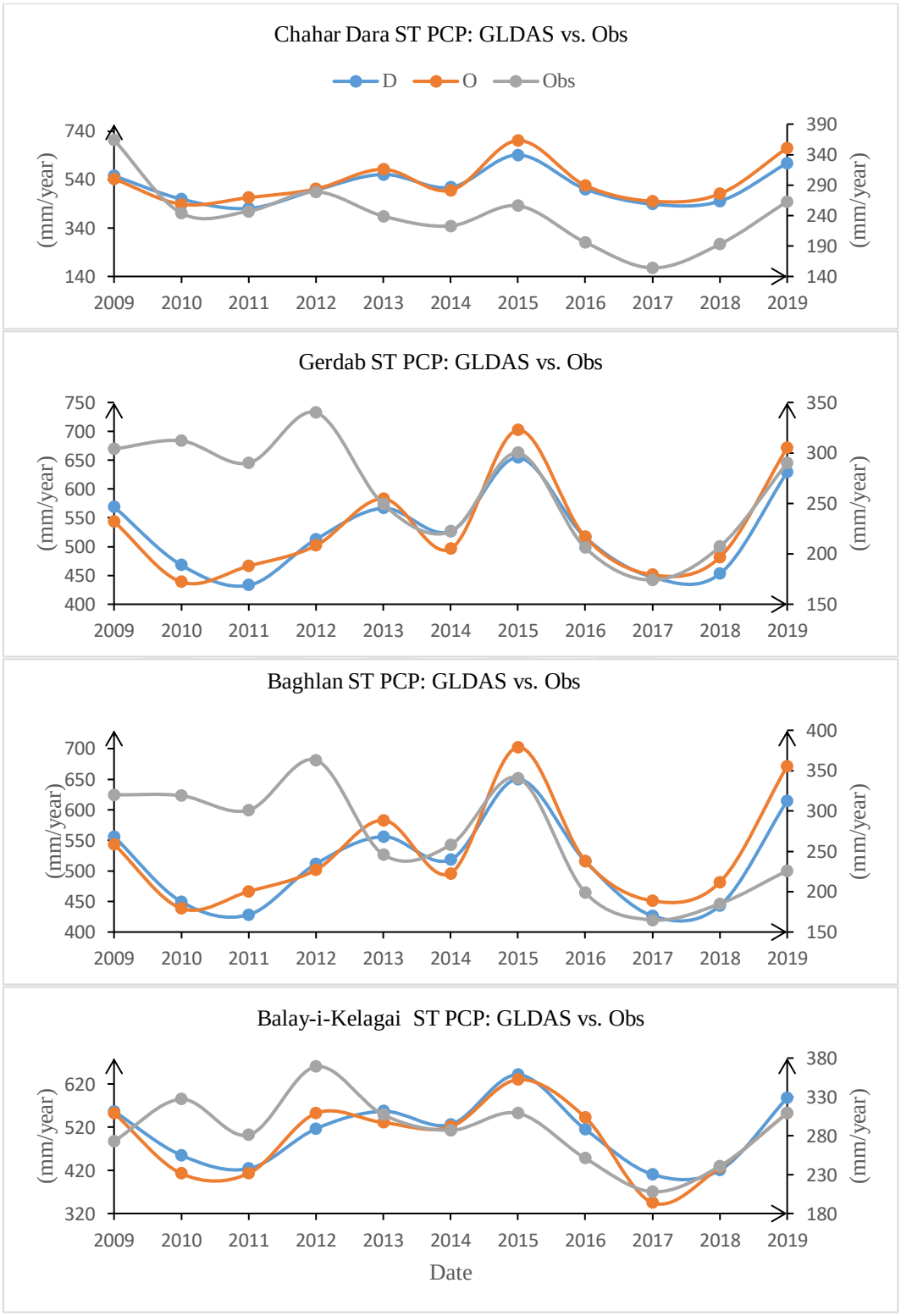

Figure 4.17 Comparison of Downscaled (D), Original (O), and Observed (Obs) Data GLDAS Precipitation data

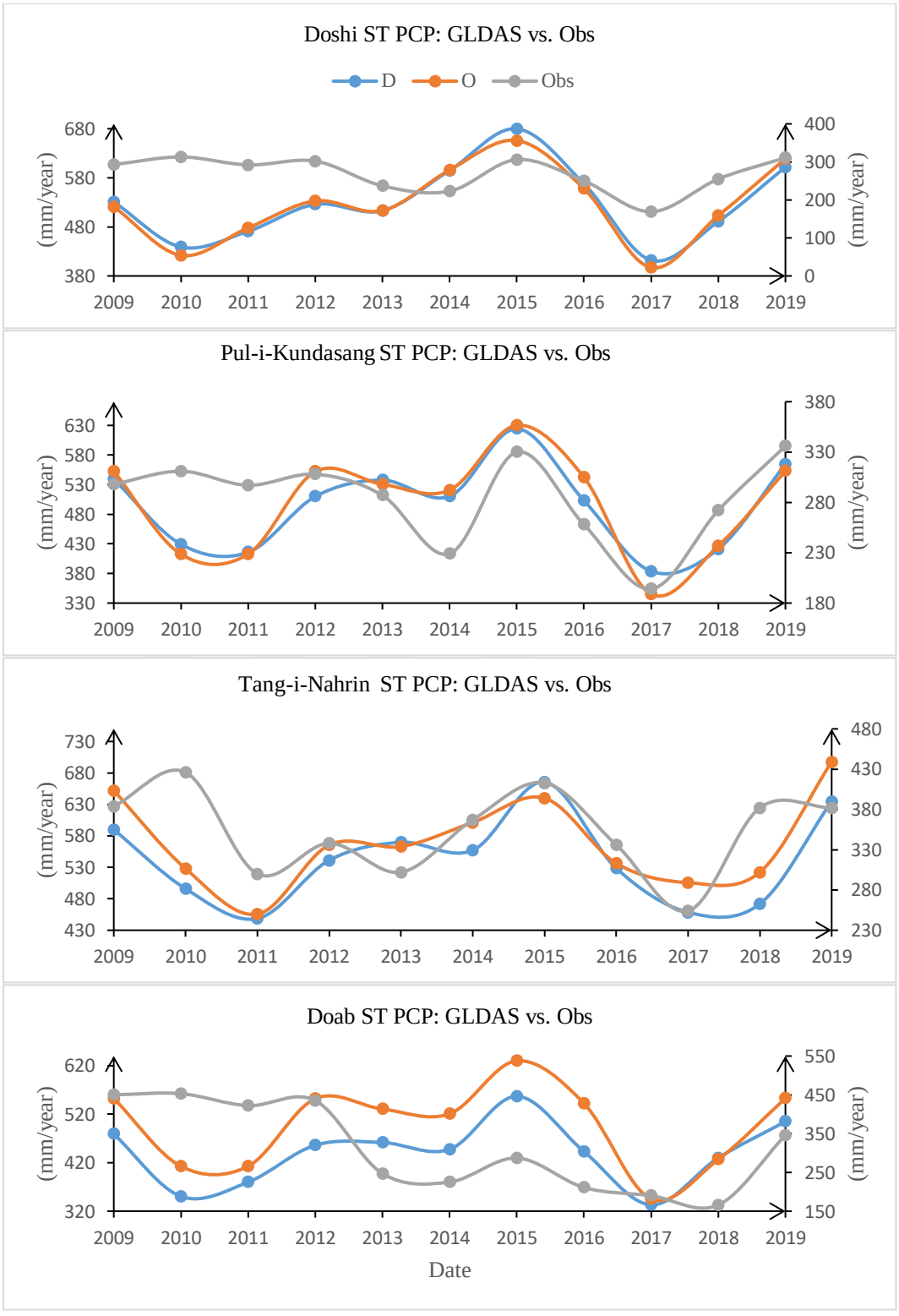

Figure 4.18 Comparison of Downscaled (D), Original (O), and Observed (Obs) Data GLDAS Precipitation data

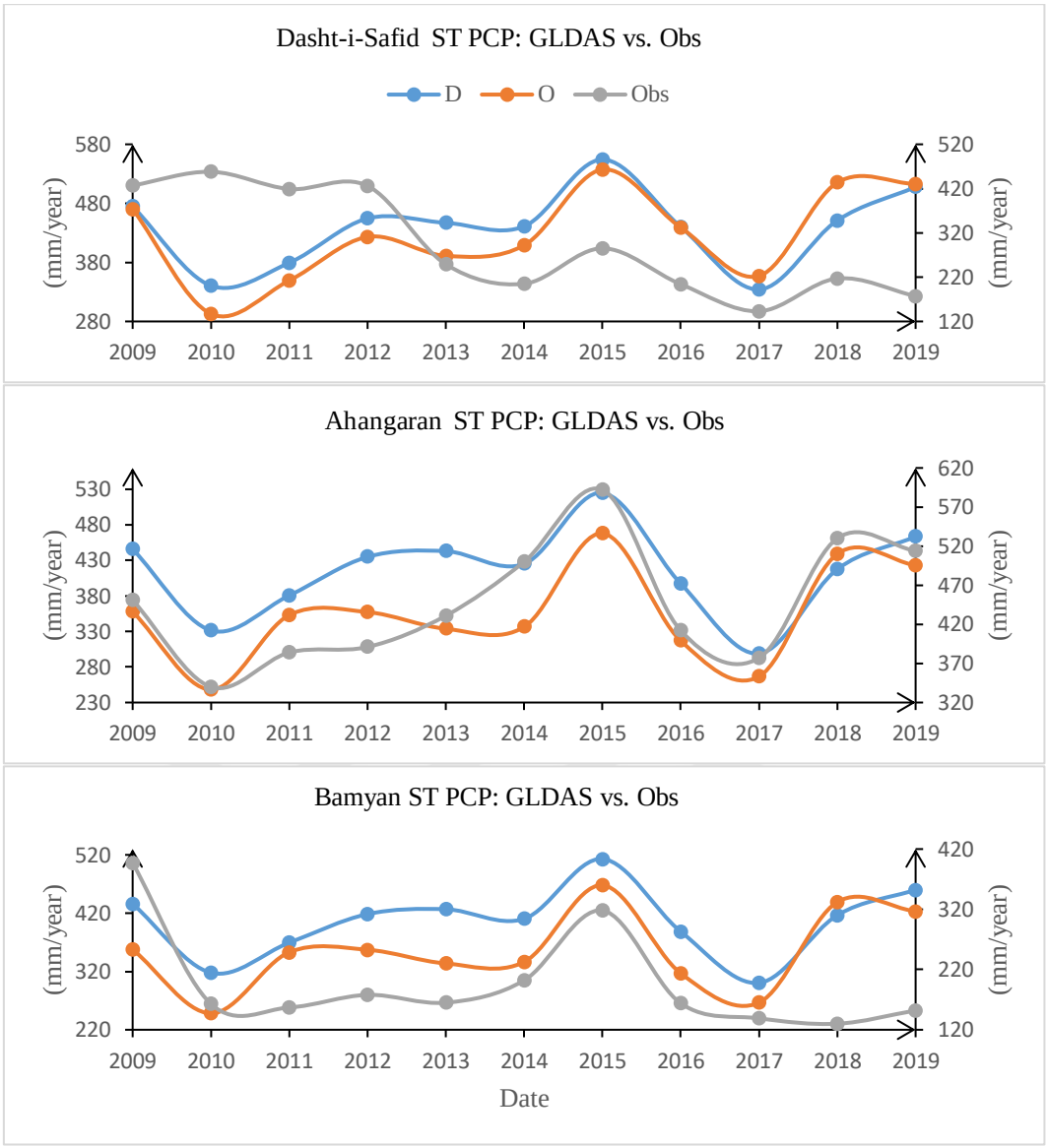

Figure 4.19 Comparison of Downscaled (D), Original (O), and Observed (Obs) Data GLDAS Precipitation data

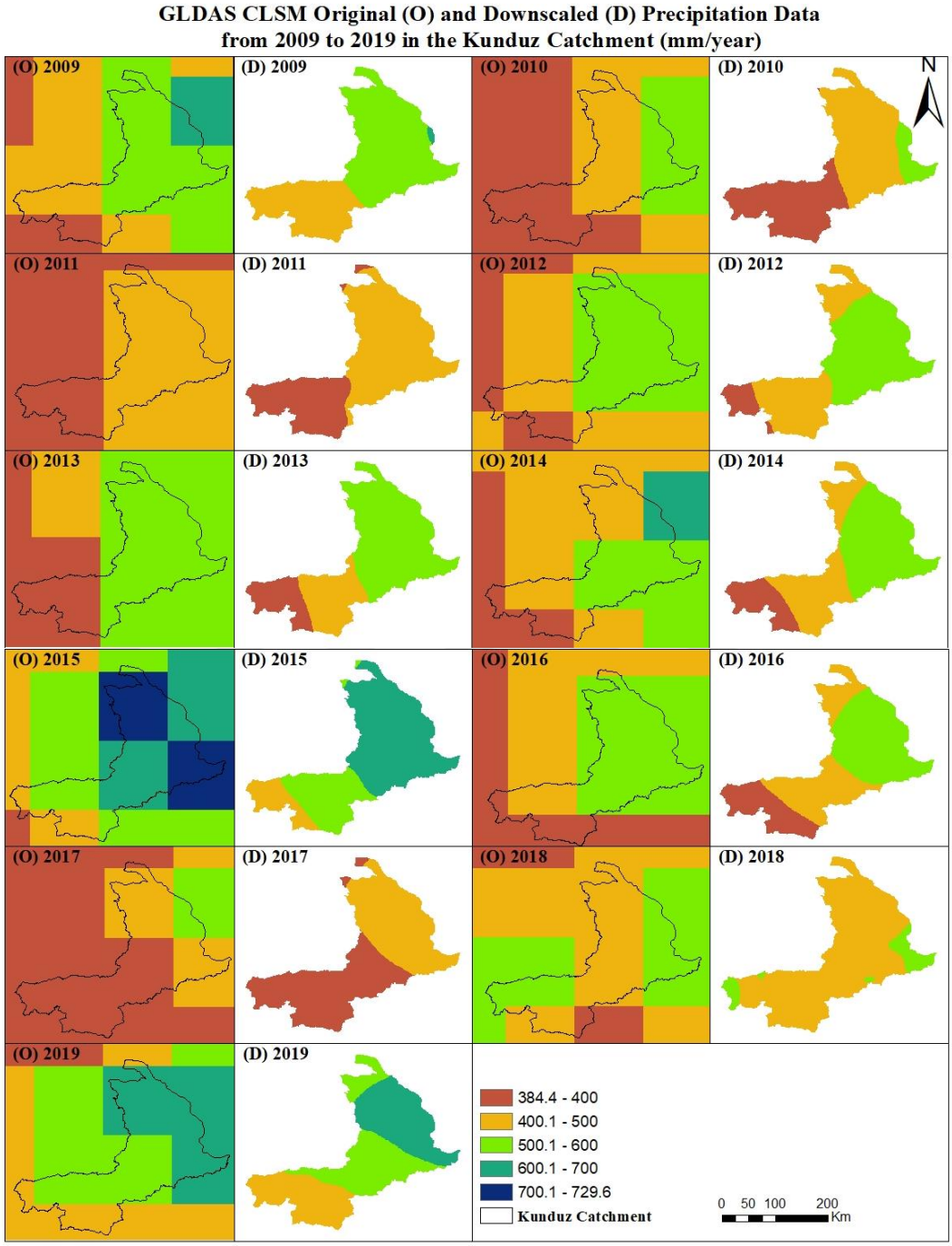

Figure 4.20 Original (O), Downscaled (D) GLDAS CLSM Precipitation data (mm/year)

Enhancements in the original dataset were investigated by performing a correlation analysis between the original and downscaled GLDAS CLSM data and gauge station data from 2009 to 2019 Table 4.7.

Table 4.7 Correlation assessment of GLDAS Downscaled (D), Original (O) vs Observed (Obs) precipitation.

Station#	GLDAS D&O vs. Obs PCP		
	Data	D	O
1	D	1.00	
	O	0.95	1.00
	Obs	0.46	0.34
2	D	1.00	
	O	0.95	1.00
	Obs	0.35	0.29
3	D	1.00	
	O	0.95	1.00
	Obs	0.30	0.17
4	D	1.00	
	O	0.94	1.00
	Obs	0.51	0.47
5	D	1.00	
	O	0.95	1.00
	Obs	0.46	0.42
6	D	1.00	
	O	0.97	1.00
	Obs	0.56	0.54
7	D	1.00	
	O	0.92	1.00
	Obs	0.53	0.50
8	D	1.00	
	O	0.94	1.00
	Obs	0.12	-0.01
9	D	1.00	
	O	0.90	1.00
	Obs	-0.35	-0.15
10	D	1.00	
	O	0.84	1.00
	Obs	0.88	0.80
11	D	1.00	
	O	0.87	1.00
	Obs	0.52	0.29

In Table 4.7 it is revealed that the highest correlation between (D) and observed (Obs) data was found at station number 6, with a correlation coefficient of 0.56. Similarly, station #6 (Pul-i-Kundasang) exhibited the second-highest correlation

when comparing (O) data with observed data (0.54). Furthermore, station #7 (Tang-i-Nahrin) showed the second-highest positive correlation of 0.53 between downscaled and observed data. Conversely, station #9 (Dasht-i-Safid) displayed a negative correlation, indicating a strong negative relationship, with downscaled data exhibiting a negative correlation coefficient of -0.35 when compared to observed data. The correlation between original and downscaled data was consistently strong, falling within the range of 0.8 to 0.9. This signifies a robust positive relationship between the two datasets.

In the monthly median analysis results, illustrated in Figure 4.21 to Figure 4.23 it was consistently observed across all stations in the Kunduz catchment that the month of February exhibited the highest median precipitation, with values ranging from approximately 68 mm/month to 129 mm/month. This observation suggests that February typically witnesses the highest levels of median precipitation in the region, and this trend agrees with the data from stations like Tang-i-Nahrin, which consistently reported the highest median precipitation levels.

Conversely, the months of June, July, August, and September consistently recorded zero median precipitation across all stations. These months are indicative of a dry spell characterized by a lack of median precipitation, as values of 0 mm/month were reported at all stations during this period.

For the remaining months, namely January, March, April, May, October, November, and December, moderate median precipitation levels were observed. Values during these months ranged from approximately 51 mm/month to 93 mm/month. While some variability was noted among stations, these months generally exhibited moderate levels of median precipitation in the Kunduz catchment. Stations such as Chahar Dara, Baghlan, Balay-i-Kelagai, Doshi, Pul-i-Kundasang, Dasht-i-Safid, Doab, and Ahangaran contributed to this observation, highlighting a pattern of moderate median precipitation throughout these months.

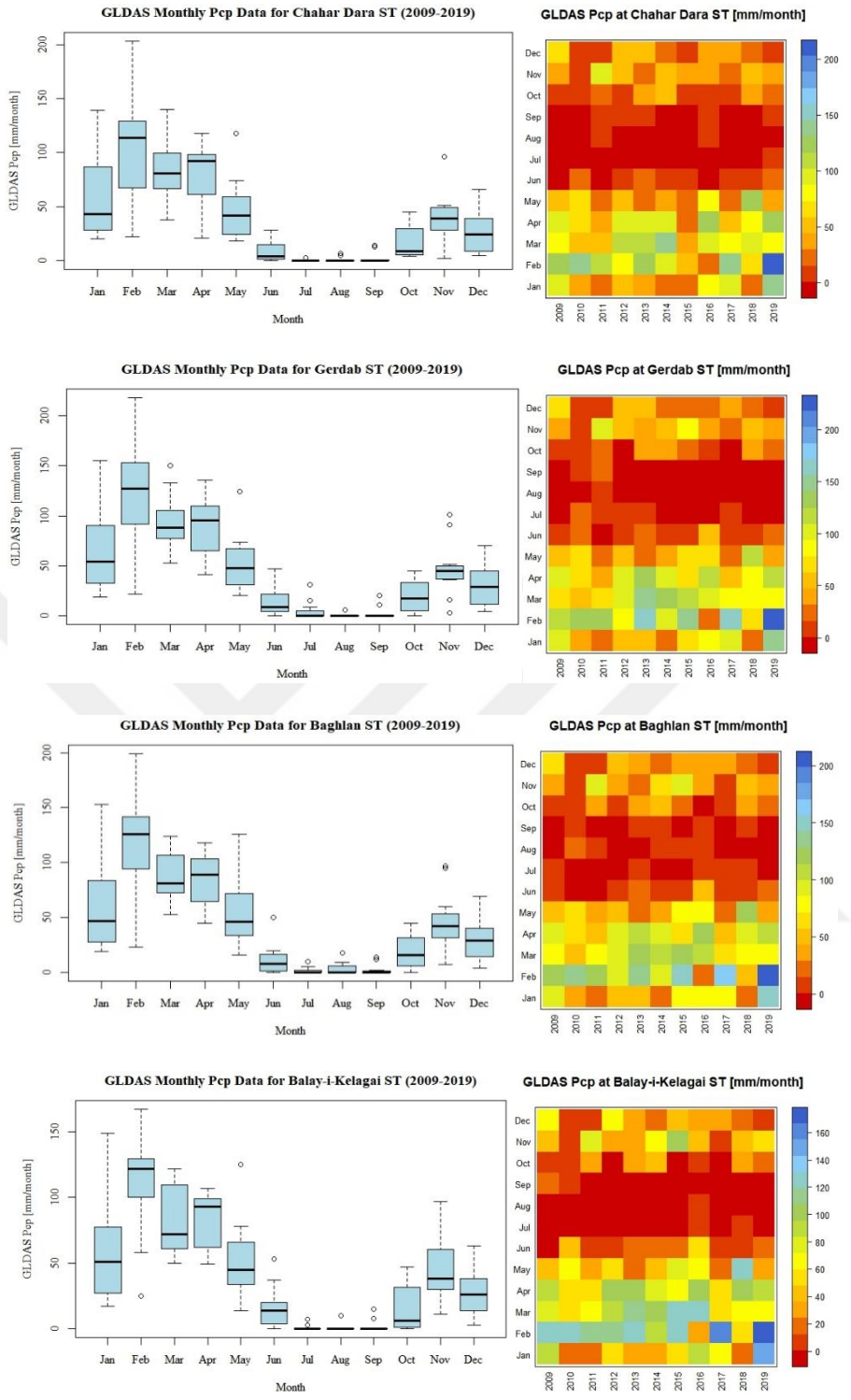

Figure 4.21 Monthly Variation of GLDAS CLSM Precipitation (Downscaled) at Chahar Dara, Gerdab, Baghlan and Balay-i-Kelagai Stations in the Kunduz Catchment from 2009 to 2019

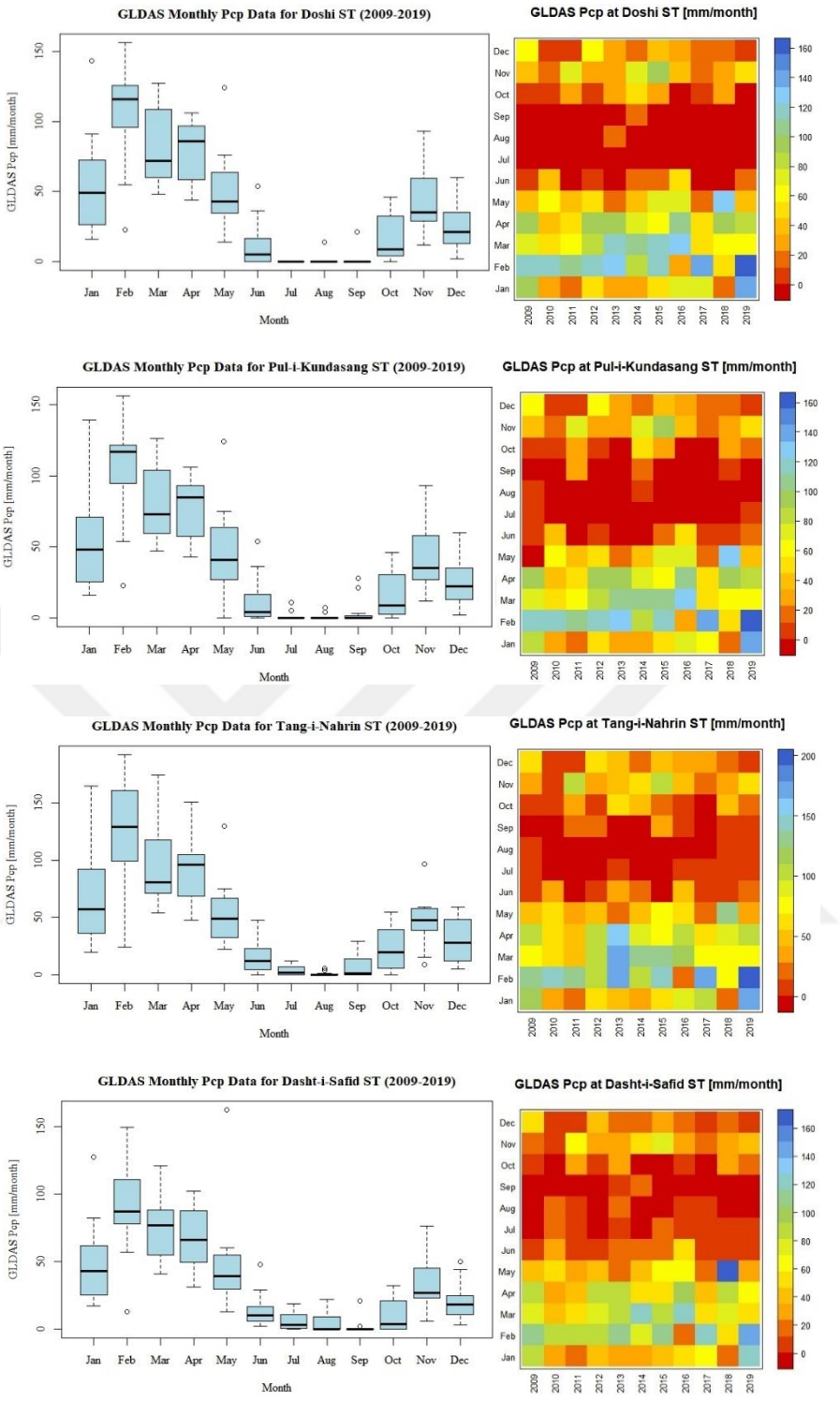

Figure 4.22 Monthly Variation of GLDAS CLSM Precipitation (Downscaled) at Doshi, Pul-i-Kundasang, Tang-i-Nahrin and Dasht-i-Safid Stations in the Kunduz Catchment from 2009 to 2019

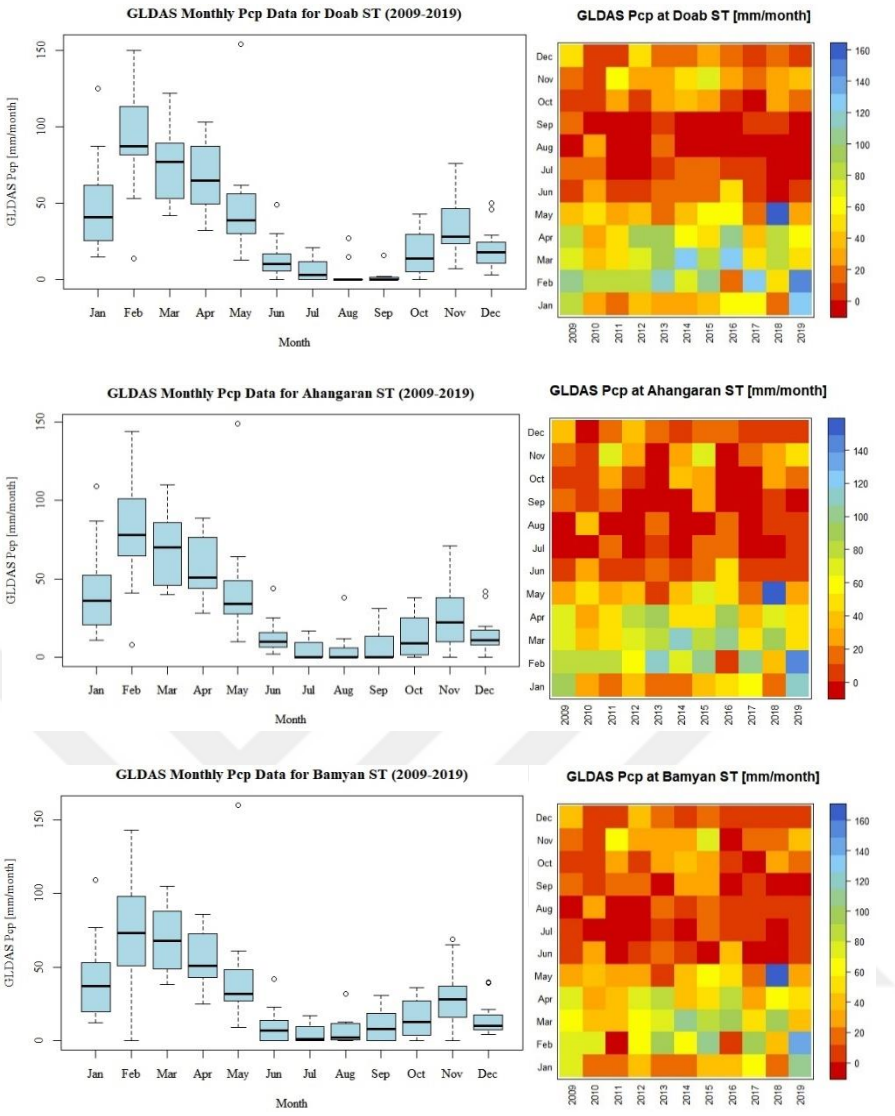

Figure 4.23 Monthly Variation of GLDAS CLSM Precipitation (Downscaled) at Doshi, Pul-i-Kundasang, Tang-i-Nahrin and Dasht-i-Safid Stations in the Kunduz Catchment from 2009 to 2019

In the analysis of the GLDAS CLSM seasonal data for various stations within the Kunduz catchment, several distinct patterns emerge. The results, presented in terms of the four seasons (DJF - Winter, MAM - Spring, JJA - Summer, SON - Autumn), reveal important insights into the precipitation characteristics in this region Figure 4.24 and Table 4.9. At the Chahar Dara station, the seasonal analysis indicates that the highest precipitation occurs during the MAM (Spring) season, with an average of approximately 210.36 mm per season. In contrast, the JJA (Summer) season experiences significantly lower precipitation, with an average of merely 10.00 mm

per season. This suggests a notable variation in seasonal precipitation, with Spring being the wettest season and Summer the driest.

Table 4.8 GLDAS CLSM Monthly Median Values Over Gauge Stations in Kunduz Catchment During 2009 to 2019.

ST#	Jan	Feb	Mar	Apr	May	Jun	Jul	Aug	Sep	Oct	Nov	Dec
1	43.0	114.0	81.0	92.0	42.0	4.0	0.0	0.0	0.0	9.0	39.0	24.0
2	54.0	127.0	88.0	95.0	48.0	9.0	0.0	0.0	0.0	17.0	45.0	29.0
3	47.0	126.0	81.0	89.0	46.0	8.0	0.0	0.0	0.0	16.0	42.0	29.0
4	51.0	122.0	72.0	93.0	45.0	14.0	0.0	0.0	0.0	6.0	38.0	26.0
5	49.0	116.0	72.0	86.0	43.0	5.0	0.0	0.0	0.0	9.0	35.0	21.0
6	48.0	117.0	73.0	85.0	41.0	4.0	0.0	0.0	0.0	9.0	35.0	22.0
7	57.0	129.0	81.0	96.0	49.0	12.0	2.0	0.0	1.0	20.0	48.0	28.0
8	43.0	87.0	77.0	66.0	39.0	10.0	3.0	0.0	0.0	4.0	27.0	18.0
9	41.0	87.0	77.0	65.0	39.0	10.0	3.0	0.0	0.0	14.0	28.0	18.0
10	36.0	78.0	70.0	51.0	34.0	10.0	0.0	0.0	0.0	9.0	22.0	11.0
11	37.0	73.0	68.0	51.0	32.0	7.0	1.0	2.0	8.0	13.0	28.0	10.0

Note: Table name and numbers explained in Table 2.1.

Moving to Gerdab station, a similar pattern is observed. The MAM (Spring) season continues to exhibit the highest precipitation levels, averaging around 235.91 mm per season. Conversely, the JJA (Summer) season records the lowest precipitation, with an average of 20.45 mm per season. This consistent pattern aligns with the broader seasonal climate trends in the region.

At the Baghlan station, the data demonstrates a parallel trend. The MAM (Spring) season is the wettest, with an average of approximately 226.64 mm per season. Similarly, the JJA (Summer) season exhibits the least precipitation, averaging 17.55 mm per season. This seasonal contrast is characteristic of many regions with distinct wet and dry periods.

Balay-i-Kelagai also follows this trend, with the MAM (Spring) season registering the highest average precipitation at 217.27 mm per season, while the JJA (Summer) season reports the lowest, with an average of 18.09 mm per season. This consistency in seasonal precipitation patterns reflects the larger climatic influences within the Kunduz catchment. Doshi station demonstrates a comparable pattern, with the MAM (Spring) season as the wettest, recording an average of

approximately 211.00 mm per season, and the JJA (Summer) season as the driest, with an average of 14.36 mm per season. These findings align with the anticipated seasonal fluctuations in precipitation. Pul-i-Kundasang station exhibits a similar trend, with the MAM (Spring) season experiencing the highest precipitation at an average of 204.00 mm per season, while the JJA (Summer) season encounters the lowest, with an average of 15.27 mm per season. These consistent patterns provide a valuable understanding of the seasonal dynamics. Tang-i-Nahrin station reports the highest average precipitation during the MAM (Spring) season, with approximately 241.73 mm per season, while the JJA (Summer) season witnesses the lowest precipitation, averaging 20.64 mm per season. These findings align with established climatic patterns for the region. Dasht-i-Safid station demonstrates a distinct pattern, with the JJA (Summer) season exhibiting the highest average precipitation, approximately 25.64 mm per season, while the DJF (Winter) season records the lowest, with an average of 160.09 mm per season. This unexpected seasonal distribution highlights the unique climate of the station. The Doab station data also deviates from the typical pattern, with the JJA (Summer) season experiencing the highest average precipitation at 25.09 mm per season, and the DJF (Winter) season reporting the lowest, averaging 160.36 mm per season. This distinctive pattern underscores the local climate's nuances. At the Ahangaran station, the MAM (Spring) season stands out with the highest average precipitation of approximately 173.00 mm per season, while the JJA (Summer) season registers the lowest, averaging 24.18 mm per season. These findings provide insights into the station's unique precipitation dynamics. Finally, the Bamyan station presents the highest average precipitation during the MAM (Spring) season, with approximately 170.36 mm per season, while the JJA (Summer) season reports the lowest, with an average of 22.27 mm per season. These results align with broader seasonal climatic patterns. the seasonal analysis of GLDAS CLSM data across various Kunduz catchment stations unveils consistent trends in the seasonal distribution of precipitation. The MAM (Spring) season consistently records the highest levels of precipitation, while the JJA (Summer) season consistently experiences the lowest. These findings contribute to a deeper understanding of the climatic dynamics within the Kunduz catchment area and are valuable for local water resource management and planning.

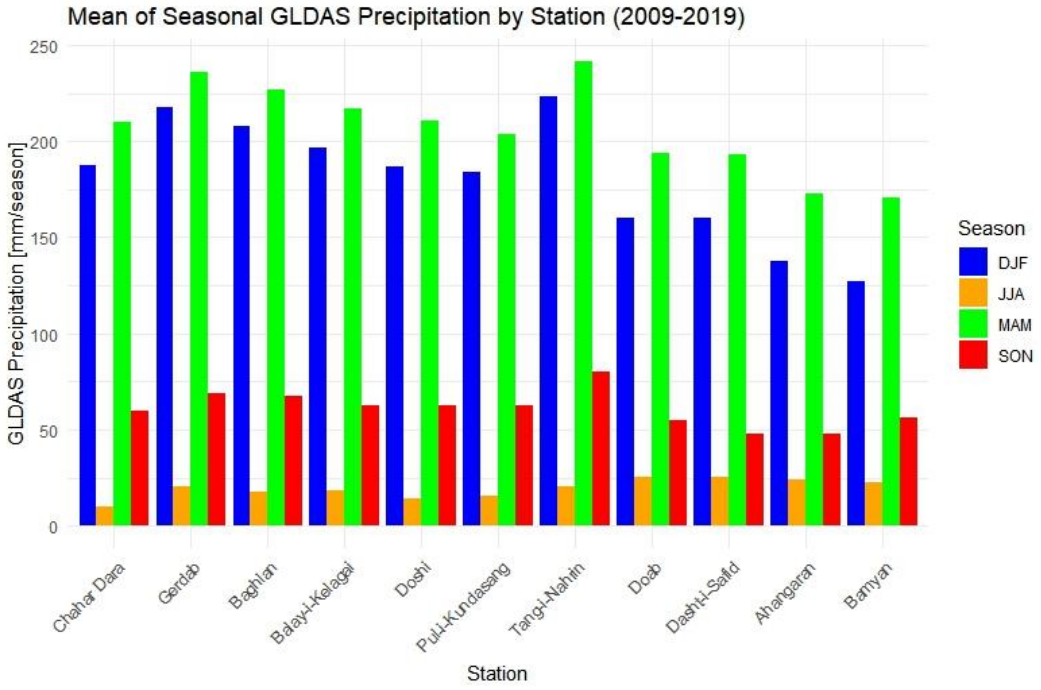

Figure 4.24 Seasonal (DJF, MAM, JJA, SON) Mean of Downscaled GLDAS CLSM Precipitation in Kunduz Catchment (2009-2019) by Station (mm/season)

Table 4.9 Seasonal Mean of Downscaled RS-Based GLDAS CLSM Precipitation in Kunduz Catchment (2009-2019) by Station (mm/season).

Station	DJF	MAM	JJA	SON
Chahar Dara	189.6	206.7	22	67.3
Gerdab	197.5	212.4	21.4	70.6
Baghlan	195.6	215.6	26.9	67.2
Balay-i-Kelagai	204.3	232.5	16.3	71.3
Doshi	198.6	229.6	24.6	73.6
Pul-i-Kundasang	189.4	217.7	21.8	45
Tang-i-Nahrin	207.9	232.2	20.3	62.2
Doab	177.6	209.6	23.6	63.3
Dasht-i-Safid	177.1	206.9	23.2	63.6
Ahangaran	129.3	180.6	21.7	59.1
Bamyan	159.6	178.4	19.4	52.6

The discussion of results, as evidenced in the analysis of CHIRPS, PERSIANN, and GLDAS CLSM datasets, reveals shared patterns and disparities in precipitation overestimations and seasonal variations within the Kunduz catchment. A consistent

theme across all three datasets is the overestimation of precipitation compared to observed values, aligning with findings in numerous global studies [15, 18, 25].

The wettest year in the CHIRPS dataset is identified as 2019 show good agreement with [77], characterized by notably higher rainfall volume within the catchment. In contrast, both 2015 and 2019 are emphasized as the wettest years in the PERSIANN dataset, reflecting elevated precipitation levels during these periods. Notably, the years 2011 and 2012 are concurred upon as the driest years in both CHIRPS and PERSIANN datasets, signifying a robust characterization of years with limited rainfall, consistent with a recent study published in 2023 [165].

In simple contrast, the GLDAS CLSM dataset indicates that 2019 received the most rainfall which is consistent with this study finding as there was a flash flood in Kunduz catchment during 2019 based on the report [166], followed by 2015 and 2014. However, this dataset exhibits notable discrepancies, including instances of both overestimations and underestimations, underscoring the inherent variations in precipitation estimates among different years. The overestimation of observed data is a common phenomenon in scientific research, with variations often attributed to the differences between satellite-derived data and ground-based observations. In the context of the Kunduz catchment, additional factors such as the geographical location and data quality contribute to the underestimation of precipitation. The gauge stations have been operational since 2008, facing intermittent challenges related to electricity supply and personnel training, which can impact data quality. Furthermore, the scarcity of observation stations in relation to the catchment's size introduces a limitation in data collection, further complicating the accurate characterization of precipitation. Significant heterogeneity in precipitation and temperature within the Kunduz catchment can be primarily attributed to its extensive elevation range, as depicted in Figure 2.1. According to the Köppen–Geiger climate classification scheme, the Kunduz Catchment is predominantly characterized by a mid-latitude steppe climate (Bsk), signifying a cold semi-arid climate, with some regions influenced by a Mediterranean-influenced subarctic climate (Dsc). Notably, low precipitation levels characterize the months of September, marked by scant rainfall. Conversely, most of the annual precipitation is concentrated between January and April at the Kunduz station, aligning with the

study's findings, which indicate that February consistently receives the highest amount of rainfall during the entire study period, based on data from three precipitation datasets: CHIRPS, PERSIANN, and GLDAS CLSM.

Consistently, monthly precipitation patterns emphasize February as the month with the highest recorded precipitation levels across all monitoring stations. In stark contrast, a prolonged dry period, devoid of recorded precipitation, collectively spans the months from June through September, aligning with the climatic characteristics of the Kunduz catchment as expounded upon by reference [77]. This concurrence highlights the data's reliability, as it harmonizes with the established climate patterns within the region.

Variations in precipitation levels are observed across monitoring stations in all datasets during different seasons. The DJF (Winter) season consistently records the highest precipitation levels across all datasets, albeit with station-specific nuances. In the MAM (Spring) season, CHIRPS and PERSIANN data show relatively uniform precipitation levels among most stations, while the GLDAS CLSM dataset displays distinct patterns. In contrast, the JJA (Summer) season consistently emerges as the driest across all datasets, characterized by specific variations among monitoring stations. Conversely, the SON (Autumn) season uniformly experiences an increase in precipitation levels across all datasets, reflecting the prevalent seasonal patterns within the region.

In Afghanistan, the greatest precipitation is observed in the higher northeastern regions, where the convergence and interaction of Westerly Winds, orographic precipitation, and monsoon winds contribute to the highest moisture levels. These intricate weather and climate patterns may be adversely influenced by the ongoing climate change, a phenomenon discussed in [167], aligning with the findings of this study.

4.2 Evapotranspiration (ET)

The second crucial component of the water budget, as elucidated in the previous section, is Evapotranspiration (ET). In this study, various ET estimation methods based on remote sensing data sources, including Landsat 8 data and MODIS

SSEBop ET, were employed, alongside remote sensing-based data from GLDAS CLSM ET in both Original (OD) and Downscaled (DD) data. The study's results will be presented separately in the following sections.

The Landsat 8 ET estimation using the SEBAL algorithm demonstrated that in catchments with limited or nonexistent ET data, high-resolution, freely available remote sensing data can be employed for water budget analyses or related water management studies by decision-makers or water authorities. This approach effectively addresses the ET data gap in regions like Afghanistan, particularly the Kunduz catchment, where ET data is scarce or non-existent. Therefore, the utilization of remote sensing-based or data-assimilated sources, such as GLDAS, in conjunction with ET calculations based on meteorological data, emerges as the sole available option for water resources studies and their management. The results of MODIS SSEBop ET and GLDAS CLSM are presented through monthly mean analyses based on pixel base as (gauge station location), encompassing the entire Kunduz catchment, and providing insights into the range of ET values.

4.2.1 ET Rates Using Local Meteorological Station Data

Local meteorological data from Kunduz Catchment stations were utilized, employing six widely recognized ET calculation methods: PM, HS, PT, Lin, Mak, and Abt (as shown in Table 4.10). A comparative evaluation of these methods' performance was conducted through statistical analyses, including MAD, RMSE, and NSE (refer to Table 4.22). Among the conventional ET calculation methods, PM demonstrated the most favorable performance, supported by calculated ET values of 6.76 mm/day for Baghlan and 7.00 mm/day for Kotal-i-Shibar stations (refer to Figure 2.1). Consequently, the remaining methods were ranked in order of performance as Lin, HS, Mak, Abt, and PT.

Table 4.10 ET Values (mm/day) on September 18th and September 27th, 2016: SEBAL and Widely Used Conventional Methods.

Stations	SEBAL		PM	HS	Lin	Mak	Abt	PT
Baghlan	7.56		6.76	10.92	8.71	10.05	4.69	1.81
Kotal-i-Shibar	5.98		7.00	7.85	9.05	9.18	1.63	1.41

Three radiation-based methods, namely Mak, PT, and Abt, were employed, in addition to three temperature-based methods, namely Lin, HS, and PM. Among the radiation-based methods, Mak demonstrated superior performance compared to the other two, consistent with the findings of previous studies conducted in various regions worldwide [168]. However, it is important to note that the remaining two radiation-based methods, Abt and PT, did not exhibit satisfactory performance in this study area, even though such methods may perform better in humid climate conditions [169].

Among the temperature-based methods considered, the method that yields the most favorable results for the study area is Lin. PM, Lin, and HS methods are applicable over various time scales, including hourly, daily, and monthly intervals. As these methods are specifically designed for arid and semi-arid climate conditions, the study demonstrates that the PM method achieves the lowest RMSE and the highest NSE. This study substantiates that the PM method outperforms all other methods, encompassing both radiation and temperature-based approaches, with Lin following as the next best alternative. In contrast, although the HS method is tailored for arid and semi-arid regions and has previously exhibited success [169], it did not perform well in the current study area. The HS method has shown suboptimal performance in various regions, primarily due to its dependence on parameters of extraterrestrial solar radiation, which other methods exclude [168].

4.2.2 SEBAL ET Result

During the SEBAL calculation process, various parameters, including solar radiation parameters such as NDVI, LAI, LST, and surface albedo, were computed, as depicted in Figure 4.25 and Table 4.23. NDVI, a widely utilized vegetation index, and LAI, a crucial variable linked to plant biomass production, were examined. Elevated values of NDVI and LAI indicate agricultural land, rangeland, and forest categories, while lower values signify bare soil and water bodies.

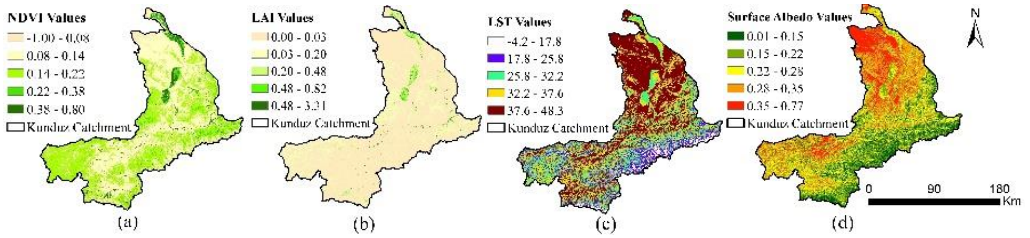

Figure 4.25 Normalized Difference Vegetation Index (NDVI) – (*a)*; Leaf Area Index (LAI) – (*b)*; Surface Temperature – (c), and Surface Albedo values – (*d*)in Kunduz Catchment, North of Afghanistan

The results obtained from the SEBAL method and Landsat-8 OLI imagery reveal pixel-wise variations in ET patterns. Instantaneous ET values range from 0.0 to 1.31 mm/hour across all land cover classes, with the minimum and maximum values associated with rangeland and snow cover due to sublimation, respectively. In this study, the predominant land cover class, rangeland, which covers 57% of the study area, exhibits a maximum ET value of 11.3 mm/day. Additionally, the maximum daily ET value for the agricultural land cover class is 17.4 mm/day (refer to Table 4.24 and Figure 4.26).

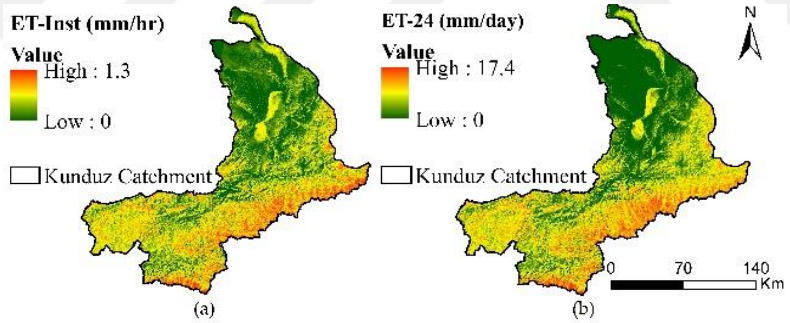

Figure 4.26 Instantaneous hourly ET – (*a*) and ET daily – (*b)* for 18th and 27th September 2016

4.2.3 MODIS SSEBop Evapotranspiration

In Figure 4.27, MODIS SSEBop for the Kunduz Catchment is illustrated, the year 2015 stands out with the highest ET value, reaching 1858 mm/year, demonstrating a particularly substantial level of evapotranspiration. This year is clearly classified as having the highest ET value within the study period.

In the category of moderate ET values, years such as 2009, 2010, 2012, 2014, 2017, and 2019 are observed, with ET values ranging between 1641 mm/year and 1777 mm/year. These years exhibit moderate levels of evapotranspiration when compared to the highest values in the dataset.

Conversely, years with lower ET values, denoting comparatively reduced evapotranspiration levels, include 2011, 2013, 2016, and 2018, with ET values between 1668 mm/year and 1692 mm/year. These years clearly show a lower degree of ET within the Kunduz catchment.

The results, as presented in Figures 4.29 to 4.32 and Table 4.11, were obtained through an analytical approach that incorporates the plotting of ET data against CHIRPS data. This methodology provides a comprehensive understanding of the dynamics of evapotranspiration within the Kunduz catchment by enabling an examination of variations in ET values in relation to precipitation levels. It is apparent that the months of January through March, as well as October through December, consistently exhibit lower to the lowest ET variations across all stations. Conversely, the higher and highest ET variations are notably observed in the months when precipitation is absent, spanning from May through September. This observed pattern underscores the influence of precipitation on the ET dynamics within the Kunduz catchment. Notably, Gerdab exhibits significant variations in ET values over the course of the year, with its highest values reaching a peak of 267 mm in the summer months of June and July, indicating substantial evapotranspiration. However, the depths of winter, specifically January and September, see ET values plummet to as low as 0 mm. In contrast, the Baghlan station consistently maintains moderate ET values across various months, notably in January, February, and March, with values ranging from 17 mm to 40 mm. This pattern reflects a relatively steady, moderate rate of evapotranspiration. The station sees its peak ET values of up to 144 mm during the spring months of May and June. Balay-i-Kelagai Station aligns closely with Baghlan in showcasing moderate ET values, especially in the early months of the year, particularly in January, February, and March. Conversely, the highest ET values, reaching up to 105 mm, emerge in the months of May and June. Doshi exhibits considerable variations in ET values. The station observes its highest ET values in May and June, ranging from 83 mm

to 112 mm, representing notable evapotranspiration during these months. Conversely, the station experiences a decline in ET values, dropping as low as 15 mm in September and October. Pul-i-Kundasang consistently registers moderate ET values throughout the year. May and June stand out as the months with the highest values, reaching up to 224 mm, indicative of increased evapotranspiration. Tang-i-Nahrin Station, similar to Pul-i-Kundasang, maintains moderate ET values, with peak values observed in May and June. Ahangaran exhibits moderate ET values, with May and June marking the months with the highest ET values, reaching up to 47 mm. Similarly, Bamyan Station portrays moderate ET values, with the highest values occurring in May and June, reaching up to 47 mm. Dasht-i-Safid consistently records some of the lowest ET values, primarily during the winter months of January, February, and March, where values drop as low as 0 mm. However, May and June see a slight increase in ET values. Doab Station generally maintains low ET values throughout the year, with May and June showcasing the highest ET values, reaching up to 26 mm. Chahar Dara Station stands out with the highest ET values, notably in July, reaching up to 267 mm, a month characterized by peak evapotranspiration. Conversely, January and February record the lowest ET values, with values as low as 1 mm.

Seasonal analysis of SSEBop ET presented in Table 4.12 show variations in ET values during the winter months, several stations displayed low ET values. Among them, Chahar Dara, Baghlan, Balay-i-Kelagai, Doshi, Pul-i-Kundasang, Tang-i-Nahrin, Doab, Dasht-i-Safid, Ahangaran, and Bamyan consistently registered relatively low ET values, ranging from 0 to 23.3 mm/season. Notably, January emerged as the month with the lowest ET values for most stations with the onset of spring, a marked increase in ET values was observed across most stations. Chahar Dara, Gerdab, Baghlan, Balay-i-Kelagai, Doshi, Pul-i-Kundasang, Tang-i-Nahrin, Doab, Dasht-i-Safid, Ahangaran, and Bamyan all recorded heightened ET values, ranging from 37.3 to 95 mm/season. March saw Chahar Dara exhibits its highest ET value at 93.7 mm/season. Other stations, such as Gerdab, Baghlan, and Balay-i-Kelagai, showed peak ET values in May, ranging from 6.7 to 84.3 mm/season. As the summer season unfolded, June and July marked the peak months for ET values in many stations. Gerdab, Balay-i-Kelagai, Doshi, Pul-i-Kundasang, and Tang-i-

Nahrin consistently exhibited the highest ET values during these months, with values reaching as high as 195 mm/season in Chahar Dara. Some stations, like Baghlan, Ahangaran, and Bamyan, recorded their highest ET values in May and June, with values ranging from 6.7 to 84.3 mm/season. With the arrival of autumn in September and October, a decline in ET values was witnessed across most stations, resulting in the lowest values for the year. However, some stations, like Baghlan and Doshi, managed to maintain moderate ET values during this period, with values ranging from 7.7 to 53.7 mm/season.

4.2.4 GLDAS CLSM Evapotranspiration

GLDAS CLSM ET presented in Figure 4.28 showing values for the Kunduz catchment in both the Downscaled Data (DD) and Original Data (OD) form, these datasets revealing intriguing patterns in evapotranspiration (ET). These values are presented in high and low ranges, offering a comprehensive perspective on ET dynamics over the years. Comparison across the years within the Kunduz catchment shows that 2015 consistently had the highest ET values in both the DD and OD datasets. The greatest demand for ET throughout the year was evident this year. Conversely, the year 2011 stands out as the period with the lowest ET values, reflecting comparatively reduced evapotranspiration. When comparing the DD and OD, it becomes apparent that the DD consistently reports higher ET values across all the years. This suggests that more significant ET rates in the Kunduz catchment are depicted in the DD than in the OD. To delve deeper into this comparison in 2015, a high ET of 578.6 mm and a low ET of 388.5 mm were recorded in the DD. In contrast, a high ET of 619.6 mm and a low ET of 343.6 mm were reported in the OD. Significant evapotranspiration was observed in both datasets, with the DD values slightly lower than those in the OD. In the lowest ET year, 2011, a high ET of 415.8 mm and a low ET of 270.2 mm were recorded in the. The OD for the same year reported a high ET of 407.8 mm and a low ET of 221.5 mm. Here, the difference in ET values between the two datasets is more pronounced, with consistently higher ET rates observed in the DD. Overall, higher ET values were consistently portrayed in the DD throughout the entire study period compared to the OD, with the year 2015 standing out as a year with notably elevated ET rates. These variations may have implications for hydrological and environmental studies

within the Kunduz catchment. Further analysis may be needed to understand the factors contributing to these differences and their potential consequences.

The results, as presented in Figures 4.29 to 4.32 and Table 4.13, reveal that GLDAS CLSM monthly mean ET, similar to SSEBop ET, exhibits consistent lower to the lowest variations during January through March and October through December. In contrast, higher and highest ET variations are consistently observed from May through September, coinciding with periods of scarce precipitation. This highlights the significant influence of precipitation availability on the ET dynamics within the Kunduz catchment. Chahar Dara Station variations in ET values were noted, with the highest ET values recorded in March, reaching 44mm/month. In contrast, the lowest ET values were observed in November and December, with values of 11 and 10 mm/month, respectively. Gerdab Station ET values remained relatively consistent throughout the year. The highest ET was observed in June, with a value of 82mm/month. Conversely, the lowest ET values were recorded in January and February, with values of 10 and 17mm/month, respectively. Baghlan station exhibited moderate ET values, with the highest values occurring in May and June, reaching 91 and 77mm/month, respectively. January marked the lowest ET value at 12. Balay-i-Kelagai Station: Similar to Baghlan, Balay-i-Kelagai displayed moderate ET values. The months of May and June featured the highest ET values, reaching 85 and 81mm/month, respectively. January registered the lowest ET value at 13mm/month. Doshi Station ET values at Doshi showcased variations throughout the year. May exhibited the highest ET values, reaching 85mm/month, while the lowest ET values were recorded in September and October, with values of 29 and 25mm/month, respectively. Pul-i-Kundasang Station This station consistently maintained moderate ET values, with the highest ET values found in May and June, reaching 92 and 88mm/month, respectively. August recorded the lowest ET value at 44mm/month. Tang-i-Nahrin Station ET values were also consistent at Tang-i-Nahrin, with peak values in May and June, reaching 92 and 88mm/month, respectively. November exhibited the lowest ET value at 15mm/month. Doab Station Generally, Doab maintained moderate ET values, with May and June showcasing the highest ET values, reaching 70mm/month. January marked the lowest ET value at 12mm/month. Dasht-i-Safid Station consistently displayed low

ET values throughout the year. May had the highest ET value, reaching 70mm/month, while January exhibited the lowest ET value at 12mm/month. Ahangaran Station presented moderate ET values, with the highest values observed in May and June, reaching 65mm/month. November registered the lowest ET value at 13mm/month. Bamyan Station similarly recorded moderate ET values, with the highest values observed in May and June, reaching 65mm/month. The lowest ET values were observed in January and December, with values of 14mm/month.

A seasonal result presented in Table 4.14 shows that during the winter season, most stations showed moderate ET values, with a range of 12 to 14 mm/season. Chahar Dara and Gerdab stations registered the lowest ET values in this season. While Chahar Dara exhibited ET values of 12 mm/season, Gerdab had slightly higher values at 12.5 mm/season. With the arrival of spring, there was a noticeable increase in ET values for all stations. Chahar Dara, Gerdab, Baghlan, Balay-i-Kelagai, Doshi, Pul-i-Kundasang, Tang-i-Nahrin, Doab, Dasht-i-Safid, Ahangaran, and Bamyan consistently displayed higher ET values ranging from 40.8 to 61.3 mm/season. The highest ET values were observed at Baghlan station, reaching 61.3 mm/season. Summer months saw a peak in ET values for most stations, particularly in June and July. Stations like Chahar Dara, Gerdab, Baghlan, Balay-i-Kelagai, Doshi, Pul-i-Kundasang, Tang-i-Nahrin, Doab, Dasht-i-Safid, Ahangaran, and Bamyan registered significantly higher ET values, ranging from 63.3 to 80 mm/season. Chahar Dara reported the highest ET values in this season at 67.3 mm/season. As the autumn season unfolded in September and October, there was a decrease in ET values across most stations, resulting in the lowest values for the year. These ET values ranged from 13.3 to 16.3 mm/season. The highest ET values were observed at Baghlan station, reaching 16.3 mm/season.

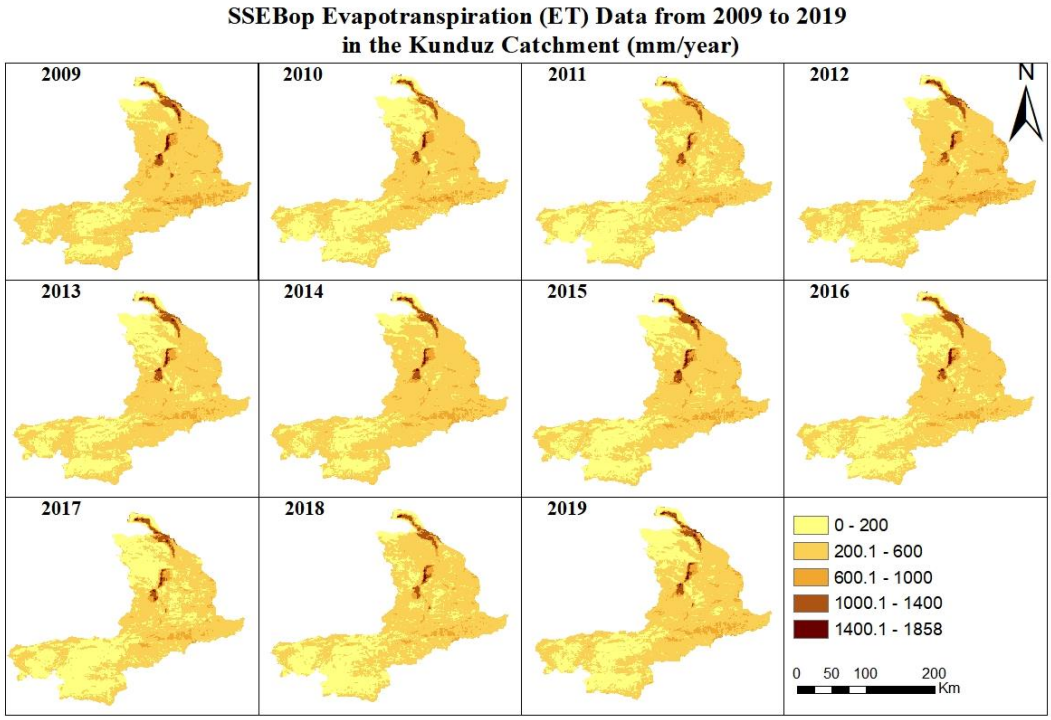

Figure 4.27 ET values derived from MODIS SSEBop model for the period spanning from 2009 to 2019 in Kunduz Catchment

Table 4.11 Presents the Monthly Mean MODIS SSEBop ET data for gauge stations within the Kunduz Catchment from 2009 to 2019 (mm/month).

Month	ST#1	ST#2	ST#3	ST#4	ST#5	ST#6	ST#7	ST#8	ST#9	ST#10	ST#11
Jan	18	5	17	8	7	3	3	0	0	0	0
Feb	28	19	24	15	11	3	7	1	1	0	0
Mar	59	25	40	44	33	14	20	4	3	3	1
Apr	124	51	105	96	83	55	65	29	23	26	7
May	176	67	144	105	112	63	97	47	40	55	7
Jun	224	82	136	93	106	38	77	47	42	38	11
Jul	267	57	102	54	88	25	46	20	26	10	2
Aug	203	10	50	25	52	6	13	4	6	2	0
Sep	122	4	36	22	28	3	5	1	0	0	0
Oct	53	4	26	27	15	2	3	1	0	0	0
Nov	22	5	21	17	12	1	5	2	1	0	0
Dec	14	7	12	13	8	3	7	2	1	0	0

Note: Station name and numbers explained in Table 2.1.

Table 4.12 Seasonal Mean of RS-Based MODIS SSEBop ET in Kunduz Catchment (2009-2019) by Station (mm/season).

ST#	Station	DJF	MAM	JJA	SON
1	Chahar Dara	23.3	93.7	195	61.3
2	Gerdab	10.3	47.3	73.7	22
3	Baghlan	18.7	96.3	97.7	53.7
4	Balay-i-Kelagai	13.3	84.3	75.3	27.3
5	Doshi	10.3	74.7	93.7	27
6	Pul-i-Kundasang	3.3	37.3	25.3	9.7
7	Tang-i-Nahrin	6.7	47.3	50	18.7
8	Doab	1.3	26.7	35.3	9.7
9	Dasht-i-Safid	0.7	22.7	32.7	7.7
10	Ahangaran	0.7	28.7	27.7	11.7
11	Bamyan	0	6.7	7.7	2

Table 4.13 Presents the Monthly Mean GLDAS CLSM ET data for gauge stations within the Kunduz Catchment from 2009 to 2019 (mm/month).

Month	ST#1	ST#2	ST#3	ST#4	ST#5	ST#6	ST#7	ST#8	ST#9	ST#10	ST#11
Jan	10	10	12	13	14	13	14	12	12	12	12
Feb	19	17	17	17	18	17	18	15	15	14	14
Mar	44	40	38	37	38	36	40	34	34	32	32
Apr	65	61	62	61	58	55	58	52	52	50	50
May	95	89	91	85	85	77	92	70	70	65	65
Jun	81	82	77	81	82	77	88	65	66	59	59
Jul	63	65	66	66	70	64	75	58	59	57	57
Aug	37	40	44	53	55	51	44	35	36	36	36
Sep	20	24	25	29	30	27	25	26	28	31	31
Oct	15	16	17	21	25	24	19	16	16	14	14
Nov	11	12	12	18	21	20	15	14	14	13	13
Dec	10	10	11	15	18	16	14	14	14	14	14

Note: Station name and numbers explained in Table 2.1.

Table 4.14 Seasonal Mean of GLDAS CLSM ET in Kunduz Catchment (2009-2019) by Station (mm/season).

ST#	Station	DJF	MAM	JJA	SON
1	Chahar Dara	12	40.8	67	13.3
2	Gerdab	12.5	45	69	13.8
3	Baghlan	13	61.3	79	16.3
4	Balay-i-Kelagai	13	59.3	80	14.8
5	Doshi	14	57	77	16
6	Pul-i-Kundasang	13.3	58.5	78	14.8
7	Tang-i-Nahrin	14.3	59	76	15
8	Doab	13	53	63	13.8
9	Dasht-i-Safid	13	51	62	13.3
10	Ahangaran	13	54.5	69	14
11	Bamyan	13	51.3	68	13.8

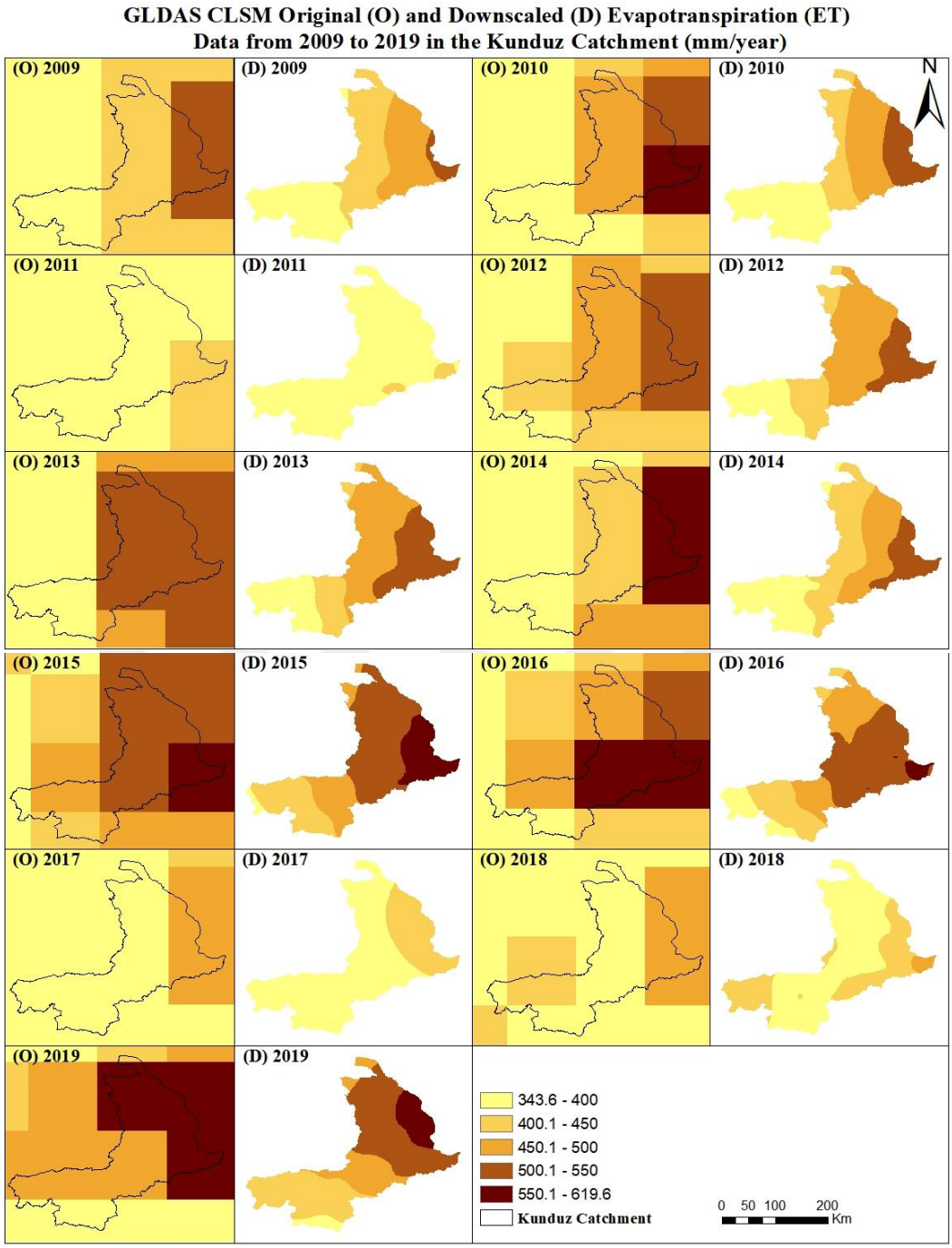

Figure 4.28 ET values derived from GLDAS CLSM Original (O), Downscaled DD model for the period spanning from 2009 to 2019 in Kunduz Catchment

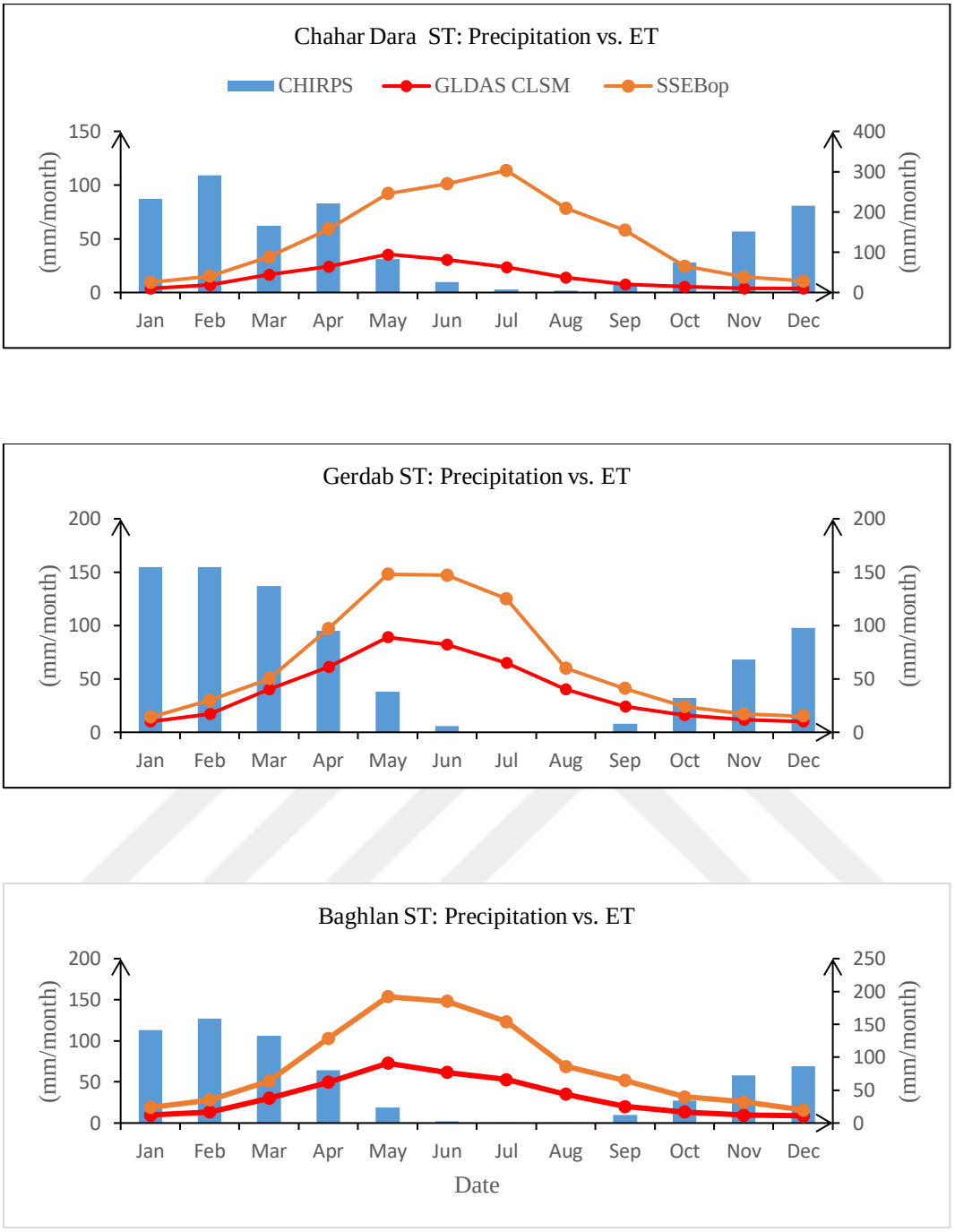

Figure 4.29 ET values vs precipitation from downscaled RS-Base precipitation in Chahar Dara, Gerdab and Baghlan stations for the period spanning from 2009 to 2019 in Kunduz Catchment

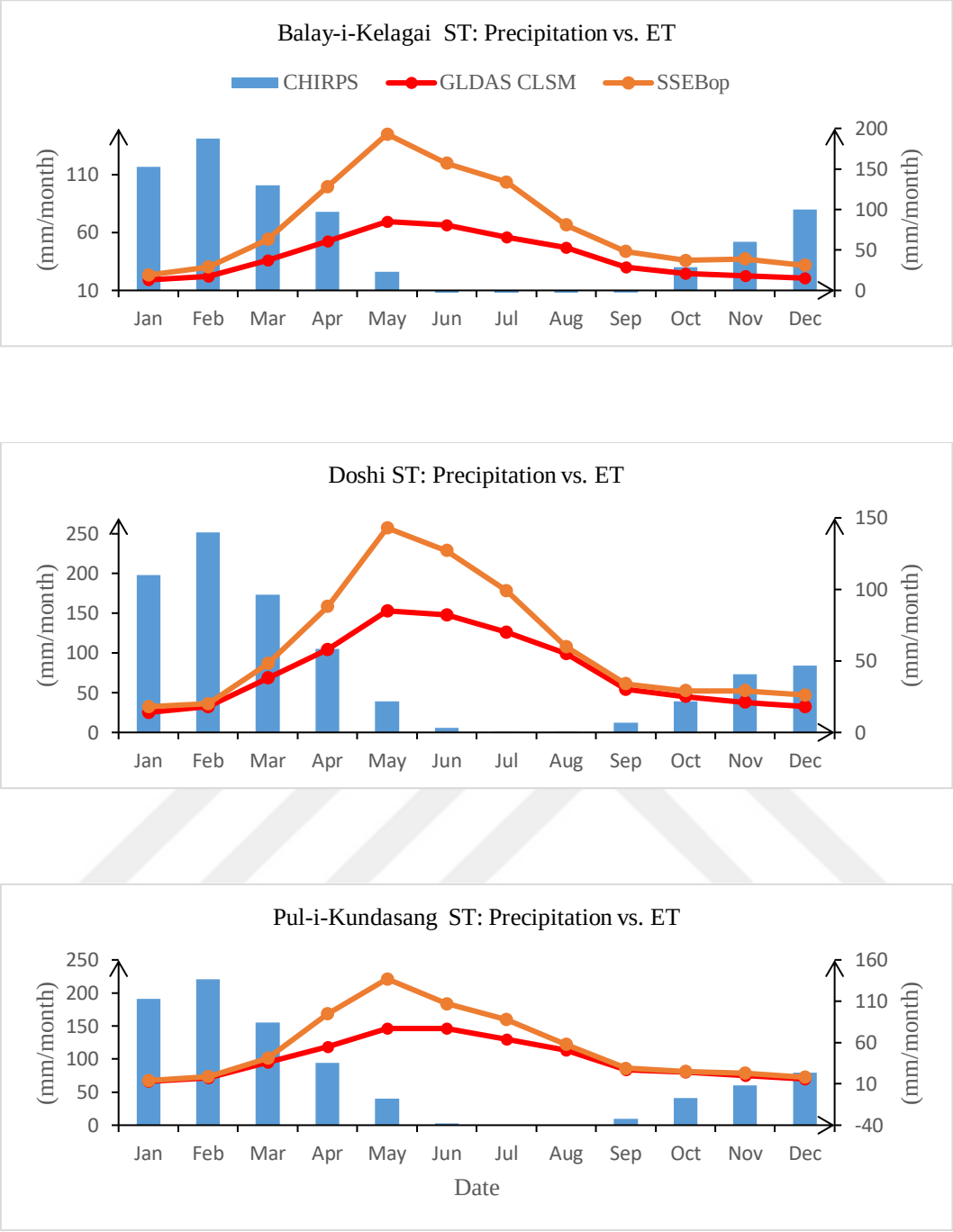

Figure 4.30 ET values vs precipitation from downscaled Rs-base precipitation in Balay-i-Kelagai. Doshi and Pul-i-Kundasang for the period spanning from 2009 to 2019 in Kunduz Catchment

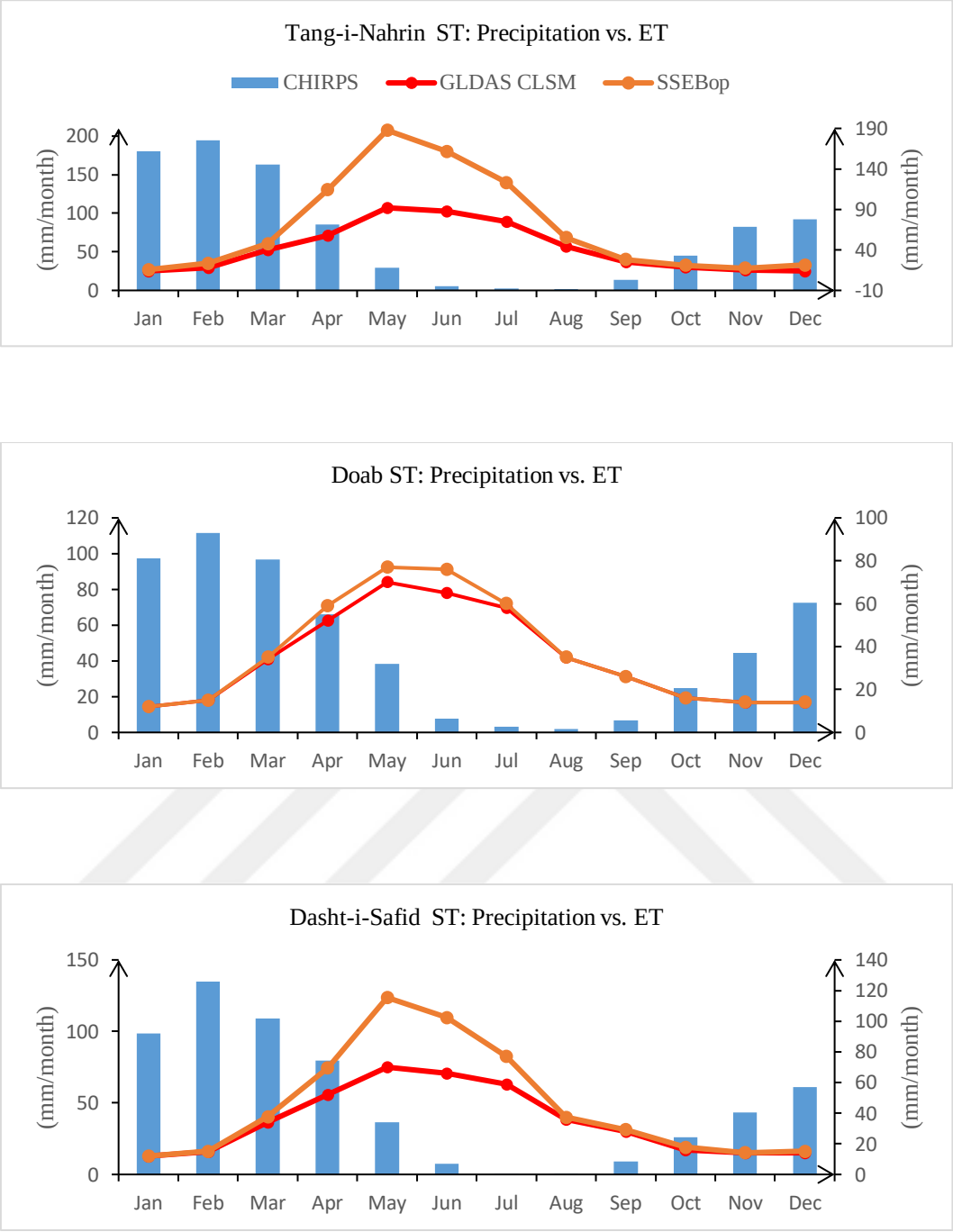

Figure 4.31 ET values vs precipitation from downscaled Rs-base precipitation in Tang-i-Nahrin, Doab and Dasht-i-Safid for the period spanning from 2009 to 2019 in Kunduz Catchment

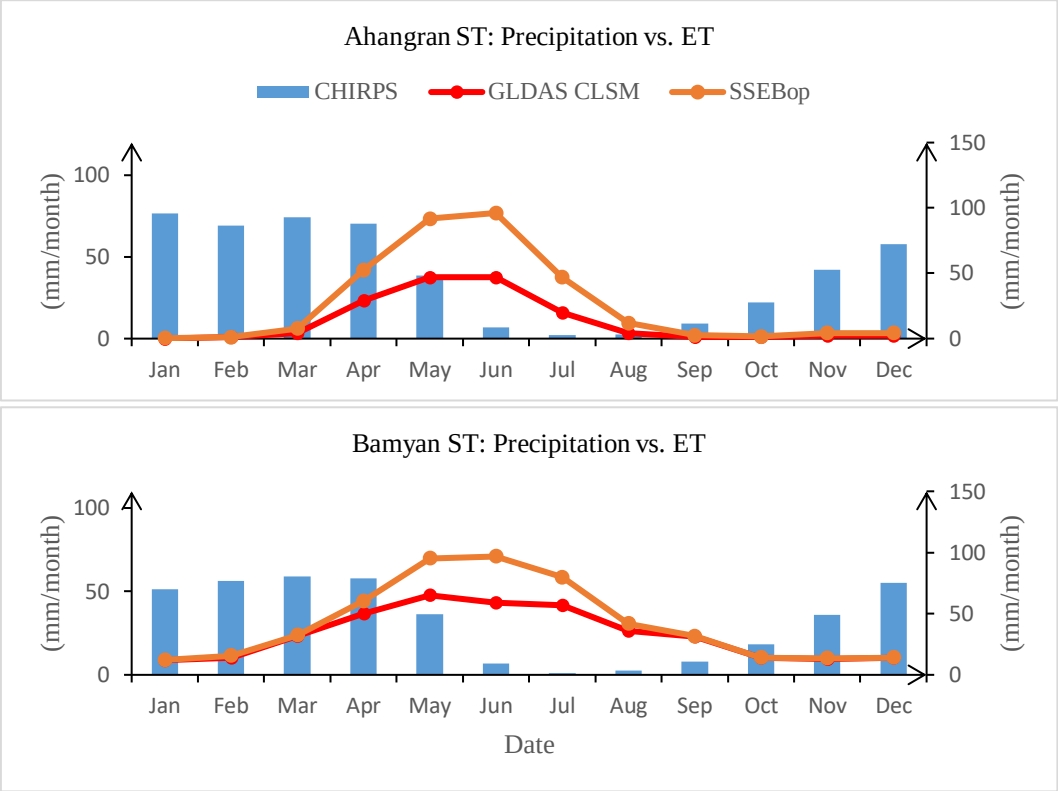

Figure 4.32 ET values vs precipitation from downscaled RS-base precipitation Ahangran and Bamyan stations for the period spanning from 2009 to 2019 in Kunduz Catchment

Upon examining the ET variations in the Kunduz Catchment, both on a catchment-wide (Figure 4.27 and 28, and Tables 4.11 to 4.14) and monthly mean pixel location basis (Figures 30 to 32), several key findings become evident. The discussion about ET values could be elaborated in this section. Notably, lower ET variations occur during the winter season, while higher ET values are evident during the summer months, defining a distinct seasonal pattern in ET dynamics within the study area.

Furthermore, the figures denoted as 2.2, 2.14, and 2.15 provide valuable insights into the underlying factors contributing to these ET variations. Land cover, NDVI, and Land Surface Temperature (LST) variations are identified as key influencers of SSEBop and GLDAS CLSM ET values within the Kunduz Catchment. Specifically, regions characterized by bare soil demonstrate elevated ET values in both SSEBop and GLDAS ET datasets. Notably, agricultural land exhibits the highest ET variations across the entire Kunduz Catchment, with SSEBop indicating

the most substantial ET variation in such areas. Additionally, mountainous regions consistently display heightened ET values in both ET datasets, which may be attributed to orographic winds and sublimation with the presence of snow cover in Kunduz's mountainous terrain. In the Kunduz Catchment, the absence of evapotranspiration data limits the ability to directly align the findings of this study. However, it is noteworthy that a recent article focusing on the Kabul River Basin, which represents an arid and semi-arid climate region in Afghanistan, presents results that closely support the observations made in this study. Specifically, the findings from the Kabul River Basin study indicate that higher ET values are recorded during the summer months, with values that are more or less similar to those observed in this study. Conversely, lower ET values are consistently observed during the winter months in both studies, highlighting a parallel pattern of ET dynamics [170]. As emphasized by previous studies [28, 31, 32], it should be noted that evapotranspiration (ET) estimation carries inherent uncertainties linked to various basin characteristics. Given that ET is a crucial component in water budget assessments and obtaining in situ ET measurements is a challenging task, the decision was made to utilize two primary sources for ET data within the Kunduz Catchment. The first source is the SSEBop model ET product, which relies on satellite thermal data, while the second source is the GLDAS CLSM ET data, which is grounded in remote sensing data assimilation and meteorological field information [29]. The evaluation of SSEBop ET data was conducted by [28]. Within their assessment, the advantages and limitations of SSEBop in various land cover classes were highlighted. Owing to data scarcity, the estimation of water budget often resorts to the utilization of ensemble mean ET data from Land Surface Models (LSMs), as observed in studies by [14, 171-174].

4.3 GRACE and GLDAS CLSM Terrestrial Water Storage (TWS)

Figure 4.33 presents the results for GRACE Terrestrial Water Storage (TWS), while Figure 4.34 displays GLDAS CLSM original data. TWS data serves as a fundamental element within the hydrological cycle, integrated into the framework of the water budget. A basic visual interpretation of Figure 4.33 reveals that the

majority of annual TWS layers depict higher terrestrial storage, with the exceptions of 2016. It is crucial to emphasize that a comprehensive comprehension of alterations in terrestrial water storage necessitates supplementary analysis and calculation of the TWS layer, as previously documented [135]. For GRACE TWS, it is worth noting, as referenced in Table 2.3, that except for the years 2009 and 2010, a significant number of months in each year until 2017 contain missing data [97]. These missing months have a notable impact on the overall data quality of GRACE TWS, thus influencing the decision to limit the focus of this study to GRACE TWS data only up to 2017. To address the issue of missing data, specific methods outlined in [14, 135] were employed for data imputation.

It is evident that the GLDAS CLSM TWS dataset demonstrates the lowest water storage in the year 2011 when compared to the years 2009 through 2019. Conversely, the years 2009, 2013, 2018, and 2019 exhibit the highest levels of water storage in the TWS layer, respectively.

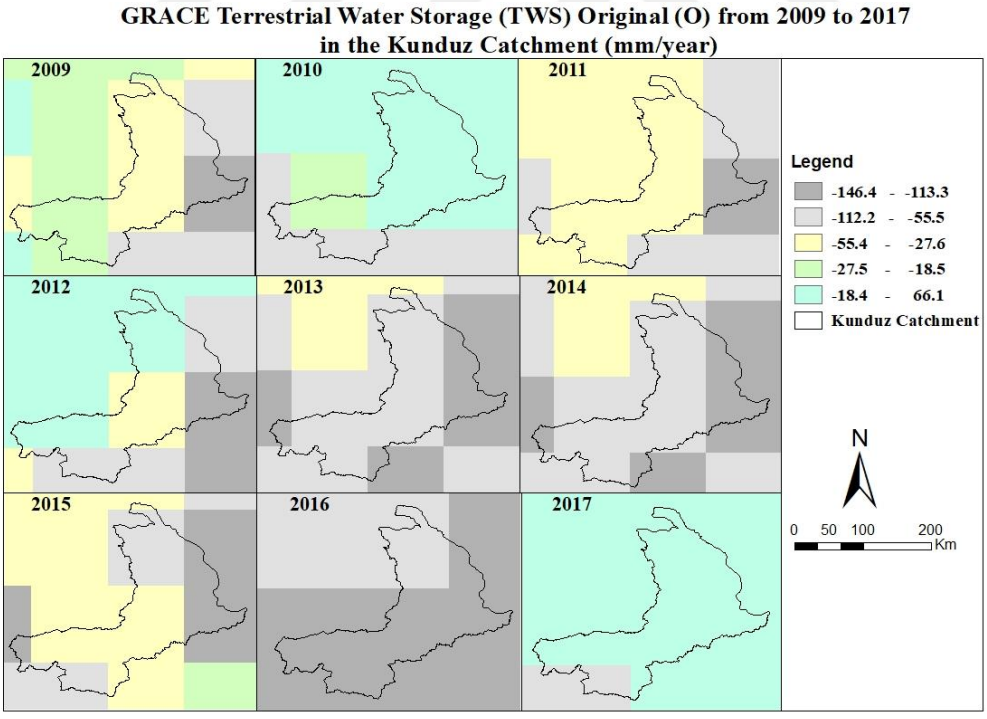

Figure 4.33 Original GRACE JPL Data (O) for Total Water Storage Availability in the Kunduz Catchment

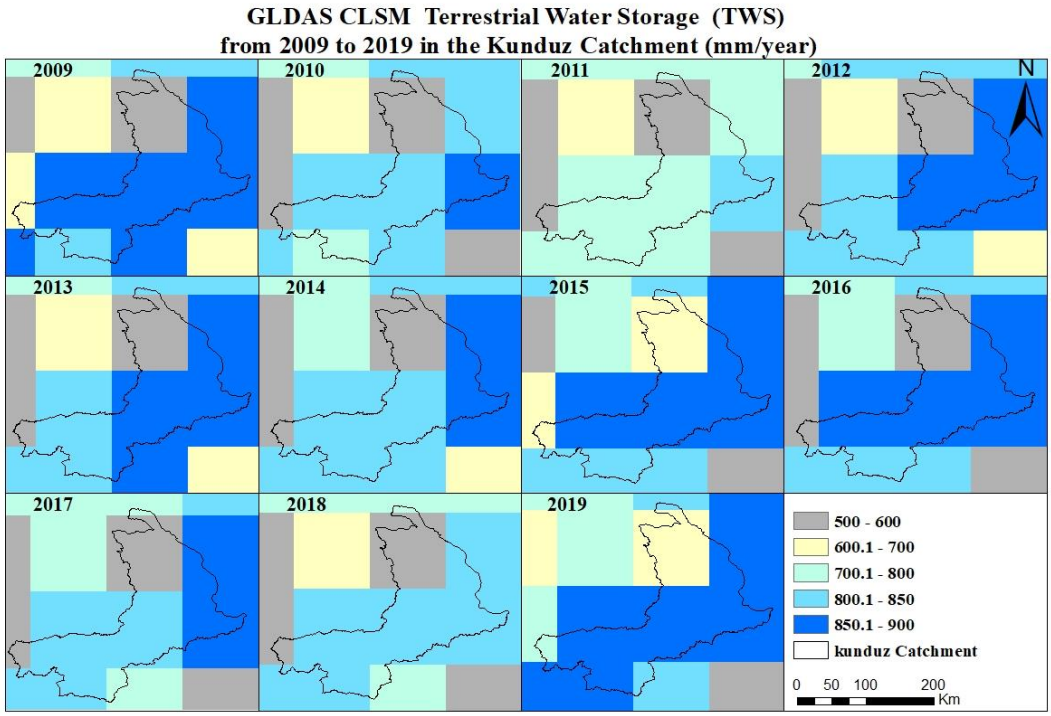

Figure 4.34 Original GLDAS Data (O) for Total Water Storage (TWS) Availability in the Kunduz Catchment

However, its direct application in completing the water balance equation is limited until the real changes in water storage are accurately calculated, following the method expounded by [135]. In many studies, TWS is primarily employed to discern trends in water storage, rather than determining the actual changes in storage. The forthcoming section will delve into the comprehensive explanation of total water storage changes, denoted as TWSC.

4.4 Temporal Variations in Terrestrial Water Storage Change (TWSC)

The estimates of Total Water Storage Change (TWSC) were derived from both the GRACE and GLDAS models by calculating the monthly differences explained in [14, 135] in TWS over the study period. The changes in TWS, as obtained from the two model outputs and the GRACE product, are presented in Figures 4.35 and 4.36, illustrating the yearly catchment-wise TWSC from GRACE, both in Downscaled (DD) and Original (OD) data formats. Simultaneously, Figure 4.37 depicts the mean monthly variations in changes in terrestrial water storage, represented as DD

and OD, based on GRACE data. In addition, Figure 4.38 provides insight into the relationship between the DD and OD versions of the mean monthly variation of GRACE TWSC in the Kunduz catchment.

Similarly, Figures 4.39 to 4.40 detail the TWSC from GLDAS on a catchment basis, while Figures 4.41 and 4.42 exhibit the mean monthly variations in this data. These figures collectively contribute to a comprehensive understanding of the dynamics of TWSC in the study area. In Figure 4.37, a comparison is made between the monthly basin-averaged values of TWSC. Significant gaps in the GRACE dataset have been observed and are well-documented in Table 2.3 of this study, indicating which specific months are missing from the data records. It is imperative to recognize that the recurring issue of data gaps in GRACE observations has been persistent since the year 2011. These data gaps primarily stem from the implementation of active battery management practices to extend the operational life of aging satellite batteries [97, 175]. The resulting interruptions in data availability hold profound implications for the comprehensive analysis and interpretation of TWSC trends and patterns. These insights play a pivotal role in enhancing the overall understanding of water storage dynamics within the study area.

In the case of missing data for specific months, this study has employed an alternative approach recommended by [176]. These recommended interpolation methods involve using data from the adjacent two months to fill in the gaps within the monthly dataset. In this study, Inverse Distance Weighting (IDW) interpolation was applied to address the gaps in GRACE data. Consequently, the utilization of interpolation methods for certain months has introduced significant variations in both catchment-wise and mean monthly TWSC patterns when comparing GRACE and GLDAS CLSM, as depicted in Figures 4.35 to 4.42. Furthermore, apart from the evident data gaps, variations in the datasets can be attributed to a multitude of factors, which are elaborated upon in the GRACE L-3 Product User Handbook [175]. The examination of GRACE TWSC data in the Kunduz Catchment for the years spanning from 2009 to 2017 reveals distinctive patterns in annual water storage variations. Notably, the year 2014 recorded the most substantial change in TWSC, manifesting a significant positive value of 247.7 mm/year in the DD and

1.5 mm/year in the OD. This value indicates a substantial surge in water storage within the catchment for that particular year in the DD, while the OD shows a negligible change. Subsequently, the year 2017 exhibited considerable positive alterations in TWSC, with a value of 243.7 mm/year in the DD and 12.6 mm/year in the OD. These values signify another year marked by notable growth in water storage, with the DD showing more significant changes than the OD. In stark contrast, 2012 stands out as the year featuring the most significant depletion in water storage, characterized by a negative value of -135.9 mm/year in the DD and -8.6 mm/year in the OD, signifying a substantial reduction in water storage within that period in both datasets. Similarly, 2013 also displayed significant depletion in water storage, with a negative value of -102.8 mm/year in the DD and -2.3 mm/year in the OD. These values suggest pronounced water storage depletion in both datasets for that year. In summary, the analysis of GRACE TWSC data for the Kunduz Catchment underscores the remarkable variations in water storage over the years. Specifically, 2014 and 2017 are marked by the highest positive changes in water storage, indicating increased water storage in the DD, while the OD showed smaller changes. In contrast, 2012 and 2013 represent the years with the most pronounced negative changes, signifying substantial water storage depletion in both datasets. Mean monthly variation are for GRACE both DD and OD explained in Figure 4.37.

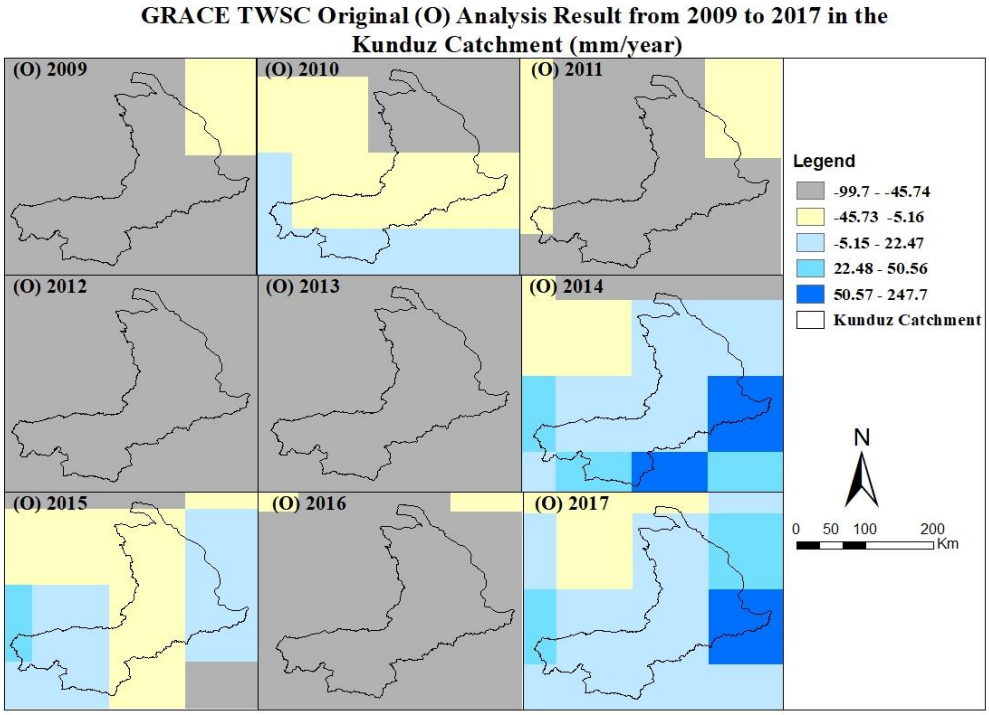

Figure 4.35 Original (O) Total Water Storage Change (TWSC) in the Kunduz Catchment from 2009 to 2017

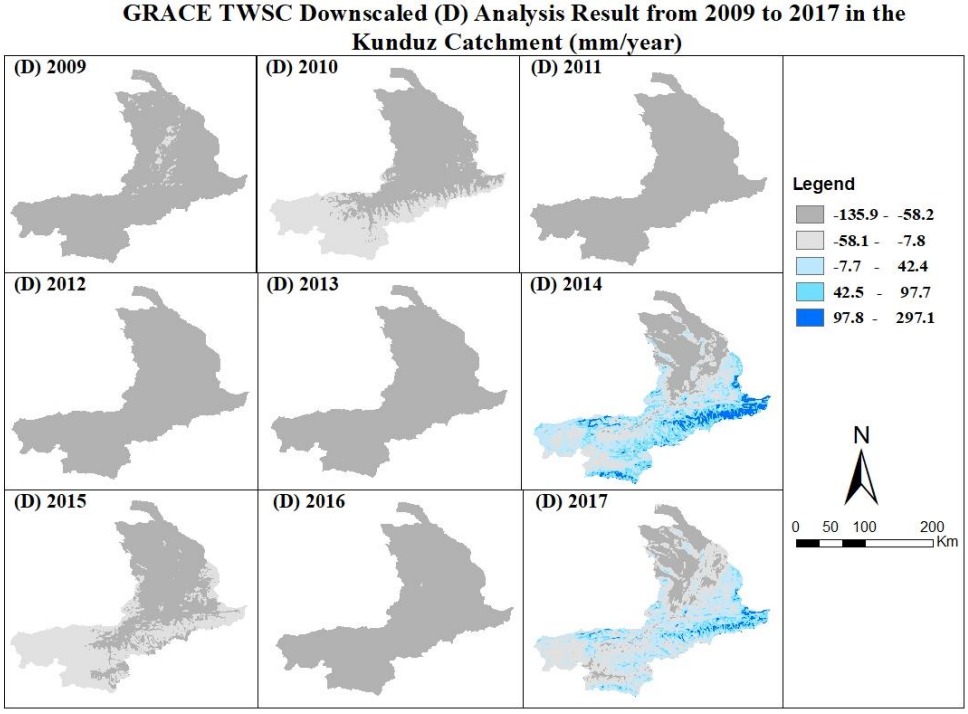

Figure 4.36 Downscaled (D) Total Water Storage Change (TWSC) in the Kunduz Catchment from 2009 to 2017

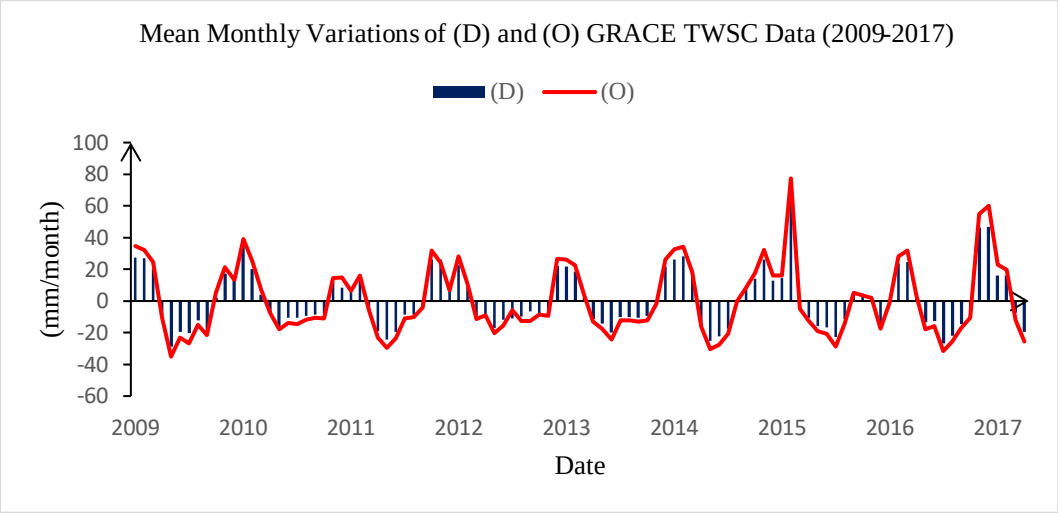

Figure 4.37 illustrates the Mean Monthly Basin-wise Downscaled (D) Total Water Storage Change (TWSC) in the Kunduz Catchment from 2009 to 2019

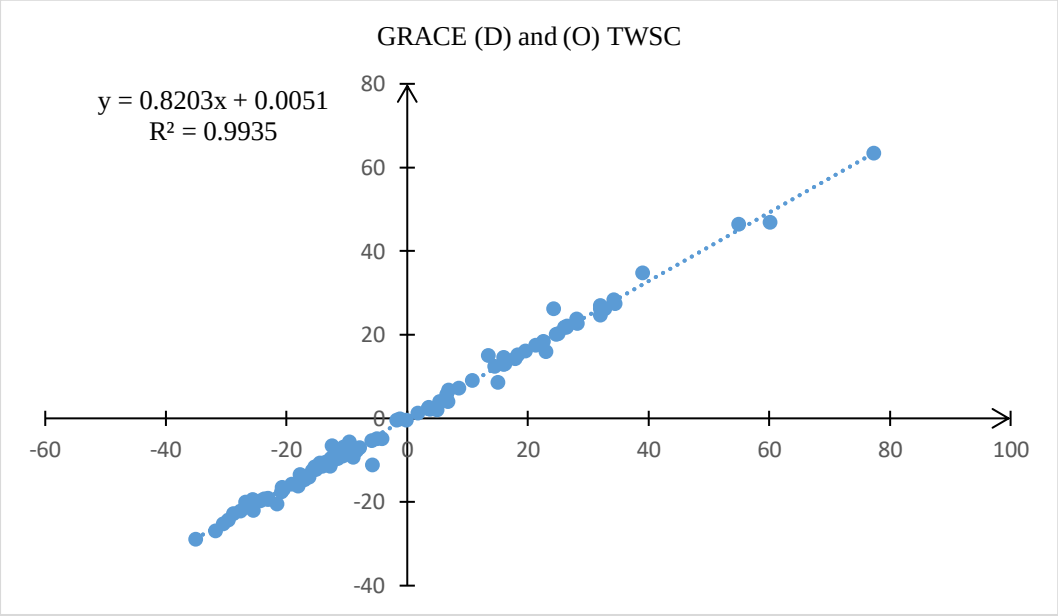

Figure 4.38 Presents a scatter plot comparing the Mean Monthly (D) and (O) datasets of GRACE from 2009 to 2019

The analysis of TWSC data from the GLDAS dataset in the Kunduz Catchment for the years spanning from 2009 to 2019 reveals notable variations in yearly water storage fluctuations. The data from both the GLDAS OD and DD are compared for each year. In 2011, the GLDAS OD recorded a high change in TWSC with a value of 95.0 mm/year and a low of 31.9 mm/year. On the other hand, the GLDAS DD for the same year also showed significant changes, with a high of 91.6 mm/year and a low of 16.1 mm/year. In 2014, both GLDAS OD and DD demonstrated high

values of 29.0 mm/year and low values of -12.7 mm/year. These values indicate significant changes in water storage within the catchment. Conversely, 2016 displayed moderate changes in both datasets, with high values of 14.8 mm/year in GLDAS OD and -84.8 mm/year in GLDAS DD. Additionally, in 2017, the datasets showed relatively low changes, with high values of -3.9 mm/year in GLDAS OD and -46.3 mm/year in GLDAS DD. In summary, the analysis of GLDAS TWSC data for the Kunduz Catchment demonstrates the annual fluctuations in water storage. Specifically, 2011 and 2014 experienced the highest changes, while 2016 and 2017 had moderate to low changes in both GLDAS OD and DD. These findings offer insights into the dynamics of water resources within the catchment.

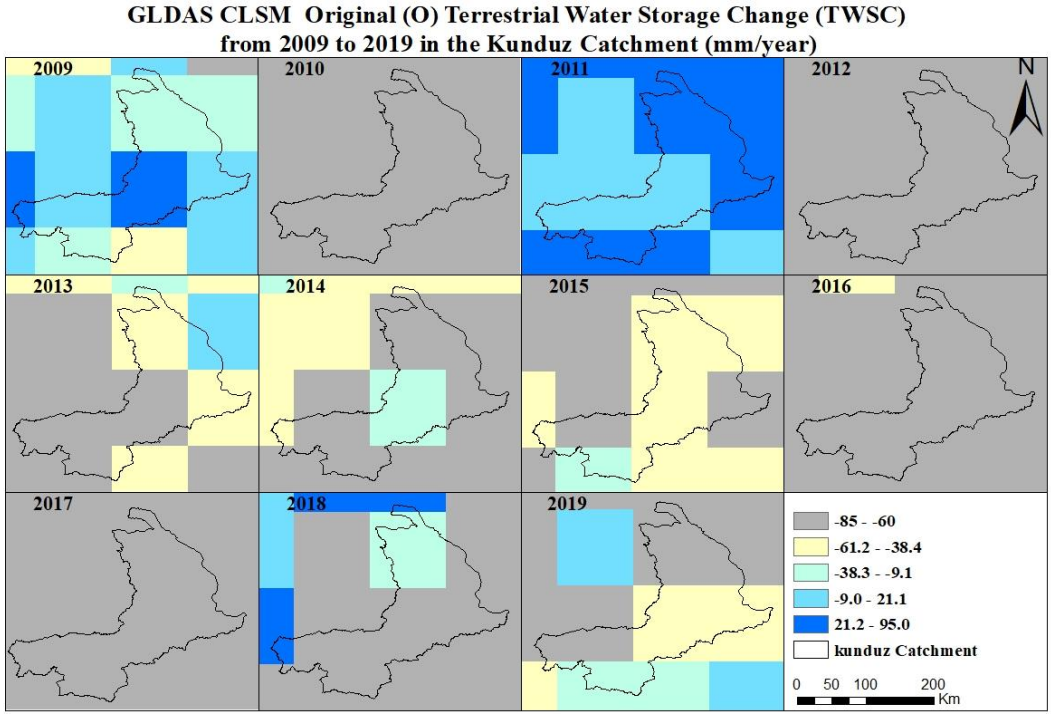

Figure 4.39 Original (O) Total Water Storage Change (TWSC) in the Kunduz Catchment from 2009 to 2019

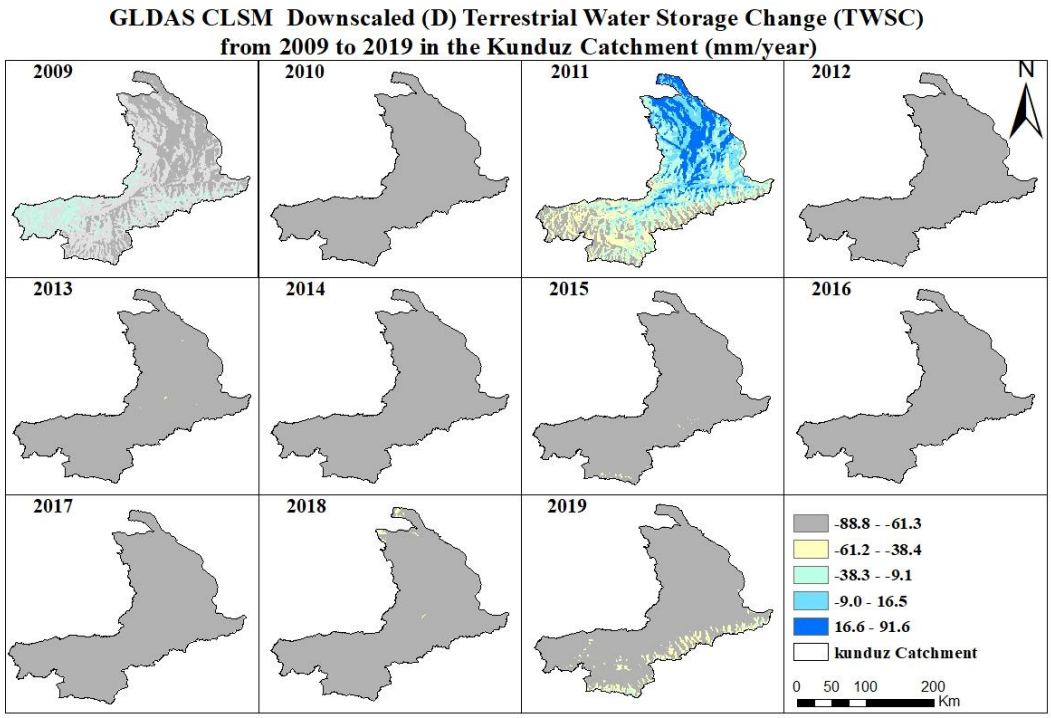

Figure 4.40 Downscaled (D) Total Water Storage Change (TWSC) in the Kunduz Catchment from 2009 to 2019

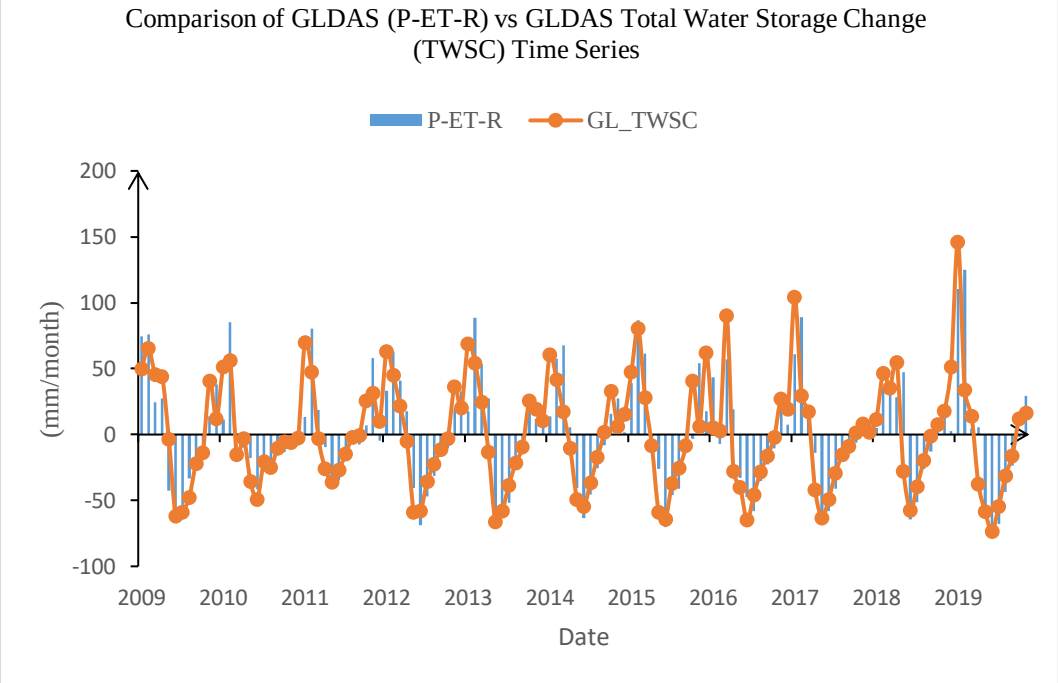

Figure 4.41 illustrates the Mean Monthly Basin-wise GLDAS CLSM (P-ET-SR) vs GLDAS CLSM in the Kunduz Catchment from 2009 to 2019

To discuss both GRACE and GLDAS CLSM datasets provide valuable information regarding TWSC in the Kunduz Catchment. These datasets share some

commonalities and exhibit distinct differences, offering a comprehensive understanding of water storage dynamics in the region.

Similarities High Positive Changes: In both GRACE and GLDAS CLSM datasets, the years 2014 and 2017 indicate the highest positive changes in water storage. This alignment signifies a consensus between the datasets regarding substantial increases in water storage during these particular years. GRACE's DD recorded 247.7 mm/year, while the OD showed 1.5 mm/year in 2014, mirroring GLDAS, which displayed high values in both OD and DDfor the same year. Negative Changes: Additionally, both GRACE and GLDAS datasets concur on significant water storage depletion in 2012 and 2013. These datasets reveal negative changes, emphasizing substantial reductions in water storage during these years. Dataset Discrepancies: While both datasets identify the years with the highest positive changes, differences in the magnitude of changes become apparent. GRACE's DD demonstrates more significant increases in 2014 and 2017 compared to the GLDAS DD. This highlights the need to consider the specific dataset when analyzing water storage variations.

Data Gaps: Notably, a significant difference lies in the presence of data gaps in the GRACE dataset, which can impact the analysis. Conversely, the GLDAS dataset does not encounter similar data gap challenges. These gaps, as elaborated in Table 2.3, have been a recurring issue in GRACE observations since 2011 due to satellite battery management practices. In case of GRACE data, it is worth noting that the coarse spatial resolution of GRACE, approximately (330 by 330) kilometers, can lead to spatial signal leakage [15, 43, 175]. Additionally, during close-proximity orbits, the monthly grids exhibit increased inaccuracies, which consequently affect the precision of gravity field calculations [175] generate more uncertainties for TWS data. Moreover, uncertainties in precipitation (P), evapotranspiration (ET), and runoff introduce inherent uncertainties in the estimation of TWSC. These discrepancies between GLDAS CLSM TWSC and GRACE can also be attributed to the absence of lake and river modules in the GLDAS model, as noted in prior studies [15, 34]. Considering the relatively low spatial resolution of both GRACE and GLDAS datasets, comparable TWSC results are more likely to be obtained over larger basins exceeding 150,000 km². This alignment is primarily due to the

effective spatial resolution of GRACE, estimated at approximately 150 km² [177, 178]. GRACE and GLDAS data have been widely employed in numerous water balance studies to derive TWS anomalies and TWSC for specific time intervals [27, 52, 97, 178-180]. Nonetheless, it is essential to acknowledge that the presence of data gaps in the GRACE archive poses a significant challenge when estimating monthly TWSC Figure 4.37 [10, 181]. Additionally, due to the relatively coarse sensor resolution, GRACE data may not be suitable for smaller-scale basins [34, 182], which represents a notable limitation of both GRACE and GRACE-FO represented in Table 2.3. TWSC in smaller watersheds are estimated using remote sensing data for precipitation (P) and evapotranspiration (ET), in combination with surface runoff data from observation stations. To mitigate uncertainties associated with model-derived data (GLDAS CLSM), the ensemble mean approach of Land Surface Models (LSMs) is applied as recommended by [181]. A study by [34] explored the correlation between P-ET-R and TWSC across major river basins globally. Their findings indicated R^2 values ranging from 0.35 to 0.9, which closely aligns with the results of this study's monthly mean variation analysis presented in Figures 4.41 and 4.42, utilizing GLDAS CLSM for the Kunduz Catchment over the period 2009 to 2019. The researchers concluded that human activities have a notable impact on the water systems within these basins. Basins with lower human influence, such as the Amazon River Basin, exhibited reduced uncertainty in total water alterations. Variations in TWS can also be attributed to surface water components, including lakes, reservoirs, and snowmelt.

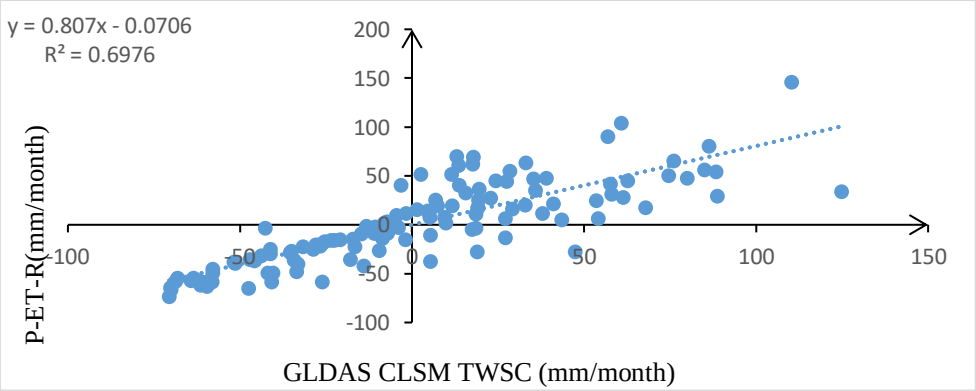

Figure 4.42 Scatter plot of P-ET-R from GLDAS CLSM with GLDAS CLSM TWSC

4.5 Runoff

As previously discussed, the direct estimation of runoff within a catchment using remote sensing data remains unfeasible, as elucidated by[13-15]. Nevertheless, it is possible to generate an inferred runoff dataset through the subtraction of precipitation from evapotranspiration and terrestrial water storage layers. This inferred runoff data retains its utility for water resource management, particularly in catchments characterized by limited data availability, as it provides valuable information regarding the presence of water deficits or surpluses within the catchment based on its unique characteristics. Figures 4.43 and 4.44 depict the annual inferred runoff, which represents the inferred runoff based on Remote Sensing (RS) data for the years 2009 to 2017 in both DD layers. Figure 4.43, using CHIRPS data, reveals two years with the lowest values, signifying water deficiencies in 2010 and 2014. On the other hand, Figure 4.44 showcases the agreement between the remote sensing datasets CHIRPS and PERSIANN in identifying water deficits in 2010. Additionally, the PERSIANN dataset indicates that 2017 is the year when the catchment received rainfall, accompanied by higher evapotranspiration rates, resulting in fluctuations in TWSC and a negative residual value for that year.

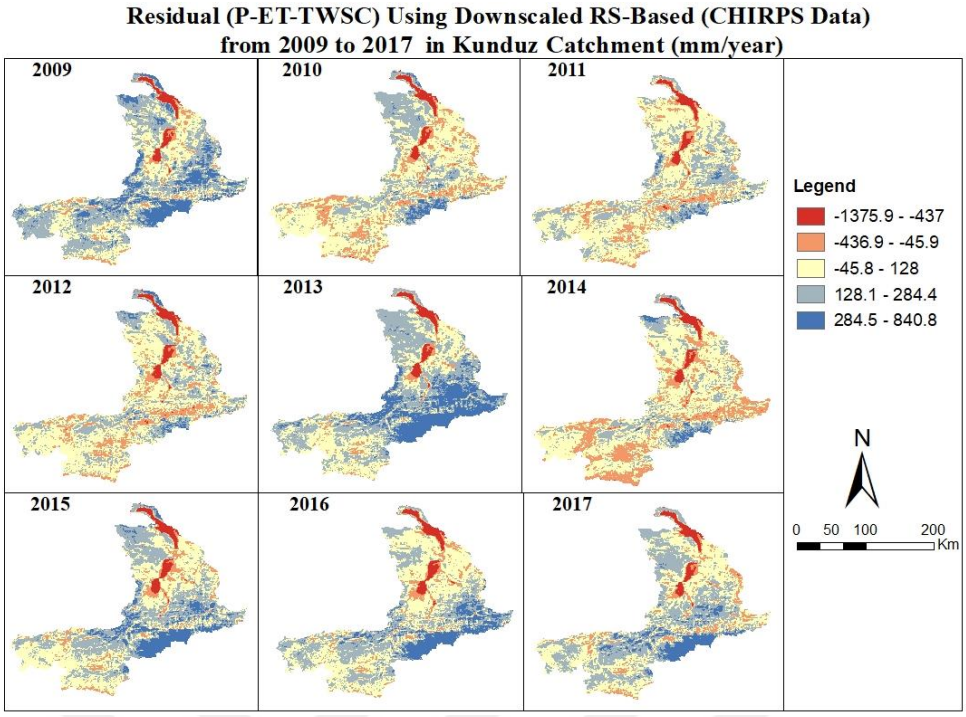

Figure 4.43 illustrates the residual from CHIRPS, a RS-based dataset, from 2009 to 2017

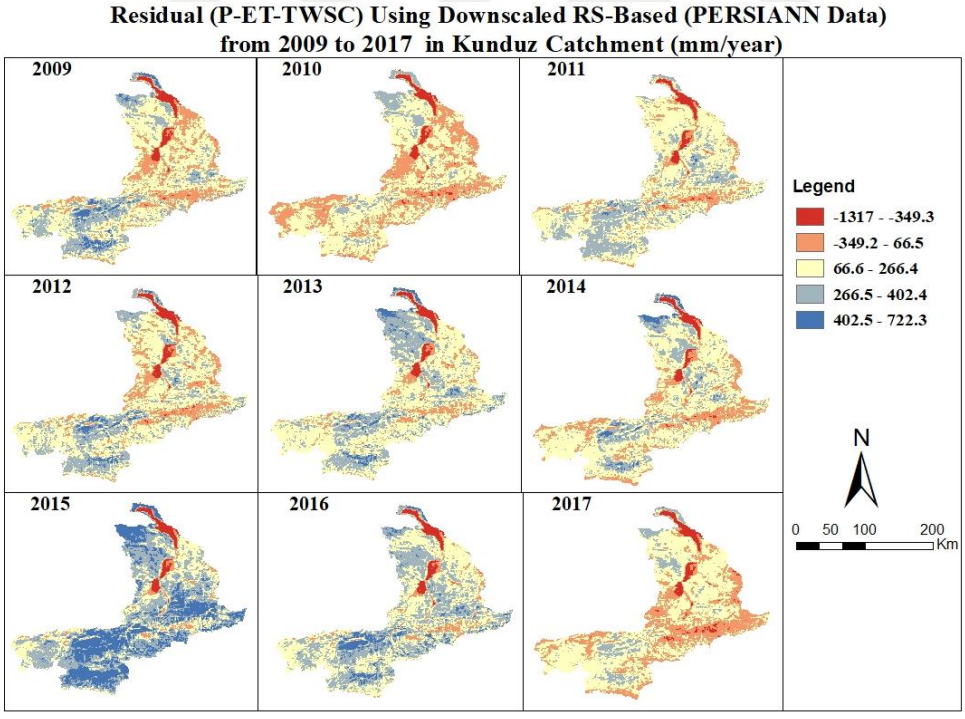

Figure 4.44 illustrates the residual from PERSIANN, a RS-based dataset, from 2009 to 2017

The interpretation of Figures 4.45 and 4.46, which present GLDAS OD and DD datasets, indicates that, in the years 2011, 2013, and 2014, the Kunduz Catchment experienced increased precipitation and higher evapotranspiration levels, resulting in significant fluctuations in TWSC. Consequently, these specific years demonstrated the most pronounced instances of water deficits across various locations within the catchment. Additionally, the analysis highlights that GLDAS CLSM data exhibited substantial agreement in the residual layer, particularly with the years 2010 and 2014.

In the Kunduz Catchment, the influence of landcover characteristics on the residual, as depicted in Figure 2.2, is readily apparent. The lower part of the catchment, predominantly covered by barren soil and deserted land, exhibits the most pronounced water deficit, signifying a scarcity of water resources. Remote sensing-based data has proven to be effective in discerning areas with water availability and deficiency, particularly in mountainous regions, where the RS data aligns with the GLDAS CLSM layer for most of the analyzed years.

The agricultural land cover class consistently demonstrates elevated levels of water deficit within the Kunduz Catchment, primarily attributed to the higher rates of evapotranspiration associated with agricultural activities. This is evidenced by RS data. In contrast, forested areas exhibit substantial fluctuations in water availability over time, underscoring the dynamic nature of water resources in these regions. Furthermore, the rangeland experiences occasional precipitation; however, the catchment's higher evapotranspiration rates lead to instances of water deficits. This analysis underscores the significant impact of landcover characteristics on water resource dynamics within the Kunduz Catchment, with agricultural land exhibiting the most consistent water deficits.

This analysis underscores the pivotal role of landcover characteristics in shaping water availability and deficiency within the Kunduz Catchment. Remote sensing-based data provides valuable insights into these dynamics, contributing to a comprehensive understanding of water resources in different landcover classes within the catchment.

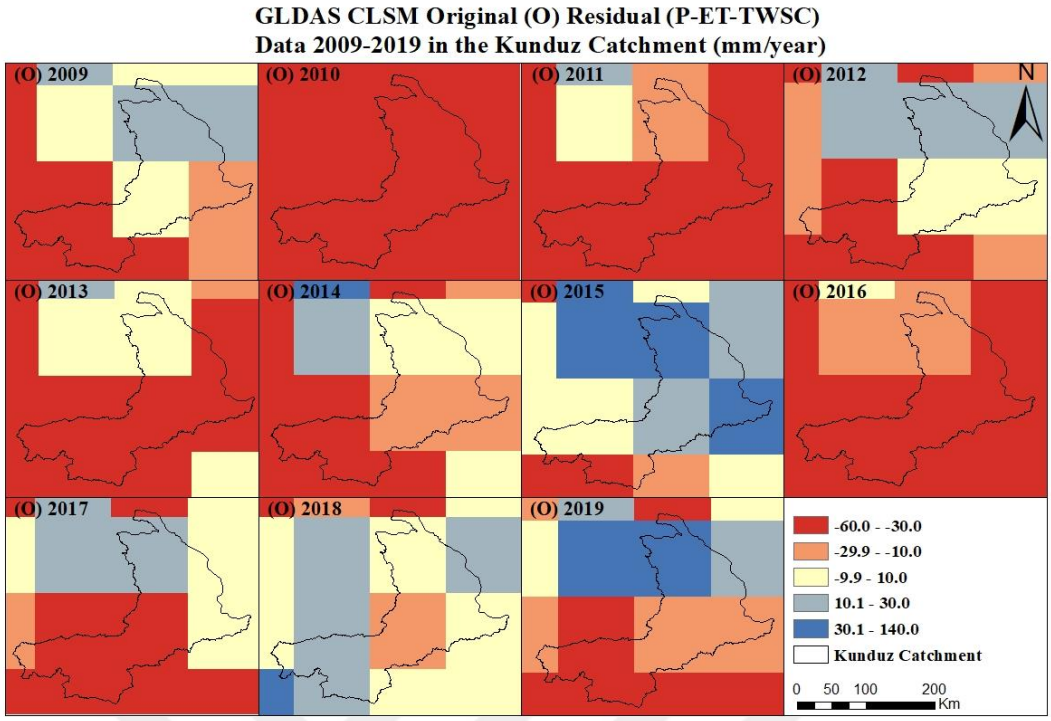

Figure 4.45 Present the residual from GLDAS CLSM (O) dataset, from 2009 to 2019

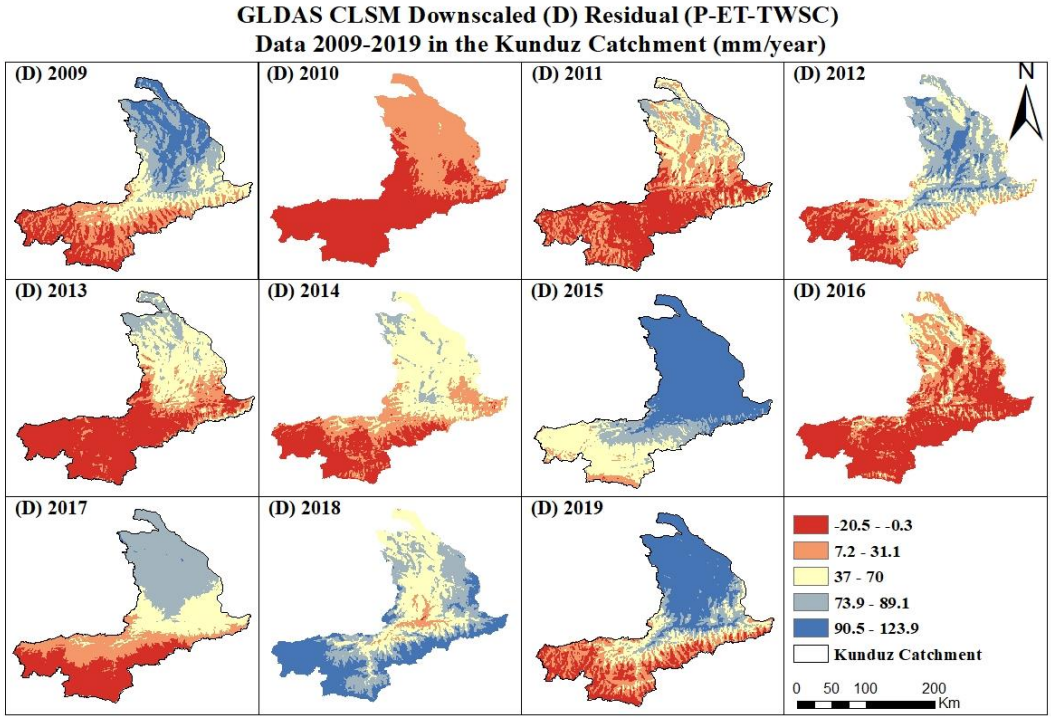

Figure 4.46 Present the residual from GLDAS CLSM (D) dataset, from 2009 to 2019

In various water budget studies, it is widely acknowledged that directly estimating surface runoff through remote sensing data is generally impractical. Instead, researchers often rely on assimilated surface runoff data from GLDAS CLSM as a valuable alternative. Nevertheless, it is imperative to recognize that the utility of such data is constrained by several limitations, including spatial resolutions and other associated constraints.

Figure 4.47 plays a pivotal role in conveying annual catchment-wise surface runoff data, while Figure 4.48 compares monthly catchment-wise observed runoff with GLDAS CLSM Surface runoff. These figures provide essential insights into the dynamics of runoff within the Kunduz Catchment. The surface runoff (SR) data derived from GLDAS, encompassing both the OD and DD, unveils significant variations in surface runoff over the years from 2009 to 2019. The analysis reveals that the years 2010, 2011, 2012, and 2017 exhibit lower surface runoff, while 2015 and 2019 witnessed the highest levels of surface runoff. Conversely, 2018 stands out as the period with the lowest surface runoff levels. During this time, the catchment experienced a notable decrease in surface runoff, signifying relatively lower water runoff levels. In contrast, 2019 emerges as the year characterized by the highest surface runoff levels in both datasets. This year experienced a substantial increase in surface runoff, indicative of notably higher water runoff within the Kunduz Catchment. Regarding the monthly comparison, GLDAS CLSM's monthly surface runoff is assimilated, primarily influenced by precipitation and other hydrological components. It closely mirrors the seasonal precipitation patterns in the Kunduz Catchment. In this region, the rainy season predominantly occurs in the winter and autumn months. Therefore, the monthly surface runoff exhibits higher values during these months.

In contrast, the observed runoff displays a distinct pattern. Given that the flow in the Kunduz Catchment is primarily driven by snowmelt, the highest surface runoff typically occurs during the spring months extending into the early summer months. This noteworthy disparity between the pattern of surface runoff and observed runoff is evident in Figure 4.47. The substantial discrepancies between observed runoff and GLDAS CLSM surface runoff may arise due to the absence of streamflow routing in the GLDAS-2.1 simulations, resulting in notable discrepancies between

modeled GLDAS CLSM SR values and observed values. The analysis shows that GLDAS SR values exhibit significant variation from observed streamflow, and this inconsistency aligns with findings in previous studies [14, 17, 19, 42, 43, 183].

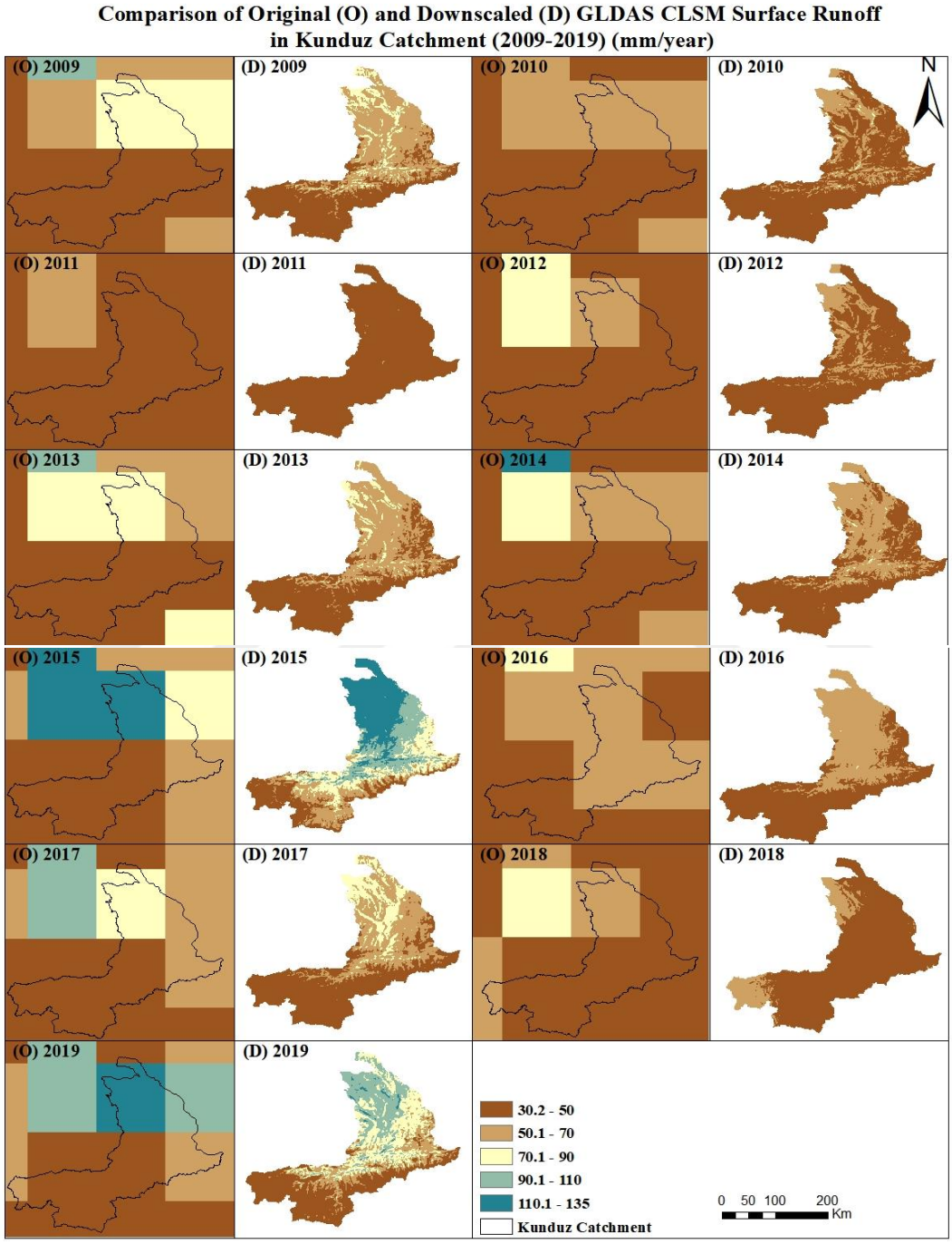

Figure 4.47 GLDAS CLSM Surface Runoff - Original (O) and Downscaled (D) in Kunduz Catchment (2009-2019) (mm/year)

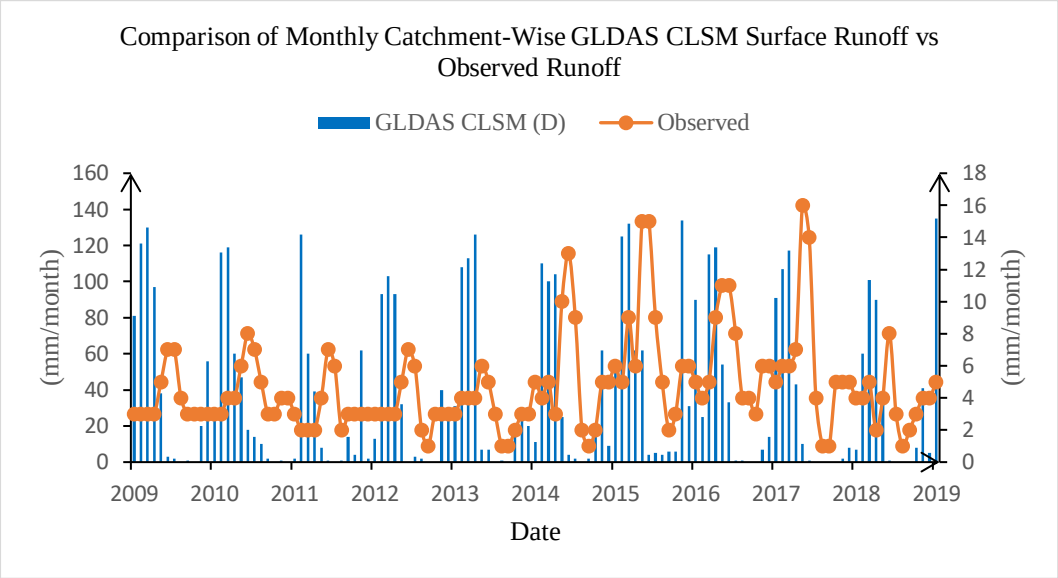

Figure 4.48 illustrates the monthly comparison between GLDAS CLSM surface runoff and observed runoff within the Kunduz Catchment for the period spanning from 2009 to 2019

4.6 Assessment of Water Budget Estimation Using Remote Sensing-Based and GLDAS CLSM Data

Table 4.15 presents the assessment of total water budget components for the Kunduz catchment, incorporating both Original (OD) and Downscaled (DD) datasets. The data in this table, along with the accompanying Figures 4.49 to 4.51 for OD and Figures 4.52 to 4.54 for DD, have been derived from remote sensing and GLDAS CLSM sources. This approach enables a comprehensive evaluation of the water budget components within the study area, enhancing the depth of analysis. The incorporation of figures in the form of Figures 4.49 to 4.51 and Figures 4.52 to 4.54 serves to visually illustrate the dynamics and trends observed in the data. This visual representation complements the tabulated information, offering a more holistic understanding of the water budget assessment. Furthermore, all results from the years 2009 to 2017 representing remote sensing datasets and, simultaneously, from 2009 to 2019 representing GLDAS CLSM datasets have been compiled. This compilation collectively offers a comprehensive overview of the water budget assessment, enabling a thorough analysis of the data. In the realm of RS-based (CHIRPS) precipitation datasets, distinctive patterns and temporal variations were observed. The (OD precipitation dataset exhibited particular intricacies during the

study period. In the year 2010, a notable reduction in precipitation was evident, with OD values decreasing by approximately 25.79% in comparison to the preceding year (2009). This declining trend persisted into 2011, marking a further decrease of 11.01%. However, the year 2012 witnessed a reversal of this trend, reflecting an increase of 10.47% in OD precipitation. Subsequently, 2013 recorded a substantial increment of 27.16% relative to the year 2012, followed by a relatively stable year in 2014, characterized by a marginal percentage change of -5.50%. In 2015, OD precipitation registered an increase of 2.42%, while 2016 experienced a decline of 12.47%. The final year, 2017, witnessed a positive percentage change of 9.86%, indicating a resurgence in precipitation.

Conversely, within the CHIRPS framework, the DD precipitation dataset displayed its own temporal fluctuations throughout the stipulated period. Notably, in 2010, DD precipitation exhibited a significant decrease, declining by approximately 21.55% in relation to the prior year (2009). This declining trend persisted into the subsequent years, as 2011 marked a further reduction of 10.81%. Nevertheless, 2012 deviated from this trend, with a positive percentage change of 10.28% compared to the preceding year. The year 2013 witnessed a substantial increase in DD precipitation, surging by 18.81% relative to 2012. In 2014, DD values remained relatively stable, with a marginal percentage change of 0.27%. The year 2015 recorded a modest increase of 3.33% in DD precipitation, while 2016 experienced a noticeable decrease of 12.60%. The concluding year, 2017, witnessed a reversal in this trend, with a positive percentage change of 9.83%. These observations collectively reveal the intricate dynamics of precipitation within the CHIRPS dataset. Within the OD precipitation dataset of the PERSIANN model, the year 2010 witnessed a decline of approximately 6.49% in precipitation compared to the prior year (2009). However, 2011 saw a notable upswing, signifying a percentage change of 10.77%. This upward trajectory continued into 2012, with an increase of 10.60%. The year 2013 exhibited a slight decrease of 3.27%, and 2014 recorded a substantial increase of 14.97%. Notably, in 2015, OD precipitation increased by 16.57%, but it witnessed a considerable decrease of 20.23% in 2016. This downward trend persisted into 2017, with a further reduction of 21.23%.

Similarly, the DD precipitation dataset under the PERSIANN model experienced noteworthy fluctuations. Commencing in 2010, there was a decrease of approximately 6.36% in DD precipitation compared to the preceding year (2009). However, in 2011, DD precipitation displayed an upsurge, registering an increment of 11.15%. The subsequent year, 2012, maintained this positive trajectory with a slight percentage change of 2.97%. The year 2013 exhibited an increase of 3.46% in DD precipitation. In 2014, DD values surged by 14.97%, while 2015 marked a substantial increment of 15.96%. Conversely, the year 2016 displayed a stark decrease of 20.37%, which was followed by a further downturn of 21.23% in 2017. As elucidated through the OD precipitation dataset within the GLDAS CLSM model, the year 2010 bore witness to a decrease of approximately 14.68% compared to the preceding year (2009). The year 2011 saw a further decline of 6.15%. Nevertheless, 2012 reflected an upswing in precipitation, with a substantial percentage change of 18.31%. 2013 displayed a minor percentage change of 1.79%, and 2014 registered a decrease of -2.83%. In stark contrast, the year 2015 saw a considerable increase of 23.92%. However, 2016 marked a noticeable decrease of 21.74%, followed by a further reduction of 17.40% in 2017. Subsequently, 2018 and 2019 witnessed substantial increments of 22.38% and 20.63%, respectively, in OD precipitation.

In the context of the GLDAS CLSM model, the DD precipitation dataset underscored its own nuances. The year 2010 marked a discernible decrease, with DD values dropping by approximately 23.25% compared to the previous year (2009). However, 2011 saw a positive percentage change of 4.35%, followed by a substantial increment of 19.18% in 2012. In 2013, DD precipitation showed a minute percentage change of 0.91%. Conversely, 2014 witnessed a slight decrease of -3.39%. The year 2015 registered a noteworthy increase of 27.76%, which was followed by a considerable decline of 21.35% in 2016. The final years of the dataset, 2017 to 2019, demonstrated consistent decreases in DD precipitation, with percentage changes of -20.94%, 22.35%, and 20.62%, respectively. Table 4.15 provides an overview of the assessment of the MODIS SSEBop ET dataset for the years 2010 to 2009. During this period, there was a notable reduction in ET from 9.83 BCM/year in 2009 to 8.93 BCM/year in 2010, resulting in a percentage change

of approximately -9.14%. This decrease indicates a significant decline in ET. The subsequent year, 2011, witnessed a further decrease in ET, as it decreased to 7.87 BCM/year from 8.93 BCM/year in 2010, marking a percentage change of approximately -11.91%. This reduction implies a continued decline in ET. However, in 2012, there was a notable increase in ET to 9.06 BCM/year from 7.87 BCM/year in 2011, resulting in a percentage change of approximately 15.15%. This change indicates a significant recovery in ET. The year 2013 saw a slight decrease in ET, as it decreased from 9.06 BCM/year in 2012 to 8.93 BCM/year in 2013, leading to a percentage change of approximately -1.43%. This change suggests relative stability in ET during this period. In 2014, ET exhibited a slight increase, rising from 8.93 BCM/year to 9.03 BCM/year, resulting in a percentage change of approximately 1.12%. This marginal increase implies a modest recovery in ET. The year 2015 witnessed a significant decrease in ET, as it dropped from 9.03 BCM/year to 8.35 BCM/year, resulting in a percentage change of approximately -7.54%. This reduction signifies a substantial decline in ET.

ET increased notably from 8.35 BCM/year in 2015 to 8.93 BCM/year in 2016, indicating a percentage change of approximately 6.99%. This change reflects a noteworthy recovery in ET. Conversely, in 2017, there was a significant decrease in ET from 8.93 BCM/year in 2016 to 7.02 BCM/year in 2017, resulting in a percentage change of approximately -21.38%. This decrease indicates a substantial decline in ET during this period. From 2010 to 2009, there was a marginal increase in ET, rising from 11.19 BCM/year in 2009 to 11.23 BCM/year in 2010, resulting in a percentage change of approximately 0.36%. This change suggests relative stability in ET during this period. However, in 2011, there was a significant decrease in ET, as it reduced to 8.59 BCM/year from 11.23 BCM/year in 2010, resulting in a percentage change of approximately -23.49%. This substantial decrease highlights a significant reduction in ET. In 2012, ET exhibited a notable increase, rising to 11.88 BCM/year from 8.59 BCM/year in 2011, marking a percentage change of approximately 38.45%. This change signifies a substantial recovery in ET. The year 2013 saw a marginal increase in ET, as it rose from 11.88 BCM/year in 2012 to 12.08 BCM/year in 2013, resulting in a percentage change of approximately 1.68%. This change suggests relative stability in ET during this

period. In 2014, ET witnessed a decrease, falling from 12.08 BCM/year to 11.45 BCM/year, leading to a percentage change of approximately -5.21%. This reduction implies a modest decline in ET. ET increased significantly in 2015, rising to 13.25 BCM/year from 11.45 BCM/year in 2014, resulting in a percentage change of approximately 15.68%. This increase highlights a significant recovery in ET. Conversely, in 2016, there was a notable decrease in ET, reducing from 13.25 BCM/year in 2015 to 12.00 BCM/year in 2016, leading to a percentage change of approximately -10.63%. This decrease indicates a notable reduction in ET. ET decreased further from 12.23 BCM/year in 2016 to 9.88 BCM/year in 2017 in 2017, resulting in a percentage change of approximately -19.21%. This reduction reflects a substantial decrease in ET. In 2018, ET increased to 10.53 BCM/year from 9.88 BCM/year in 2017, resulting in a percentage change of approximately 6.57%. This change suggests a moderate recovery in ET. The year 2019 experienced a notable increase in ET, rising to 13.29 BCM/year from 10.53 BCM/year in 2018, marking a percentage change of approximately 26.21%. This increase signifies a significant recovery in ET during this period. The discussion that could be made of this result is highlight the temporal variability in ET estimations provided by the MODIS SSEBop and GLDAS CLSM datasets. The distinct patterns of change, including periods of decline, stability, and recovery, indicate the sensitivity of ET to environmental and climatic factors. The observed decreases in ET, such as in 2011 and 2017 for both datasets, may be attributed to factors such as reduced precipitation and elevated temperatures. Conversely, notable recoveries in ET, such as in 2012 and 2019, may result from favorable environmental conditions.

Regarding TWSC both in OD and DD from RS-Based data such as CHIRPS and PERSIANN dataset along with GLDAS CLSM TWSC is also presented in Table 4.15 In 2009, In 2009, the CHIRPS based TWSC OD recorded -0.41 BCM/Year, signifying a decline. Subsequently, in 2010, TWSC (CH) increased by 0.31 BCM/Year, a 175.61% change. 2011 saw a minor increase of 0.03 BCM/Year, approximately -90.32%. However, 2012 witnessed a significant decrease of -1.09 BCM/Year, about -3766.67%. This decreasing trend continued in 2013 with -0.74 BCM/Year, a change of 32.11%. In 2014, there was a substantial recovery in TWSC (CH) with 2.07 BCM/Year, a positive change of 378.38%. 2015 showed a modest

increase of 0.56 BCM/Year, approximately -72.95%. In 2016, TWSC (CH) decreased by -0.52 BCM/Year, around -192.86%. In 2017, a significant increase was observed, with 1.77 BCM/Year, marking a positive change of approximately 440.38%. TWSC OD was derived from the GRACE original TWS layer for comparison with the PERSIANN dataset. The PERSIANN OD exhibited similar patterns to CHIRPS OD. Shifting to the DD form of CHIRPS and PERSIANN precipitation data against TWSC DD, in 2009, TWSC DD registered -0.510 BCM/Year, indicating a decrease. In 2010, a value of 0.380 BCM/Year was observed, a change of approximately 175.61%. In 2011, there was a minor increase of 0.040 BCM/Year, approximately -90.32%. In 2012, a significant decrease of -1.000 BCM/Year occurred, reflecting a substantial reduction, around -3766.67%. This trend continued into 2013 with -0.650 BCM/Year, a change of 32.11%. In 2014, a substantial recovery was observed with 1.830 BCM/Year, representing a positive change of approximately 378.38%. In 2015, a modest increase of 0.490 BCM/Year was recorded, about -72.95%. In 2016, there was a decrease of -0.450 BCM/Year, around -192.86%. The PERSIANN DD exhibited similar values to the CHIRPS DD TWSC solution. Turning to the GLDAS CLSM OD TWSC dataset, in 2009, it reported 1.040 BCM/Year. However, in 2010, there was a substantial decrease with a DD TWSC value of -1.23 BCM/Year, a negative change of approximately -218.08%. 2011 witnessed an increase with 1.450 BCM/Year, a positive change of approximately 219.23%. In 2012, there was a decrease with a DD TWSC value of -0.37 BCM/Year, about -125.97%. 2013 showed a slight increase of 0.160 BCM/Year, a positive change of approximately 143.75%. In 2014, a marginal increase of 0.210 BCM/Year was noted, a positive change of approximately 131.25%. 2015 demonstrated a further increment with 0.360 BCM/Year, marking a positive change of approximately 171.43%. In 2016, there was a significant decline with a DD TWSC value of -0.930 BCM/Year, around -258.33%. This decrease continued in 2017 with a value of -0.690 BCM/Year, reflecting a change of approximately -74.19%. 2018 exhibited a slight increase with 0.110 BCM/Year, a positive change of approximately 114.67%. The final year, 2019, experienced a minor increment with a value of 0.230 BCM/Year, a positive change of approximately 109.09%. Similarly, the GLDAS CLSM DD TWSC dataset exhibited its variations. In 2009, it reported 1.07 BCM/Year. However, in

2010, there was a significant decrease with a TWSC DD value of -1.33 BCM/Year, a negative change of approximately -224.30%. 2011 saw an increase with 1.55 BCM/Year, a positive change of approximately 239.25%. 2012 witnessed another decrease with a TWSC DD value of -0.37 BCM/Year, around -23.87%. 2013 showed a slight increase of 0.16 BCM/Year, a positive change of approximately 43.24%. In 2014, a marginal increase of 0.21 BCM/Year was noted, a positive change of approximately 131.16%. 2015 demonstrated a further increment with 0.44 BCM/Year, marking a positive change of approximately 209.52%. However, in 2016, there was a significant decline with a TWSC DD value of -0.98 BCM/Year, around -222.73%. The decrease continued in 2017 with a value of -0.75 BCM/Year, reflecting a change of approximately -76.53%. 2018 showed a slight increase with 0.11 BCM/Year, a positive change of approximately 114.67%. The final year, 2019, experienced a minor increment with a value of 0.15 BCM/Year, a positive change of approximately 36.59%.

The result discussion for all the water budget components over Kunduz catchment both in OD and DD form of the datasets as the CHIRPS framework, the DD precipitation dataset displayed its own fluctuations. Notably, in 2010, there was a significant decrease, declining by approximately 21.55% compared to 2009. This declining trend persisted into the subsequent years, with a further reduction of 10.81% in 2011. Nevertheless, 2012 deviated from this trend with a 10.28% positive change. The year 2013 witnessed a substantial 18.81% increase in DD precipitation, while 2014 remained stable with a marginal percentage change of 0.27%. 2015 recorded a 3.33% increase, and 2016 experienced a noticeable 12.60% decrease. The concluding year, 2017, saw a reversal in this trend with a positive percentage change of 9.83%. In the PERSIANN model, the OD precipitation dataset for 2010 saw a decline of approximately 6.49% compared to 2009, but 2011 marked a notable upswing with a 10.77% increase. This upward trajectory continued into 2012 with a 10.60% increase. However, 2013 showed a slight decrease of 3.27%, and 2014 recorded a substantial 14.97% increase. In 2015, precipitation increased by 16.57%, but a considerable decrease of 20.23% was observed in 2016, which persisted into 2017 with a further reduction of 21.23%. The DD precipitation dataset under the PERSIANN model experienced

fluctuations. In 2010, there was a decrease of approximately 6.36% compared to the preceding year, but 2011 displayed an upsurge with an increment of 11.15%. The subsequent year, 2012, maintained this positive trajectory with a 2.97% increase, followed by a 3.46% increase in 2013. In 2014, values surged by 14.97%, while 2015 marked a substantial 15.96% increase. Conversely, the year 2016 displayed a 20.37% decrease, followed by a further downturn of 21.23% in 2017. In the GLDAS CLSM model, both in its OD and DD forms, variations in precipitation were observed. In 2009, there was a 14.68% decrease compared to the preceding year. In 2011, there was a further decline of 6.15%. However, 2012 witnessed an increase of 18.31%. The subsequent years exhibited mixed patterns, with increases and decreases in both OD and DD forms. These precipitation variations had noticeable impacts on evapotranspiration (ET). When precipitation increased, as seen in 2012 and 2019 for CHIRPS OD, ET also displayed an increasing trend, signifying a positive correlation between precipitation and ET. Conversely, periods of precipitation decrease, such as in 2011 and 2017 for CHIRPS OD, were accompanied by a decline in ET, indicating a negative relationship between the two. These nuanced responses highlight the complex dynamics of the hydrological system within the Kunduz catchment. Furthermore, the variations in precipitation also had consequences for TWSC. In the CHIRPS dataset, an increase in precipitation in 2014, observed in both OD and DD forms, corresponded with a substantial recovery in TWSC. Conversely, years of reduced precipitation, like 2012 in CHIRPS DD, exhibited a decrease in TWSC, highlighting the close linkage between precipitation and TWSC dynamics. The ET dataset displayed a contrasting pattern. In years with increased precipitation, such as 2015 and 2019, ET increased significantly. Conversely, years with declining precipitation, like 2017, were associated with a decrease in ET. This suggests a positive relationship between precipitation and ET, where more precipitation allows for higher ET rates.

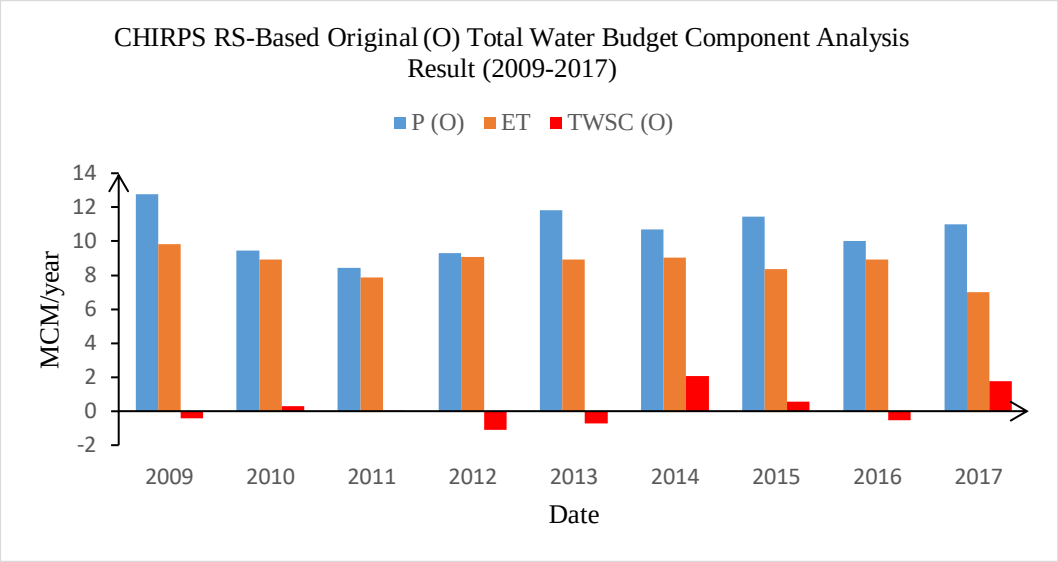

Figure 4.49 Original (O) Total Amount of RS-Based (CHIRPS) Water Budget Components in Kunduz Catchment (2009-2017)

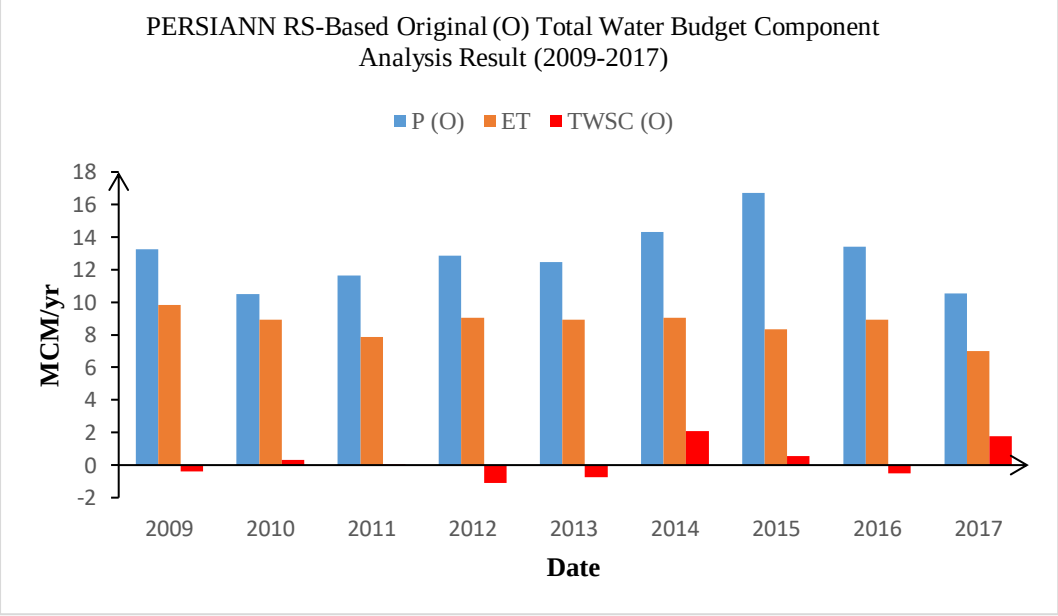

Figure 4.50 Original (O) Total Amount of RS-Based (PERSIANN Data) Water Budget Components in Kunduz Catchment (2009-2017)

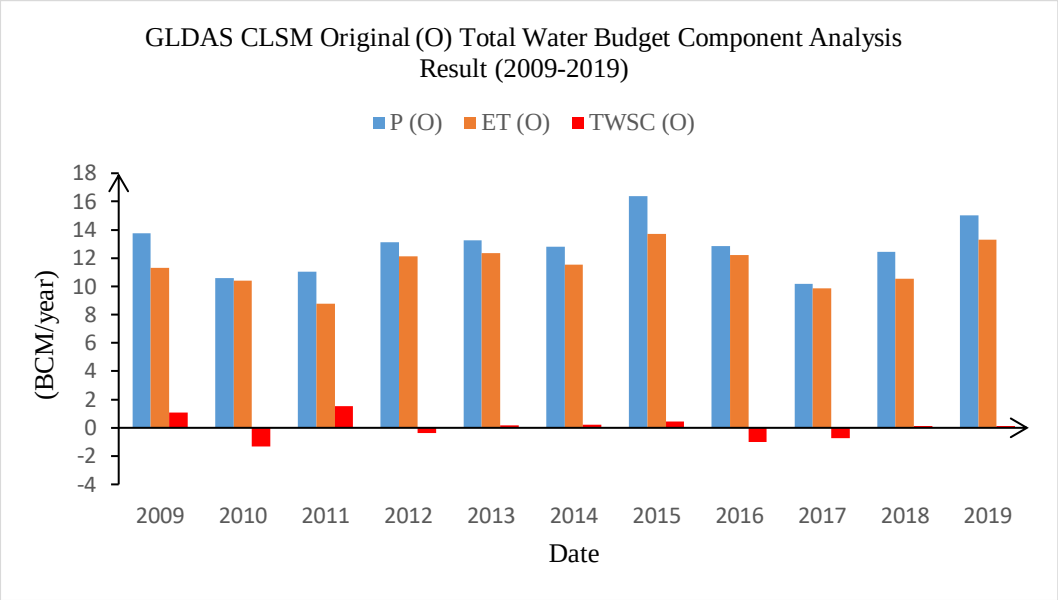

Figure 4.51 Original (O) Total Amount of GLDAS CLSM Data Water Budget Components in Kunduz Catchment (2009-2019)

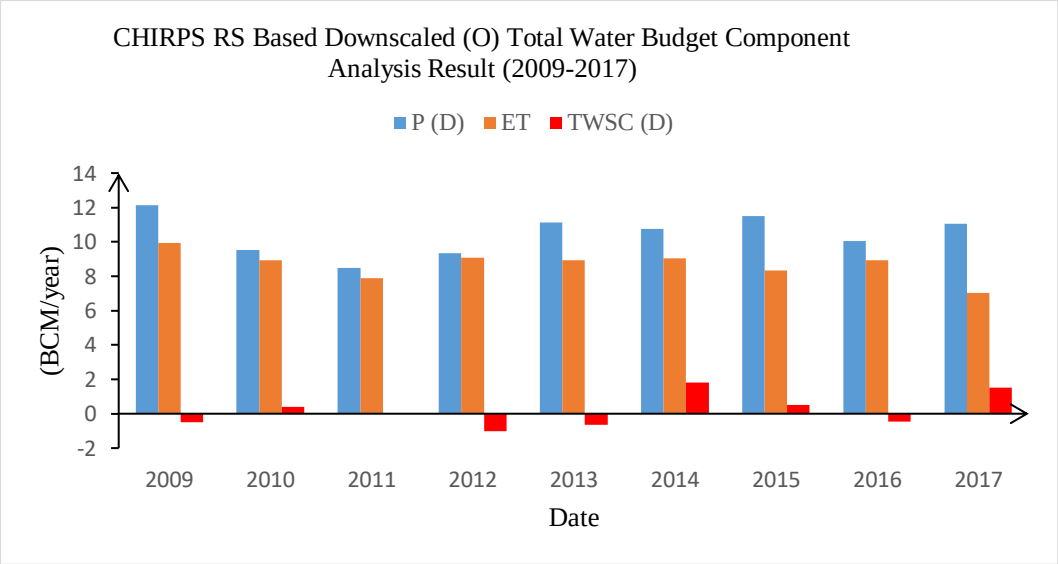

Figure 4.52 Downscaled (D) Total Amount of RS-Based (CHIRPS Data) Water Budget Components in Kunduz Catchment (2009-2017)

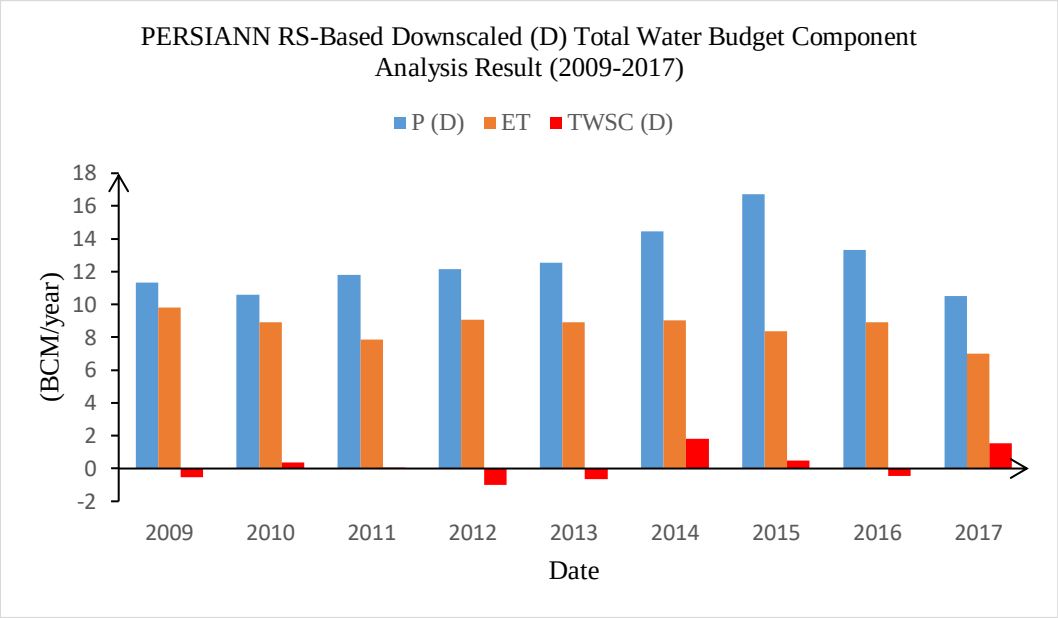

Figure 4.53 Downscaled (D) Total Amount of RS-Based (PERSIANN Data) Water Budget Components in Kunduz Catchment (2009-2017)

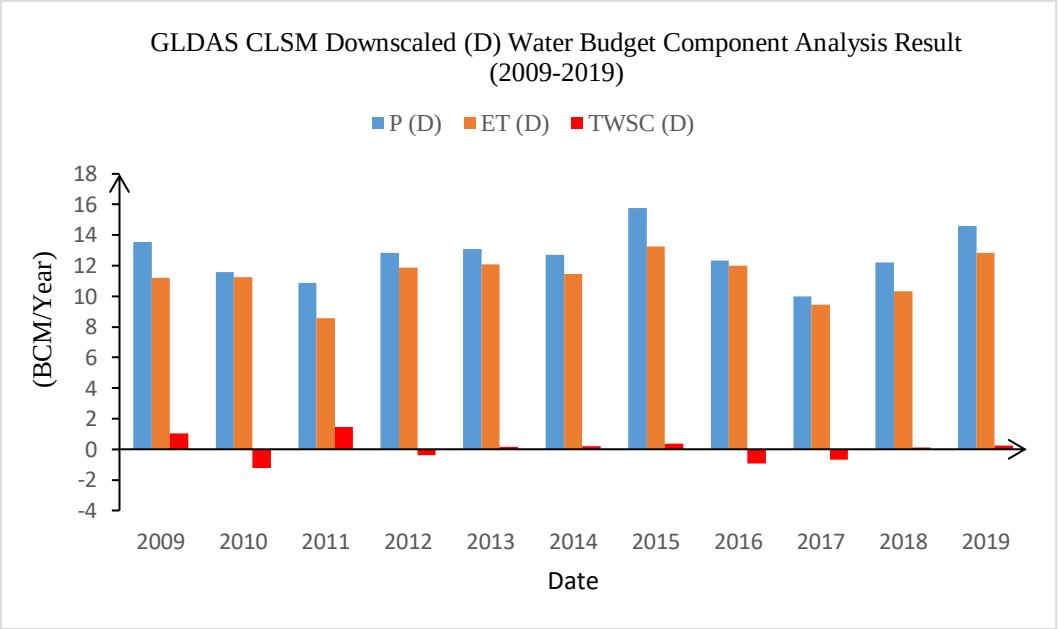

Figure 4.54 Downscaled (D) Total Amount of GLDAS CLSM Data Water Budget Components in Kunduz Catchment (2009-2019)

Table 4.15 Comparison of RS-Based and GLDAS CLSM Total Water Budget Components - Original (O) and Downscaled (D).

Dataset	Date	P (BCM/Year)		ET (BCM/Year)		TWSC (BCM/Year)	
		(O)	(D)	(O)	(D)	(O)	(D)
RS-Based (CHIRPS)	2009	12.76	12.12	9.83	9.83	-0.41	-0.51
	2010	9.46	9.51	8.93	8.93	0.31	0.38
	2011	8.42	8.48	7.87	7.87	0.03	0.04
	2012	9.3	9.35	9.06	9.06	-1.09	-1
	2013	11.83	11.11	8.93	8.93	-0.74	-0.65
	2014	11.18	11.14	9.03	9.03	2.07	1.83
	2015	11.45	11.51	8.35	8.35	0.56	0.49
	2016	10.02	10.06	8.93	8.93	-0.52	-0.45
	2017	11.01	11.05	7.02	7.02	1.77	1.53
RS-Based (PERSIANN)	2009	11.24	11.33	9.83	9.83	-0.41	-0.51
	2010	10.51	10.61	8.93	8.93	0.31	0.38
	2011	11.64	11.79	7.87	7.87	0.03	0.04
	2012	12.88	12.14	9.06	9.06	-1.09	-1
	2013	12.46	12.56	8.93	8.93	-0.74	-0.65
	2014	14.33	14.44	9.03	9.03	2.07	1.83
	2015	16.71	16.74	8.35	8.35	0.56	0.49
	2016	13.41	13.33	8.93	8.93	-0.52	-0.45
	2017	10.52	10.5	7.02	7.02	1.77	1.53
GLDAS CLSM	2009	13.56	13.77	11.19	11.31	1.04	1.07
	2010	11.57	10.57	11.23	10.41	-1.23	-1.33
	2011	10.86	11.03	8.59	8.79	1.45	1.55
	2012	12.85	13.14	11.88	12.12	-0.37	-0.37
	2013	13.08	13.26	12.08	12.37	0.16	0.16
	2014	12.71	12.81	11.45	11.53	0.21	0.21
	2015	15.75	16.37	13.25	13.69	0.36	0.44
	2016	12.33	12.87	12	12.23	-0.93	-0.98
	2017	9.98	10.18	9.45	9.88	-0.69	-0.75
	2018	12.22	12.46	10.32	10.53	0.11	0.11
	2019	14.6	15.03	12.83	13.29	0.23	0.15

4.7 Uncertainty Analysis

Tables 4.16 to 4.18 provide a detailed analysis of the uncertainty associated with each water budget component. These tables present the uncertainty data for both the OD and DD versions of the datasets for the years 2009 to 2019, except for the GRACE TWSC dataset, which is reported only up to 2017. Table 4.16 provides a comprehensive overview of key statistics and uncertainty levels for three distinct precipitation datasets, RS-Based CHIRPS, PERSIANN and GLDAS CLSM (P) over a period spanning from 2009 to 2019. The data is presented in terms of the OD and DD, and the uncertainty percentages (U) are calculated for each year. In the RS-Based CHIRPS (P) dataset, various statistics are observed to exhibit consistent patterns across the years. The minimum, maximum, mean, and standard deviation values in both OD and DD are relatively similar, suggesting good agreement. Moreover, the uncertainty percentages remain steady at 31% for the entire study period, indicating a consistent level of uncertainty. Similarly, the RS-Based PERSIANN (P) dataset demonstrates coherence between OD and DD in terms of the minimum, maximum, mean, and standard deviation values. The uncertainty percentages are relatively low, ranging from 7% to 17%, affirming the dataset's stability and reliability. In the case of the GLDAS CLSM (P) dataset, statistical values between the OD and DD also display close alignment. Although the uncertainty percentages vary somewhat, ranging from 6% to 26%, they remain within a moderate range.

In the context of ET uncertainty analysis, the study meticulously scrutinized the OD and DD for the RS-Based (MODIS SSEBop) and (GLDAS CLSM) ET components. The datasets characteristics and the mean uncertainty percentages (U) for both OD and DD are systematically summarized in Table 4.17. For the RS-Based SSEBop ET dataset, it is apparent that across the study period from 2009 to 2019, the dataset consistently displayed an uncertainty level of 67%, as reflected in both the OD and DD. This dataset presented maximum and minimum values that remained identical for both OD and DD, further reinforcing the stability of the uncertainty characteristics. Conversely, the GLDAS ET dataset demonstrated varying uncertainty levels over the study years. For this dataset, the OD uncertainty ranged from 15% in 2018 to 23% in 2010, with mean uncertainty percentages

between 16% and 20%. In the DD, the mean uncertainty ranged from 6% in 2018 to 16% in 2010. These variations suggest that the GLDAS ET dataset exhibited a degree of variability in uncertainty levels over time, with the Downscaled dataset generally displaying lower uncertainty compared to the original dataset. In summary, the RS-Based (MODIS SSEBop ET) dataset exhibited consistent uncertainty levels throughout the study period, while the GLDAS (ET) dataset displayed some variability in uncertainty, with the Downscaled dataset generally showing improved stability and lower uncertainty compared to the original dataset. These findings provide valuable insights into the reliability and consistency of these datasets in the context of evapotranspiration analysis.

Table 4.18 provides a comprehensive overview of the uncertainty analysis for TWSC data, particularly focusing on the GRACE and GLDAS datasets. Firstly, in the GRACE dataset, it is evident that there is substantial variation in uncertainty percentages. The minimum uncertainty for the original dataset ranged from 83% in 2012 to 310% in 2011, while the Downscaled dataset exhibited a similar trend, with minimum uncertainties varying from 69% to 208%. These high percentages of uncertainty indicate the challenging nature of TWSC estimation using GRACE data. Conversely, the GLDAS dataset showed a comparatively lower range of uncertainty percentages. The minimum uncertainty in the original dataset for GLDAS ranged from 20% in 2009 to 52% in 2017. In the Downscaled dataset, the minimum uncertainty varied between 12% and 29%. While these percentages are notably lower than those observed for the GRACE dataset, they still indicate the presence of significant uncertainty in TWSC estimation. Additionally, it is interesting to note that in 2018 and 2019, both datasets for GRACE and GLDAS showed 0% uncertainty. However, this could be attributed to specific data characteristics or limitations for those particular years. In conclusion, the GRACE dataset exhibited substantially higher uncertainty percentages compared to the GLDAS dataset, suggesting that the latter may be more reliable for TWSC estimation.

Table 4.16 Uncertainty Analysis of the Precipitation (P) Water Budget Component from RS-Based and GLDAS CLSM Sources in Both (O) and (D) Datasets, Including Minimum (Min), Maximum (Max), Standard Deviation (Std Dev), and Uncertainty (U).

Data	Year	Min (O)	Min (D)	Max (O)	Max (D)	Mean (O)	Mean (D)	Std Dev (O)	Std Dev (D)	U (O) (%)	U (D) (%)
RS-Based (CHIRPS (P))	2009	225.6	233.6	1000.0	967.5	490.3	489.3	152.7	149.5	31%	31%
	2010	144.8	152.9	764.5	781.3	363.2	362.4	117.3	115.3	32%	32%
	2011	123.0	126.7	671.6	642.2	324.7	324.2	104.6	101.8	32%	31%
	2012	133.9	140.0	689.2	674.5	360.0	358.9	120.2	117.5	33%	33%
	2013	158.4	167.9	1199.3	1118.6	451.6	450.0	198.5	194.9	44%	43%
	2014	170.9	180.2	980.7	957.5	409.2	408.5	144.4	141.5	35%	35%
	2015	144.4	167.6	1132.0	1058.7	437.7	436.8	170.0	167.0	39%	38%
	2016	164.8	173.0	936.3	903.9	382.0	381.0	154.0	150.5	40%	40%
	2017	196.7	207.0	1086.3	974.9	417.6	416.8	151.9	149.3	36%	36%
	2018	195.8	213.2	1112.7	1122.0	452.3	451.1	188.5	185.3	42%	41%
	2019	252.9	265.2	1205.7	1141.3	565.2	563.2	170.3	165.5	30%	29%
RS-Based (PERSIANN (P))	2009	357.8	403.8	652.0	602.8	482.1	516.6	79.5	57.3	17%	11%
	2010	289.0	278.9	537.9	557.7	409.4	404.0	64.1	60.3	16%	15%
	2011	342.4	365.4	574.9	569.5	448.5	447.0	51.5	43.5	11%	10%
	2012	387.0	404.9	606.8	639.5	493.9	490.9	56.0	52.8	11%	11%
	2013	368.3	353.6	594.3	598.6	479.5	476.5	51.9	49.9	11%	10%
	2014	445.4	425.0	730.2	773.7	553.2	547.3	80.3	79.8	15%	15%
	2015	525.9	504.9	861.6	913.2	642.4	633.7	90.6	86.5	14%	14%
	2016	391.9	380.1	651.5	621.6	514.4	504.2	68.5	59.9	13%	12%
	2017	346.6	337.2	517.4	525.0	404.2	398.0	44.1	38.6	11%	10%
	2018	420.1	404.6	637.2	630.9	516.1	512.0	47.6	51.8	9%	10%
	2019	503.3	509.1	755.6	724.6	584.8	578.9	49.1	41.9	8%	7%
GLDAS CLSM (P)	2009	357.8	403.8	652.0	602.8	482.11	516.6	79.5	57.3	17%	11%
	2010	240.9	265.0	556.1	525.3	378.33	404.9	99.0	74.6	26%	18%
	2011	318.4	342.7	494.2	490.3	389.95	413.0	57.6	37.3	15%	9%
	2012	304.5	382.5	593.3	580.8	443.71	488.6	83.6	54.0	19%	11%
	2013	322.3	340.7	583.0	570.7	463.84	499.2	101.1	70.9	22%	14%
	2014	330.5	357.0	601.2	583.7	454.28	484.3	81.8	61.5	18%	13%
	2015	384.4	448.4	729.6	680.2	729.61	599.1	101.1	65.7	14%	11%
	2016	308.8	350.0	548.0	530.7	420.05	469.1	84.7	55.3	20%	12%
	2017	259.3	280.2	505.7	474.3	359.68	381.4	77.6	54.9	22%	14%
	2018	320.4	411.8	533.8	537.5	445.34	462.5	65.7	25.9	15%	6%
	2019	397.5	446.6	697.6	647.1	508.22	555.9	97.3	61.4	19%	11%

Table 4.17 Uncertainty Analysis of Evapotranspiration (ET) Component from RS- Based and GLDAS CLSM Sources in Both (O) and (D) Datasets.

Data	Year	Min (O)	Min (D)	Max (O)	Max (D)	Mean (O)	Mean (D)	Std Dev (O)	Std Dev (D)	U (O) (%)	U (D) (%)
RS-Based (MODIS SSEBop ET)	2009	0.0	0.0	1724.0	1724.0	376.4	376.4	218.7	218.7	58%	58%
	2010	0.0	0.0	1777.0	1777.0	316.4	316.4	212.5	212.5	67%	67%
	2011	0.0	0.0	1641.0	1641.0	286.6	286.6	198.5	198.5	69%	69%
	2012	0.0	0.0	1783.0	1783.0	365.7	365.7	223.4	223.4	61%	61%
	2013	0.0	0.0	1692.0	1692.0	315.0	315.0	209.9	209.9	67%	67%
	2014	0.0	0.0	1748.0	1748.0	344.4	344.4	208.1	208.1	60%	60%
	2015	0.0	0.0	1658.0	1658.0	320.5	320.5	228.9	228.9	71%	60%
	2016	0.0	0.0	1695.0	1695.0	303.9	303.9	213.7	213.7	70%	70%
	2017	0.0	0.0	1696.0	1696.0	269.1	269.1	209.8	209.8	78%	78%
	2018	0.0	0.0	1668.0	1668.0	293.8	293.8	199.9	199.9	68%	68%
	2019	0.0	0.0	1756.0	1756.0	317.9	317.9	220.7	220.7	70%	70%
GLDAS (ET)	2009	309.3	343.9	541.2	510.8	399.9	426.2	64.8	45.6	16%	11%
	2010	279.7	303.5	562.5	532.6	396.0	429.3	90.8	66.8	23%	16%
	2011	221.5	270.2	407.8	415.8	299.7	325.4	57.6	34.0	19%	10%
	2012	324.2	354.5	549.3	530.4	417.4	452.3	71.6	46.6	17%	10%
	2013	303.2	342.2	532.3	529.5	421.9	459.9	83.3	52.3	20%	11%
	2014	316.5	334.5	556.3	546.9	403.6	436.4	78.9	53.1	20%	12%
	2015	343.6	388.5	619.6	578.6	462.6	503.7	81.0	49.2	18%	10%
	2016	306.8	368.3	579.9	560.7	424.7	479.4	86.7	49.7	20%	10%
	2017	249.1	275.5	469.1	440.2	337.3	360.8	67.1	45.2	20%	13%
	2018	284.5	337.9	463.5	467.4	371.3	390.9	57.1	24.3	15%	6%
	2019	336.2	388.9	608.6	568.3	447.0	488.5	84.7	51.6	19%	11%

Table 4.18 Uncertainty Analysis of TWSC Component from RS- Based (GRACE) and GLDAS CLSM Sources in Both (O) and (D) Datasets.

Data	Year	Min (O)	Min (D)	Max (O)	Max (D)	Mean (O)	Mean (D)	Std Dev (O)	Std Dev (D)	U (O) (%)	U (D) (%)
GRACE (TWSC)	2009	-99.7	-91.7	15.2	26.4	-19.0	-18.9	29.8	24.7	260%	131%
	2010	-5.7	-14.8	70.9	62.2	14.3	14.1	19.9	16.0	139%	114%
	2011	-10.5	-9.2	20.5	10.5	2.2	1.6	6.7	3.3	310%	208%
	2012	-112.3	-136.0	-8.6	9.9	-39.9	-37.4	33.0	25.7	83%	69%
	2013	-86.6	-102.8	-2.3	14.0	-24.8	-24.2	23.6	20.0	95%	83%
	2014	1.5	-45.4	247.7	297.1	67.5	67.7	73.8	64.2	109%	95%
	2015	-19.2	1.8	100.1	64.7	16.9	18.3	25.6	11.1	151%	61%
	2016	-65.7	-79.3	9.7	17.9	-15.3	-16.6	22.3	19.2	146%	116%
	2017	12.6	-26.8	203.9	243.7	59.9	57.0	52.9	44.6	88%	78%
	2018	0.0	0.0	0.0	0.0	0.0	0.0	0.0	0.0	0.0	0.0
	2019	0.0	0.0	0.0	0.0	0.0	0.0	0.0	0.0	0.0	0.0
GLDAS (TWSC)	2009	10.7	18.9	60.6	61.3	33.7	38.8	14.3	7.6	42%	20%
	2010	-65.9	-60.6	-9.4	-24.8	-42.9	-46.4	13.5	5.4	32%	12%
	2011	31.9	43.8	95.0	122.7	58.2	83.0	17.9	24.3	31%	29%
	2012	-56.7	-53.8	7.8	26.4	-22.7	-14.6	19.9	16.7	88%	115%
	2013	-18.7	-27.7	32.7	41.1	9.2	6.2	13.3	12.1	144%	195%
	2014	-12.7	-21.1	29.0	26.8	7.7	7.6	14.7	6.4	192%	83%
	2015	-27.0	-8.0	29.5	42.1	6.8	13.3	15.8	9.6	231%	72%
	2016	-84.8	-88.8	14.8	0.1	-30.2	-34.8	22.3	14.7	74%	42%
	2017	-46.3	-43.7	-3.9	-6.2	-22.9	-25.9	11.8	7.5	52%	29%
	2018	-28.9	-45.6	74.7	42.5	10.3	3.8	32.3	17.7	314%	470%
	2019	-28.5	-34.4	37.9	57.9	5.1	8.3	22.5	19.8	440%	237%

4.8 Statistical Tests and Findings

In the context of performance analysis, the study conducted crucial correlation tests, with a specific focus on Tables 4.1, 4.4, and 4.7, to assess the degree of correlation between the original and downscaled datasets in comparison to observed precipitation collected from Kunduz catchment gauge stations (as shown in Figure 2.3 and Table 2.1). This assessment primarily pertained to precipitation (P), the first component of the water budget. Additionally, monthly downscaled evapotranspiration (ET) values, representing the second component of the water budget, were visually examined in relation to downscaled CHIRPS precipitation data. This examination provided insights into the dynamics of ET concerning precipitation patterns within the Kunduz catchment Figure 4.29 to 4.32.

Due to limited groundwater data availability within the Kunduz catchment, a direct comparison with GRACE or GLDAS TWS data was infeasible. However, the presence of runoff data from gauge stations (Figure 2.3) within the Kunduz catchment allowed for a comparative analysis between remote sensing-based residual (P-ET-TWSC) and GLDAS CLSM inferred runoff, as well as GLDAS CLSM surface runoff, in both OD and DD. These parameters constitute the third component of the water budget. The primary objective of these tests was to determine if water budget outcomes, either in their original form or as downscaled versions, originating from the Rs-based dataset or the GLDAS CLSM dataset, with a specific focus on residual or inferred runoff components, exhibited a significant level of concordance with observed runoff data. This analysis aimed to identify which of the two approaches demonstrated superior alignment with observed runoff.

In Table 4.19, Table 4.20 (annual), and Table 4.21 (monthly), the statistical test results for three datasets, namely CHIRPS, PERSIANN, and GLDAS CLSM, were presented in comparison to observed runoff. Table 4.20 (annual) specifically focused on the statistical test results for three datasets, namely CHIRPS, PERSIANN, and GLDAS CLSM, both in comparison to observed runoff and GLDAS CLSM surface runoff. These analyses centered on their residuals (P-ET-TWSC), referred to as inferred runoff, and aimed to assess the model's performance concerning the water budget components. The results were rigorously compared against the observed runoff data collected within the Kunduz catchment. Furthermore, in Table 4.21 (monthly), the statistical test results for the same datasets—CHIRPS, PERSIANN, and GLDAS CLSM—were examined on a monthly scale, focusing on their correlations with observed runoff.

Before proceeding with the presentation of the statistical test results for the water budget components, a brief explanation of the applied metrics is warranted. The first statistical test, Percent Bias (PBIAS), was utilized to evaluate the average tendency of the simulated values to deviate from their observed counterparts. An optimal PBIAS value of 0.0 was aimed for, with lower-magnitude values indicating precise model simulations. Positive PBIAS values denoted a bias toward overestimation, while negative values indicated a bias toward underestimation

within the model. This metric was employed to assess the accuracy of the model's predictions regarding observed runoff.

The second test employed was the Nash-Sutcliffe Efficiency (NSE), a normalized statistic used to evaluate the relative magnitude of the residual variance (termed "noise") compared to the variance of the measured data (referred to as "information"). NSE provided values ranging from (-Inf to 1), with values approaching 1 signifying a more accurate model. In other words, the closer the NSE value was to 1, the better the model's accuracy [184]. The third test, denoted as (r), represented Pearson's correlation coefficient, indicating the Mean Squared Error. It quantified the degree of linear association between simulated and observed values. The fourth statistical test was the Coefficient of Determination (R^2), calculated by multiplying the slope of the regression line between simulated and observed values, considering any treatment of missing values.

The sixth statistical test was KGE, a goodness-of-fit measure developed to provide a diagnostically interesting decomposition of the Nash-Sutcliffe efficiency (and hence MSE). It facilitated the analysis of the relative importance of its different components, including correlation, bias, and variability, in the context of hydrological modeling. The last statistical test, VE (Volumetric Efficiency), was proposed to circumvent some problems associated with the Nash-Sutcliffe efficiency. VE ranged from 0 to 1 and represented the fraction of water delivered at the proper time, with its complement signifying the fractional volumetric mismatch [185].

Regarding the performance analysis, both the original and downscaled forms of CHIRPS (CH) exhibited underestimations, with the original CHIRPS dataset showing approximately -7.30 and the downscaled CHIRPS water budget residual demonstrating a -12 bias in estimation. PERSIANN, on the other hand, exhibited overestimations in both the OD and downscaled DD. For GLDAS CLSM, underestimations were observed, with the GLDAS CLSM D dataset showing approximately -21.5 and the GLDAS CLSM O dataset exhibiting -32.4.

For the NSE metric, considering the CHIRPS dataset, the NSE value for the CH (D) dataset yielded a mean value of -0.84, whereas the NSE for the original CHIRPS dataset resulted in a comparatively lower mean value of -1.89, indicating

that the NSE for CH DD outperformed its original counterpart. In the case of the PERSIANN dataset, the downscaled version exhibited a mean NSE value of -11.53, while the PERS OD had a mean NSE value of -12.2. This observation implies that the NSE for the PERS DD performed slightly better than the original one. Shifting our focus to the GLDAS CLSM dataset, the analysis revealed that the GL DD dataset achieved a mean NSE value of -0.44, while the original GLDAS CLSM dataset recorded a mean NSE value of -0.54. These findings suggest that, although the results are relatively similar, the GL DD exhibited slightly superior performance in terms of NSE.

For the (r) Pearson's correlation coefficient, in the CHIRPS (CH), the dataset CH (DD) demonstrated a mean (r) value of 0.43, whereas the original CHIRPS dataset CH (OD) yielded a slightly lower mean (r) value of 0.27. These results indicated that the CH (DD) exhibited a relatively stronger correlation compared to the CH (OD). In the case of the PERSIANN dataset, the (PERS (DD) exhibited a mean (r) value of 0.24, while the original PERSIANN dataset (PERS (OD) showed a lower mean (r) value of 0.19, suggesting that the PERS (DD) had a somewhat stronger correlation than the original PERSIANN dataset. Turning to the GLDAS CLSM dataset, the analysis revealed that the GL (DD) achieved a mean (r) value of 0.49, whereas the GL (O) dataset recorded a mean (r) value of 0.42. These findings indicated that the GL (DD) exhibited a slightly stronger correlation compared to the GL (OD).

In the CHIRPS dataset, the CH (DD) achieved a mean R^2 value of 0.18, indicating a moderate level of explained variance. In comparison, the CH (OD) exhibited a lower mean R^2 value of 0.07, suggesting a weaker explanatory power. In the PERSIANN dataset, the PERS (DD) showed a mean R^2 value of 0.06, implying a relatively lower level of variance explanation. Similarly, the PERS (OD) displayed a slightly lower mean R^2 value of 0.04, suggesting a comparable degree of variance explanation. Within the GLDAS CLSM dataset, the GL (DD) yielded a mean R^2 value of 0.24, indicating a moderate level of variance explanation. The GL (OD) recorded a mean R^2 value of 0.18, suggesting a similar level of explained variance. For KGE In the CHIRPS dataset, the CH (DD) demonstrated a mean KGE value of 0.15, reflecting a moderate level of goodness-of-fit. The CH (OD) resulted in a

lower mean KGE value of 0.06, indicating a weaker goodness-of-fit. Within the PERSIANN dataset, the PERS (DD) exhibited a mean KGE value of 0.03, suggesting a relatively lower level of goodness-of-fit. The PERS (OD) had a slightly lower mean KGE value of 0.02, implying a similar level of goodness-of-fit. In the GLDAS CLSM dataset, the GL (DD) recorded a mean KGE value of 0.15, indicating a moderate level of goodness-of-fit. The GL (OD) displayed a mean KGE value of 0.11, suggesting a comparable goodness-of-fit level. For VE (Volumetric Efficiency) In the CH (DD) presented a mean VE value of 0.29, signifying a relatively high proportion of water delivered at the proper time. In contrast, the original CH (OD) exhibited a mean VE value of 0.01, implying a significantly lower fraction of water delivered at the correct timing. For the PERSIANN dataset, the PERS (DD) resulted in a mean VE value of -0.96, indicating that a substantial volumetric mismatch occurred. The original PERSIANN dataset PERS (OD) had a mean VE value of -1.06, suggesting a comparable volumetric mismatch. Within the GLDAS CLSM dataset, the GL (DD) achieved a mean VE value of 0.27, indicating a relatively high fraction of water delivered at the correct time. The GL (OD) displayed an identical mean VE value of 0.16, signifying a similar proportion of water delivered at the proper time.

Table 4.19 Statistical Analysis of Rs-Based CHIRPS Downscaled (CH (D)) and Original (CH (O)), PERSIANN Downscaled (PERS (D)) and Original (PERS (O)), and GLDAS CLSM Downscaled (GL (D)) and Original (GL (O)) Residuals (Inferred Runoff) Compared to Observed Runoff from Kunduz Catchment Gauge Stations.

Dataset	PBIAS %	NSE	r	R^2	KGE	VE
CH (D)	-12	-0.84	0.43	0.18	0.29	0.53
CH (O)	-7.30	-1.89	0.27	0.07	0.01	0.42
PERS(D)	102.3	-11.53	0.24	0.06	-0.96	-0.14
PERS(O)	101.9	-12.2	0.19	0.04	-1.06	-0.17
GL (D)	-31.5	-0.44	0.49	0.24	0.27	0.64
GL (O)	-32.4	-0.54	0.42	0.18	0.16	0.64

In another attempt A comprehensive statistical analysis was conducted to gain a profound understanding of surface runoff fluctuations using remote sensing

datasets and GLDAS CLSM. This analysis encompassed a comparison of GLDAS CLSM Surface Runoff with observed runoff, as well as the residual (inferred runoff) derived from both RS-based datasets in their downscaled and original forms. The study focused on three primary datasets: CHIRPS, PERSIANN, and GLDAS CLSM. Within Table 4.20, and Figures 4.55 and 4.56, GL SR (DD) designates the downscaled GLDAS CLSM Surface Runoff, while GL SR (O) denotes the original GLDAS CLSM Surface Runoff. Overall, the analysis revealed a scenario of underestimation for GLSR, with downscaled datasets displaying lower estimated values, while original datasets exhibited higher underestimations. However, when comparing GLSR (DD) with GLSR (OD), an overestimation trend becomes apparent. The most favorable performance in terms of NSE is evident in the comparison between CH (DD) and GLSR (DD), exhibiting a strong concurrence with the observed data. Furthermore, a notably high positive correlation (r) of 0.71 is identified between GLSR (DD) and observed runoff, with the highest correlation observed between CH (DD) and GLSR (DD). In contrast, the weakest correlation is observed between PERS (OD) and GLSR (OD). Notably, the R-squared (R^2) values for the downscaled datasets indicate significant improvements for GLDAS and CHIRPS datasets, as depicted in Figure 4.55, as well as for GLDAS and observed runoff, as shown in Figure 4.56.

KGE values indicate that the performance of GLSR (DD) is superior to other datasets, especially when compared to CH (DD), which again displays the highest KGE among all the datasets. In the VE statistical test presented in Table 4.20, it's evident that volumetric efficiency shows a significant improvement for the downscaled dataset. This improvement supports the overall enhancement of the CHIRPS downscaled data. Specifically, approximately 60 percent of the flow volume is accurately represented at the appropriate time within the flow dynamics. On the other hand, the comparison of GLDAS downscaled data against observed runoff reveals even more favorable results. Among the downscaled datasets, GLSR (DD) stands out as the top performer, particularly when contrasted with CH (DD).

Table 4.20 Statistical Analysis of Rs-Based CHIRPS Downscaled (CH (D)) and Original (CH (O)), PERSIANN Downscaled (PERS (D)) and Original (PERS (O)), and GLDAS CLSM Surface Runoff Downscaled (GLSR (D)) and Original Surface Runoff (GLSR (O)) Residuals (Inferred Runoff) Compared to Observed Runoff from Kunduz Catchment Gauge Stations.

Dataset	PBIAS %	NSE	r	R^2	KGE	VE
GLSR (D)	-39.9	-0.67	0.71	0.51	0.22	0.60
GLSR (O)	-41.2	-1.82	0.65	0.42	0.15	0.59
GLSR (D) vs PERS (D)	-69.5	-1.84	0.54	0.29	-0.19	0.31
GLSR (O) vs PERS (O)	-70	-1.73	0.49	0.24	-0.23	0.3
GLSR (D) vs CH (D)	-29.8	0.1	0.75	0.56	0.16	0.49
GLSR (O) vs CH (O)	-3470	-0.01	0.68	0.46	0.06	0.41
GLSR (D) vs GL (D)	-39.9	-0.67	0.71	0.51	0.22	0.6
GLSR (O) vs GL (O)	-41.2	-0.82	0.65	0.42	0.15	0.59
GLSR(D) vs GL (D)	14	-0.69	0.59	0.35	0.39	0.77
GLSR(O) vs GL (O)	14.9	-0.8	0.59	0.35	0.38	0.73

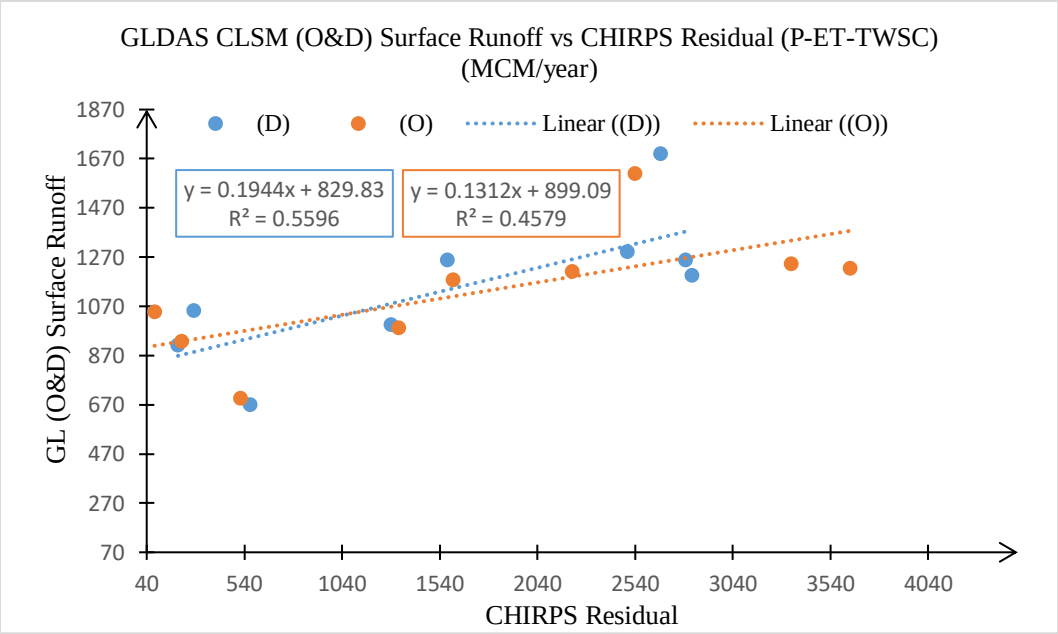

Figure 4 55 GLDAS CLSM Downscaled and Original Surface Runoff vs CHIRPS Downscaled and Original Residual

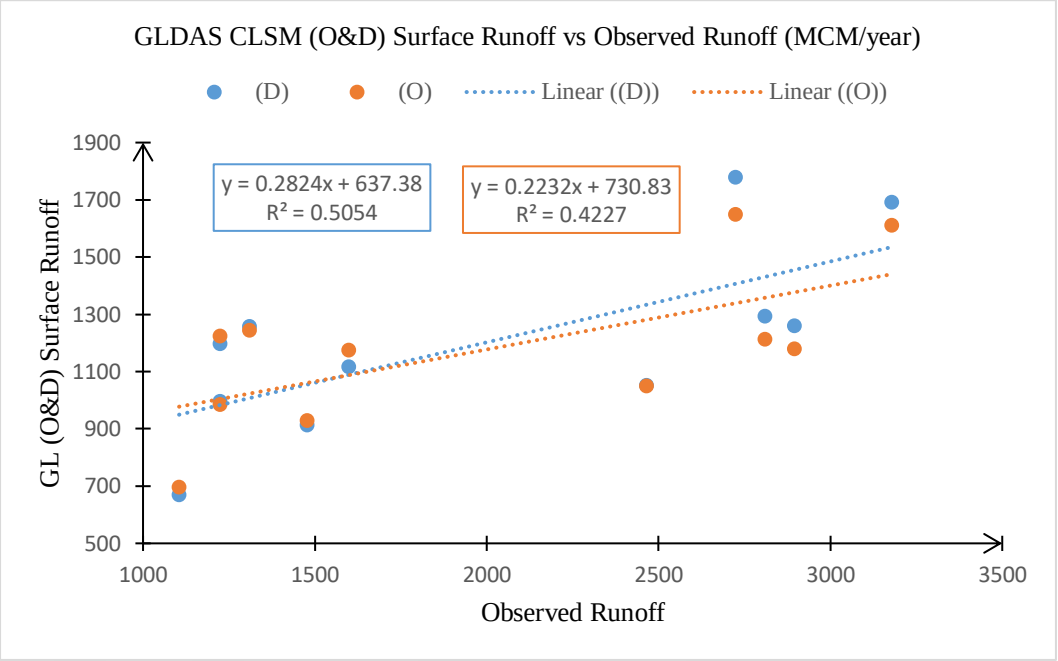

Figure 4 56 GLDAS CLSM Downscaled and Original Surface Runoff vs Observed Runoff

In Table 4.21, a monthly-scale analysis of the statistical results suggests that the computation of a monthly water budget in the Kunduz catchment was unattainable. It can be inferred that none of the statistical tests exhibit optimal performance.

Table 4.21 Monthly statistical analysis result for Rs based and GLDAS CLSM residual (P-ET-TWSC) vs observed runoff.

Dataset	PBIAS %	NSE	r	R^2	KGE	VE
CH (D)	623.1	-329.4	-0.1	0.0	-15.0	-8.2
CH (O)	576.8	-287.5	-0.3	0.1	-13.8	-8.2
PERS (D)	52.3	-123.0	0.1	0.0	-9.2	-4.6
PERS (O)	91.4	-114.2	0.1	0.0	-8.8	-4.6
GL (D)	-152.3	-117.5	-0.3	0.1	-8.5	-5.0
GL (O)	-46.1	-211.2	-0.3	0.1	-12.3	-7.0

In this study, additional statistical results for SEBAL evapotranspiration are provided in Table 4.22 through Table 4.24. These findings are presented to demonstrate that SEBAL, along with other conventional evapotranspiration calculation methods, serves as a valuable alternative data source in data-scarce

catchments. This approach is instrumental in acquiring essential hydrological parameters, particularly evapotranspiration, through remote sensing techniques.

Table 4.22 Accuracy assessment of SEBAL result using two meteorological station data.

Equations	ET_{HS}	ET_{PM}	ET_{Lin}	ET_{Mak}	ET_{Abt}	ET_{PT}
MAD	2.61	0.90	2.10	2.84	3.61	5.15
RMSE	2.72	0.91	2.31	2.86	3.68	5.19
NSE	0.40	0.99	0.61	0.29	-0.13	-1.32

MAD - Median absolute deviation; RMSE - Root-Mean-Square Error; NSE - Nash Sutcliffe Error.

Descriptive statistical parameters (i. e, minimum, maximum and mean values) produced by zonal statistics using GIS tools, are used (Tables 4.22).

Table 4.23 Statistics of albedo, Nb-Emissivity, NDVI, LAI, and LST in Kunduz Catchment.

Values	Albedo	Nb-Emissivity	NDVI	LAI	LST (°C)
Minimum	0.00	0	-1.00	0.00	- 4.2
Maximum	0.70	0.98	0.80	3.32	48.39
Mean	0.27	0.96	0.15	0.06	28.73
Std	0.10	0.061	0.09	0.10	7.309

NDVI - Normalized Difference Vegetation Index; LAI - Leaf Area Index; LST - Land Surface Temperature; Nb-Emissivity - Narrow Band Emissivity.

Table 4.24 Statistical properties of energy balance parameters, in Kunduz Catchment.

Values	Rn	G	H	ET-Inst	ET-24
Min	25.7	20.1	94.5	0.0	0.0
Max	840.3	435.1	505.1	1.3	17.4
Mean	450.1	87.2	299.8	0.5	8.7
Std	51.2	20.3	68.8	2.9	0.2

Rn - Net Radiation; G - Soil heat flux; H - Sensible heat flux; ET-Inst - Hourly ET values; ET-24 - ET Values for one day.

When widely used ET methods compared with SEBAL results, PM resulted with the highest estimation followed by Lin. HS and Mak were acceptable and applicable, while PT and Abt were not good enough to estimate ET in the study area (Table 4.22). Similar to this research [169], Grosso et al. studied the SEBAL

results with also no measured validation data. They compared SEBAL with PM and a three-dimensional soil-plant simulation. Moreover, in SEBAL analysis part of this study the comparison was made not only PM but also with three temperatures and three radiation-based methods. Both results proved the potential of SEBAL with lack of measured data.

4.9 Discussion of Statistical Result

The discussion of the statistical results concerning remote sensing based and GLDAS CLSM water components in this study reveals several key findings. Firstly, the study showed an overestimation of precipitation when compared to observed precipitation collected from gauge stations, both in their original data (OD) and downscaled (DD) data formats. Simultaneously, the observed runoff, as per CHIRPS and GLDAS datasets, displayed an underestimation, indicating that the surface runoff was underestimated. This observation is consistent with findings from a previous study conducted by [15]. However, in contrast to the underestimation observed with CHIRPS and GLDAS, the PERSIANN dataset exhibited an overestimation of surface runoff. This finding aligns with a minor variation in the utilization of precipitation datasets [18]. While overestimation and underestimation in water budget studies can be attributed to numerous sources of error, it is believed that the primary source of this discrepancy may lie in the precipitation data sources. This study concurs with previous research by [13, 15, 40], which also suggested precipitation as a potential contributing factor.

In the Kunduz catchment, one of the potential factors contributing to the underestimation of runoff could be the variations in ET values Table 4.24 explain the (ET Percentages). This phenomenon was particularly evident in the CHIRPS and GLDAS CLSM datasets, both in their OD and DD. These datasets exhibited exceptionally high ET percentages, ranging from 75% to 98%, indicating that a significant proportion of the precipitation was being consumed through evapotranspiration. This high ET rate may have contributed to the underestimation of runoff within the Kunduz catchment. Conversely, the utilization of the PERSIANN precipitation data in conjunction with SSEBop ET values revealed a lower rate of evapotranspiration. This, in turn, could lead to an overestimation of

runoff. Studies, such as the one conducted by[48] have reported fluctuations in ET that can significantly influence the hydrological dynamics of a basin. These findings suggest that variations in evapotranspiration play a pivotal role in altering the runoff patterns within the Kunduz catchment. Climate change is a critical factor that could contribute to the overestimation of runoff within the Kunduz catchment. As reported by [77] the temperature trend in the Kunduz catchment has exhibited a consistent increment. This upward trend in temperature can lead to accelerated snowmelt, resulting in an increased volume of runoff. Consequently, this elevated runoff caused by climate change may not be accurately accounted for in the Rs-based and GLDAS CLSM estimated water budget, potentially leading to the underestimation of runoff.

Furthermore, it's worth noting that the Kunduz catchment has been experiencing ongoing drought conditions since 2008, as reported by [165]. These prolonged drought conditions can further contribute to snowmelt over the mountains, generating higher runoff throughout the year. This dual influence of rising temperatures due to climate change and recurrent drought episodes may collectively explain the discrepancies and overestimation of runoff in the Kunduz catchment.

Table 4.25 MODIS SSEBop and GLDAS CLSM ET Percentages (CHIRPS (CH), PERSIANN (PERS) and GLDAS (GL) %).

Dataset		2009	2010	2011	2012	2013	2014	2015	2016	2017
CH	O	77	94	93	97	75	81	73	89	64
	D	81	94	93	97	80	81	73	89	64
PERS	O	87	85	68	70	72	63	50	67	67
	D	87	84	67	75	71	63	50	67	67
GL	O	83	97	79	92	92	90	84	97	95
	D	82	98	80	92	93	90	84	95	97

Note: the other two years of GLDAS CLSM data are as for (OD) 84 and 85and for (DD) are 88&88%.

Satellite-based precipitation datasets commonly do not differentiate snowfall from rainfall, especially in case of PERSIANN and GLDAS CLSM precipitation and treat them collectively as precipitation. This approach may have had an impact on

the accuracy or proximity of the total basin discharge compared to the in-situ runoff measurements as explained in the [186].

Further investigations by [187] focused on estimating water budgets across ten global river basins using satellite data but faced challenges in achieving water budget closure. Similar difficulties were reported by other researchers studying water budget closure in different river basins, such as [9, 14, 18, 188]. These studies consistently underscored the recurring issues of overestimated runoff and underestimated evapotranspiration, highlighting the persistent obstacles in achieving water budget closure.

Despite these challenges, satellite data remains a valuable tool for evaluating trends and changes in the water balance. Although the closure of water budget using residue analysis of RS-based and GLDAS data may pose challenges in accurately estimating evapotranspiration and precipitation, satellite data provides valuable insights into the overall patterns and variations in water balance components.

The results of this study clearly demonstrate the superiority of the downscaling procedure for each parameter when compared to the original dataset. These findings highlight that enhancing the spatial resolution of the dataset can significantly improve the accuracy of water budget estimation, even in the case of a small basin like Kunduz, where observed data are limited. These observations are thoroughly explained in Table 4.19 and 4.20. These studies [11, 61, 62, 67, 70, 118, 120, 123, 189-196] emphasize the vital role and significance of downscaling procedures in water budget assessments worldwide and supporting the finding of this study. Downscaling has proven to be instrumental in enhancing the quality of remote sensing data, especially for layers like GRACE and GLDAS, as well as precipitation data from sources such as CHIRPS and PERSIAN, in addition to evapotranspiration data. The findings highlight the potential for downscaling to improve the accuracy and reliability of data used in hydrological studies. This is of great importance, particularly in regions with limited access to ground-based observations.

5
CONCLUSION

5.1 General Conclusion

This study concludes that there is an ongoing challenge when it comes to achieving closure in the water budget estimation for the Kunduz catchment. The challenges primarily revolve around the issues of both underestimation and overestimation detailed in Table 4.19 and Table 4.20 of surface runoff. These challenges persist whether one uses downscaled or original remote sensing and GLDAS CLSM data, especially when compared to observed runoff data. This research is essential in addressing specific challenges and limitations that are encountered in water budget assessments, especially in the context of smaller basins such as the Kunduz catchment. Smaller basins typically suffer from a shortage of high-quality observed data, making it more difficult to achieve accurate estimations. Historically, research in this field has predominantly focused on larger global basins. This emphasis on larger basins was primarily due to the constraints associated with the GRACE satellite mission, which provided precise data for larger basins. Unfortunately, its accuracy diminished as the size of the basin decreased. Considering these findings, it becomes evident that there is a pressing need for the development of improved methodologies and the utilization of more reliable data sources for water budget estimation in smaller river basins.

In response to this, the study aims to apply GRACE data to the Kunduz catchment, which encompasses an area of 28,042 km^2. Additionally, the research incorporates data from GLDAS TWS to comprehensively address the water budget, offering a more holistic understanding of the basin's water dynamics.

The challenges associated with coarser spatial resolution in estimating water budget components using remote sensing and GLDAS datasets are widespread and affect decision-making in many regions worldwide. To address these challenges, this study underscores the significant role of downscaling techniques, specifically through the implementation of Geographically Weighted Regression (GWR) methodology. Coarse resolution impacts all water budget components, including

precipitation, evapotranspiration, and TWS. It is essential to acknowledge that these challenges often lead decision-makers to be cautious when using such data for their decisions. Hence, this study utilizes GWR to mitigate these challenges and enhance the accuracy of water budget component estimates by employing downscaled remote sensing data and GLDAS CLSM.

The unique aspect of this study lies in its comprehensive approach, applying downscaling methods to all water balance components, resulting in a more holistic comprehension of the dynamics of the water cycle. It signifies a noteworthy advancement in the application of downscaling techniques to water budget analysis, particularly within an academic context. The geographical focus on the Kunduz catchment, situated in the northern region of Afghanistan with transboundary water issues involving neighboring countries, is of strategic importance for the area's agricultural productivity. This aspect sets this study apart as the first-ever investigation employing remote sensing and GLDAS layers to study water budget components, addressing a critical gap in the existing literature concerning the Kunduz catchment.

The study addresses four key research questions related to water budget estimation using remote sensing and the distribution of water budget components, providing valuable insights into the accuracy and reliability of remote sensing data for estimating water budgets. This information is crucial for informed decision-making in water resource management, especially in basins with limited quality data available for most environmental features, including water, precipitation, evapotranspiration, and terrestrial water storage. The study underscores the significance and necessity of using remote sensing and GLDAS data in a basin where it acts as a transboundary remote sensing base, and data assimilated sources, such as GLDAS, serve as the best alternative, whether in their downscaled or original form. Various GIS software platforms are employed for the processing of these steps.

5.2 Precipitation

In conclusion, the analysis of CHIRPS, PERSIANN, and GLDAS CLSM datasets in the Kunduz catchment sheds light on precipitation distribution. These datasets

reveal both shared patterns and disparities in estimating precipitation within the region. A consistent trend in all three datasets is the overestimation of precipitation concerning observed values, in alignment with findings in various global studies. The identification of the wettest and driest years displays a significant level of agreement among these datasets, enhancing result reliability. Notably, CHIRPS and GLDAS CLSM datasets highlight 2019 as the wettest year, and this is in line with the occurrence of a flash flood in that year, further validating this study's findings. Conversely, both CHIRPS and PERSIANN datasets point to 2011 and 2012 as the driest years, indicating minimal rainfall during these periods. However, these datasets also reveal notable discrepancies, including both overestimations and underestimations, emphasizing inherent variations in precipitation estimates over different years. The persistent overestimation of observed data underscores the complexities of remote sensing-based precipitation estimation, influenced by differences between satellite-derived data and ground-based observations, geographical factors, and data quality. Furthermore, the rough terrain and the scarcity of observation stations in the study area add to the intricacies of data collection. Monthly precipitation patterns consistently identify February as the month with the highest recorded precipitation levels, consistent with established climate patterns in the Kunduz catchment. Seasonal fluctuations in precipitation levels, evident across all datasets, reinforce data reliability. Given the geographical influence on precipitation patterns and the intricate interplay of weather and climate in Afghanistan, especially in the Kunduz catchment, these regions are vulnerable to the ongoing impacts of climate change. This study contributes to a deeper understanding of precipitation dynamics within the Kunduz catchment.

5.3 Evapotranspiration (ET)

In conclusion, the examination of ET variations within the Kunduz Catchment reveals distinct seasonal patterns in ET dynamics. Lower ET variations occur during the winter season, while higher ET values are evident during the summer months. The analysis further identifies key influencers of SSEBop and GLDAS CLSM ET values, including land cover, NDVI, and Land Surface Temperature (LST) variations. Notably, agricultural land demonstrates the most substantial ET

variations across the entire Kunduz Catchment, with SSEBop ET indicating the highest variability in these areas. Mountainous regions consistently exhibit heightened ET values, likely influenced by orographic winds and snow cover in the mountainous terrain. Comparisons with a recent study in the Kabul River Basin support these findings, emphasizing parallel patterns of ET dynamics. These findings contribute to the understanding of ET dynamics in arid and semi-arid regions like Kunduz. The inherent uncertainties associated with ET estimation, linked to various basin characteristics, highlight the complexity of this essential component in water budget assessments. Utilizing both SSEBop and GLDAS CLSM ET data sources provides a comprehensive perspective on ET dynamics within the Kunduz Catchment. Future research in this region can benefit from these insights and contribute to improved water resource management and climate resilience strategies.

5.4 Runoff

In conclusion, this study highlights the value of using inferred runoff data derived from remote sensing in water resource management, especially in regions with limited data availability. The analysis of inferred runoff, based on CHIRPS, PERSIANN, and GLDAS datasets, offers insights into water deficits and surpluses within the Kunduz Catchment.

The influence of landcover characteristics on water resource dynamics is evident, with barren soil areas and agricultural land consistently exhibiting water deficits. This underscores the role of landcover in shaping water availability and deficiency within the catchment. The examination of surface runoff dynamics, both catchment-wise and monthly, reveals significant variations in surface runoff levels over the years. GLDAS CLSM surface runoff closely aligns with seasonal precipitation patterns in the Kunduz Catchment, while observed runoff is primarily driven by snowmelt, leading to a distinct pattern. Discrepancies between GLDAS CLSM surface runoff and observed runoff are noted, primarily attributed to the absence of streamflow routing in the simulations. This inconsistency emphasizes the importance of considering the limitations of assimilated surface runoff data in water resource studies. In summary, the combination of inferred runoff and surface runoff

data provides valuable insights into the dynamics of water resources within the Kunduz Catchment, contributing to informed water resource management decisions. The findings of this study enhance the understanding of water availability and its seasonal variations in this region, emphasizing the complex interplay of climatic and hydrological factors.

5.5 Terrestrial Water Storage (TWS)

In conclusion, the analysis of TWS data from GRACE and GLDAS CLSM provides valuable insights into the dynamics of water storage within the Kunduz Catchment. Visual interpretation of the data reveals annual variations in terrestrial water storage, with some years exhibiting higher storage levels while others experience lower storage. It's essential to note that GRACE TWS data has limitations, particularly the presence of missing data in multiple months from 2009 to 2017. This limitation influenced the decision to focus on GRACE TWS data only up to 2017, and data imputation methods were employed to address the missing data issue. The GLDAS CLSM TWS dataset indicates that 2011 had the lowest water storage levels compared to the years from 2009 to 2019. On the other hand, the years 2009, 2013, 2018, and 2019 stood out with the highest water storage levels in the TWS layer. Overall, the examination of TWS data contributes to our understanding of the dynamics of terrestrial water storage within the Kunduz Catchment, highlighting variations and trends in water storage levels over the years. This information is valuable for water resource management and decision-making in the region.

5.6 Water Budget (WB)

The assessment of water budget components in the Kunduz catchment, utilizing both Original (OD) and Downscaled (DD) datasets from remote sensing-based sources and GLDAS CLSM, revealed intricate and dynamic patterns in precipitation, evapotranspiration, and TWSC over the study period. These datasets illustrated a complex interplay of factors influencing the hydrological system within the region. The observed fluctuations in precipitation, notably in the CHIRPS, PERSIANN, and GLDAS CLSM datasets, indicated temporal variability in rainfall

patterns. Precipitation reductions, such as in 2010 and 2011, were associated with decreased evapotranspiration and total water storage, while years of increased precipitation, like 2014 and 2019, corresponded with notable recoveries in TWSC. Evapotranspiration demonstrated a positive correlation with precipitation, where increased rainfall led to higher evapotranspiration rates and vice versa. This positive relationship underscored the sensitivity of evapotranspiration to environmental conditions, particularly precipitation. TWSC exhibited close linkage with precipitation variations. Increased precipitation contributed to TWSC recovery, whereas decreased precipitation was associated with declining TWSC, emphasizing the role of precipitation in shaping TWSC dynamics. In conclusion, this study highlights the intricate relationships between precipitation, evapotranspiration, and total water storage change within the Kunduz catchment, underlining the need for a comprehensive understanding of these components for effective water resource management and decision-making in the region.

5.7 Reducing Water Budget Uncertainty through Downscaling in Kunduz Catchment

The analysis of RS-Based CHIRPS (P) and RS-Based PERSIANN (P) precipitation datasets suggests that the impact of downscaling on these datasets is relatively minimal in terms of uncertainty levels. In both the OD and DD versions of these datasets, consistent statistical patterns were observed, with similar minimum, maximum, mean, and standard deviation values. The uncertainty percentages for CHIRPS precipitation remained stable at 31% throughout the study period, indicating a consistent level of uncertainty. In the case of PERSIANN precipitation, the uncertainty percentages remained relatively low, ranging from 7% to 17%. These findings imply that the downscaling process has a limited impact on the uncertainty of CHIRPS and PERSIANN precipitation datasets, and they maintain their reliability and stability in both OD and DD forms. Regarding the GLDAS CLSM (P) dataset, it also demonstrated coherence between the OD and DD, with similar statistical values. While there was some variability in uncertainty percentages, ranging from 6% to 26%, these variations generally remained within a moderate range. This suggests that downscaling in GLDAS CLSM precipitation

has a relatively minor impact on the dataset's uncertainty levels, and it remains a reliable source of precipitation data. In summary, the impact of downscaling on RS-Based CHIRPS, PERSIANN, and GLDAS CLSM precipitation datasets appears to be minor with regard to uncertainty levels due to the size of the catchment. These datasets maintain their reliability and stability in both OD and DD format. Figure 4.55 visually illustrates the influence of downscaling on both GLDAS and CHIRPS data. When comparing the two linear regression models, it's apparent that the first model ($y = 0.1944x + 829.83$) displays a steeper positive slope, indicating a more pronounced rate of change between the variables. In contrast, the second model ($y = 0.1312x + 899.09$) exhibits a comparatively shallower slope. Furthermore, the first model features a higher coefficient of determination ($R^2 = 0.55$) compared to the second model ($R^2 = 0.45$), indicating a superior goodness-of-fit in explaining the variance in the dependent variable. The first model explains approximately 16% more of the variance than the original dataset.

A similar pattern emerges in the GLDAS CLSM surface runoff data, where downscaled data demonstrate higher coefficients of determination, elucidating about 8% more of the observed runoff compared to the original dataset. To sum up, the downscaling process has a relatively minor impact on precipitation datasets uncertainty levels. Downscaled data consistently display improved performance in elucidating the variance in surface runoff data compared to the original datasets.

The analysis of downscaling effects on precipitation datasets, including RS-Based CHIRPS, PERSIANN and GLDAS CLSM precipitation, reveals the constructive impact of downscaling on data reliability. Both the OD and downscaled DD versions of these datasets consistently exhibit reliability and stability. This finding holds significant value for researchers and decision-makers who depend on precipitation data for various applications, such as hydrology, agriculture, and disaster management. It implies that downscaled dataset versions can be confidently utilized, offering higher spatial resolution without introducing substantial uncertainty.

Comparing linear regression models, as illustrated in Figures 4.55 and 4.56 and supported by the data in Table 4.19 and 4.20, consistently demonstrates that downscaled data leads to an enhanced goodness-of-fit. This improvement is evident

through higher Pearson correlation values, better KGE scores, and more accurate volumetric fractions, all contributing to the overall model performance. These positive outcomes are accompanied by higher coefficients of determination (R^2), further affirming the advantages of downscaled data in various aspects of the analysis. This suggests that downscaled data provides a more accurate representation of relationships between variables, which is invaluable for modeling and prediction tasks. In practical terms, this implies that when modeling the impact of precipitation on various processes, utilizing downscaled data can lead to superior results and more precise predictions.

For regions with limited data, remote sensing, and data assimilated sources like GLDAS prove to be the most reliable choices. These research outcomes have practical implications for decision support systems that depend on precipitation and evapotranspiration data.

The study demonstrates that the downscaling process does not significantly augment uncertainty in precipitation datasets and, in certain cases, reduces uncertainty. Therefore, decision-makers can confidently employ downscaled data to inform choices in domains like water resource management, drought monitoring, and climate change adaptation. Furthermore, these findings suggest avenues for future research. While the current study underscores the advantages of downscaling in specific scenarios, further research is warranted to comprehend the impacts of downscaling on other climatic and environmental datasets. Additionally, delving into the specific mechanisms contributing to the reduction in uncertainty and improved model fit could yield insights for refining downscaling techniques.

In summation, the study's results contribute to the field by emphasizing the benefits of downscaling in maintaining data reliability, enhancing model fit, and augmenting decision support in applications related to precipitation and hydrological processes. These implications hold both theoretical and practical significance, advocating for the continued utilization and development of downscaling methods in climate and environmental research.

5.8 Recommendations for the Study Area

- Annual Water Budget Study: It is recommended that water budget studies be conducted on an annual basis or even seasonal basis, emphasizing a shift from a monthly scale. This adjustment will allow for a more comprehensive understanding of water dynamics and enable the effective capture of long-term trends.
- Integration of GRACE Data: Consideration should be given to the integration of all available GRACE datasets (JPL, GFZ and CSR), with a focus on the amalgamation of three different sources. The creation of a mean value from these sources can contribute to a more reliable and consistent water budget study.
- Catchment Size for Downscaling: When employing downscaling techniques, it is advisable to concentrate on larger basins. Larger catchments may yield more accurate results for water budget studies when closely aligned with observed data.
- Hydrological Modeling: Incorporation of hydrological models, such as VIC, SWAT, or WASIM, should be considered in water budget studies, depending on availability. The selection of a model that demands minimal field data while preserving result accuracy is encouraged.
- Remote Sensing Analysis: The utilization of remote sensing analysis is recommended in areas where field surveys are either impractical or impossible or there is absence of observed data. This approach will broaden the scope of the study to regions that might otherwise remain inaccessible, facilitating a more comprehensive assessment of water resources.

By implementing these recommendations, future water budget studies can attain greater accuracy, consistency, and applicability in both local and broader contexts.

5.9 Future Works

Given the imminent global challenges, the meticulous management of water resources within defined boundaries, especially in regions with shared borders like Afghanistan, requires prompt and deliberate action. The utilization of freely available remote sensing sources, systematically processed, should be a serious consideration. Future efforts should prioritize the refinement of water budget estimations, inclusive engagement with diverse stakeholders, and the adoption of a comprehensive approach to water budget modeling that leverages remote sensing data. Special attention should be given to incorporating anthropogenic influences within the basins, particularly by integrating land-use characteristics into hydrological models.

Furthermore, proactive measures are necessary to address the complexities associated with springtime snow runoff, a challenge characterized by significant disparities in remote sensing data. By comprehensively addressing these prospects, we can promote sustainable water resource management in response to evolving global concerns.

REFERENCES

[1] State of the world's drinking water, World Health Organization, 2022. [Online]. Available: https://cdn.who.int/media/docs/default-source/wash-documents/water-safety-and-quality/state-of-drinking-water-report-web.2_v-lowres.pdf?sfvrsn=e2479151_3.

[2] FAO. 2020. The State of World Fisheries and Aquaculture 2020. Rome, https://doi.org/10.4060/ca9229en

[3] UNESCO, "The United Nations World Water Development Report 2021: Valuing Water," United Nations, 2021.

[4] V. Masson-Delmotte, P. Zhai, H. O. Pörtner, D. Roberts, J. Skea, and P. R. Shukla, "Global Warming of 1.5°C: IPCC special report on impacts of global warming of 1.5°C above pre-industrial levels in context of strengthening response to climate change, sustainable development, and efforts to eradicate poverty," Cambridge University Press, 2022.

[5] P. Steduto, J. M. Faurès, J. Hoogeveen, J. Winpenny, and J. Burke, "Coping with water scarcity: An action framework for agriculture and food security," Food and Agriculture Organization of the United Nations, Rome, 2012.

[6] Kayan, G., Erten, E., Mercan, H., & Ozcan, O. "Understanding of Cyprus total water storage under climate change," presented at the 2017 IEEE International Geoscience and Remote Sensing Symposium (IGARSS), Fort Worth, TX, USA, July 23-28, 2017, Paper number 5591-5594.

[7] Z. Luo, Q. Shao, W. Wan, H. Li, X. Chen, S. Zhu, and X. Ding, "A new method for assessing satellite-based hydrological data products using water budget closure," *Journal of Hydrology*, vol. 594, p. 125927, 2021..

[8] A. L. Atchley and R. M. Maxwell, "Influences of subsurface heterogeneity and vegetation cover on soil moisture, surface temperature and evapotranspiration at hillslope scales," *Hydrogeology Journal*, vol. 19, no. 2, pp. 289-305, 2011.

[9] H. Wang, H. Guan, H. A. Gutiérrez-Jurado, and C. T. Simmons, "Examination of water budget using satellite products over Australia," *Journal of Hydrology*, vol. 511, pp. 546-554, 2014.

[10] Wang, Q., Xia, J., She, D., Zhang, X., Liu, J., & Zhang, Y. (2021). Assessment of four latest long-term satellite-based precipitation products in capturing the extreme precipitation and streamflow across a humid region of southern China. *Atmospheric Research*, 257, 105554.

[11] S. Spak, T. Holloway, B. Lynn, and R. Goldberg, "A comparison of statistical and dynamical downscaling for surface temperature in North America,"*Journal of Geophysical Research: Atmospheres*, vol. 112, no. D8, 2007.

[12] S. Wongchuig-Correa, R. C. D. de Paiva, S. Biancamaria, and W. Collischonn, "Assimilation of future SWOT-based river elevations, surface

extent observations and discharge estimations into uncertain global hydrological models," *Journal of Hydrology*, vol. 590, 2020, 125473.

[13] J. Sheffield, C. R. Ferguson, T. J. Troy, E. F. Wood, and M. F. McCabe, "Closing the terrestrial water budget from satellite remote sensing," *Geophysical Research Letters*, vol. 36, no. 7, 2009..

[14] M. Lv, Z. Ma, X. Yuan, M. Lv, M. Li, and Z. Zheng, "Water budget closure based on GRACE measurements and reconstructed evapotranspiration using GLDAS and water use data for two large densely-populated mid-latitude basins," *Journal of Hydrology*, vol. 547, pp. 585-599, 2017.

[15] H. Gao, Q. Tang, C. R. Ferguson, E. F. Wood, and D. P. Lettenmaier, "Estimating the water budget of major US river basins via remote sensing," *International Journal of Remote Sensing*, vol. 31, no. 14, pp. 3955-3978, 2010.

[16] H. Rui, H. Beaudoing, and C. Loeser, "README document for NASA GLDAS version 2 data products, Goddard Earth Sciences Data and Information Services Center *(GES DISC)*," 2020.

[17] N. R. Nelli, M. Temimi, R. M. Fonseca, M. J. Weston, M. S. Thota, V. K. Valappil, O. Branch, et al., "Impact of roughness length on WRF simulated land-atmosphere interactions over a hyper-arid region,"*Earth and Space Science*, vol. 7, no. 6, 2020, p.e2020EA001165.

[18] Oliveira, P. T. S., Nearing, M. A., Moran, M. S., Goodrich, D. C., Wendland, E., & Gupta, H. V. (2014). Trends in water balance components across the Brazilian Cerrado. *Water Resources Research*, 50(9), 7100-7114.

[19] P. Bai, X. Liu, T. Yang, K. Liang, and C. Liu, "Evaluation of streamflow simulation results of land surface models in GLDAS on the Tibetan plateau,"*Journal of Geophysical Research: Atmospheres*, vol. 121, no. 20, pp. 12-180, 2016.

[20] C. Kidd, A. Becker, G. J. Huffman, C. L. Muller, P. Joe, G. Skofronick-Jackson, and D. B. Kirschbaum, "So, how much of the Earth's surface is covered by rain gauges?," *B. Am. Meteorol. Soc.*, vol. 98, no. 1, pp. 69-78, 2017.

[21] Shen, Z., B. Yong, J. J. Gourley, W. Qi, D. Lu, J. Liu, et al., "Recent global performance of the Climate Hazards group Infrared Precipitation (CHIRP) with Stations (CHIRPS)," *Journal of Hydrology*, vol. 591, 125284, 2020.

[22] Patil, M., A. S. H. A. Arnab, S. M. Pingale, D. S. Rathore, and V. C. Goyal, "Identification of potential zones for the estimation of direct runoff and soil erosion in an ungauged watershed using remote sensing and GIS techniques," *International Journal of Engineering and Geosciences*, vol. 8, no. 3, pp. 224-238.

[23] Le, H. M., J. R. Sutton, D. D. Bui, J. D. Bolten, and V. Lakshmi, "Comparison and bias correction of TMPA precipitation products over the lower part of the Red–Thai Binh River basin of Vietnam," *Remote Sensing*, vol. 10, no. 10, p. 1582, 2018.

[24] Hsu, J., W. R. Huang, P. Y. Liu, and X. Li, "Validation of CHIRPS precipitation estimates over Taiwan at multiple timescales," *Remote Sensing*, vol. 13, no. 2, p. 254, 2021.

[25] Hosseini-Moghari, S. M., and Q. Tang, "Validation of GPM IMERG V05 and V06 precipitation products over Iran," *Journal of Hydrometeorology*, vol. 21, no. 5, pp. 1011-1037, 2020.

[26] C. Funk, et al., "The climate hazards infrared precipitation with stations—a new environmental record for monitoring extremes," *Scientific data*, vol. 2, no. 1, pp. 1-21, 2015.

[27] Y. Jia, et al., "Terrestrial water storage change retrieved by GRACE and its implication in the Tibetan Plateau: Estimating areal precipitation in Ungauged Region," *Remote Sensing*, vol. 12, no. 19, pp. 3129, 2020.

[28] N. M. Velpuri, et al., "A comprehensive evaluation of two MODIS evapotranspiration products over the conterminous United States: Using point and gridded FLUXNET and water balance ET," *Remote Sensing of Environment*, vol. 139, pp. 35-49, 2013.

[29] G. B. Senay, et al., "Operational evapotranspiration mapping using remote sensing and weather datasets: A new parameterization for the SSEB approach," *JAWRA Journal of the American Water Resources Association*, vol. 49, no. 3, pp. 577-591, 2013.

[30] D. Long, L. Longuevergne, and B. R. Scanlon, "Uncertainty in evapotranspiration from land surface modeling, remote sensing, and GRACE satellites," *Water Resources Research*, vol. 50, no. 2, pp. 1131-1151, 2014..

[31] S. Dzikiti, et al., "Comparison of two remote sensing models for estimating evapotranspiration: algorithm evaluation and application in seasonally arid ecosystems in South Africa," *Journal of Arid Land*, vol. 11, pp. 495-512, 2019.

[32] J. P. Du and R. Sun, "Estimation of evapotranspiration for ungauged areas using MODIS measurements and GLDAS data," *Procedia Environmental Sciences*, vol. 13, pp. 1718-1727, 2012.

[33] H. Chen, et al., "Evaluation of evapotranspiration models using different LAI and meteorological forcing data from 1982 to 2017," *Remote Sensing*, vol. 12, no. 15, pp. 2473, 2020.

[34] V. Lakshmi, J. Fayne, and J. Bolten, "A comparative study of available water in the major river basins of the world," *Journal of Hydrology*, vol. 567, pp. 510-532, 2018..

[35] R. G. Allen, et al., "Evapotranspiration information reporting: I. Factors governing measurement accuracy," *Agricultural Water Management*, vol. 98, no. 6, pp. 899-920, 2011.

[36] G. Tang, et al., "Statistical and hydrological comparisons between TRMM and GPM level-3 products over a midlatitude basin: Is day-1 IMERG a good

successor for TMPA 3B42V7?," *Journal of Hydrometeorology*, vol. 17, no. 1, pp. 121-137, 2016.

[37] M. Azarderakhsh, W. B. Rossow, F. Papa, H. Norouzi, and R. Khanbilvardi, "Diagnosing water variations within the Amazon basin using satellite data," *Journal of Geophysical Research: Atmospheres*, vol. 116, no. D24, 2011.

[38] M. N. Islam and H. Uyeda, "Use of TRMM in determining the climatic characteristics of rainfall over Bangladesh," Remote Sensing of Environment, vol. 108, no. 3, pp. 264-276, 2007.

[39] X.-H. Li, Q. Zhang, and C.-Y. Xu, "Suitability of the TRMM satellite rainfalls in driving a distributed hydrological model for water balance computations in Xinjiang catchment, Poyang lake basin," *Journal of Hydrology*, vol. 426, pp. 28-38, 2012.

[40] A. A. Moreira, A. L. Ruhoff, D. R. Roberti, V. de Arruda Souza, H. R. da Rocha, and R. C. D. de Paiva, "Assessment of terrestrial water balance using remote sensing data in South America," *Journal of Hydrology*, vol. 575, pp. 131-147, 2019.

[41] Q. Tang, H. Gao, H. Lu, and D. P. Lettenmaier, "Remote sensing: hydrology," *Progress in Physical Geography*, vol. 33, no. 4, pp. 490-509, 2009.

[42] Y. Pan, et al., "Detection of human-induced evapotranspiration using GRACE satellite observations in the Haihe River basin of China," *Geophysical Research Letters*, vol. 44, no. 1, pp. 190-199, 2017.

[43] W. Yin, L. Hu, S. C. Han, M. Zhang, and Y. Teng, "Reconstructing terrestrial water storage variations from 1980 to 2015 in the Beishan area of China," *Geofluids*, 2019.

[44] W. G. Bastiaanssen, H. Pelgrum, J. Wang, Y. Ma, J. F. Moreno, G. J. Roerink, and T. Van der Wal, "A remote sensing surface energy balance algorithm for land (SEBAL).: Part 2: Validation," *Journal of Hydrology*, vol. 212, pp. 213-229, 1998.

[45] A. L. Ruhoff, A. R. Paz, W. Collischonn, L. E. Aragao, H. R. Rocha, and Y. S. Malhi, "A MODIS-based energy balance to estimate evapotranspiration for clear-sky days in Brazilian tropical savannas," *Remote Sensing*, vol. 4, no. 3, pp. 703-725, 2012.

[46] S. Tarul, T. Praveen, N. Bhaskar, and V. Garg, "Water budget components estimation using satellite data and a hydrological model," *in Proceedings of Hydro International*, 2013, pp. 4-6.

[47] Q. Tang and X. Zhang, "Mapping evapotranspiration using MODIS and GRACE data," *in 2011 19th International Conference on Geoinformatics*, June 2011, pp. 1-4. IEEE.

[48] N. C. Penatti, T. I. R. de Almeida, L. G. Ferreira, A. E. Arantes, and M. T. Coe, "Satellite-based hydrological dynamics of the world's largest continuous wetland," *Remote Sensing of Environment*, vol. 170, pp. 1-13, 2015.

[49] D. E. Armanios and J. B. Fisher, "Measuring water availability with limited ground data: assessing the feasibility of an entirely remote-sensing-based hydrologic budget of the Rufiji Basin, Tanzania, using TRMM, GRACE, MODIS, SRB, and AIRS," *Hydrological Processes*, vol. 28, no. 3, pp. 853-867, 2014.

[50] M. Alfaloji, "A water budget estimation using remote sensing observations and GLDAS-CLSM for Limpopo River Basin," *Advanced Remote Sensing*, vol. 2, no. 2, pp. 85-93, 2022.

[51] T. H. Syed, J. S. Famiglietti, M. Rodell, J. Chen, and C. R. Wilson, "Analysis of terrestrial water storage changes from GRACE and GLDAS," *Water Resources Research*, vol. 44, no. 2, 2008.

[52] Z. Rzepecka and M. Birylo, "Groundwater storage changes derived from GRACE and GLDAS on smaller river basins—A case study in Poland," *Geosciences*, vol. 10, no. 4, 2020, pp. 124.

[53] S. Z. Yirdaw, K. R. Snelgrove, and C. O. Agboma, "GRACE satellite observations of terrestrial moisture changes for drought characterization in the Canadian Prairie," *Journal of Hydrology*, vol. 356, no. 1-2, 2008, pp. 84-92.

[54] A. Singh, F. Seitz, and C. Schwatke, "Inter-annual Water Storage Changes in the Aral Sea from Multi-mission Satellite Altimetry, Remote Sensing, and GRACE Satellite Gravimetry," *in Geodetic Week 2011, Nuremberg, Germany*, 2011.

[55] A. Kuss, W. T. Brandt, J. Randall, B. Floyd, M. Newcomer, C. Schmidt, and J. W. Skiles, "Groundwater Storage Estimates in the Central Valley Aquifer Using GRACE Data.

[56] M. Rodell, P. Houser, C. Peters-Lidard, H. Kato, S. Kumar, J. Gottschalck, and J. Meng, "Nasa/Noaa's global land data assimilation system (GLDAS): Recent results and future plans," *in Proceedings of the ECMWF/ELDAS Workshop on Land Surface Assimilation, Shinfield, UK*, November 2004, pp. 8-11.

[57] Draft Handbook For Water Budget Development With or Without Models," February 2020. [Online]. Available:[https://groundwaterexchange.org/news-post/draft-handbook-for-water-budget-development-released-webinar-scheduled/]. Accessed on: May 2023.

[58] N. Mohammed, J. D. Bolten, R. Srinivasan, and V. Lakshmi, "Satellite observations and modeling to understand the Lower Mekong River Basin streamflow variability," *Journal of Hydrology*, vol. 564, pp. 559-573, 2018.

[59] S. Moghim, "Impact of climate variation on hydrometeorology in Iran," *Global and Planetary Change*, vol. 170, pp. 93-105, 2018.

[60] S. Pan, N. Pan, H. Tian, P. Friedlingstein, S. Sitch, H. Shi, and S. W. Running, "Evaluation of global terrestrial evapotranspiration using state-of-the-art approaches in remote sensing, machine learning and land surface modeling," *Hydrology and Earth System Sciences*, vol. 24, no. 3, pp. 1485-1509, 2020.

[61] P. López López, W. W. Immerzeel, E. A. Rodríguez Sandoval, G. Sterk, and J. Schellekens, "Spatial downscaling of satellite-based precipitation and its impact on discharge simulations in the Magdalena River basin in Colombia," *Frontiers in Earth Science*, vol. 6, p. 68, 2018.

[62] G. Sposito, "Upscaling and downscaling methods for environmental research-Developments in Plant and Soil Sciences, vol. 88, MFP Bierkens, PA Finke, and P. de Willigen, Kluwer Academic Publishers, Dordrecht, 2000, Hardcover, ISBN 0-7923-6339-6; US $88, 190 pp.+ CD-ROM," *Geoderma*, vol. 103, pp. 354-355, 2001.

[63] M. El Maayar and J. M. Chen, "Spatial scaling of evapotranspiration as affected by heterogeneities in vegetation, topography, and soil texture," *Remote Sensing of Environment*, vol. 102, no. 1-2, pp. 33-51, 2006.

[64] S. H. Hong, J. M. Hendrickx, and B. Borchers, "Down-scaling of SEBAL derived evapotranspiration maps from MODIS (250 m) to Landsat (30 m) scales," *International Journal of Remote Sensing*, vol. 32, no. 21, pp. 6457-6477, 2011.

[65] D. T. Price, D. W. McKenney, I. A. Nalder, M. F. Hutchinson, and J. L. Kesteven, "A comparison of two statistical methods for spatial interpolation of Canadian monthly mean climate data," *Agricultural and Forest Meteorology*, vol. 101, no. 2-3, pp. 81-94, 2000.

[66] S. F. Liu, J. Xiong, and B. F. Wu, "ETWatch: A method of multi-resolution ET data fusion," *Journal of Remote Sensing*, vol. 15, no. 2, pp. 255-269, 2011.

[67] Y. Ke, J. Im, S. Park, and H. Gong, "Downscaling of MODIS one kilometer evapotranspiration using Landsat-8 data and machine learning approaches," *Remote Sensing*, vol. 8, no. 3, p. 215, 2016.

[68] M. Pan and E. F. Wood, "Data assimilation for estimating the terrestrial water budget using a constrained ensemble Kalman filter," *Journal of Hydrometeorology*, vol. 7, no. 3, pp. 534-547, 2006.

[69] J. Roads, R. Lawford, E. Bainto, E. Berbery, S. Chen, B. Fekete, and E. Yarosh, "GCIP water and energy budget synthesis (WEBS)," *Journal of Geophysical Research: Atmospheres*, vol. 108, no. D16, 2003.

[70] J. V. Haynes and G. B. Senay, "Evaluation of the relation between evapotranspiration and normalized difference vegetation index for downscaling the simplified surface energy balance model," Reston, VA, USA: US Department of the Interior, US Geological Survey, 2012.

[71] M. Rodell, J. Chen, H. Kato, J. S. Famiglietti, J. Nigro, and C. R. Wilson, "Estimating groundwater storage changes in the Mississippi River basin (USA) using GRACE," *Hydrogeology Journal*, vol. 15, pp. 159-166, 2007.

[72] M. Rodell and J. S. Famiglietti, "The potential for satellite-based monitoring of groundwater storage changes using GRACE: the High Plains aquifer, Central US," *Journal of Hydrology*, vol. 263, no. 1-4, pp. 245-256, 2002.

[73] T. H. Syed, J. S. Famiglietti, M. Rodell, J. Chen, and C. R. Wilson, "Analysis of terrestrial water storage changes from GRACE and GLDAS," *Water Resources Research*, vol. 44, no. 2, 2008.

[74] A. S. Richey, B. F. Thomas, M. H. Lo, J. T. Reager, J. S. Famiglietti, K. Voss, and M. Rodell, "Quantifying renewable groundwater stress with GRACE," *Water Resources Research*, vol. 51, no. 7, pp. 5217-5238, 2015.

[75] A. S. Richey, B. F. Thomas, M. H. Lo, J. S. Famiglietti, S. Swenson, and M. Rodell, "Uncertainty in global groundwater storage estimates in a Total Groundwater Stress framework," Water Resources Research, vol. 51, no. 7, pp. 5198-5216, 2015.

[76] G. M. Kamal, "River basins and Watersheds of Afghanistan," Afghanistan Information Management Services (AIMS), Kabul, Afghanistan, 2004, pp. 1-7.

[77] N. A. Akhundzadah, S. Soltani, and V. Aich, "Impacts of climate change on the water resources of the Kunduz River Basin, Afghanistan," *Climate*, vol. 8, no. 10, p. 102, 2020.

[78] S. Reshteen, M. K. Yosufi, A. S. Zamani, and A. Rahmatzai, "Water Balance Assessment in Three Northern (Kunduz, Balkh & Jawzjan) Provinces of Afghanistan," *Journal of Survey in Fisheries Sciences*, pp. 1318-1335, 2023.

[79] J. S. Famiglietti, M. Lo, S. L. Ho, J. Bethune, K. J. Anderson, T. H. Syed, and M. Rodell, "Satellites measure recent rates of groundwater depletion in California's Central Valley," *Geophysical Research Letters*, vol. 38, no. 3, 2011.

[80] W. Feng, M. Zhong, J. M. Lemoine, R. Biancale, H. T. Hsu, and J. Xia, "Evaluation of groundwater depletion in North China using the Gravity Recovery and Climate Experiment (GRACE) data and ground-based measurements," *Water Resources Research*, vol. 49, no. 4, pp. 2110-2118, 2013.

[81] S. Munier, M. Becker, P. Maisongrande, and A. Cazenave, "Using GRACE to detect groundwater storage variations: the cases of Canning basin and Guarani aquifer system," *International Water Technology Journal*, vol. 2, pp. 2-13, 2012.

[82] M. Rodell, I. Velicogna, and J. S. Famiglietti, "Satellite-based estimates of groundwater depletion in India," *Nature*, vol. 460, no. 7258, pp. 999-1002, 2009.

[83] G. Strassberg, B. R. Scanlon, and M. Rodell, "Comparison of seasonal terrestrial water storage variations from GRACE with groundwater-level measurements from the High Plains Aquifer (USA)," *Geophysical Research Letters*, vol. 34, no. 14, 2007.

[84] K. A. Voss, J. S. Famiglietti, M. Lo, C. De Linage, M. Rodell, and S. C. Swenson, "Groundwater depletion in the Middle East from GRACE with implications for transboundary water management in the Tigris-Euphrates-

Western Iran region," *Water Resources Research*, vol. 49, no. 2, pp. 904-914, 2013.

[85] R. Abolafia-Rosenzweig, M. Pan, J. L. Zeng, and B. Livneh, "Remotely sensed ensembles of the terrestrial water budget over major global river basins: An assessment of three closure techniques," *Remote Sensing of Environment*, vol. 252, p. 112191, 2021.

[86] F. Aires, "Combining datasets of satellite-retrieved products. Part I: Methodology and water budget closure," *Journal of Hydrometeorology*, vol. 15, no. 4, pp. 1677-1691, 2014..

[87] E. B. Balcıoğlu and B. Öztürk, "Oil pollution in the surface water of Sakarya River," *Journal of Black Sea/Mediterranean Environment*, vol. 15, no. 2, pp. 99-108, 2009.

[88] C. Cai, J. Wang, and Z. Li, "Assessment and modelling of uncertainty in precipitation forecasts from TIGGE using fuzzy probability and Bayesian theory," *Journal of Hydrology*, vol. 577, p. 123995, 2019.

[89] G. Çeribaşı and E. Doğan, "TREND ANALİZİ YÖNTEMİ KULLANILARAK BATI VE DOĞU KARADENİZ İLE SAKARYA HAVZASI AKIM MİKTARLARININ DEĞERLENDİRİLMESİ," *Uluslararası Teknolojik Bilimler Dergisi*, vol. 7, no. 2, pp. 1-12, 2015.

[90] C. L. Chang, S. L. Lo, and S. L. Yu, "Applying fuzzy theory and genetic algorithm to interpolate precipitation," *Journal of Hydrology*, vol. 314, no. 1-4, pp. 92-104, 2005.

[91] M. S. Dundar and H. Altundağ, "Determination of some major and trace elements in the lower Sakarya River water by *ICP-MS*," 2018.

[92] G. M. Foody, "Approaches for the production and evaluation of fuzzy land cover classifications from remotely-sensed data," *International Journal of Remote Sensing*, vol. 17, no. 7, pp. 1317-1340, 1996.

[93] H. T. Güner, N. Köse, and G. L. Harley, "A 200-year reconstruction of Kocasu River (Sakarya River Basin, Turkey) streamflow derived from a tree-ring network," *International Journal of Biometeorology*, vol. 61, pp. 427-437, 2017.

[94] E. Kahya and S. Kalaycı, "Trend analysis of streamflow in Turkey," *Journal of Hydrology*, vol. 289, no. 1-4, pp. 128-144, 2004.

[95] G. Kayan, "Sakarya Ve Batı Karadeniz Akarsu Havzaları İçin Taban Akışı Ayırma Modeli" [Ph.D. dissertation, Fen Bilimleri Enstitüsü], 2014.

[96] B. Khazaei and S. M. Hosseini, "Improving the performance of water balance equation using fuzzy logic approach," *Journal of Hydrology*, vol. 524, pp. 538-548, 2015.

[97] F. W. Landerer and S. C. Swenson, "Accuracy of scaled GRACE terrestrial water storage estimates," *Water Resources Research*, vol. 48, no. 4, 2012.

[98] S. Munier and F. Aires, "A new global method of satellite dataset merging and quality characterization constrained by the terrestrial water budget," *Remote Sensing of Environment*, vol. 205, pp. 119-130, 2018.

[99] M. Pan, A. K. Sahoo, T. J. Troy, R. K. Vinukollu, J. Sheffield, and E. F. Wood, "Multisource estimation of long-term terrestrial water budget for major global river basins," *Journal of Climate*, vol. 25, no. 9, pp. 3191-3206, 2012.

[100] G. Papadavid and D. G. Hadjimitsis, "Adaptation of SEBAL for estimating groundnuts evapotranspiration, in Cyprus," South-Eastern European *Journal of Earth Observation and Geomatics*, 2012.

[101] G. Papadavid, D. G. Hadjimitsis, L. Toulios, and S. Michaelides, "A modified SEBAL modeling approach for estimating crop evapotranspiration in semi-arid conditions," *Water Resources Management*, vol. 27, pp. 3493-3506, 2013.

[102] T. Partal, "Wavelet transform-based analysis of periodicities and trends of Sakarya basin (Turkey) streamflow data," *River Research and Applications*, vol. 26, no. 6, pp. 695-711, 2010.

[103] M. Querales, R. Salas, Y. Morales, H. Allende-Cid, and H. Rosas, "A stacking neuro-fuzzy framework to forecast runoff from distributed meteorological stations," *Applied Soft Computing*, vol. 118, p. 108535, 2022.

[104] A. Retalis, D. Katsanos, F. Tymvios, and S. Michaelides, "Comparison of GPM IMERG and TRMM 3B43 Products over Cyprus," *Remote Sensing*, vol. 12, no. 19, p. 3212, 2020.

[105] A. K. Sahoo, M. Pan, T. J. Troy, R. K. Vinukollu, J. Sheffield, and E. F. Wood, "Reconciling the global terrestrial water budget using satellite remote sensing," *Remote Sensing of Environment*, vol. 115, no. 8, pp. 1850-1865, 2011.

[106] T. Semeraro, G. Mastroleo, A. Pomes, A. Luvisi, E. Gissi, and R. Aretano, "Modelling fuzzy combination of remote sensing vegetation index for durum wheat crop analysis," Computers and Electronics in Agriculture, vol. 156, pp. 684-692, 2019.

[107] Z. Shao, M. E. Huq, B. Cai, O. Altan, and Y. Li, "Integrated remote sensing and GIS approach using Fuzzy-AHP to delineate and identify groundwater potential zones in semi-arid Shanxi Province, China," *Environmental Modelling & Software*, vol. 134, p. 104868, 2020.

[108] M. Silver, T. Svoray, A. Karnieli, and E. Fredj, "Improving weather radar precipitation maps: A fuzzy logic approach," *Atmospheric Research*, vol. 234, p. 104710, 2020.

[109] C. N. Solak, Ł. Peszek, E. Yilmaz, H. A. Ergül, M. Kayal, F. Ekmekçi, and É. Ács, "Use of diatoms in monitoring the Sakarya river basin, Turkey," Water, vol. 12, no. 3, p. 703, 2020.

[110] M. Uz, K. G. Atman, O. Akyilmaz, C. K. Shum, M. Keleş, T. Ay, and H. Mercan, "Bridging the gap between GRACE and GRACE-FO missions with deep learning aided water storage simulations," *Science of The Total Environment*, vol. 830, p. 154701, 2022.

[111] H. Xing, H. He, D. Hu, T. Jiang, and X. Yu, "An interval Type-2 fuzzy sets generation method for remote sensing imagery classification," *Computers & Geosciences*, vol. 133, p. 104287, 2019.

[112] Xu, J., Feng, G., Zhao, T., Sun, X., & Zhu, M. (2019). Remote sensing image classification based on semi-supervised adaptive interval type-2 fuzzy c-means algorithm. *Computers & geosciences*, 131, 132-143.

[113] S. Yaykiran, G. Cuceloglu, and A. Ekdal, "Estimation of water budget components of the Sakarya River Basin by using the WEAP-PGM model," *Water*, vol. 11, no. 2, p. 271, 2019.

[114] Y. Zhang, M. Pan, J. Sheffield, A. L. Siemann, C. K. Fisher, M. Liang, and E. F. Wood, "A Climate Data Record (CDR) for the global terrestrial water budget: 1984–2010," *Hydrology and Earth System Sciences*, vol. 22, no. 1, pp. 241-263, 2018.

[115] Y. Zhang, M. Pan, and E. F. Wood, "On creating global gridded terrestrial water budget estimates from satellite remote sensing," *Remote Sensing and Water Resources*, pp. 59-78, 2016..

[116] S. N. Bhanja, A. Mukherjee, and M. Rodell, "Groundwater storage change detection from in situ and GRACE-based estimates in major river basins across India," *Hydrological Sciences Journal*, vol. 65, no. 4, pp. 650-659, 2020.

[117] R. L. Wilby, T. M. L. Wigley, D. Conway, P. D. Jones, B. C. Hewitson, J. Main, and D. S. Wilks, "Statistical downscaling of general circulation model output: A comparison of methods," *Water Resources Research*, vol. 34, no. 11, pp. 2995-3008, 1998.

[118] R. L. Wilby, S. P. Charles, E. Zorita, B. Timbal, P. Whetton, and L. O. Mearns, "Guidelines for use of climate scenarios developed from statistical downscaling methods," Supporting material of the Intergovernmental Panel on Climate Change, available from the DDC of IPCC TGCIA, 27, 2004.

[119] E. Forootan, R. Rietbroek, J. Kusche, M. A. Sharifi, J. L. Awange, M. Schmidt, and J. Famiglietti, "Separation of large scale water storage patterns over Iran using GRACE, altimetry and hydrological data," *Remote Sensing of Environment*, vol. 140, pp. 580-595, 2014.

[120] J. T. Schoof, "Statistical downscaling in climatology," *Geography Compass*, vol. 7, no. 4, pp. 249-265, 2013.

[121] F. H. S. Chiew, D. G. C. Kirono, D. M. Kent, A. J. Frost, S. P. Charles, B. Timbal, and G. Fu, "Comparison of runoff modelled using rainfall from different downscaling methods for historical and future climates," *Journal of Hydrology*, vol. 387, no. 1-2, pp. 10-23, 2010.

[122] D. Fasbender and T. B. Ouarda, "Spatial Bayesian model for statistical downscaling of AOGCM to minimum and maximum daily temperatures," *Journal of Climate*, vol. 23, no. 19, pp. 5222-5242, 2010.

[123] A. J. Frost, S. P. Charles, B. Timbal, F. H. Chiew, R. Mehrotra, K. C. Nguyen, and D. M. Kent, "A comparison of multi-site daily rainfall downscaling techniques under Australian conditions," *Journal of Hydrology*, vol. 408, no. 1-2, pp. 1-18, 2011.

[124] J. L. Doebrich, R. R. Wahl, P. G. Chirico, C. J. Wandrey, R. G. Bohannon, G. J. Orris, and M. O. Younusi, "Geologic and mineral resource map of Afghanistan," U.S. Geological Survey, Report No. 2006-1038, 2006.

[125] T. R. Klett, C. J. Schenk, C. J. Wandrey, R. R. Charpentier, M. E. Brownfield, J. K. Pitman, and M. E. Tennyson, "Assessment of undiscovered oil and gas resources of the Amu Darya basin and Afghan-Tajik Basin provinces, Afghanistan, Iran, Tajikistan, Turkmenistan, and Uzbekistan, 2011," U.S. Geological Survey, Report No. 2011-3154, 2012.

[126] S. Kawasaki, F. Watanabe, S. Suzuki, R. Nishimaki, and S. Takahashi, "Current situation and issues on agriculture of Afghanistan," *Journal of Arid Land Studies*, vol. 22, no. 1, pp. 345-348, 2012.

[127] V. Thomas and A. M. Ramzi, "SRI contributions to rice production dealing with water management constraints in northeastern Afghanistan," *Paddy and Water Environment*, vol. 9, no. 1, pp. 101-109, 2011.

[128] M. Ahmad and M. Wasiq, "Water resource development in Northern Afghanistan and its implications for Amu Darya Basin," World Bank Publications, Report No. 36, 2004.

[129] S. Sorooshian, K. L. Hsu, X. Gao, H. V. Gupta, B. Imam, and D. Braithwaite, "Evaluation of PERSIANN system satellite-based estimates of tropical rainfall," *Bulletin of the American Meteorological Society*, vol. 81, no. 9, pp. 2035-2046, 2000.

[130] M. Rodell, P. R. Houser, U. E. A. Jambor, J. Gottschalck, K. Mitchell, C. J. Meng, and D. Toll, "The global land data assimilation system," *Bulletin of the American Meteorological Society*, vol. 85, no. 3, pp. 381-394, 2004.

[131] J. C. Derber, D. F. Parrish, and S. J. Lord, "The new global operational analysis system at the National Meteorological Center," *Weather and Forecasting*, vol. 6, no. 4, pp. 538-547, 1991.

[132] G. J. Huffman, R. F. Adler, M. M. Morrissey, D. T. Bolvin, S. Curtis, R. Joyce, and J. Susskind, "Global precipitation at one-degree daily resolution from multisatellite observations," *Journal of Hydrometeorology*, vol. 2, no. 1, pp. 36-50, 2001.

[133] R. D. Koster, M. J. Suarez, A. Ducharne, M. Stieglitz, and P. Kumar, "A catchment-based approach to modeling land surface processes in a general circulation model: 1. Model structure," J*ournal of Geophysical Research: Atmospheres*, vol. 105, no. D20, pp. 24809-24822, 2000.

[134] Q. Mu, F. A. Heinsch, M. Zhao, and S. W. Running, "Development of a global evapotranspiration algorithm based on MODIS and global meteorology data," *Remote Sensing of Environment*, vol. 111, no. 4, pp. 519-536, 2007.

[135] F. Lehmann, B. D. Vishwakarma, and J. Bamber, "How well are we able to close the water budget at the global scale?," *Hydrology and Earth System Sciences*, vol. 26, no. 1, pp. 35-54, 2022.

[136] D. Katsanos, A. Retalis, F. Tymvios, and S. Michaelides, "Analysis of precipitation extremes based on satellite (CHIRPS) and in situ dataset over Cyprus," *Natural Hazards*, vol. 83, pp. 53-63, 2016.

[137] W. Wang, W. Cui, X. Wang, and X. Chen, "Evaluation of GLDAS-1 and GLDAS-2 forcing data and Noah model simulations over China at the monthly scale," *Journal of Hydrometeorology*, vol. 17, no. 11, pp. 2815-2833, 2016.

[138] D. Lohmann, K. E. Mitchell, P. R. Houser, E. F. Wood, J. C. Schaake, A. Robock, and J. D. Tarpley, "Streamflow and water balance intercomparisons of four land surface models in the North American Land Data Assimilation System project," *Journal of Geophysical Research*: Atmospheres, vol. 109, no. D7.

[139] J. Doorenbos, "Crop water requirements," FAO Irrigation and Drainage Paper, no. 24, pp. 1-144, 1977

[140] G. H. Hargreaves and Z. A. Samani, "Reference crop evapotranspiration from temperature," *Applied Engineering in Agriculture*, vol. 1, no. 2, pp. 96-99, 1985

[141] E. Liang, X. Liu, Y. Yuan, N. Qin, X. Fang, L. Huang, and X. Shao, "The 1920s drought recorded by tree rings and historical documents in the semi-arid and arid areas of northern China," *Climatic Change*, vol. 79, pp. 403-432, 2006.

[142] E. T. Linacre, "A simple formula for estimating evaporation rates in various climates, using temperature data alone," *Agricultural Meteorology*, vol. 18, no. 6, pp. 409-424, 1977.

[143] R. G. Allen, "Crop Evapotranspiration - Guideline for computing crop water requirements," *Irrigation and Drain*, vol. 56, p. 300, 1998.

[144] W. Abtew, "Evapotranspiration measurements and modeling for three wetland systems in South Florida 1," *JAWRA Journal of the American Water Resources Association*, vol. 32, no. 3, pp. 465-473, 1996.

[147] W. G. Bastiaanssen, M. Menenti, R. A. Feddes, and A. A. M. Holtslag, "A remote sensing surface energy balance algorithm for land (SEBAL). 1. Formulation," *Journal of Hydrology*, vol. 212, pp. 198-212, 1998.

[146] W. P. Kustas and C. S. Daughtry, "Estimation of the soil heat flux/net radiation ratio from spectral data," *Agricultural and Forest Meteorology*, vol. 49, no. 3, pp. 205-223, 1990.

[147] M. Ozyavuz, B. C. Bilgili, and A. Salici, "Determination of vegetation changes with NDVI method," *Journal of Environmental Protection and Ecology*, vol. 16, no. 1, pp. 264-273, 2015.

[148] H. Rui, H. Beaudoing, and C. Loeser, "README document for NASA GLDAS version 2 data products," Goddart Earth Sciences Data and Information Services Center (GES DISC), Greenbelt, MD, USA.

[149] G. Ceccherini, I. Ameztoy, C. P. Romero Hernandez, and C. Carmona Moreno, "High-resolution precipitation datasets in South America and West Africa based on satellite-derived rainfall, enhanced vegetation index and digital elevation model," Remote Sensing, vol. 7, no. 5, pp. 6454-6488, 2015.

[150] Z. Duan and W. G. M. Bastiaanssen, "First results from Version 7 TRMM 3B43 precipitation product in combination with a new downscaling–calibration procedure," Remote Sensing of Environment, vol. 131, pp. 1-13, 2013.

[151] J. E. Hunink, W. W. Immerzeel, and P. Droogers, "A High-resolution Precipitation 2-step mapping Procedure (HiP2P): Development and application to a tropical mountainous area," *Remote Sensing of Environment*, vol. 140, pp. 179-188, 2014.

[152] A. S. Fotheringham, C. Brunsdon, and M. Charlton, "Geographically weighted regression: the analysis of spatially varying relationships," *John Wiley & Sons*, 2003.

[153] A. S. Fotheringham, "Trends in quantitative methods I: stressing the local," *Progress in human geography*, vol. 21, no. 1, pp. 88-96, 1997.

[154] A. Stewart Fotheringham, M. Charlton, and C. Brunsdon, "The geography of parameter space: an investigation of spatial non-stationarity," *International Journal of Geographical Information Systems*, vol. 10, no. 5, pp. 605-627, 1996.

[155] C. Brunsdon, A. S. Fotheringham, and M. E. Charlton, "Geographically weighted regression: a method for exploring spatial nonstationarity," *Geographical Analysis*, vol. 28, no. 4, pp. 281-298, 1996.

[156] Lindsey, James, Count Data, and J. Lindsey. "Generalized linear models." 1996.

[157] C. M. Hurvich, J. S. Simonoff, and C. L. Tsai, "Smoothing parameter selection in nonparametric regression using an improved Akaike information criterion," *Journal of the Royal Statistical Society Series B: Statistical Methodology*, vol. 60, no. 2, pp. 271-293, 1998.

[158] I. Gollini, B. Lu, M. Charlton, C. Brunsdon, and P. Harris, "GWmodel: an R package for exploring spatial heterogeneity using geographically weighted models," *arXiv preprint arXiv*:1306.0413, 2013.

[159] P. Goovaerts, "Geostatistical analysis of health data: State-of-the-art and perspectives," in GeoENV VI–Geostatistics for environmental applications:

Proceedings of the sixth European conference on Geostatistics for environmental applications, 2008, pp. 3-22.

[160] J. E. Nash, "River flow forecasting through conceptual models, I: A discussion of principles," *Journal of Hydrology*, vol. 10, pp. 398-409, 1970.

[161] J. Nossent and W. Bauwens, "Application of a normalized Nash-Sutcliffe efficiency to improve the accuracy of the Sobol'sensitivity analysis of a hydrological model," *in EGU General Assembly Conference Abstracts, April* 2012, p. 237.

[162] Yapo, P. O., Gupta, H. V., & Sorooshian, S. (1996). Automatic calibration of conceptual rainfall-runoff models: sensitivity to calibration data. *Journal of hydrology*, 181(1-4), 23-48.

[163] K. L. Hsu, H. V. Gupta, and S. Sorooshian, "Artificial neural network modeling of the rainfall-runoff process," *Water Resources Research*, vol. 31, no. 10, pp. 2517-2530, 1995.

[164] N. R. Draper and H. Smith, "Applied Regression Analysis," *John Wiley and Sons, New York*, 1981.

[165] Aydin-Kandemir, Fulya, and Dursun YILDIZ. "Assessment of growing water and food security crises in Afghanistan." *International Journal of Water Management and Diplomacy* 1.6 2023 5-28.

[166] World Vision Afghanistan, "World Vision Afghanistan Annual Report 2019," [Online]. Available: https://reliefweb.int/report/afghanistan/world-vision-afghanistan-annual-report-2019.

[167] J. F. Shroder and S. J. Ahmadzai, Transboundary Water Resources in Afghanistan: *Climate Change and Land-Use Implications*, Elsevier, 2016.

[168] B. R. Nikam, P. Kumar, V. Garg, P. K. Thakur, and S. P. Aggarwal, "Comparative evaluation of different potential evapotranspiration estimation approaches," *Int. J. Res. Eng. Technol*, vol. 3, pp. 543-552, 2014.

[169] C. Grosso et al., "Mapping maize evapotranspiration at field scale using SEBAL: A comparison with the FAO method and soil-plant model simulations," *Remote Sensing*, vol. 10, no. 9, pp. 1452, 2018.

[170] F. Akhtar et al., "Estimation of actual evapotranspiration using remote sensing-based surface energy balance system at the data-scarce Kabul River Basin of Afghanistan," *in Proceedings of the IEEE International Geoscience and Remote Sensing Symposium (IGARSS)*, 2023.

[171] Y. Yao et al., "Improving global terrestrial evapotranspiration estimation using support vector machine by integrating three process-based algorithms," *Agricultural and Forest Meteorology*, vol. 242, pp. 55-74, 2017.

[172] S. Pan et al., "Evaluation of global terrestrial evapotranspiration using state-of-the-art approaches in remote sensing, machine learning and land surface modeling," *Hydrology and Earth System Sciences*, vol. 24, no. 3, pp. 1485-1509, 2020.

[173] C. Jiménez et al., "Global intercomparison of 12 land surface heat flux estimates," *Journal of Geophysical Research: Atmospheres*, vol. 116, no. D2.

[174] R. Wartenburger et al., "Evapotranspiration simulations in ISIMIP2a—Evaluation of spatio-temporal characteristics with a comprehensive ensemble of independent datasets," *Environmental Research Letters*, vol. 13, no. 7, p. 075001, 2018.

[175] F. W. Landerer and S. S. Cooley, "GRACE D-103133 Gravity Recovery and Climate Experiment level-3 data product user handbook," NASA Jet Propulsion Laboratory Doc, 2021.

[176] D. Long, L. Longuevergne, and B. R. Scanlon, "Global analysis of approaches for deriving total water storage changes from GRACE satellites," *Water Resources Research*, vol. 51, no. 4, pp. 2574-2594, 2015.

[177] B. Li, H. Beaudoing, and M. Rodell, "GLDAS Catchment Land Surface Model L4 monthly 1.0× 1.0 degree V2. 0," Greenbelt, Maryland, USA, Goddard Earth Sciences Data and Information Services Center (GES DISC) , 2020.

[178] M. Rodell and H. Beaudoing, "GLDAS Noah Land Surface Model L4 monthly 0.25× 0.25 degree V2. 1," Greenbelt, MD: Goddard Earth Sciences Data and Information Services Center (GES DISC), 2007.

[179] R. Xiao, X. He, Y. Zhang, V. G. Ferreira, and L. Chang, "Monitoring groundwater variations from satellite gravimetry and hydrological models: A comparison with in-situ measurements in the mid-atlantic region of the United States," *Remote Sensing*, vol. 7, no. 1, pp. 686-703, 2015.

[180] Y. O. Ouma, D. O. Aballa, D. O. Marinda, R. Tateishi, and M. Hahn, "Use of GRACE time-variable data and GLDAS-LSM for estimating groundwater storage variability at small basin scales: a case study of the Nzoia River Basin," *International Journal of Remote Sensing*, vol. 36, no. 22, pp. 5707-5736, 2015.

[181] W. Li, W. Wang, C. Zhang, H. Wen, Y. Zhong, Y. Zhu, and Z. Li, "Bridging terrestrial water storage anomaly during GRACE/GRACE-FO gap using SSA method: A case study in China," *Sensors*, vol. 19, no. 19, pp. 4144, 2019.

[182] V. Lakshmi, "Beyond GRACE: using satellite data for groundwater investigations," *Groundwater*, vol. 54, no. 5, pp. 615-618, 2016.

[183] Z. Liu, Z. Yao, R. Wang, and G. Yu, "Estimation of the Qinghai-Tibetan Plateau runoff and its contribution to large Asian rivers," *Science of the Total Environment*, vol. 749, p. 141570, 2020.

[184] R. Pushpalatha, C. Perrin, N. Le Moine, and V. Andréassian, "A review of efficiency criteria suitable for evaluating low-flow simulations," *Journal of Hydrology*, vol. 420, pp. 171-182, 2012.

[185] R. E. Criss and W. E. Winston, "Do Nash values have value? Discussion and alternate proposals," *Hydrological Processes: An International Journal*, vol. 22, no. 14, pp. 2723-2725, 2008.

[186] S. N. Bhanja, X. Zhang, and J. Wang, "Estimating long-term groundwater storage and its controlling factors in Alberta, Canada," *Hydrology and Earth System Sciences*, vol. 22, no. 12, pp. 6241-6255, 2018.

[187] Y. Zou and J. A. Greenberg, "A spatialized classification approach for land cover mapping using hyperspatial imagery," *Remote Sensing of Environment*, vol. 232, p. 111248, 2019.

[188] J. L. Widlowski, C. Mio, M. Disney, J. Adams, I. Andredakis, C. Atzberger, T. Zenone, "The fourth phase of the radiative transfer model intercomparison (RAMI) exercise: Actual canopy scenarios and conformity testing," *Remote Sensing of Environment*, vol. 169, pp. 418-437, 2015.

[189] S. Xu, C. Wu, L. Wang, A. Gonsamo, Y. Shen, and Z. Niu, "A new satellite-based monthly precipitation downscaling algorithm with non-stationary relationship between precipitation and land surface characteristics," *Remote Sensing of Environment*, vol. 162, pp. 119-140, 2015.

[190] H. Wang, F. Zang, C. Zhao, and C. Liu, "A GWR downscaling method to reconstruct high-resolution precipitation dataset based on GSMaP-Gauge data: A case study in the Qilian Mountains, Northwest China," *Science of the Total Environment*, vol. 810, p. 152066, 2022.

[191] S. Tan, B. Wu, N. Yan, and W. Zhu, "An NDVI-based statistical ET downscaling method," *Water*, vol. 9, no. 12, p. 995, 2017.

[192] S. Tan, B. Wu, and N. Yan, "A method for downscaling daily evapotranspiration based on 30-m surface resistance," *Journal of Hydrology*, vol. 577, p. 123882, 2019.

[193] R. K. Singh, G. B. Senay, N. M. Velpuri, S. Bohms, and J. P. Verdin, "On the downscaling of actual evapotranspiration maps based on combination of MODIS and Landsat-based actual evapotranspiration estimates," *Remote Sensing*, vol. 6, no. 11, pp. 10483-10509, 2014.

[194] E. Sharifi, B. Saghafian, and R. Steinacker, "Downscaling satellite precipitation estimates with multiple linear regression, artificial neural networks, and spline interpolation techniques," *Journal of Geophysical Research: Atmospheres*, vol. 124, no. 2, pp. 789-805, 2019.

[195] Y.H. Kaheil et al., "Downscaling and forecasting of evapotranspiration using a synthetic model of wavelets and support vector machines," *IEEE Transactions on Geoscience and Remote Sensing*, vol. 46, no. 9, pp. 2692-2707, 2008.

[196] A. Arshad, W. Zhang, Z. Zhang, S. Wang, B. Zhang, M. J. M. Cheema, and M. J. Shalamzari, "Reconstructing high-resolution gridded precipitation data using an improved downscaling approach over the high altitude mountain regions of Upper Indus Basin (UIB)," *Science of The Total Environment*, vol. 784, p. 147140, 2021.

PUBLICATIONS FROM THE THESIS

Conference Papers

REMOTE SENSING OF EVAPOTRANSPIRATION USING SEBAL AND LANDSAT-8 IMAGERIES OVER LOWER PART OF KUNDUZ CATCHMENT, AFGHANISTAN (International Symposium on Applied Geoinformatics (ISAG-2019))

Paper

1. A. S. Frahmand Et Al., "CAN REMOTE SENSING AND SEBAL FILL THE GAP ON EVAPOTRANSPIRATION? A CASE STUDY: KUNDUZ CATCHMENT, AFGHANISTAN," JOURNAL OF ENVIRONMENTAL PROTECTION AND ECOLOGY, vol.21, no.2, pp.423-432, 2020